AN ACOUSTIC EMISSION-BASED TEST TO EVALUATE LOW TEMPERATURE BEHAVIOR OF ASPHALT MATERIALS

BY
BEHZAD BEHNIA

DISSERTATION

Submitted in partial fulfillment of the requirements
for the degree of Doctor of Philosophy in Civil Engineering
in the Graduate College of the
University of Illinois at Urbana-Champaign, 2013

Urbana, Illinois

Doctoral Committee

Professor William G. Buttlar, Chair, Director of Research
Professor Henrique Reis, Chair, Director of Research
Professor Imad L. Al-Qadi
Professor Jeff Roesler
Mr. James Barnat, Road Science, Division of ArrMaz Custom Chemicals

ABSTRACT

AN ACOUSTIC EMISSION-BASED TEST TO EVALUATE LOW TEMPERATURE BEHAVIOR OF ASPHALT MATERIALS

Behzad Behnia

Department of Civil and Environmental Engineering
University of Illinois at Urbana Champaign

William G. Buttlar, Advisor

Low temperature cracking in asphalt pavements located in cold climates is a major cause of pavement deterioration. Accurate evaluation of low temperature cracking behavior of asphalt materials is necessary in order to design pavements that are resistant to thermally induced cracking. Detrimental effects of low-temperature cracking have motivated a number of studies in an effort to experimentally design and control asphalt properties related to the low temperature performance of asphalt pavements. However, accurate predictions of thermal cracking and associated failure mechanisms still remain a challenge. In the present study, an acoustic emission-based testing method was developed to address the current shortage of a rapid and practical test to evaluate the low temperature cracking performance of asphalt binders and mixtures. The developed testing technique has been successfully implemented to assess several types of asphalt binders and mixtures including: Anti-Oxidant modified asphalt binders, SHRP core asphalt binders, asphalt concrete mixtures containing Reclaimed Asphalt Pavement (RAP) material, Warm Mix Asphalt (WMA) mixtures, Bio-Modified Binders (BMB) mixtures, etc. Results show that this technique is very sensitive to aging level of asphalt materials as well as presence of additives such as WMA additives within binder or mixture. The acoustic emission-based testing method appears to be a viable technique for characterization of low temperature behavior of asphalt materials.

IN THE NAME OF GOD, THE MOST GRACIOUS AND THE MOST MERCIFUL

To my parents
for their endless love, guidance and encouragement throughout my life

ACKNOWLEDGEMENTS

I would like to express my deepest appreciation to my advisor Prof. William G. Buttlar and my co-advisor Prof. Henrique Reis for all of their endless support, insightful guidance, invaluable suggestions and feedback, and encouragement throughout the course of this study. Their excellent knowledge, dedication to research, and great enthusiasm has always been continuous source of motivation during my study. I would also like to show my sincere thanks to my thesis committee members, Prof. Imad Al-Qadi, Prof. Jeffery Roesler, and Mr James Barnat, for their time, helpful discussions and valuable inputs to my thesis.

I would like to thank my colleagues and friends: Ms. Megan Mcgovern, Mr. Brian Hill, Dr. Eshan Dave, Mr. Salman Hakimzadeh, Dr. Sarfraz Ahmed, Mr. Nathan Abay Kebedeh, Mr. Adam Beach, Ms. Alex Haser, Mr. Jacob Arnold, Dr. Adam Senalik, Mr. Nathan Price, Mr. Thomas Suchy, Dr. Amanda Bordelon, Dr. Kerry Hall, Mr. Alireza Tofangchi and many others who always encouraged and helped me during the course of this study. Thanks for being such fantastic friends and exchanging your brilliant ideas with me. Their company made my study here at UIUC memorable.

Thanks to the National Cooperative Highway Research Program – Ideas Deserving Exploratory Analysis (NCHRP-IDEA) program manager, Dr. Inam Jawed, and Department of Civil and Environmental Engineering of University of Illinois for providing financial support to complete this research.

I finally would like express my profound appreciation to my dear family, specially my parents, for all their endless love and support throughout my life.

TABLE OF CONTENTS:

CHAPTER 1

CHAPTER 2

CHAPTER 3

CHAPTER 1

INTRODUCTION

1.1 THERMAL CRACKING IN ASPHALT PAVEMENTS

Low temperature cracking or thermal cracking is a common form of deterioration in asphalt pavements located in cold regions. This periodic crack pattern forms as a result of low pavement temperature and/or due to a high cooling rate in the pavement. As the pavement temperature reduces, thermally induced tensile stresses develop in the restrained pavement layer. The induced thermal stresses are greatest in the longitudinal direction of the pavement. In simplistic terms, thermal cracking occurs once tensile stresses reach the tensile strength of the asphalt concrete. Low temperature cracking manifests itself as transversely-oriented surface-initiated cracks of various lengths and widths [1,2]. A closely spaced thermal cracking pattern in an asphalt pavement is shown in Figure 1.1.

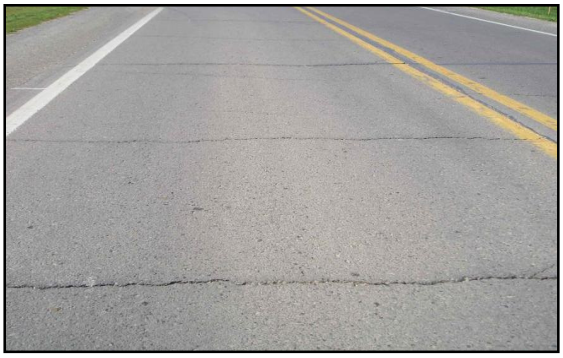

Figure1.1: Thermal Cracks in Asphalt Pavement

Thermal cracks in asphalt pavements are expensive and difficult to properly treat. They drastically affect asphalt pavement life span, rideability, and lead to millions of dollars of repair and maintenance annually. As weak zones of the pavement, thermal cracks are the starting point for other forms of deterioration. If left untreated, cracks deteriorate and widen over time, allowing moisture to readily infiltrate the pavement system and damage the road structure. Detrimental effects of low-temperature cracking have motivated a number of studies in an effort to experimentally design and control asphalt properties related to the low temperature performance of asphalt pavements. However, accurate predictions of thermal cracking and associated failure mechanisms still remain a challenge [1, 2, 3].

1.2. PROBLEM STATEMENT

As asphalt binder or mixture is cooled, it transitions from a brittle-ductile to a quasi-brittle physical state. In the quasi-brittle state, resistance to fracture is generally very low, allowing cracks to propagate readily. To complicate matters, asphalt concrete tends to become oxidized, leading to material embrittlement with time. The amount of aging, or the aging rate, has been found to vary significantly depending upon crude source, refining techniques, additives, climate, and characteristics of the mixture (asphalt content, air voids). As a consequence, one of the great challenges for the pavement engineer is to determine when a pavement surface has become vulnerable to embrittlement for a given climate. Currently, the pavement engineer lacks practical tools to determine the proper time for preventive maintenance, such as the application of a surface treatment, or to determine when a more substantial rehabilitation is required, such as pavement milling and resurfacing [1].

Another challenge facing the pavement engineer is the proliferation of new materials and the lack of field data to assess their suitability for a given climate. Such examples are:

- Recycled Asphalt Pavement (RAP) mixtures, particularly high RAP content mixtures, which are rapidly gaining popularity.
- Warm mixtures (WMA) of which several varieties exist, having markedly different modification approaches.
- Open-graded mixtures.
- Stone mastic asphalt mixtures (SMA).
- Polymer-modified and acid-modified mixtures: numerous polymers and acids exist, which impart substantially different physical properties to the mixture.
- Liquid anti-strip agents.

Combinations of these mixture types and/or modifiers are being used in the field, often without existing field performance to guide the designer in the material selection and mix design process. This can be problematic, since the result of blending acid modified mixtures with liquid anti-strip, for instance, can lead to unexpected physical property changes. In the case of RAP mixtures, the degree of blending between the new (virgin) and existing aged binder is difficult to determine, and moreover, the effect of this partial blending on the ability of the mixture to

withstand cracking under low temperatures is difficult to assess. Warm mix additives are typically proprietary products, and range from zeolite-based additives, to organic additives, to low molecular weight esterified waxes. In addition, since these mixtures are produced at markedly lower production temperatures than conventional hot-mix, a practical tool is needed to assess their resistance to low temperatures in the as-built condition.

The Superpave binder tests developed under the Strategic Highway Research Program (SHRP) have certainly improved the way in which those in the asphalt industry can specify and purchase asphalt binders (AASHTO MP1), by providing fundamental material tests over a broad range of production and service temperatures. However, these tests were not developed for highly modified binders, and were not developed for the design and control of RAP and warm-mix materials. Although the BBR has correlated well to thermal cracking in the field for straight run binders, it is more appropriate to employ the direct tension test (DTT) in conjunction with the BBR as an option in the AASHTO MP1 specification to enable a broader range of binders to be evaluated. However, the DTT device suffers from poor repeatability, is relatively expensive, and requires significant operator training and care. In addition, the combination of the BBR and DTT carries an equipment cost in the range of $60k [1].

On the mixture testing side, mechanical tests such as the Superpave Indirect Tension Test (IDT), Disk-Shaped Compact Tension Test (DC[T]), Semi- Circular Bend Test (SCB), and Thermal Stress Restrained Specimen Test (TSRST) can be used to assess thermal cracking potential. While these tools provide a closer link to field performance by testing the entire asphalt mixture, they are currently neither convenient nor cost effective for employment for practical mix design and evaluation. The cost of these devices are in the range of $50k - $150k depending upon test device features and require specimen sawing, and in some cases, coring, and notch fabrication. It is also difficult to assess near-surface properties and severe aging gradients, which may be the key to the initiation and propagation of thermal and block cracks and possibly top-down fatigue cracks [1].

For the practical low-temperature evaluation of binders, binder blends, and mixtures for the purpose of formulation, design, control, and forensics, there is still a need for a test which is: rapid; simple; compact and portable; applicable to modern materials (highly modified, recycled, warm-mix); versatile, able to test binders and mixtures and suitable for lab-produced and field materials; extendable to in-situ pavement evaluation; capable of testing thin mixture specimens,

independent of size effect, and; designed specifically to aid in the timing and selection of preventive maintenance and rehabilitation treatments [1].

Considerable interest exists for accurate, practical and cost-effective testing methods capable of predicting the low temperature behavior of asphalt binders and mixtures. As proposed herein, an acoustic emission-based (AE) test method addresses the current shortage of rapid, practical binder and mixture tests available to the pavement engineer for material formulation, selection, design, and QC/QA. This technique shows great potential in accomplishing these needs and it can be used to rapidly characterize the temperature at which material embrittlement occurs in asphalt binders and mixtures. Acoustic emission testing is a versatile NDT technique to gather information in order to detect and assess damage occurring in a wide range of materials. This study describes the development of an AE-based technique to detect and evaluate damage occurring due to thermally-induced microcracking in asphalt pavement materials [1, 3].

Acoustic emission techniques have been used extensively to study damage in many engineering materials including concrete, rock, steel, and wood. There is, however, very limited application of AE techniques for evaluating damage mechanisms in asphalt materials. A review of available literature on AE-based studies in asphalt binders and mixtures indicate that AE has been applied almost exclusively in conjunction with low temperature testing. This is to be expected since asphalt is highly temperature dependent and at warmer temperatures propagation of transient elastic waves generated by defects in a material will be severely attenuated [4]. Research involving AE in asphalt at low temperatures can be grouped into three areas: crack initiation, crack propagation, and crack source detection. The most common testing configuration used in AE testing of asphalt mixtures involved mechanical loading under isothermal conditions at single/multiple temperatures [4-8]. Another commonly used configuration involved thermally restrained specimens subjected to decreasing temperatures at specified cooling rates [7, 8]. Prior to this wor,k, no studies have been reported involving the use of AE techniques in conjunction with thermally-induced microcracking, nor has it been applied to study non-traditional mixtures like RAP, warm-mixes, porous asphalt, etc.

1.3 RESEARCH OBJECTIVES AND OUTLINE

The main objective of this research is to develop a simple and efficient acoustic emission-based testing method that can be used to accurately characterize the low temperature cracking behavior of asphalt binders as well as asphalt mixtures.

To develop a testing procedure according to the problem statement described above the major objectives for the current research were identified as follows:

- Development of an acoustic emission-based testing technique for low temperature characterization of asphalt binders.

- Use of the acoustic emission-based binder testing method to assess a wide range of asphalt binders across a range of aging levels.

- Development of an acoustic emission-based method to evaluate low temperature behavior of asphalt mixtures.

- Implementation of the AE-based mixture test to evaluate a wide range of laboratory compacted mixtures and field-cored samples.

- Application of the developed AE-based test method to assess the low temperature cracking behavior of mixtures at different aging levels, and mixtures containing Reclaimed Asphalt Pavement (RAP), Warm Mix Asphalt (WMA), and Bio-Modified Binders (BMB) mixtures.

- Implementation of the AE-based method to investigate cooling cycle effects on the low temperature behavior of asphalt concrete mixtures.

The research outline employed to meet objectives listed above is summarized in Figure 1.2.

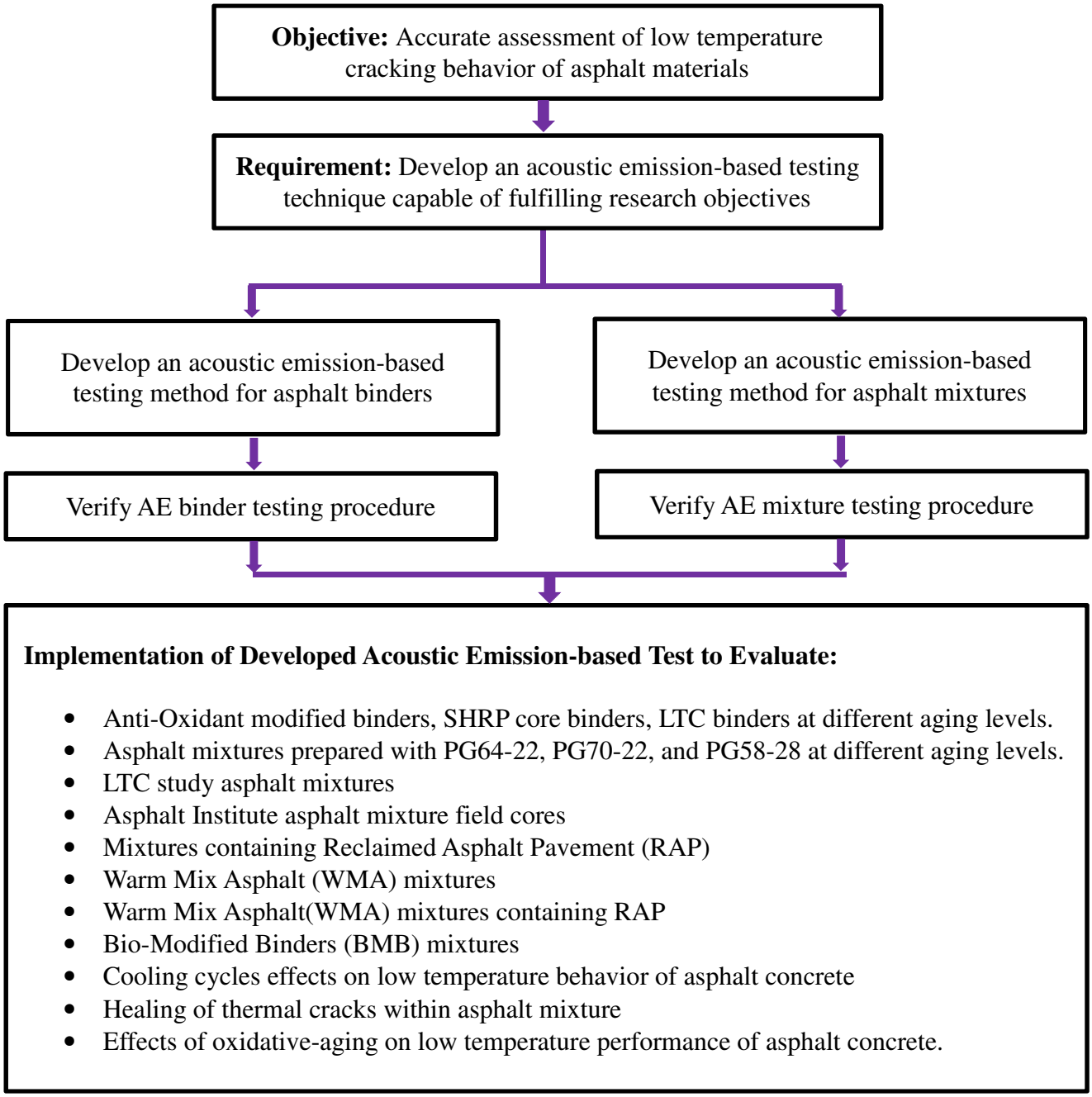

Figure1.2: Outline of the Doctorate Research

1.4. ORGANIZATION OF DISSERTATION

This dissertation is divided into ten chapters. The remaining chapters are organized as follows:

- CHAPTER 2- Background:

  This chapter provides a brief review of acoustic emission technique history. Principles of acoustic emission phenomenon in materials, propagation of AE waves in bulk medium, characteristics of AE signals, and current applications of this testing method in industry are presented in detail.

- CHAPTER 3- Developing an Acoustic Emission-based Test for Asphalt Binders:

  This chapter provides an overview of thermal cracking distress in asphalt pavements as well as a brief review of asphalt binders' conventional and current low temperature cracking tests. AE binder sample preparation procedure and analysis method are presented. Analytical explicit solution along with elastic and viscoelastic finite elements simulation results are provided and compared against each other.

- CHAPTER 4- Developing an Acoustic Emission-based Test for Asphalt Mixtures:

  Details of the AE-based approach for testing asphalt mixtures are presented in this chapter. In addition to asphalt mixtures, AE test results of binder and mastic coated aggregates are discussed.

- CHAPTER 5- Implementation of AE-based Mixture Testing Technique to Evaluate Cooling Cycle Effects on Low Temperature Cracking Characteristics of Asphalt Concrete:

  Effects of intense cooling cycles on low temperature cracking behavior of asphalt concrete mixture is investigated using developed AE-based approach. In addition to AE test, two mechanical tests, Disk-shaped Compact Tension [DC(T)] test and Indirect Tensile [ID(T)] test, along with X-ray computed tomography were employed to fully characterize the low temperature cracking performance of asphalt mixtures.

- CHAPTER 6- Application of Acoustic Emission Technique in Assessing Aging of Asphalt Concrete Mixtures:

  Detrimental effects of oxidative-aging of asphalt pavements are assessed through conducting AE-based mixture test as well as ultrasonic velocity and attenuation measurements. Critical oxidative aging time to conduct preventive maintenance for asphalt concrete mixtures is determined using AE test results.

- CHAPTER 7- Using Acoustic Emission Technique to Investigate Effects of Recycled Asphalt Pavement (RAP) Amounts on Low Temperature Cracking Performance of Asphalt Mixtures:

  This chapter investigates effects of RAP amounts on the low temperature cracking performance of asphalt mixtures. Different percentages of RAP material ranging from 0% to 50% were studied using developed AE measurement technique. In addition to AE test, the disk-shaped compact tension [DC(T)] test as well as indirect tension testing IDT were used to further characterize mixture low temperature properties.

- CHAPTER 8- Evaluation of Warm Mix Asphalt (WMA) Mixtures Containing Reclaimed Asphalt Pavement (RAP) using Acoustic Emission Technique:

  A set of WMA mixtures encompassing a variety of variables, including: four WMA additives (Evotherm 3G, Rediset LQ, Sasobit, and Advera) and presence of different amounts of RAP (0, 15, and 45%) are investigated. Fully characterization of low temperature performance of WMA RAP mixtures was achieved through conducting acoustic emission-based mixture test, DC(T), and ID(T) creep test.

- CHAPTER 9- Implementation of Acoustic Emission Technique to Characterize Low Temperature Performance of Bio-Modified Binder (BMB) Mixtures Containing Reclaimed Asphalt Pavement (RAP):

  This chapter examines the low temperature properties of virgin BMB mixtures containing RAP and to determine if these mixtures exhibit improved low temperature performance as compared to conventional asphalt concrete mixtures. Acoustic Emission,

Disk-Shaped Compact Tension (DC(T)), and Superpave Indirect Tension tests were employed to characterize low temperature properties of the asphalt mixtures.

- CHAPTER 10- Conclusions and Future Extensions
- REFERENCES

CHAPTER 2
BACKGROUND

2.1 INTRODUCTION TO ACOUSTIC EMISSION

The Acoustic Emission (AE) technique is a recognized nondestructive testing (NDT) method. AE is defined as the spontaneous release of localized strain energy in form of transient mechanical elastic waves in a stressed material. Emitted waves can be recorded using sensitive piezoelectric sensors. This technique has gained broad industrial acceptance in recent decades due to its capability to detect, locate and characterize microstructural failures in materials under stress. AE is being used in a variety of applications [4-6]:

1) As a tool for materials characterization to assess failure mechanisms and durability.
2) As a nondestructive testing tool to qualify production parts under loading condition.
3) As a structural qualification tool to locate and assess the extent of damage occurring during structural testing of components and assemblies.
4) As a health monitoring tool to assess the material stress state during thermo-mechanical processing.
5) As a design feedback tool to assess the adequacy of structural design and material processing.

There are several familiar examples of AE testing. For instance, in the case of timber subjected to loads near failure; the sounds emanating from the over stressed timber can be detected with AE equipment and used as indicators for the impending failure of a wooden structure. Another familiar example is the audible sound produced by the failure of rock; these sounds have been used to detect the impending failure of mine shafts and the onset of landslides. Emission analysis can also be used to model the fault movements that result in earthquakes; the use of seismometers to detect stress waves produced during an earthquake is another familiar application example [4-6].

The first observations of AE were documented in the 8th century by the Jabir Ibn Hayyan. In his book, Hayyan reported that tin generates a ‘harsh sound’ when it is loaded. In the middle of the nineteenth century, the acoustic emission phenomenon has been known as “tin cry”, audible emissions produced by the mechanical twinning of pure tin during plastic deformation which are

audible with the unaided ear. In the late 19th century, audible emissions produced by materials such as tin, iron, cadmium and zinc were reported. Czochralski found the correlation between tin and zinc cry and twinning. Few years later, Albert Portevin and Francois Le Chatelier reported AE emissions generated in a stressed Al-Cu-Mn (Aluminum-Copper-Manganese) alloy [9-13].

The earliest application of acoustic emission analysis probably was in seismology where stress waves produced by an earthquake were analyzed to determine the earthquake epicenter and to characterize fault movement in terms of energy released, location, and depth [12, 13]. In addition to seismology, AE was employed to detect impending rock bursts in coal mines. A German scientist, Joseph Kaiser, in the early 1950s is generally credited with initiating the present effort in acoustic emission. He was the first who used electronic instrumentation to detect and record audible sounds produced by metals during deformation. In his PhD thesis titled "Results and Conclusions from Measurements of Sound in Metallic Materials under Tensile Stress", Kaiser conducted AE tests on several metals including zinc, steel, aluminum, copper, and lead. He reported that all metals that he examined, exhibited the emission phenomena. Kaiser also observed that in cyclic loading of a material acoustic emission activity was irreversible. He showed that acoustic emissions were not generated during the reloading of a material until the stress level exceeded its previous stress level. This phenomenon is known as the "Kaiser effect" and it has proven to be very useful in acoustic emission studies. The first research program on AE in USA was initiated a few years after Kaiser's work in mid 1950s by Schofield. Research conducted by Schofield on acoustic emission led to improve in the AE instrumentation and better understanding of sources of acoustic emission phenomena. It was found that emissions from metals were mainly due to dislocation motion accompanying plastic deformation rather than being entirely due to grain boundary sliding as proposed by Kaiser. As the technology developed, AE became accepted as a NDT method. Early pioneers of the technique such as Kaiser, Dunegan, Green, Pollock, Wadley, Scruby, Birchon, Schofield, Beattie, Proctor, Harris and Ono produced outstanding scientific analyses despite the limitation of their equipment [9-13].

In 1960s, acoustic emission testing became very popular; many engineers and scientists utilized this technique in studies relating to materials research, materials characterization and evaluation, and structural evaluation. Extensive improvements in instrumentation in the early 1960s made possible many advances in acoustic emission technology. In the decade of the 1970s, implementation of acoustic emission as an NDT method continued to increase for industrial

applications. In addition research activities directed towards the formation of the working groups. In the 1980s, with the advent of computers, computer became an important component for both instrumentation and data analysis. Today AE is applied to inspect and monitor pipelines, pressure vessels, storage tanks, bridges, concrete dams, aircrafts, bucket trucks, and a variety of composite and ceramic components. It is also used in process control applications such as monitoring welding processes [14, 15].

2.2. PRINCIPLES OF ACOUSTIC EMISSION TESTING

The Acoustic Emission testing method is based on the fact that most of the materials emit mechanical stress waves when they are mechanically or thermally stressed to the point where deformation or micro-damage occurs. Mechanical elastic waves produced by a material due to the dynamic local rearrangement of its internal structure. The source of an acoustic emission is usually damage related. Micro-cracking, friction, thermal stresses, corrosion, fatigue, melting and phase transformations are common sources of AE activity in a material [4, 5].

When a load is applied to a material, it begins to deform elastically. Associated with this elastic deformation are changes in the stress distribution and storage of elastic strain energy within the material. As the load increases further, some micro-fractures may occur, which is accompanied by a release of stored energy in the form of propagating AE mechanical elastic waves. Acoustic Emission stress waves from a growing flaw travel outward from the source and propagate inside the material.

If the emitted AE stress waves are above a certain threshold level they can be detected by sensitive piezoelectric sensors mounted on the material's surface. The AE sensors convert the mechanical wave energy into voltage (AE signal). An ideal sensor would produce a voltage-time curve identical to the amplitude-time curve of the AE wave at the point where sensor is located. Many available sensors operate quite well for specific types of waves over limited ranges of parameters. Figure2.1 schematically illustrates crack nucleation and propagation and corresponding AE wave transmission and detection for a material under stress. AE waves can be considered as a link between the source and the acoustic emission signal produced by the sensor. Much of the complexity seen in acoustic emission signals is generated as the AE waves travel through the medium [4-6].

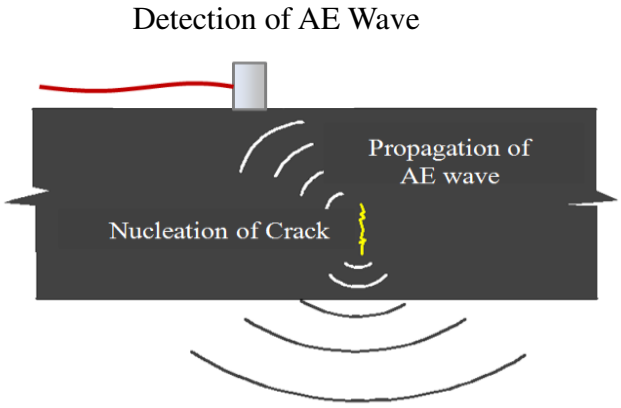

Figure 2.1: Nucleation, Propagation and Detection of AE Waves

Some distinct differences exist between the AE technique and other NDT methods. The major difference is that the AE test method is passive, whereas other NDT methods are for the most part active. With ultrasonic, radiographic or other NDT methods, the source of information is derived by creating some effect in or on the material by external application of energy or compounds. AE relies on energy that is initiated within the component or material under test. Another difference of AE compared to other NDT techniques is the possibility to observe the time-dependent damage process during the entire load history. However since AE test method detects defects in an object the moment the flaw is created, flaws cannot be retested by the AE method. In contrast, other NTD methods such as ultrasonic testing can detect and characterize flaws after they have been created [4, 6].

Some advantages of acoustic emission testing over other forms of NDT testing are: the wide volume being surveyed, the real-time nature of the technique, and the ability to continuously monitor material under stress. This technique is interesting mainly because it is non-localized, meaning that the receiver is not necessarily placed very close to the source.

2.2.1. Propagation of AE Stress Waves

Generally mechanical elastic waves can exist in any material, i.e. solids, liquids, or gases [16]. There are several different types of acoustic waves. The type of mechanical stress wave is

determined based on the relationship between particle motion and the direction of wave propagation. Velocity of stress waves is determined by the properties of the material and the types of waves generated by the geometry and boundary condition of the material. Waves traveling through a medium whose dimensions are much greater than the wavelength are classified as "bulk waves" [Reese and Kawahara, 1993]. Two main types of waves generated in bulk medium are Primary (longitudinal) wave (P wave) and Shear (transverse) wave (S wave). The type of the wave is defined based on the particle motion with respect to the direction of travel. In P waves the motion of material particles are parallel to the direction of wave propagation, whereas for S waves, material particles motion are perpendicular to the direction of wave propagation. Figure 2.2 shows propagation of AE stress waves in a solid medium along with schematic representation of P and S waves.

The P waves usually travel twice as fast as S waves. The velocities of longitudinal and shear waves are determined using equations (1) and (2) where E is Young's modulus, ν is the Poisson's ratio, and G is the shear modulus.

$$V_P = \sqrt{\frac{E(1-\nu)}{\rho(1+\nu)(1-2\nu)}} \tag{2.1}$$

$$V_S = \sqrt{\frac{G}{\rho}} = \sqrt{\frac{E}{2\rho(1+\nu)}} \tag{2.2}$$

In addition to P and S waves, waves can propagate on the surface of the material forming surface or R wave. The R waves have maximum amplitude at the surface boundary and their amplitude decrease with distance from the surface [16].

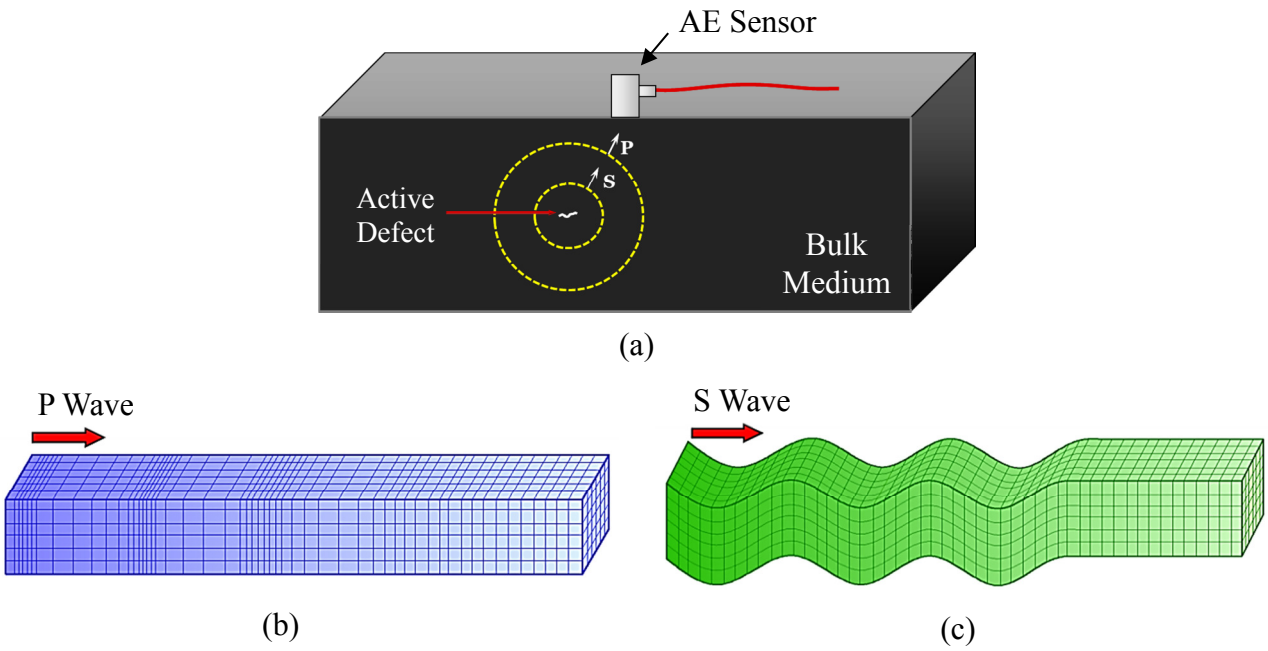

Figure 2.2: Schematic Representation of (a) P wave (b) S wave

2.2.2. Acoustic Emission Signal Characteristics

A typical AE signal lasts less than a thousandth of a second, i.e., Figure 2.3. The characteristics of AE signal are determined by the mechanism which generated the emissions, the path waves travel through the material and finally the sensor which transforms emissions in to electrical voltage versus time signal [4]. There are several parameters which are used for characterization of the AE signal. The parameters are as follows:

- **AE Event:** a rapid physical change such as micro-fracture in a material that releases energy, appearing as acoustic emission;
- **AE Event Counts:** the number of times the AE signal crosses the threshold (trigger level). A single event may provide only a few counts or it might produce hundreds of counts, depending on the size and shape of the signal. In the early years of AE, “counts” were the most common way to describe and report AE quantities. During the 1980s, energy replaced counts as the preferred measure of AE activity. However, counts are still

useful for data interpretation; used in conjunction with other parameters, they can give valuable information on signal shape [4].

- **Accumulated AE Activity:** the total number of events observed during a specific period of time;
- **Amplitude:** the largest voltage present in the signal waveform. For a signal to be detected, its amplitude must exceed a predetermined threshold.
- **Signal Duration:** the length of time from the first threshold crossing to the last, measured in microseconds. The relationship between duration and amplitude tells the user about the signal's shape: whether it is a short sharp "click," or a long drawn-out "scrape."
- **Rise Time:** the time from the crossing of the trigger level to the apex of the highest peak;
- **AE Energy:** Square of the voltage integrated over the event duration, measured for each event;
- **Cumulative AE Energy:** The total amount of energy recorded progressively since the beginning of the AE test.

Other signal features may be measurable, depending on the equipment available, but those noted above are the most widely used.

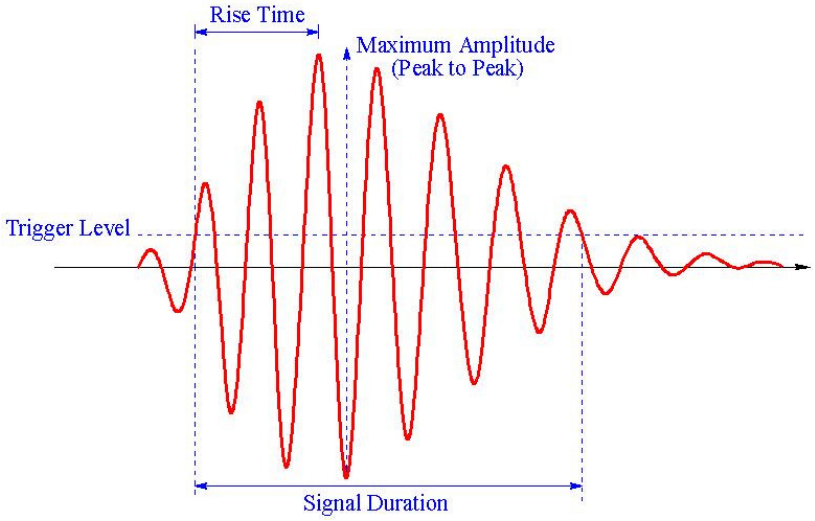

Figure 2.3: Typical Acoustic Emission Signal

There are two types of emissions in the material: burst emission and continuous emission. Acoustic Emission happens by the fracture in the crystallites of the material in the form of discrete packets of mechanical elastic waves. Packets of mechanical elastic waves produced when the stress in the material exceeds the level necessary to fracture the crystallites. These high amplitude discrete packets of acoustic energy are known as “burst emission”. The superposition of bursts produces continuously occurring acoustic waves are called “continuous emission”. Both burst and continuous AE signals are generated by discrete processes. The amplitude of the continuous emission is usually much lower than that of burst emission [16]. Both types of emission are depicted in Figure 2.4.

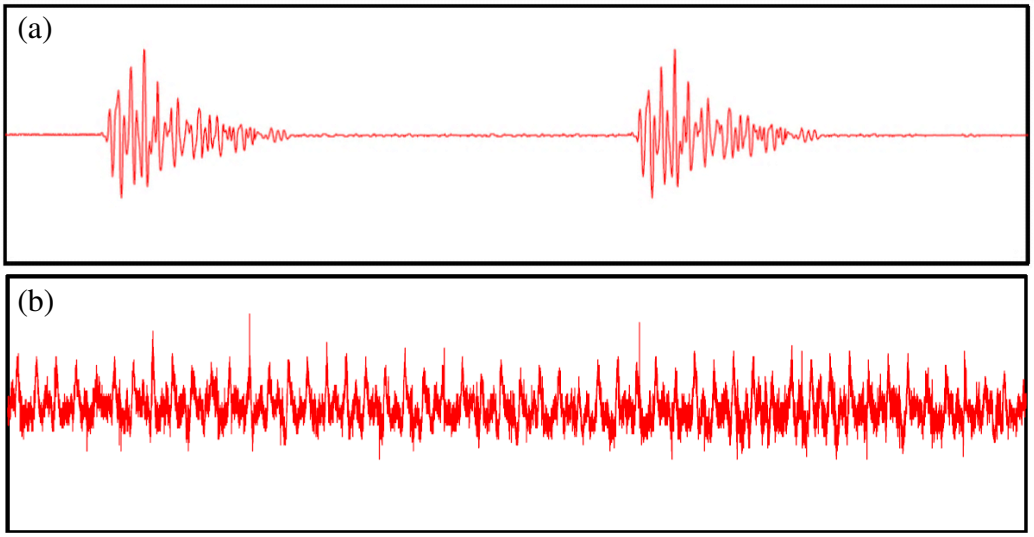

Figure 2.4: Two Types of Emissions: (a) Burst Emission (b) Continuous Emission.

2.2.3 Acoustic Emission Testing Setup

Acoustic Emission stress waves can be measured using piezoelectric transducers. Problems arise in the low level magnitude of the emission activity and the high frequency of the signal. The microfracturing processes leading to failure of a material are generally short-lived events with rise times on the order of 10^{-6} to 10^{-4} seconds. Emissions or stress waves generated by these processes are low level in magnitude; therefore, special electronic equipment is required for

detection, recording, and analysis. Figure 2.5 schematically represents a typical AE testing setup. A well-conceived test procedure, good equipment, and adequately skilled personnel are prerequisites for successful AE testing. The test procedure must take into account probable sources of emission, possible background noise, and load history of the material [4-6].

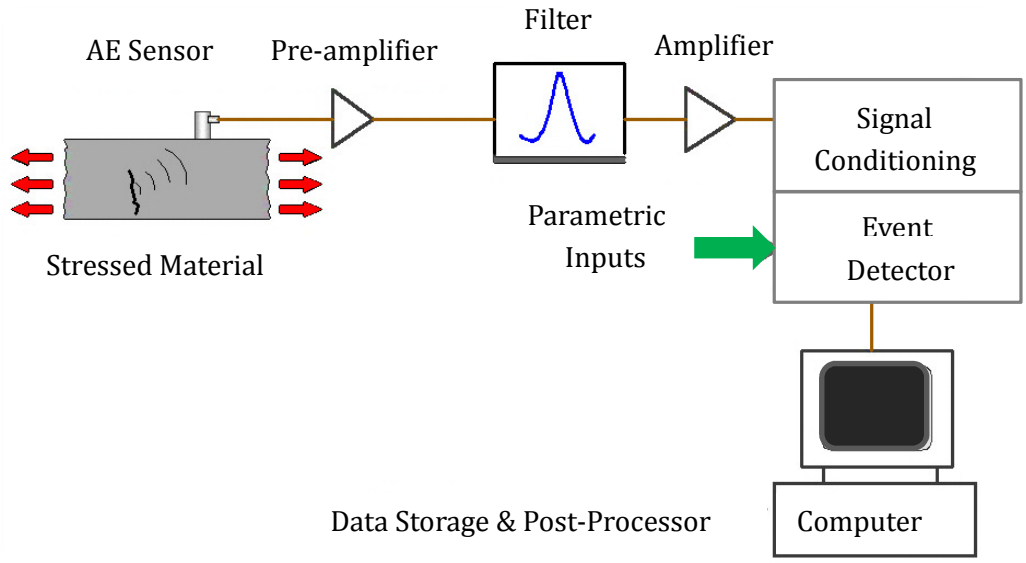

Figure 2.5: Schematic Representation of a Typical Acoustic Emission Testing Setup. AE Stress Waves are Detected with Piezoelectric Sensors, Amplified, Filtered, and then Recorded.

The acoustic emission technique uses sensitive piezoelectric sensors capable of detecting AE stress waves generated by failures occurring within the material. AE sensors are generally mounted on the surface of the material being tested but can also be embedded inside the material. They contain piezoelectric crystal embedded in the sensor. They generate electrical signal when they are stimulated by AE stress waves. Figure 2.6 illustrates a typical AE sensor. The magnitude of the AE signals are very small, so a preamplifier is used to amplify the voltage to a more suitable range. After being amplified, the AE signals are transmitted to an AE data acquisition system to filter unwanted signals or frequencies and to further amplify the signals. Finally signals are sent to a computer for storage and post-processing. Computer also have the ability to record, organize and plot graphs of the AE data which is very helpful for inspectors to understand what is happening during testing [10, 16].

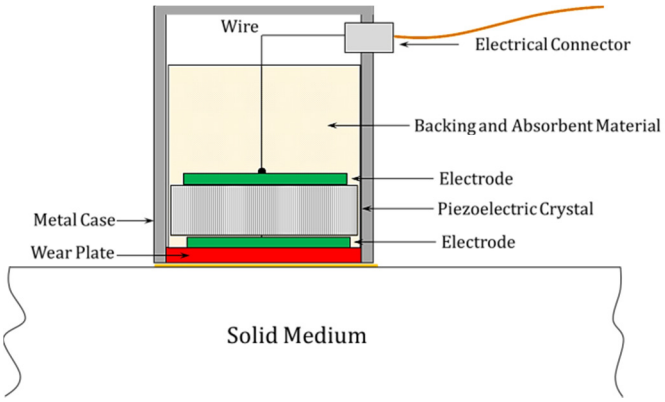

Figure 2.6: Acoustic Emission Piezoelectric Sensor

2.3. APPLICATIONS OF ACOUSTIC EMISSION TECHNIQUE

Acoustic Emission method can be used wherever the stresses in a material stimulate the release of energy as a detectable indication of the possible future failure. This technique has proven itself to be a powerful tool for examining the behavior of materials under stress. It has been extensively applied for condition assessment and damage detection for many materials such as: metals (steel, stainless steel, carbon steel, aluminum and its alloys, magnesium alloys, copper and its alloys, uranium alloys, titanium, and zirconium alloys, etc.), composite materials and polymers (sandwich composite, glass-reinforced plastic (GRP) and carbon fiber), concrete, reinforced concrete, rocks and woods. Almost all materials produce acoustic emissions when they are stressed beyond their normal design ranges to final failure.

AE can be applied to determine the level of strain when a specific material becomes significantly damaged, which is useful for design criteria [17, 18]. Now conducting Acoustic emission is a mandatory in the American Society of Mechanical Engineers (ASME) Code in order to assess composite pressure vessels. Other important applications of AE testing are cooling tower fan blades (ASTM E2076), aerospace structures [19-22], pipe [23], and FRP bridge beams [24,25].

Summary of applications of AE testing method in different areas is listed below:

- Civil Engineering:
    - ❖ Bridges, suspension cable bridges, reinforced concrete structures, tunnels, towers, dams, weld monitoring, railroad tank cars.
- Seismology:
    - ❖ Seismic waves produced by an earthquake are analyzed to characterize fault movement in terms of energy released, location, and depth.
- Aircraft and Aerospace:
    - ❖ Aerospace structures, wings, bulkhead, fuel tanks, Rocket engine, real time monitoring;
- Petrochemical and Chemical Engineering:
    - ❖ Storage tanks, reactor vessels, offshore and onshore platforms, drill pipe, pipeline;
- Marine:
    - ❖ Corrosion, composite shell, engine and power plant;
- Material Research:
    - ❖ Investigation of material properties, fracture mechanisms and damage behavior.

Some advantages of AE technique include high sensitivity, real-time capability, and location of damaged regions [20]. One disadvantages of AE is its dependence on application of load to activate the damage mechanisms (typically mechanical or thermal). Depending upon the material and applied load, some damages within the material may not generate detectable AE waves. Another disadvantage of AE is noises coming from either the applied load or surrounding environment. Noise negatively affects AE test accuracy.

CHAPTER 3

DEVELOPING ACOUSTIC EMISSION-BASED TEST FOR ASPHALT BINDERS

Acoustic emission testing is a versatile NDT technique for the detection and assessment of damage in a wide range of materials. The current study attempts to develop an AE-based technique to detect and evaluate damage occurring due to thermal cracking in asphalt materials including asphalt binders as well as asphalt concrete mixtures. This chapter focuses on the AE-based technique developed to evaluate asphalt binders. Several technical details such as original AE test setup, sample preparation methods, cooling and rate effect, and development of analysis methods are presented in following sections.

3.1 INTRODUCTION

A major form of deterioration in asphalt pavements built in cold climates is low temperature (thermal) cracking which results from the restrained contraction of the asphalt mixture under temperature changes [1, 2, 25, 26]. Pavement temperature during winter is lowest at the surface and temperature changes are highest there. Contraction strains induced by pavement cooling lead to thermal tensile stress development in the restrained pavement layer [3]. The induced thermal stresses are greatest in the longitudinal direction of the pavement. Thermal cracking in the pavement manifests itself as transversely-oriented surface-initiated cracks of various lengths and widths. Thermal cracking in the pavement along with the induced thermal stresses are schematically illustrated in Figure 3.1. For very severe cooling cycles (very low temperatures and/or very fast cooling rates) transverse thermal cracks may develop at specific locations within the pavement under one or very few cooling cycles [3]. This is generally referred to as low-temperature cracking or single-event thermal cracking. Additional cracks will develop at different locations as the pavement is exposed to subsequent cooling cycles. For milder cooling conditions, cracks may advance and develop at a slower rate, such that it may take several cooling cycles for cracks to propagate completely through the surface layer. This is generally referred to as thermal fatigue cracking. Both phenomena are typically classified under the general category of thermal cracking in pavement engineering [3].

A typical thermal cracking pattern occurring in asphalt pavements is shown in Figure 3.2. This form of distress drastically affects asphalt pavement life span, rideability and leads to millions of

dollars of repair and maintenance annually. If left untreated, thermal cracks will continue to deteriorate and widen over time, allowing moisture to readily infiltrate the pavement system. Detrimental effects of low-temperature cracking have motivated a number of studies in an effort to experimentally design and control asphalt properties related to the low temperature performance of asphalt pavements. However, accurate predictions of thermal cracking and associated failure mechanisms still remain a challenge [1].

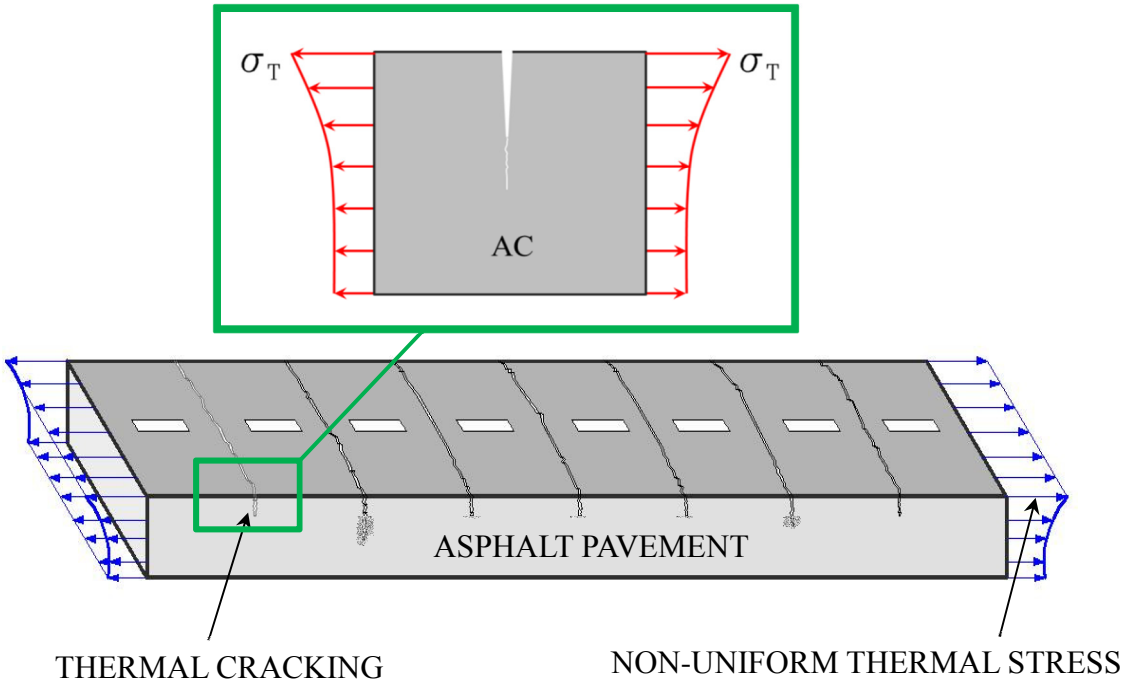

Figure 3.1: Thermal Cracking Formation and Non-uniform Thermal Stresses Distribution through the Pavement Thickness

Figure 3.2: Typical Thermal Cracking in Asphalt Pavement [27]

Over the past decades several testing methods have been developed to characterize the low temperature properties of asphalt binders. The following section briefly reviews conventional as well as current low temperature testing techniques. Today some of these methods, such as the Bending Beam Rheometer (BBR) test, are widely used in United States and Canada to assess thermal cracking resistance of asphalt materials. The present study used the BBR test to determine thermal cracking properties of the asphalt materials. Obtained results were compared with embrittlement temperatures obtained from the AE-based test.

3.1.1. Reviewing Asphalt Binder Thermal Cracking Evaluation Tests

Over the past half century, a number of testing methods have been developed to characterize the low temperature properties of asphalt binders. The strengths and weaknesses of these tests are reviewed in the following sections.

3.1.1.1 Conventional Test Methods

Early attempts to evaluate thermal cracking of asphalt binders yielded several empirical methods such as Fraass Brittle Point Test, and Temperature Susceptibility parameters based on penetration and viscosity test results. These techniques are briefly discussed in the following sections.

3.1.1.1.1 Fraass Brittle Point Test

The Fraass brittle point test is one of the earliest techniques to characterize the low temperature performance of asphalt binders. It has been standardized by the Institute of Petroleum (IP-80153) [28]. The testing sample consists of a thin film of asphalt binder bonded to a thin steel plate. Coating of the plate with binder is performed at an elevated temperature, 90°C (194°F), to ensure proper bonding between the binder and steel plate. In this technique, the steel plate is flexed repeatedly (once per minute), while it is cooled down at a constant rate. A thermocouple positioned in direct contact with the back of the steel plate constantly records the temperature. The Fraass brittle point temperature is the temperature at which the first crack is observed in the asphalt coating. Thenoux et al. [29] found that the Fraass brittle point corresponded to a stiffness modulus of between 0.8 to 2×10^8 Pa. There are some general concerns expressed in the literature regarding this test. For instance, due to repeated loading of testing samples, some argue that this test is actually more like a fatigue test and may not be a good technique to evaluate

thermal cracking of binders. Another issue is due to test limitations as test results could not be obtained below about -35°C. In addition, a relatively high strain level is used, probably due to limitations in strain control and measurement present at the time the test was introduced. The Fraass test has not been popular in the United States and there is not enough data available to correlate the Fraass brittle point temperature and asphalt properties obtained from other tests [30].

3.1.1.1.2. Temperature Susceptibility Test:

Various test parameters and temperature susceptibility-based criteria have been proposed in the past to help control thermal cracking of asphalt pavements. These include: penetration at 25°C, kinematic viscosity at 135°C, McLeod's dimensionless Pen-Vis Number (PVN) and Penetration Index (PI) [31]. McLeod's dimensionless Pen-Vis Number (PVN) is defined by the following relation [31, 32]:

$$PVN = \frac{-1.5(L - \log_{10}\eta)}{(L - M)} \tag{3.1}$$

Where:

$$L = 4.25800 - 0.79674\log_{10}(PEN)$$

$$M = 3.46289 - 0.61094\log_{10}(PEN)$$

η= Kinematic viscosity at 135°C (cSt)

PEN = Penetration at 25°C (dmm)

Susceptibility criteria of the asphalt binder have been defined as follows:

PVN > -0.6 low thermal susceptibility

-1.0 < PVN < -0.6 moderate thermal susceptibility

PVN < -1.0 high thermal susceptibility

Penetration Index (PI) is defined by the following relationship:

$$PI = \frac{20 - 500B}{50B + 1} \tag{3.2}$$

where

$$B = \frac{\log_{10}(PEN(T_1)) - \log_{10}(PEN(T_2))}{T_1 - T_2} \quad (3.3)$$

B represents the slope of the log penetration versus temperature relationship. Asphalt binders with PI values below -1.5 are considered to be susceptible to thermal cracking [31]. However, since the tests are generally conducted at or above 4 Celsius, considerable extrapolation of results is needed in order to assess thermal cracking at low temperatures. Also, the precise interpretation of empirical needle penetration test results is a subject of debate.

3.1.1.2 Current Test Methods

In the early 1990's, Superpave binder tests developed under the Strategic Highway Research Program (SHRP) resulted in developing two test methods for low temperature assessment of asphalt binders: the Bending Beam Rheometer (BBR) test and the Direct Tension Test (DTT).

3.1.1.2.1 Bending Beam Rheometer (BBR) Test

The Bending Beam Rheometer (BBR) test was developed under SHRP program to determine the propensity for thermal cracking in asphalt binders. It measures the flexural creep stiffness or compliance and the m-value (slope of log stiffness-time curve) of asphalt binders by measuring the mid-point deflection of a simply supported beam shaped asphalt samples subjected to a constant creep load applied to the mid-point of the beam. Flexural creep stiffness of asphalt binder correlates to the amount of thermal stress that will develop in the asphalt binder during cooling and thermal contraction in a pavement. High thermal stresses can in turn lead to thermal cracking in a pavement. A higher creep stiffness value indicates higher thermal stresses. The m-value indicates the rate of stress relaxation in asphalt material. It is a measure of the asphalt's ability to relieve stress from an applied load. The higher the m-value, the higher the resistance against low temperature cracking in pavements according to SHRP researchers [28, 33]. The BBR test is conducted in accordance with ASTM D6648-01 and AASHTO T313-02. The test apparatus is designed for testing within the temperature range from 0 to -36°C. The beam shaped BBR testing samples are 101.60 mm long by 12.70 mm wide by 6.35 mm, Figure 3.3.

The BBR testing set-up is illustrated in Figure 3.3(a). It consists of a loading cell, a thermoelectric-based controlled temperature liquid bath which maintains the test beam at the test

temperature, and a computer-controlled automated data acquisition system. A linear variable differential transducer (LVDT) device is located axially above the blunt-nosed loading shaft and is capable of resolving a linear movement ≤ 0.15μm. The computer-controlled data acquisition system records applied creep load, deflection of midpoint of asphalt beam, and loading time during the test [28].

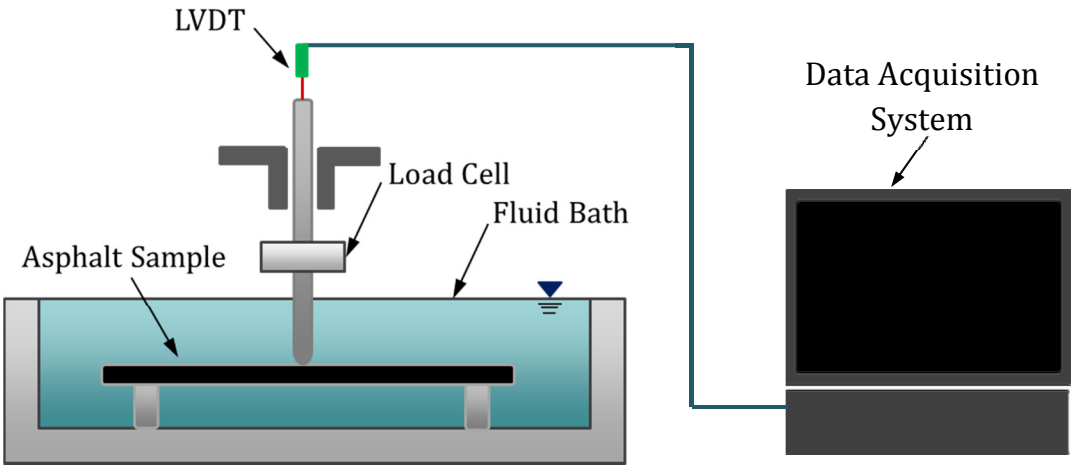

(a)

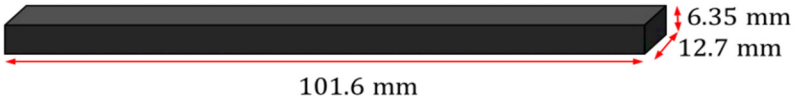

(b)

Figure 3.3: (a) Schematic Representation of Bending Beam Rheometer Testing Setup (b) BBR Beam Dimensions

Prior to conducting the test, BBR specimen is submerged and conditioned for 60 minutes in the fluid bath held at the target temperature. A 981mN creep load is applied for 240 seconds and the deflection is measured by the LVDT. Having length to depth ratio of 16:1, BBR beams behave like a Bernoulli beam and the contribution of shear to deflection of the beam can be neglected. The mid-span deflection of the beam can be calculated using the following equation:

$$\delta(t) = \frac{PL^3}{48EI} \ , \ I = \frac{bh^3}{12} \qquad (3.4)$$

Rearranging the equation above and replacing elastic modulus, E, with 1/D(t), which is equivalent to S(t), results in the following equation to calculate the stiffness of binder samples:

$$S(t) = \frac{PL^3}{4bh^3\delta(t)} \qquad (3.5)$$

Where:

S(t) = flexural creep stiffness at t=60 sec, MPa;

P = applied creep load, N;

L= beam span length, mm;

b = width of beam, mm;

h = thickness of beam, mm;

δ(t) = deflection of beam, mm;

Typical BBR test results including typical plots of deflection and flexural stiffness vs. loading time are shown in Figure 3.4. The flexural creep stiffness of asphalt binder and the slope of the log creep stiffness versus log loading time curve at t=60 sec are considered the creep stiffness and the m-value of the asphalt material, respectively.

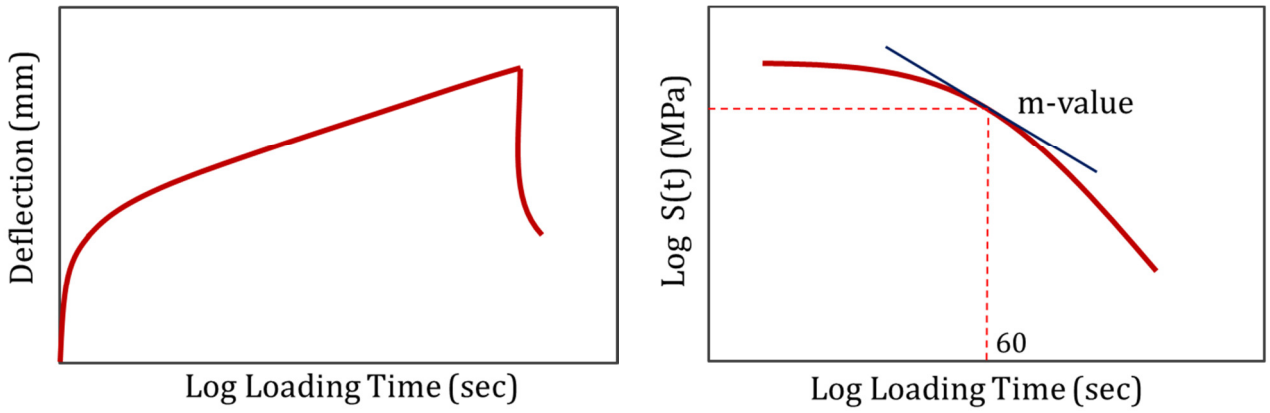

(a) (b)

Figure 3.4: (a) Typical Plot of Deflection vs. Loading Time. (b) Typical Plot of Flexural Stiffness vs. Loading Time

3.1.1.2.2 Direct Tension Test (DTT)

The Direct Tension Test (DTT) test is another important Superpave test developed under the SHRP program. This test evaluates low temperature stiffness and relaxation properties of asphalt binders. The DTT test is used in conjunction with the BBR test to determine an asphalt binder's low temperature PG grade. The testing setup consists of a temperature controlled fluid bath, tensile loading machine, real-time loading system and elongation measuring device, and data acquisition system. The DTT test is standardized in ASTM D6723. The dog bone shaped DTT asphalt samples of 40mm long and 6mm thick are conditioned at the target temperature and then pulled apart at a constant strain rate of 3% per minute until failure. Figure 3.5 schematically illustrates a typical plot of tensile stress vs. tensile strain obtained from the DTT test [28, 34].

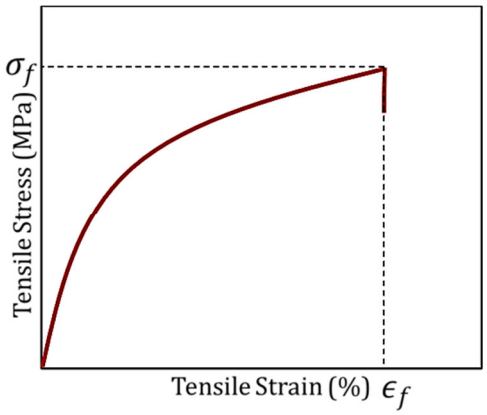

Figure 3.5: Typical Plot of Tensile Stress vs Tensile Strain

Failure stress of the sample is calculated by dividing the measured failure load (P_f) by the original cross sectional area of the test specimen, equation (3.6):

$$\sigma_f = \frac{P_f}{A} \qquad (3.6)$$

Where:

σ_f : failure stress, MPa;

P_f: failure load, N;

A : original cross-sectional area;

Failure strain is calculated by dividing the amount of elongation at failure by the effective original length of sample, Figure 3.6:

$$\epsilon_f = \frac{\Delta L}{L_e} \qquad (3.7)$$

Where:

ϵ_f : failure strain (mm/mm);

ΔL: Sample alongation at failure (mm);

L_e: Effective gage length (mm);

According to Superpave MP1 specification, the flexural creep stiffness (S) of PAV binder must not exceed 300 MPa and the m-value must be greater than 0.300. In case the creep stiffness of a binder is between 300 MPa and 600 MPa and its m-value is greater than 0.300, the asphalt binder is only acceptable if the failure strain of DTT test is more than 1.0 percent. The limiting values of stiffness and m-value were determined based on experience and pavement thermal cracking field data [28].

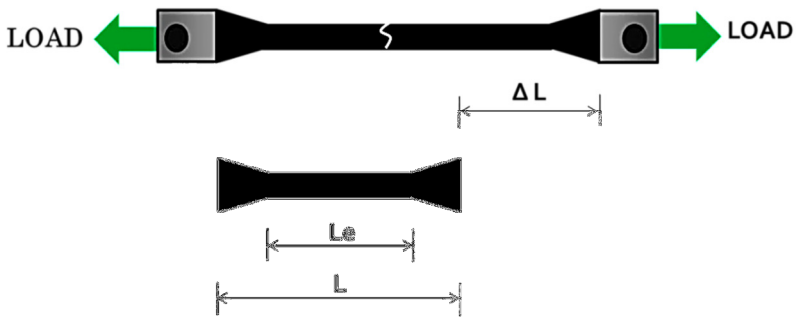

Figure 3.6: Schematic Representation of Direct Tension Test (DTT)

3.1.1.2.3. Asphalt Binder Cracking Device (ABCD) Test

The Asphalt Binder Cracking Device (ABCD) was developed by Kim [28, 35-37] to determine the critical cracking temperature of asphalt binders. The device consists of a 12.7 mm high metal ring of uniform thickness and an electrical strain gauge mounted on the inside of the metal ring to monitor and record the thermal strains. Figure 3.7 schematically shows the asphalt binder cracking device. The outside surface of metal ring is bonded to a thick layer of asphalt binder. When subjected to cold temperatures, tensile stresses are induced within asphalt sample due to dissimilar thermal expansion/contraction coefficients of asphalt binder and metal ring. As the temperature is lowered, thermally induced tensile stresses continue to increase until they reach

the tensile strength of the material which is accompanied with the formation of thermal cracks inside the sample. Thermal cracking of asphalt sample is detected by an instant drop in the strain reading of strain gauge. The cracking temperature is the temperature at which the drop occurs on a plot of strain versus temperature [35-37].

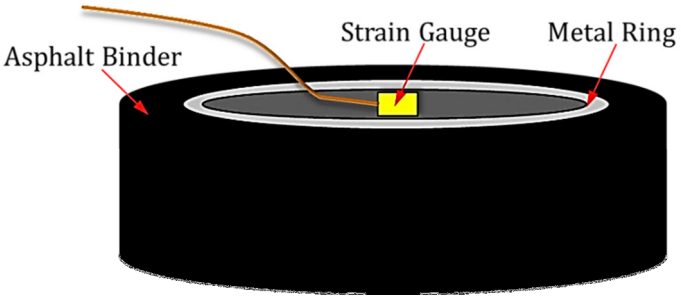

Figure 3.7: The Asphalt Binder Cracking Device

3.1.1.2.4. MPla Specification

The AASHTO MPla specification incorporates strength data along with thermal stress to predict a critical cracking temperature of asphalt binder. The critical cracking temperature is determined using the thermal stress data from the BBR and tensile strength data from the DTT. The thermal stress and tensile strength of the material are plotted versus temperature in a graph. The temperature corresponding to the intersection of these two plots is considered as the single event thermal cracking temperature as illustrated in Figure 3.8 [28, 38, 39].

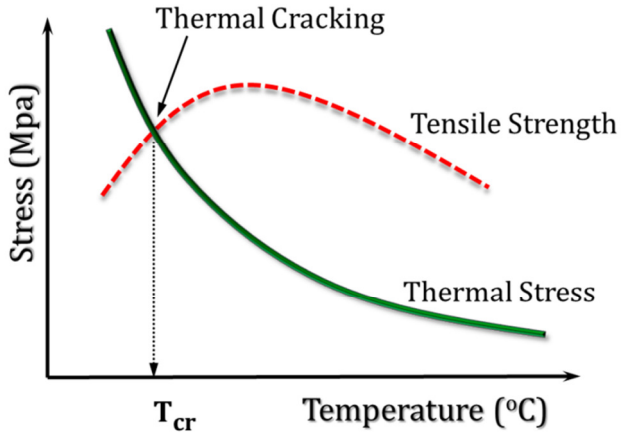

Figure 3.8: MPla Prediction of Single Event Thermal Crack

BBR data are used to generate the creep compliance master curve using the time temperature superposition method. The creep compliance master curve is then converted into a relaxation modulus. Having the relaxation modulus of asphalt material, the thermal stress can be calculated through a convolution integral as follows: Where:

$$\sigma(t) = \int_0^t E(t-\tau)\frac{d\varepsilon(\tau)}{d\tau}d\tau \qquad (3.8)$$

$\sigma: Thermal\ Stress(MPa)$

$E: Relaxation\ Modulus(MPa)$

$\varepsilon: Thermal\ Strain$

3.1.1.2.5. Acoustic Emission Technique

Acoustic emission monitoring has been used extensively to characterize the microscopic fracture processes and to evaluate damage growth in materials. The use of acoustic emission testing for evaluating asphalt materials dates back several decades. Khosla and Goetz [40] used AE techniques to detect crack initiation and propagation in indirect tensile (IDT) specimens at -23ºC. The study found that failure by fracture is indicated by a sharp increase in total AE counts and that significant AE counts occur at about 80% of the peak load. Valkering and Jongeneel [7] used the AE technique to monitor temperature cycling tests with restrained asphalt concrete specimens at low temperatures (10ºC to -40ºC). The Thermal Stress Restrained Specimen Test (TSRST) was used, where a closed loop servohydraulic system is used to maintain constant sample (beam) length as temperature is dropped, thereby inducing thermal tensile strain. They observed that the repeatability of AE measurements is good, the AE activity (number of events) correlates with thermal fracture temperatures, and the AE activity in restrained specimens at low temperatures is caused by defect initiation in the binder. Hesp, et al. [8] used AE measurements to detect crack initiation and propagation in restrained TSRST specimens at low temperatures (-32º to -20ºC). They concluded that the SBS-modified mixes produced less AE activity than unmodified mixes. Li et al. [41-45] in several studies used AE techniques to characterize fracture properties of asphalt specimens at low temperatures. They concluded that large amounts of accumulated AE events occur at 70% of material strength, that the maximum intensity of AE peaks correlates with the development of macrocracks, and that the location of AE events

suggests that a several centimeter-sized process zone forms before peak load. Nesvijski and Marasteanu [46, 47] used an AE spectral analysis approach to characterize fracture in semi-circular bend asphalt specimens at low temperatures, and concluded that an AE approach could be used for evaluation of asphalt pavements. It should be noted that all of the previous studies involved the need for mechanical tests, which are relatively expensive and time-consuming to perform as compared to the techniques developed herein.

3.2 ACOUSTIC EMISSION-BASED METHOD FOR TESTING ASPHALT BINDERS

The current study implements the AE technique to assess low temperature cracking performance of both asphalt materials. The AE binder sample is a thin film of asphalt binder bonded to granite substrate. The sample is exposed to decreasing temperatures, ranging from 20 °C to -50 °C. Differential thermal contraction between granite substrate and asphalt binder induces progressively higher thermal stresses in the binder resulting in thermal crack formation, which is accompanied by a release of elastic energy in the form of transient waves. The critical cracking temperatures of the asphalt binders tested were predicted by processing and analyzing the emitted elastic waves captured during the tests using the AE technique. Figure 3.9 schematically illustrates an AE testing sample of asphalt binder with a granite substrate. [1, 2, 25].

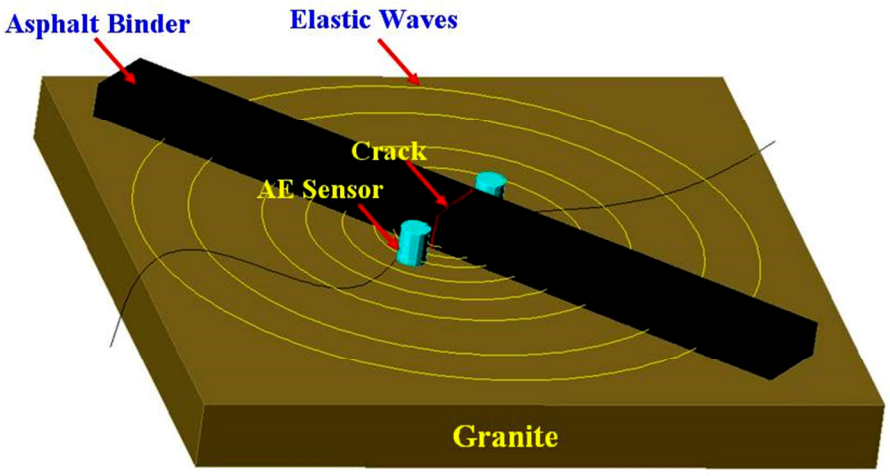

Figure 3.9: Schematic Representation of AE Testing of Asphalt Binders

3.2.1. Experimental Procedure

This section explains the experimental procedure developed for AE testing of asphalt binders. It focuses on several important aspects of AE testing, including: AE testing setup, tested asphalt materials, AE sample preparation, and AE signal analysis.

3.2.1.1 Asphalt Materials

The AE testing technique was employed to evaluate the low temperature cracking behavior of a wide range of asphalt binders. Several different types of asphalt binders at different aging levels were tested as follows:

- Strategic Highway Research Program (SHRP) core asphalt binders:
  - ❖ AAA-1 (PG 58-28),
  - ❖ AAB-1 (PG 58-22),
  - ❖ AAC-1 (PG 58-16),
  - ❖ AAD-1 (PG 58-28),
  - ❖ AAF-1 (PG 64-10),
  - ❖ AAG-1 (PG 58-10),
  - ❖ AAK-1 (PG 64-22),
  - ❖ AAM-1 (PG 64-16),
- Asphalt Binders from the pooled fund study (#776) on low-temperature cracking:
  - ❖ PG64-22 (NY),
  - ❖ PG58-28 (MN/Road-section20),
  - ❖ PG58-34 (MN/Road- section22)
- Anti-Oxidant (AOX) Modified Asphalt Binders:
  - ❖ PG64-22, AOX-modified PG64-22,
  - ❖ PG70-22, AOX-modified PG70-22

All binders were aged using the Rolling Thin Film Oven (RTFO) according to ASTM D2872–04 [48] and the Pressure Aging Vessel (PAV) in accordance with ASTM D6521–05[49]. The RTFO test is a short-term sample conditioning procedure for asphalt binders which simulates the aging that takes place during hot-mix production and about two years of in-field aging. During the

RTFO test, a 35 g asphalt sample in the form of a 1.25 mm thin film of asphalt is exposed to both heat (163 ºC) and air flowing at a rate 400ml/min for 85 minutes in an oven with a rotating rack revolving at speed of 15 rpm. The PAV test simulates the long term aging of the binder after approximately 10 years of service. During PAV testing, a 50 g sample of RTFO-aged sample is subjected to 2.1 MPa air pressure at a temperature of 100 ºC for 20 hours. Figure 3.10 shows the RTFO and PAV test equipment used in this study [13].

(a) (b)

Figure 3.10: (a) Rolling Thin Film Oven Test Setup for Short-Term Aging. (b) Pressure Aging Vessel setup for Long-Term Aging [50].

To prepare AOX-modified binders, two asphalt binders, namely PG 64-22 and PG 70-22 were selected, primarily because they exhibit very different aging and thermal cracking susceptibility characteristics. In addition, half of the asphalt binder samples were modified using an antioxidant (AOX) treatment prior to conditioning and testing. Among several different antioxidant materials, a combination of two additives, namely: Dilaurylthiodipropionate (DLTDP) and Furfural together with hydrochloric acid as a catalyst was used in this study. Apeagyei et al. [8] showed that this combination provided the best resistance to oxidative aging in laboratory-aged asphalt binders. AOX-modified asphalt binders were prepared by mixing antioxidants in the following order: Hydrochloric acid (1.2%), Furfural (2%), and DLTDP (1.5%), as illustrated in Figure 3.11. A Barnant mixer operating at a speed of 750 rpm was used to incorporate the

antioxidants into the base asphalt. The total mixing time was 4 hours; DLTDP was introduced after the second hour in three divided portions. The mixing temperature was kept constant at about 115 ºC. During this period the mixture was continuously stirred with the Barnant Mixer. Un-aged (tank) samples of all the binders were tested. In addition, both unmodified and AOX-modified asphalt binders were short-term aged using the Rolling Thin Film Oven (RTFO) in accordance to standard ASTM D2872–04 and long-term aged in a pressure aging vessel (PAV) in accordance with ASTM D6521–05 [1,2,50].

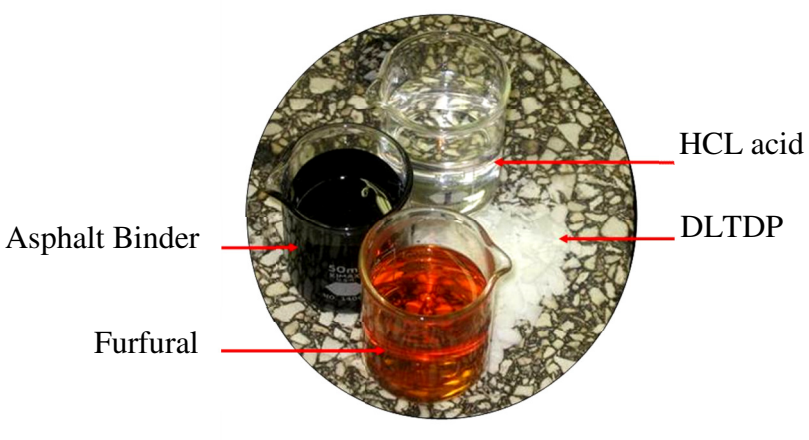

Figure 3.11: Antioxidant Materials Utilized to Modify Asphalt Binders [50].

3.2.1.2 AE Binder Sample Preparation

The thin, rectangular asphalt binder samples used in the AE test were generally molded to be identical to standard BBR sample dimensions. Teflon tape was used as a debonding aid during molding, as shown in Figures 3.12 and 3.13. A 10 mm thick square granite slab (150 mm by 150 mm) was used as the substrate. In order to ensure proper bonding and restraint between the asphalt binder sample and the substrate, the granite substrate was preheated to approximately 120°C. The mold was placed on the heated slab and asphalt binder at a temperature of 135°C was poured into the mold. The AE sample preparation procedure is shown in Figure 3.12. At the end of each test, bonding was verified by the absence of visual debonding, even after visible transverse cracks at regular spacing were present, Figure 3.13(b). It was observed that the sample preparation procedure guaranteed a quality bond in each of the binder samples tested [1,2, 25].

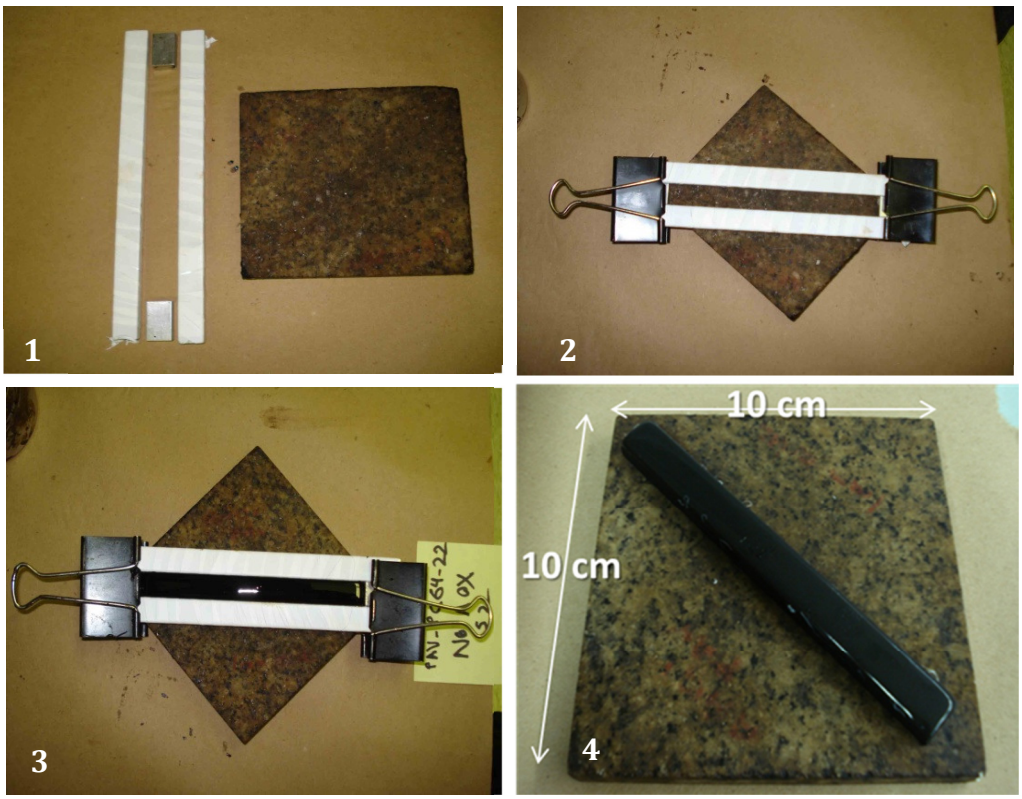

Figure 3.12: Acoustic Emission Asphalt Binder Sample Preparation Procedure

(a) (b)

Figure 3.13:(a) Top: Molds for Fabricating AE Samples; Bottom: Completed AE Sample in the Molds; (b) Typical Crack Patterns in Asphalt Binder Sample after AE Testing [25, 26].

3.2.1.3 Acoustic Emission Testing Setup

A typical AE system consists of sensors, pre-amplification, data acquisition, and processing and analysis software. In the present study, wideband AE sensors (Digital Wave, Model B1025) with a nominal frequency range of 20 kHz to 1.5 MHz were utilized to monitor and record acoustic activities of the sample during the test, Figure 3.14(a). High-vacuum grease was used to couple the AE sensors to the test sample. AE signals were pre-amplified 20dB using broad-band pre-amplifiers to reduce extraneous noise. The signals were then further amplified 21 dB (for a total of 41 dB) and filtered using a 20 kHz high-pass double-pole filter using the Fracture Wave Detector (FWD) signal condition unit, Figure 3.14(c). The signals were then digitized using a 16-bit analog to digital converter (ICS 645B-8) using a sampling frequency of 2 MHz and a length of 2048 points per channel per acquisition trigger. The outputs were stored for later processing using Digital Wave software (Wave-Explorer TM V7.2.6). AE samples were cooled down using a Shuttle ULT-25 portable freezer, Figure 3.14(e). Temperature of the sample was recorded using a K-type thermocouple connected to 4 channel temperature data logger, Figure 3.14(d) [1]

Figure 3.14: Acoustic Emission Testing Setup (a) AE sensors (Digital Wave, Model B1025)

(b)Broad Band Pre-Amplifier (c) Fracture Wave Detector (FWD) Signal Condition Unit (d) 4 Channel Temperature Data Logger along with the K-Type Thermocouple (e) Shuttle ULT-25 Portable Freezer

3.2.1.4 Conducting Acoustic Emission Test

Prepared AE samples are positioned inside the ULT-25 Portable Freezer as shown in Figure 3.15. AE sensors are carefully positioned and bonded to the specimen using vacuum grease as the couplant. A poorly coupled sensor with air bubbles in the couplant can drastically affect the sensor output and it should be avoided. Temperature is recorded using a K-type thermocouple, which is placed adjacent to the asphalt sample at the interface between the substrate and asphalt binder specimen. Figure 3.16 shows a typical temperature versus time cooling profile.

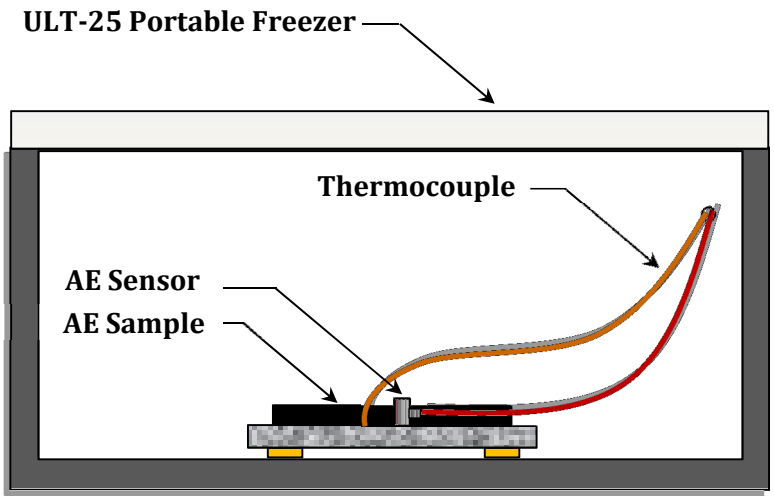

Figure 3.15: Schematic Presentation of AE Binder Testing Setup.

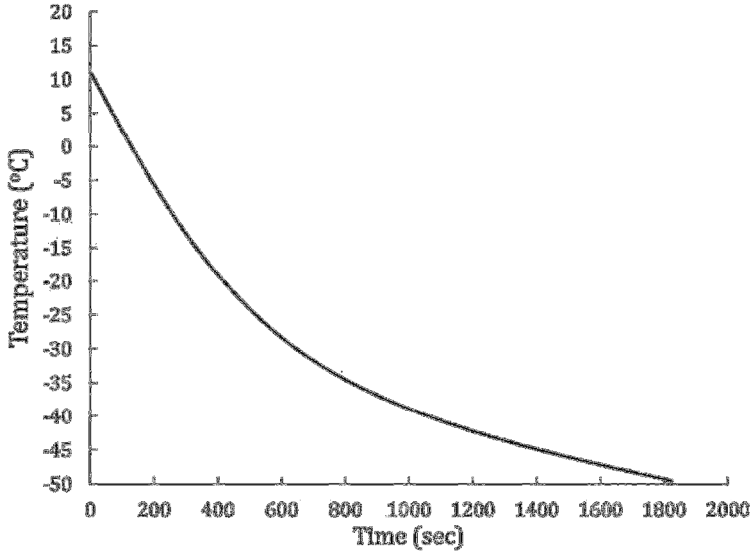

Figure 3.16: Typical Temperature vs. Cooling Time Plot.

3.2.1.5 Analysis of Acoustic Emission Results

There are two main techniques available to analyze the AE test results. One is the "*classical*" or "*parameter-based*" AE technique and the other one which is newer is the "*quantitative*" or "*signal-based*" approach. In traditional classical AE analyses techniques only AE parameters are recorded, not the AE signals, whereas in signal-based techniques AE signals are recorded and used to evaluate materials behavior. Damage and failure processes often generate several thousand AE events from one damage zone within a very short time interval, producing a huge amount of data. With parameter-based AE techniques a fast but only rudimentary analysis can be performed. On the other hand, signal-based AE technique can provide more comprehensive assessment of performance of the material. However it needs careful interpretation by an expert processing the data [1].

In the current study, evaluation of AE activity during thermal loading of asphalt binder samples is performed on recorded AE signals and associated test temperature using both parameter-based and signal-based techniques. A typical waveform associated with an AE event is shown in Figure 3.17. An AE event is hereafter referred to as a local material change giving rise to a measurable acoustic emission. It is an individual waveform having a threshold voltage of 0.1 V and energy equal to or greater than 4 V^2-μs. The emitted energy associated with each event is one of the

characteristics of an AE signal and can be computed using the equation shown below, where E_{AE} is the AE energy of an event (V^2- μsec) with duration of time t (μsec) and recorded voltage of V(t) [1].

$$E_{AE} = \int_0^t V^2(t)dt \qquad (3.9)$$

"Noise" is a major issue in acoustic emission analysis, where noise is simply defined as any unwanted signal captured by the AE system. There is a need to separate genuine stress wave emissions, originating from within the material, from noises such as environmental noise, mechanical noise (movement of the component or sensor during testing), electrical noise, etc. An essential step in a properly conducted AE test is the elimination or filtering of noise, which can be accomplished through appropriate equipment design and testing techniques. Much of this can be achieved by careful electronic filtering of the received AE data, but best practice involves the identification and removal of as many sources of extraneous noise as possible prior to testing. In this study, to minimize the amount of extraneous data including electronic noise, the piezoelectric AE sensors were conditioned in the cooling chamber prior to starting of test. In addition, all events with energy lower than 4 V^2-μs were filtered out. All results presented hereafter are based on the above filtering procedures [1].

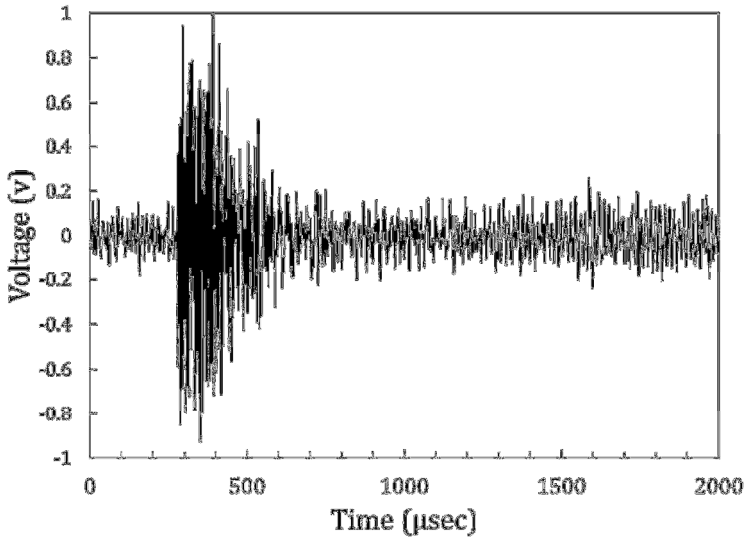

Figure 3.17: Typical Waveform Associated with an AE Event.

A typical plot of AE events counts versus temperature for typical asphalt binder AE tests is shown in Figure 3.18. Four distinct regions were found to exist in AE event counts versus

temperature in the plot, namely: pre-cracking, transition, stable cracking, and fully cracked regions. During the pre-cracking region, differential thermal contraction between the asphalt binder and the granite substrate cause thermal stresses to accumulate in the binder specimen eventually leading to material fracture. In the "pre-cracking region," no AE events are detected. Progressively higher thermal stresses in the specimen result in the formation of thermal microcracks in the material which is accompanied by the release of mechanical elastic waves. This manifests itself as a cluster of high amplitude waves during the test. The transition region is defined as the point in time when thermal microcracking in the specimen, as indicted by higher energy events, begins to occur. The temperature corresponding to the event with the first peak energy level has been termed the "Embrittlement temperature," as shown in Figure 3.19. The embrittlement temperature shows the onset of damage in asphalt material. It is hypothesized that the embrittlement temperature represents a fundamental material state which is independent of material constraint, sample size (as long as a statistically representative volume or larger is used), and sample shape [1, 2, 25].

The "transition region" can be considered as the region where material behavior gradually changes from a quasi-brittle to a brittle state where resistance to fracture is generally very low, allowing cracks to propagate readily. The "stable cracking region" usually initiates at a very low temperature, when the material is brittle and generates a significant amount of AE activity. The AE events count versus temperature plot in this region usually has a steep slope that remains relatively constant. Based upon examination of the study data, this region is thought to be below the glass transition region of the binder [1].

The "fully cracked region" starts right after the stable cracking region when the rate of AE activity of the asphalt sample begins to reduce until it reaches zero at the end of this region. Considering the fact that the source of AE activities is generation of new microdamage inside the sample, reduction in the rate of AE activity is an indication of the presence of plenty of microdamage in the sample. It should be noted that in the AE test the fully cracked region is not usually observed unless the sample is cooled down to very cold temperatures allowing all microdamage to develop within the sample.

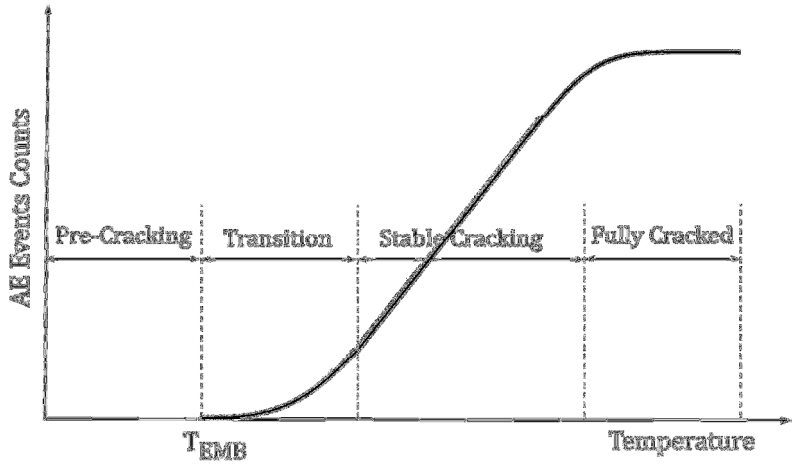

Figure 3.18: Typical AE event Counts vs Temperature Plot Regions.

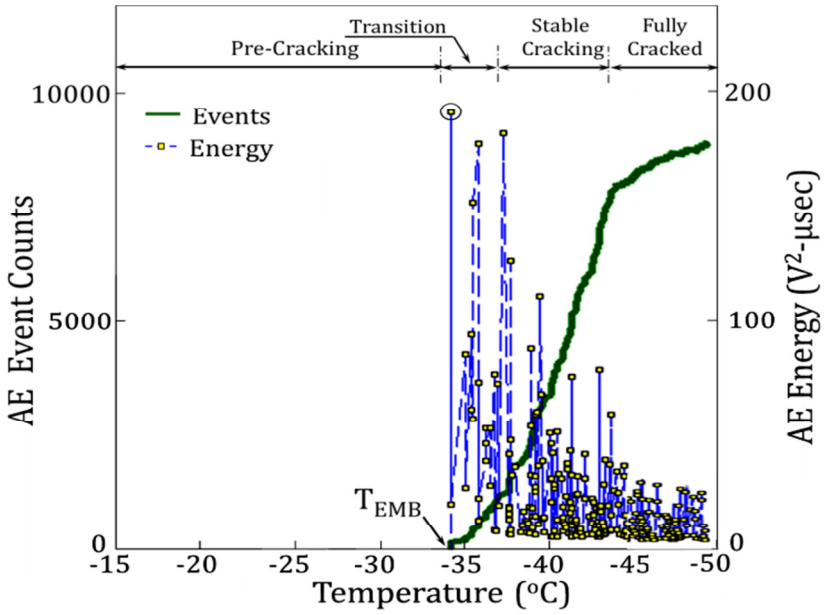

Figure 3.19: Typical Plot of Event Count and AE Energy vs Temperature.

The typical envelope locus of AE events energies is depicted in Figure 3.20, which schematically illustrates the intensity of the released energies of AE events. The envelope locus is zero in the pre-cracking region, then suddenly jumps to its maximum magnitude at the beginning of the transition region. As the sample cools down, the magnitude of AE events energies gradually tapers off until reaching almost zero in the fully cracked region.

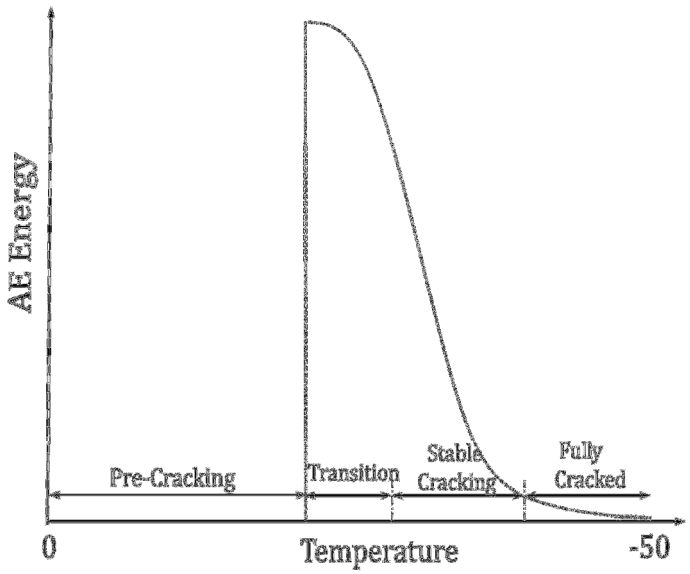

Figure 3.20: Typical Envelope Locus of AE Events Energy During Thermal Cooling

The graphical representation of the distribution of AE events energies is presented as a histogram in Figure 3.21. It is seen that the majority of AE events are low energy events; only a small portion of AE events contain high energy. The energy content of an event depends on the size of the microdamage generating that event. The high energy events result from the formation of large microcracks which are probably visible by naked eye, whereas low level energy events are produced by hairline microcracks within the sample such as formation of spiral cracking.

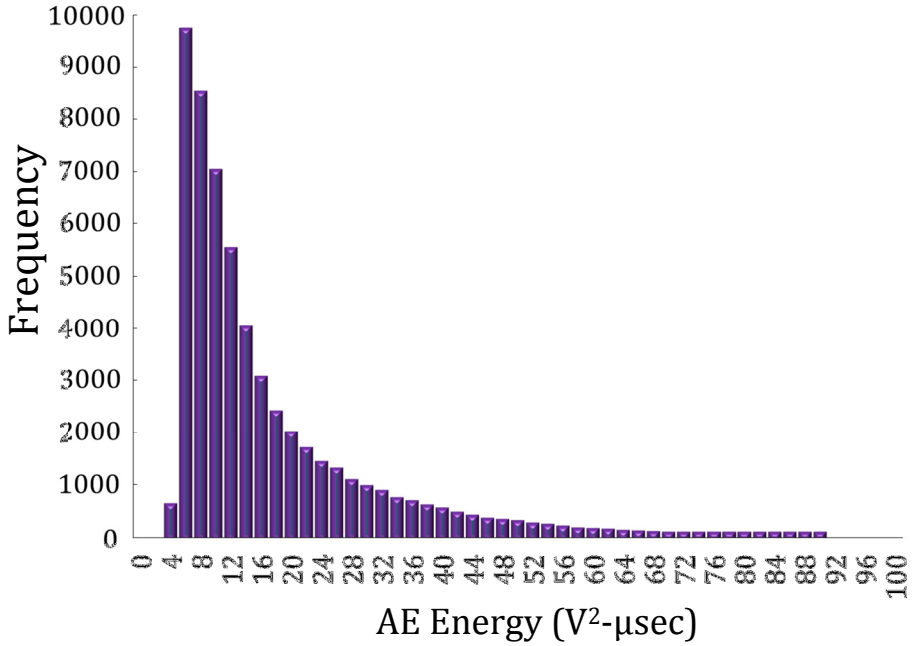

Figure 3.21: Typical Histogram of AE Events Energies of Asphalt Binder Sample.

3.2.1.6 Investigating the Cooling Rate Effect on Embrittlement Temperature

An important aspect in developing AE testing of asphalt material is determining an appropriate cooling rate to conduct the AE test. The available cooling device is capable of applying a maximum average cooling rate of 3^{o}C/min. It is desirable to apply the highest possible cooling rate to reduce the testing time as much as possible. However, before selecting the cooling rate, it was necessary to explore effects of cooling rate on the embrittlement temperature of asphalt materials. Accordingly, different cooling rates ranging from 0.2 to 3^{o}C/min were applied to asphalt samples prepared from two asphalt binders namely, tank PG64-22 and Tank PG70-22. AE embrittlement temperature results along with the average testing time of AE test for different cooling rates are presented in Table 3.1. It is seen that lower cooling rates yield lower embrittlement temperature. At lower cooling rates, asphalt material has more time to relax thermally induced stresses which delays formation of thermal microcracks in the sample. Results show that there is not a significant difference between the embrittlement temperature of asphalt binder at cooling rates slower than 2^{o}C/min. The difference between the embrittlement temperatures of 2^{o}C/min and 0.2^{o}C/min is less than 1^{o}C for PG64-22 and is approximately 1.3^{o}C for PG70-22. This suggests that the 2^{o}C/min rate can be considered as an appropriate cooling rate for AE binder samples.

3.2.1.7 Determining the Proper Location to Measure AE Asphalt Sample Temperature

In addition to cooling rate, another critical requirement of the AE-based test is to monitor and record temperature of the asphalt sample throughout the test. It is acknowledged that temperature gradients will exist in specimens, which needs to be understood, characterized, and accounted for. It is very important to measure the temperature which represents a known and useful temperature condition in the sample, such as surface temperature or average sample temperature. To determine the proper location to measure temperature of the AE binder sample, three thermocouples were employed. One thermocouple was positioned adjacent to the sample right at the interface of the binder and granite. The other two thermocouples were embedded within the sample, one 3mm deep and the other one 6mm deep inside the sample, Figure 3.22. Figure 3.23 shows the temperature vs. time plot of the AE asphalt sample measured by provided thermocouples. It is seen that initially at the beginning of the test there is a thermal lag of 6^{o}C between outside and inside of the sample. This thermal lag gradually decreases as the sample

cools down until it becomes almost zero when temperature approaches -10°C. At temperatures below -10°C, the temperature of all three thermocouples of A, B, and C are almost the same. Considering the fact that the embrittlement temperature of almost all asphalt binders is below -10°C, the interface of asphalt binder and granite, point A, appears to be a proper location to position thermocouples to measure the temperature of asphalt sample during AE test.

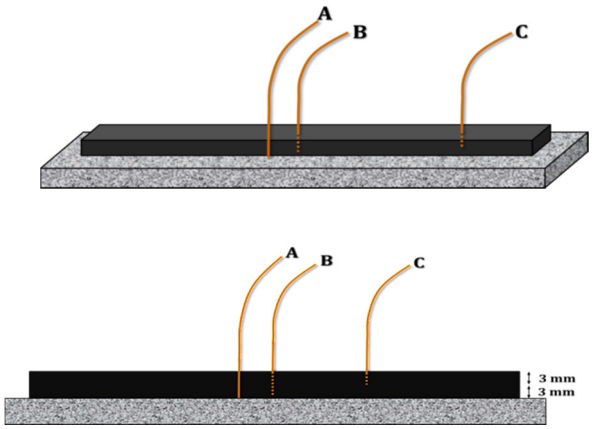

Figure 3.22: (a) Position of Thermocouples within the Asphalt Sample (b) Profile View of Thermocouples within Asphalt Sample

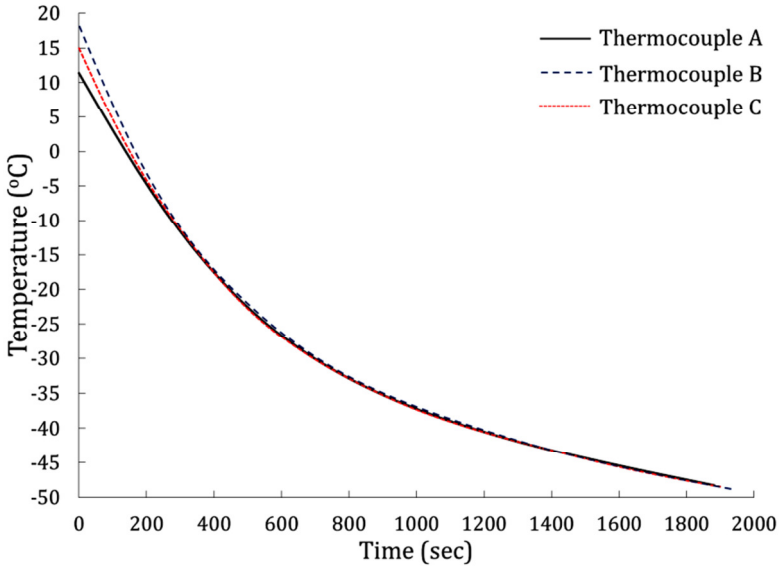

Figure 3.23: Typical Plot of Temperature vs Time of AE Asphalt Sample Obtained from Three Thermocouples of A, B, and C.

TABLE 3.1: Acoustic Emission Test Results for Different Cooling Rates

Average Cooling Rate (^oC/min)	AE Test Duration (min)	Rep#	TANK PG64-22			TANK PG70-22		
			T_{EMB} (^oC)	Average	CoV%	T_{EMB} (^oC)	Average	CoV%
3.00	20	#1	-25.41	-24.98	1.85%	-32.01	-32.13	1.93%
		#2	-24.32			-32.77		
		#3	-25.06			-32.42		
		#4	-25.11			-31.33		
2.00	30	#1	-28.11	-27.32	3.16%	-32.56	-33.43	1.81%
		#2	-27.52			-33.52		
		#3	-27.56			-33.95		
		#4	-26.09			-33.69		
1.50	40	#1	-27.34	-27.09	1.92%	-34.02	-33.69	2.97%
		#2	-26.93			-33.11		
		#3	-26.44			-32.69		
		#4	-27.64			-34.94		
1.00	60	#1	-25.70	-27.74	4.97%	-34.59	-34.30	1.72%
		#2	-28.62			-33.98		
		#3	-28.54			-34.97		
		#4	-28.08			-33.66		
0.67	90	#1	-26.80	-27.85	2.62%	-33.25	-33.96	2.88%
		#2	-27.90			-34.67		
		#3	-28.40			-33.00		
		#4	-28.29			-34.93		
0.50	120	#1	-28.14	-28.12	3.28%	-33.79	-34.51	1.94%
		#2	-28.43			-34.22		
		#3	-29.04			-34.67		
		#4	-26.85			-35.36		
0.34	176	#1	-28.01	-27.96	2.63%	-34.15	-34.99	1.97%
		#2	-26.91			-35.04		
		#3	-28.52			-34.92		
		#4	-28.41			-35.83		
0.20	300	#1	-27.21	-28.04	3.55%	-35.16	-34.77	1.42%
		#2	-27.17			-34.09		
		#3	-28.69			-35.11		
		#4	-29.09			-34.70		

3.2.1.8 Investigating Substrate Material Effect on Embrittlement Temperature of Asphalt Binder

One important issue regarding AE binder test is effect of using different substrate material on the embrittlement temperature of asphalt binder. Granite was originally utilized as the substrate material because its thermal expansion coefficient, $\alpha=7.9\times10^{-6}$ m/m ^{o}K, was very close to other aggregates such as limestone, $\alpha=8\times10^{-6}$ m/m ^{o}K, which are commonly used in production of asphalt mixtures. To explore effects of using different material as the substrate on the embrittlement temperature of asphalt binder, AE binder samples were prepared using Aluminum as the substrate material with thermal expansion coefficient of 22.2×10^{-6} m/m ^{o}K, Figure 3.24. AE results are presented in Table 3.2. It is seen that embrittlement temperature of AE samples with granite as the substrate are slightly warmer than those of with Aluminum substrate. This could be linked to greater difference between thermal expansion coefficient of asphalt binder and granite as compared to that of aluminum substrate. Differential thermal expansion coefficients of asphalt binder and substrate material is the main source of thermally induced stresses within AE binder sample. The higher the difference between thermal expansion coefficient of asphalt binder and substrate material, the higher the thermally induced stresses within the sample leading to warmer embrittlement temperature. However, it is observed that the difference between embrittlement temperatures of samples with Aluminum and granite substrates is not significant.

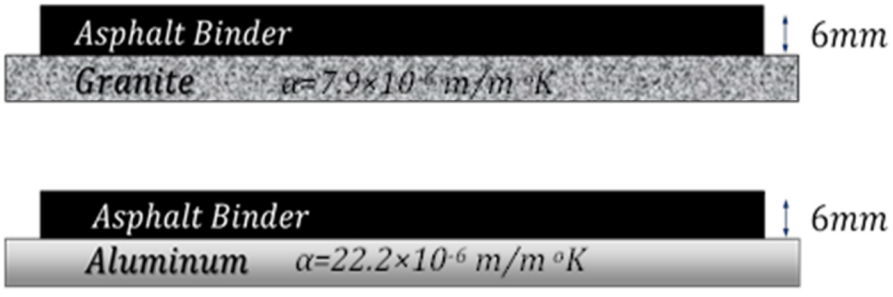

Figure 3.24**:** AE Binder Sample with Granite and Aluminum Substrates

TABLE 3.2: AE Embrittlement Temperature of PG64-22 Binder

Substrate Material	Granite ($\alpha=7.9\times10^{-6}$ m/m ^{o}K)				Aluminum ($\alpha=22.2\times10^{-6}$ m/m ^{o}K)			
Asphalt Binder ID	Rep#	AE Embrittlement Temp (^{o}C)			Rep#	AE Embrittlement Temp (^{o}C)		
		T_{EMB} (^{o}C)	Average	CoV%		T_{EMB} (^{o}C)	Average	CoV%
TANK	#1	-26.99	-28.21	2.90%	#1	-28.01	-28.49	3.44%
	#2	-27.97			#2	-27.32		
	#3	-28.67			#3	-30.14		
	#4	-29.45			#4	-28.02		
	#5	-28.04			#5	-28.43		
	#6	-28.11			#6	-29.00		
RTFO	#1	-26.32	-26.16	2.38%	#1	-27.71	-26.81	2.74%
	#2	-27.12			#2	-26.44		
	#3	-26.34			#3	-26.37		
	#4	-25.87			#4	-25.98		
	#5	-25.23			#5	-27.72		
	#6	-26.10			#6	-26.62		
PAV	#1	-25.11	-24.65	2.26%	#1	-25.51	-25.02	3.94%
	#2	-24.42			#2	-24.17		
	#3	-24.49			#3	-24.11		
	#4	-25.52			#4	-26.42		
	#5	-24.02			#5	-25.71		
	#6	-24.32			#6	-24.22		

3.2.1.9 Investigating Sample Thickness Effects on Embrittlement Temperature of Asphalt Binder

Originally when developing AE-based test for asphalt binders, 6mm thick asphalt sample was selected as AE asphalt sample. To investigate the effects of sample thickness on embrittlement temperature, several AE binder samples with different thicknesses including: 6, 3, 1, and less than 1mm, were examined. Figure 3.25 schematically shows AE samples with different thicknesses. Table 3.3 presents AE test results for AE samples with different thicknesses. Results suggest that the embrittlement temperature of asphalt binder is a size-dependent parameter; the thinner the sample the lower its embrittlement temperature. In other words, the onset of thermal microdamage in thicker samples occurs at warmer temperatures. This can be linked to the higher resistance of thinner films of asphalt material to thermal cracking. One important observation is the significant changes in coefficient of variation (COV) of AE tests with changes in sample thickness. Results show that reduction in sample thickness drastically affects repeatability of the AE test, as the COV of the AE test changes from 2.7% for 6mm sample to 11.2% for 3mm thick samples and it reaches more than 20% for 1mm thick samples. This can be associated to the fact that 6mm thick samples are statistically better representatives of tested asphalt material. Results indicate that 6mm samples yield more reliable results in terms of repeatability and they appear to be a better and more reliable size for AE-based binder samples.

Figure 3.25: AE Asphalt Binder Samples with Different Thicknesses

TABLE 3.3: AE Test Results for Tank PG64-22 Asphalt Samples with Different Thicknesses

Sample Thickness (mm)	Rep#	AE Embrittlement Temperature		
		T_{EMB}(°C)	Average	Cov %
6 mm	#1	-28.49	-28.37	2.7%
	#2	-29.61		
	#3	-28.36		
	#4	-27.09		
	#5	-27.95		
	#6	-28.84		
	#7	-28.22		
3 mm	#1	-29.04	-29.57	11.2%
	#2	-30.07		
	#3	-26.96		
	#4	-33.99		
	#5	-32.30		
	#6	-25.07		
1 mm	#1	-26.01	-34.37	20.2%
	#2	-39.71		
	#3	-39.83		
	#4	-27.51		
	#5	-41.86		
	#6	-31.32		
< 1mm	#1	-28.45	-35.43	18.2%
	#2	-41.01		
	#3	-30.11		
	#4	-40.92		
	#5	-41.92		
	#6	-30.19		

3.3. RESULTS AND DISCUSSION

The embrittlement temperature (T_{EMB}) of asphalt binders evaluated through AE testing is compared against the critical cracking temperature (T_{CR}) obtained from the Superpave asphalt binder test procedures. The critical cracking temperature for the asphalt binders were determined using the test results described by Marasteanu et al. [32] and using the procedure described in NCHRP Report 452. Two asphalt binder parameters, creep stiffness and m-value, are determined based upon the BBR test results at a loading time of 60 seconds. The cracking temperature is defined as the temperature at which either the stiffness is 300 MPa or the m-value is 0.3, whichever gives a higher cracking temperature value [1,2,25]. The equations used for determining critical temperature using Superpave tests are shown below:

$$T_{cr-S} = T_1 + [\frac{log(300) - log(S_1)}{log(S_2) - log(S_1)}](T_2 - T_1) \quad (3.10)$$

$$T_{cr-m} = T_1 + [\frac{log(0.300) - log(m_1)}{log(m_2) - log(m_1)}](T_2 - T_1) \quad (3.11)$$

$$T_{CR} = max(T_{cr-S}, T_{cr-m}) \quad (3.12)$$

Where, S_1 and S_2 are BBR creep stiffnesses and m_1 and m_2 are the m-values of asphalt binders at test temperatures of T_1 and T_2, respectively. When using direct tension test (DTT) results, a similar interpolation technique can be used to determine the temperature at which a failure strain of 1% is reached. BBR test results along with the BBR-based critical cracking temperatures of all SHRP binders are presented in Table 3.4 to 3.111.

TABLE3.4: BBR Test Results along with the Critical Cracking Temperature of SHRP AAA1 Asphalt Binder

Asphalt Binder ID	Rep #	Stiffness (MPa)									m-value									$T_{Stiffness}$ (^oC)	$T_{m\text{-}value}$ (^oC)	T_{BBR} (^oC)
		Temp=-12°C			Temp=-18°C			Temp=-24°C			Temp=-12°C			Temp=-18°C			Temp=-24°C					
		S(t) (MPa)	Average	CoV%	S(t) (MPa)	Average	CoV%	S(t) (MPa)	Average	CoV%	m-value	Average	CoV %	m-value	Average	CoV %	m-value	Average	CoV%			
TANK AAA1 (PG58-28)	#1	32	30	13.70%	76	81	17.29%	256	262	7.54%	0.555	0.507	6.48%	0.469	0.453	7.04%	0.379	0.359	6.62%	-24.69	-28.65	-34.69
	#2	29			89			289			0.491			0.422			0.336					
	#3	33			63			242			0.500			0.489			0.380					
	#4	24			94			260			0.482			0.430			0.341					
RTFO AAA1 (PG58-28)	#1	49	46	14.41%	126	132	11.30%	352	366	5.34%	0.495	0.461	8.87%	0.347	0.373	6.86%	0.324	0.303	5.33%	-22.83	-24.26	-32.83
	#2	52			114			349			0.431			0.391			0.303					
	#3	37			148			391			0.498			0.399			0.285					
	#4	44			139			372			0.421			0.356			0.299					
PAV AAA1 (PG58-28)	#1	88	73	15.74%	251	250	6.98%	609	616	8.07%	0.414	0.405	3.00%	0.342	0.317	6.41%	0.234	0.238	11.48%	-19.21	-19.16	-29.16
	#2	64			274			669			0.401			0.294			0.253					
	#3	76			241			634			0.416			0.323			0.201					
	#4	64			234			551			0.390			0.310			0.263					

TABLE 3.5:BBR Test Results along with the Critical Cracking Temperature of SHRP AAB1 Asphalt Binder

Asphalt Binder ID	Rep #	Stiffness (MPa)									m-value									$T_{Stiffness}$ (^oC)	$T_{m\text{-}value}$ (^oC)	T_{BBR} (^oC)
		Temp=-12°C			Temp=-18°C			Temp=-24°C			Temp=-12°C			Temp=-18°C			Temp=-24°C					
		S(t) (MPa)	Average	CoV%	S(t) (MPa)	Average	CoV%	S(t) (MPa)	Average	CoV%	m-value	Average	CoV %	m-value	Average	CoV %	m-value	Average	CoV %			
TANK AAB1 (PG58-22)	#1	37	43	14.34%	129	134	7.55%	393	375	8.13%	0.466	0.467	1.63%	0.469	0.454	3.67%	0.334	0.331	3.29%	-22.70	-25.83	-32.70
	#2	49			145			352			0.478			0.446			0.342					
	#3	38			138			347			0.465			0.434			0.316					
	#4	47			122			409			0.460			0.466			0.330					
RTFO AAB1 (PG58-22)	#1	64	58	18.13%	186	162	19.21%	432	418	3.27%	0.462	0.460	1.32%	0.427	0.440	2.25%	0.287	0.290	4.58%	-21.90	-23.51	-31.90
	#2	45			129			401			0.451			0.439			0.296					
	#3	55			142			413			0.463			0.445			0.304					
	#4	69			191			425			0.464			0.450			0.273					
PAV AAB1 (PG58-22)	#1	108	121	8.61%	314	313	3.86%	783	542	6.42%	0.422	0.416	2.28%	0.279	0.294	3.95%	0.199	0.211	4.88%	-17.73	-17.64	-27.64
	#2	118			323			722			0.404			0.301			0.209					
	#3	131			296			764			0.425			0.305			0.211					
	#4	128			320			709			0.413			0.291			0.224					

TABLE3.6: BBR Test Results along with the Critical Cracking Temperature of SHRP AAC1 Asphalt Binder

Asphalt Binder ID	Rep #	Stiffness (MPa)									m-value									$T_{Stiffness}$ (^oC)	$T_{m\text{-}value}$ (^oC)	T_{BBR} (^oC)
		Temp=-6°C			Temp=-12°C			Temp=-18°C			Temp=-6°C			Temp=-12°C			Temp=-18°C					
		S(t) (MPa)	Average	CoV%	S(t) (MPa)	Average	CoV%	S(t) (MPa)	Average	CoV%	m-value	Average	CoV%	m-value	Average	CoV%	m-value	Average	CoV%			
TANK AAC1 (PG58-16)	#1	106	97	8.99%	172	187	6.52%	499	498	3.14%	0.411	0.413	1.05%	0.388	0.379	2.36%	0.309	0.313	2.04%	-14.90	-25.36	-24.90
	#2	101			193			517			0.409			0.379			0.314					
	#3	94			183			479			0.419			0.383			0.322					
	#4	86			200			495			0.412			0.367			0.308					
RTFO AAC1 (PG58-16)	#1	145	136	11.86%	316	319	5.21%	561	565	3.85%	0.398	0.399	0.83%	0.340	0.339	2.84%	0.288	0.287	0.92%	-11.58	-22.37	-21.58
	#2	129			341			572			0.395			0.352			0.286					
	#3	153			301			538			0.399			0.336			0.289					
	#4	117			316			590			0.403			0.329			0.283					
PAV AAC1 (PG58-16)	#1	252	263	11.66%	454	452	6.23%	799	822	3.00%	0.351	0.368	3.50%	0.307	0.314	2.51%	0.241	0.247	2.01%	-7.48	-19.14	-17.48
	#2	284			472			829			0.371			0.314			0.253					
	#3	224			469			853			0.366			0.310			0.246					
	#4	290			411			805			0.382			0.325			0.248					

TABLE 3.7: BBR Test Results along with the Critical Cracking Temperature of SHRP AAD1 Asphalt Binder

Asphalt Binder ID	Rep #	Stiffness (MPa)									m-value									$T_{Stiffness}$ (^oC)	$T_{m\text{-}value}$ (^oC)	T_{BBR} (^oC)
		Temp=-12°C			Temp=-18°C			Temp=-24°C			Temp=-12°C			Temp=-18°C			Temp=-24°C					
		S(t) (MPa)	Average	CoV%	S(t) (MPa)	Average	CoV%	S(t) (MPa)	Average	CoV%	m-value	Average	CoV %	m-value	Average	CoV %	m-value	Average	CoV%			
TANK AAD1 (PG58-28)	#1	45	49	29.76%	134	150	7.87%	284	294	5.35%	0.440	0.437	1.98%	0.404	0.407	1.90%	0.352	0.340	3.30%	-24.17	-28.16	-34.17
	#2	52			156			304			0.447			0.398			0.332					
	#3	67			148			311			0.431			0.412			0.329					
	#4	32			161			278			0.428			0.415			0.347					
RTFO AAD1 (PG58-28)	#1	71	60	14.49%	238	257	5.13%	384	389	2.39%	0.417	0.409	1.94%	0.369	0.366	1.33%	0.304	0.314	2.37%	-20.24	-25.78	-30.24
	#2	62			259			392			0.401			0.360			0.313					
	#3	50			268			401			0.415			0.365			0.318					
	#4	58			263			380			0.404			0.371			0.321					
PAV AAD1 (PG58-28)	#1	107	105	5.44%	382	367	3.35%	482	500	2.68%	0.354	0.351	2.52%	0.311	0.317	1.70%	0.280	0.278	2.05%	-17.03	-20.51	-27.03
	#2	102			352			504			0.340			0.318			0.275					
	#3	99			369			499			0.361			0.316			0.271					
	#4	112			366			514			0.349			0.324			0.284					

TABLE 3.8:BBR Test Results along with the Critical Cracking Temperature of SHRP AAF1 Asphalt Binder

Asphalt Binder ID	Rep #	Stiffness (MPa)									m-value									$T_{Stiffness}$ (^oC)	$T_{m\text{-}value}$ (^oC)	T_{BBR} (^oC)
		Temp=0°C			Temp=-6°C			Temp=-12°C			Temp=0°C			Temp=-6°C			Temp=-12°C					
		S(t) (MPa)	Average	CoV%	S(t) (MPa)	Average	CoV%	S(t) (MPa)	Average	CoV%	m-value	Average	CoV %	m-value	Average	CoV %	m-value	Average	CoV%			
TANK AAF1 (PG64-10)	#1	35	41	14.33%	134	139	11.73%	239	228	10.72%	0.349	0.343	3.95%	0.304	0.305	2.29%	0.274	0.249	7.00%	-21.36	-6.49	-16.49
	#2	42			142			256			0.328			0.297			0.240					
	#3	48			120			212			0.337			0.314			0.235					
	#4	37			159			203			0.359			0.305			0.246					
RTFO AAF1 (PG64-10)	#1	68	70	11.99%	173	178	7.35%	320	330	3.59%	0.317	0.311	2.84%	0.263	0.263	2.48%	0.227	0.228	3.00%	-15.37	-0.47	-10.47
	#2	60			164			322			0.320			0.271			0.231					
	#3	73			180			346			0.302			0.255			0.235					
	#4	80			195			330			0.305			0.263			0.219					
PAV AAF1 (PG64-10)	#1	112	114	8.68%	204	228	8.85%	372	409	6.44%	0.281	0.286	4.22%	0.241	0.242	3.41%	0.214	0.209	2.66%	-14.39	1.69	-8.31
	#2	114			219			408			0.272			0.252			0.201					
	#3	103			239			431			0.293			0.244			0.211					
	#4	127			249			424			0.299			0.232			0.209					

TABLE 3.9: BBR Test Results along with the Critical Cracking Temperature of SHRP AAG1 Asphalt Binder

Asphalt Binder ID	Rep #	Stiffness (MPa)									m-value									$T_{Stiffness}$ (°C)	$T_{m\text{-}value}$ (°C)	T_{BBR} (°C)
		Temp=0°C			Temp=-6°C			Temp=-12°C			Temp=0°C			Temp=-6°C			Temp=-12°C					
		S(t) (MPa)	Average	CoV%	S(t) (MPa)	Average	CoV%	S(t) (MPa)	Average	CoV%	m-value	Average	CoV %	m-value	Average	CoV %	m-value	Average	CoV%			
TANK AAG1 (PG58-10)	#1	31	38	17.05%	111	115	10.90%	190	199	6.11%	0.388	0.390	2.21%	0.344	0.338	1.72%	0.271	0.278	4.72%	-22.48	-9.63	-19.63
	#2	35			115			212			0.394			0.337			0.292					
	#3	46			101			187			0.399			0.330			0.285					
	#4	40			131			206			0.379			0.339			0.263					
RTFO AAG1 (PG58-10)	#1	52	59	15.45%	141	147	9.28%	291	298	4.18%	0.344	0.350	2.19%	0.309	0.318	3.09%	0.253	0.254	1.48%	-16.63	-7.56	-17.56
	#2	50			167			303			0.352			0.315			0.250					
	#3	63			136			284			0.344			0.316			0.259					
	#4	69			145			312			0.360			0.332			0.255					
PAV AAG1 (PG58-10)	#1	132	134	5.74%	267	241	10.45%	378	375	4.53%	0.312	0.309	2.27%	0.267	0.264	3.90%	0.200	0.218	5.70%	-14.23	-1.08	-11.08
	#2	145			217			391			0.316			0.249			0.219					
	#3	128			258			351			0.300			0.270			0.229					
	#4	130			222			380			0.306			0.271			0.222					

TABLE 3.10: BBR Test Results along with the Critical Cracking Temperature of SHRP AAK1 Asphalt Binder

Asphalt Binder ID	Rep #	Stiffness (MPa)									m-value									$T_{Stiffness}$ (^oC)	$T_{m\text{-}value}$ (^oC)	T_{BBR} (^oC)
		Temp=-12°C			Temp=-18°C			Temp=-24°C			Temp=-12°C			Temp=-18°C			Temp=-24°C					
		S(t) (MPa)	Average	CoV%	S(t) (MPa)	Average	CoV%	S(t) (MPa)	Average	CoV%	m-value	Average	CoV %	m-value	Average	CoV %	m-value	Average	CoV%			
TANK AAK1 (PG64-22)	#1	83	89	11.05%	172	174	9.90%	390	385	6.21%	0.418	0.415	2.18%	0.361	0.381	4.03%	0.322	0.319	2.88%	-22.12	-26.07	-32.12
	#2	92			195			371			0.425			0.398			0.307					
	#3	101			153			416			0.411			0.380			0.329					
	#4	79			176			362			0.404			0.385			0.318					
RTFO AAK1 (PG64-22)	#1	113	111	9.00%	274	263	3.94%	459	486	4.96%	0.384	0.386	3.02%	0.330	0.334	2.03%	0.272	0.268	4.39%	-19.29	-20.92	-29.29
	#2	122			249			473			0.389			0.326			0.254					
	#3	98			263			499			0.399			0.341			0.265					
	#4	109			265			512			0.371			0.337			0.282					
PAV AAK1 (PG64-22)	#1	187	192	11.00%	394	401	3.81%	595	606	4.52%	0.341	0.342	2.13%	0.262	0.254	4.37%	0.202	0.194	4.10%	-15.65	-14.63	-24.63
	#2	199			407			634			0.352			0.248			0.193					
	#3	165			418			622			0.339			0.241			0.183					
	#4	215			383			573			0.335			0.264			0.196					

TABLE 3.11: BBR Test Results along with the Critical Cracking Temperature of SHRP AAM1 Asphalt Binder

Asphalt Binder ID	Rep #	Stiffness (MPa)									m-value									$T_{Stiffness}$ (^oC)	$T_{m\text{-}value}$ (^oC)	T_{BBR} (^oC)
		Temp=-6°C			Temp=-12°C			Temp=-18°C			Temp=-6°C			Temp=-12°C			Temp=-18°C					
		S(t) (MPa)	Average	CoV%	S(t) (MPa)	Average	CoV%	S(t) (MPa)	Average	CoV%	m-value	Average	CoV%	m-value	Average	CoV%	m-value	Average	CoV%			
TANK AAM1 (PG64-16)	#1	118	120	11.58%	229	242	7.32%	399	423	6.08%	0.389	0.383	3.53%	0.351	0.340	2.64%	0.295	0.288	2.33%	-14.32	-22.55	-24.32
	#2	139			241			420			0.390			0.340			0.279					
	#3	106			267			459			0.363			0.329			0.289					
	#4	116			230			413			0.391			0.341			0.290					
RTFO AAM1 (PG64-16)	#1	181	184	12.80%	339	326	6.52%	552	539	6.29%	0.352	0.358	2.25%	0.325	0.327	2.67%	0.281	0.278	1.47%	-11.13	-21.17	-21.13
	#2	192			349			505			0.361			0.329			0.272					
	#3	153			306			518			0.368			0.337			0.279					
	#4	209			310			580			0.351			0.316			0.280					
PAV AAM1 (PG64-16)	#1	342	342	6.80%	518	529	7.33%	781	786	3.27%	0.341	0.333	2.70%	0.307	0.305	3.22%	0.267	0.259	4.72%	-4.21	-18.61	-14.21
	#2	355			479			752			0.322			0.296			0.271					
	#3	361			556			811			0.340			0.299			0.244					
	#4	309			563			799			0.330			0.318			0.255					

AE embrittlement temperatures along with BBR-based critical cracking temperatures of various asphalt binders tested at different age conditioning levels are provided in Table 3.12 through 3.22. In all cases, a minimum of 4 replicates were used to produce the average values and statistical measures presented in this section. The COV is computed by dividing the standard deviation of a population (in this case, embrittlement temperature or cracking temperature) by the absolute value of the sample mean. Strictly speaking, the COV statistic is the most appropriate for data measured on a ratio scale, unlike temperature, which is expressed on an interval scale. Thus, the COV statistic will be temperature-scale dependent (different results would be obtained for results expressed in degrees Kelvin versus degrees Celsius, for instance), and would produce infinite values for means approaching zero. For the present application, where embrittlement temperatures were in a relatively narrow range and sufficiently below zero, the COV statistic was deemed to be a useful statistical parameter to describe the repeatability of the measurements obtained [1].

Results shows that both AE embrittlement temperature and BBR critical cracking temperature of asphalt binders are sensitive to aging level, where $T_{cracking}$ (TANK) < $T_{cracking}$ (RTFO) < $T_{cracking}$ (PAV). The COV values of AE tests conducted on the SHRP and LTC study binders are lower than the COV values obtained when testing the AOX-modified binders. This is due to pre-conditioning the AE sensors in the cooling chamber prior to testing of the SHRP and LTC study binders. Comparing the AE and BBR results shows that in almost all cases, the embrittlement temperature of the asphalt material is lower than its BBR-based critical cracking temperature. This can be attributed to the fact that the BBR stiffness and m-value thresholds (upper limit of S=300 MPa and lower limit of m-value=0.300) do not explicitly define the development of thermal cracks within the sample. In fact, the BBR thresholds were established with an inherent factor of safety to avoid low temperature cracking. They are only practical values based on the performance of asphalt materials in the field. In the case of the AE test, thermal microcracks develop within the sample as soon as the temperature reaches the embrittlement temperature. The fact that BBR critical temperature of most binders is warmer than the embrittlement temperature of that particular material, this result indicates that BBR thresholds are somewhat conservative and in most cases low temperature performance of asphalt binders is better than what their PG low temperature grades suggest. AOX-modified PG64-22

and PG70-22 results show that embrittlement temperatures of AOX-modified binders are lower than those of unmodified binders. This suggests that adding AOX to asphalt binder improves its low temperature performance by lowering its embrittlement temperature which is consistent with the results obtained from BBR testing [1].

TABLE 3.12: AE Embrittlement Temperature along with BBR-based Critical Cracking Temperatures of SHRP AAA1 Asphalt Binder

Asphalt Binder ID	Rep#	AE Embrittlement Temp (^oC)			BBR Cracking Temp (^oC)
		T_{EMB} (^oC)	Average	CoV%	
TANK AAA1 (PG58-28)	#1	-39.10	-37.58	2.98%	-34.69
	#2	-36.12			
	#3	-37.14			
	#4	-38.01			
	#5	-36.70			
	#6	-38.41			
RTFO AAA1 (PG58-28)	#1	-34.11	-35.78	3.68%	-32.83
	#2	-35.09			
	#3	-37.83			
	#4	-36.22			
	#5	-35.00			
	#6	-36.42			
PAV AAA1 (PG58-28)	#1	-33.03	-32.09	3.74%	-29.16
	#2	-31.11			
	#3	-30.29			
	#4	-32.71			
	#5	-33.40			
	#6	-32.00			

TABLE 3.13: AE Embrittlement Temperature along with BBR-based Critical Cracking Temperatures of SHRP AAB1 Asphalt Binder

Asphalt Binder ID	Rep#	AE Embrittlement Temp (°C)			BBR Cracking Temp (°C)
		T_{EMB} (°C)	Average	CoV%	
TANK AAB1 (PG58-22)	#1	-30.80	-30.46	3.56%	-32.70
	#2	-28.78			
	#3	-31.13			
	#4	-29.49			
	#5	-31.61			
	#6	-30.92			
RTFO AAB1 (PG58-22)	#1	-28.46	-29.45	2.21%	-31.90
	#2	-29.20			
	#3	-29.74			
	#4	-30.44			
	#5	-29.50			
	#6	-29.36			
PAV AAB1 (PG58-22)	#1	-25.05	-24.33	3.25%	-27.64
	#2	-24.32			
	#3	-24.90			
	#4	-23.21			
	#5	-23.53			
	#6	-24.96			

TABLE 3.14: AE Embrittlement Temperature along with BBR-based Critical Cracking Temperatures of SHRP AAC1 Asphalt Binder

Asphalt Binder ID	Rep#	AE Embrittlement Temp (°C)			BBR Cracking Temp (°C)
		T_{EMB} (°C)	Average	CoV%	
TANK AAC1 (PG58-16)	#1	-28.84	-29.36	3.77%	-24.90
	#2	-30.83			
	#3	-28.18			
	#4	-30.65			
	#5	-28.63			
	#6	-29.03			
RTFO AAC1 (PG58-16)	#1	-28.10	-27.77	1.26%	-21.58
	#2	-27.79			
	#3	-27.66			
	#4	-28.22			
	#5	-27.26			
	#6	-27.60			
PAV AAC1 (PG58-16)	#1	-21.14	-21.86	5.30%	-17.48
	#2	-21.56			
	#3	-22.98			
	#4	-20.34			
	#5	-23.44			
	#6	-21.69			

TABLE 3.15: AE Embrittlement Temperature along with BBR-based Critical Cracking Temperatures of SHRP AAD1 Asphalt Binder

Asphalt Binder ID	Rep#	AE Embrittlement Temp (°C)			BBR Cracking Temp (°C)
		T_{EMB} (°C)	Average	CoV%	
TANK AAD1 (PG58-28)	#1	-39.11	-39.09	2.66%	-34.17
	#2	-37.56			
	#3	-38.11			
	#4	-40.01			
	#5	-39.85			
	#6	-39.91			
RTFO AAD1 (PG58-28)	#1	-38.22	-37.93	2.07%	-30.24
	#2	-37.14			
	#3	-37.11			
	#4	-38.59			
	#5	-37.51			
	#6	-38.98			
PAV AAD1 (PG58-28)	#1	-35.29	-35.19	2.79%	-27.03
	#2	-33.76			
	#3	-34.20			
	#4	-35.89			
	#5	-35.98			
	#6	-36.01			

TABLE 3.16: AE Embrittlement Temperature along with BBR-based Critical Cracking Temperatures of SHRP AAF1 Asphalt Binder

Asphalt Binder ID	Rep#	AE Embrittlement Temp (°C)			BBR Cracking Temp (°C)
		T_{EMB} (°C)	Average	CoV%	
TANK AAF1 (PG64-10)	#1	-25.70	-24.47	4.74%	-16.49
	#2	-23.80			
	#3	-23.72			
	#4	-24.67			
	#5	-25.92			
	#6	-23.03			
RTFO AAF1 (PG64-10)	#1	-22.02	-22.29	3.35%	-10.47
	#2	-21.93			
	#3	-22.12			
	#4	-22.47			
	#5	-21.50			
	#6	-23.67			
PAV AAF1 (PG64-10)	#1	-18.11	-17.30	5.15%	-8.31
	#2	-17.39			
	#3	-15.71			
	#4	-17.69			
	#5	-16.90			
	#6	-17.98			

TABLE 3.17: AE Embrittlement Temperature along with BBR-based Critical Cracking Temperatures of SHRP AAG1 Asphalt Binder

Asphalt Binder ID	Rep#	AE Embrittlement Temp (°C)			BBR Cracking Temp (°C)
		T_{EMB} (°C)	Average	CoV%	
TANK AAG1 (PG58-10)	#1	-27.14	-26.48	3.56%	-19.63
	#2	-25.19			
	#3	-27.63			
	#4	-27.04			
	#5	-25.70			
	#6	-26.15			
RTFO AAG1 (PG58-10)	#1	-23.15	-24.12	2.55%	-17.56
	#2	-24.71			
	#3	-24.45			
	#4	-24.68			
	#5	-23.72			
	#6	-24.00			
PAV AAG1 (PG58-10)	#1	-19.10	-19.54	5.39%	-11.08
	#2	-20.99			
	#3	-19.71			
	#4	-18.01			
	#5	-20.36			
	#6	-19.08			

TABLE 3.18: AE Embrittlement Temperature along with BBR-based Critical Cracking Temperatures of SHRP AAK1 Asphalt Binder

Asphalt Binder ID	Rep#	AE Embrittlement Temp (°C)			BBR Cracking Temp (°C)
		T_{EMB} (°C)	Average	CoV%	
TANK AAK1 (PG64-22)	#1	-33.19	-31.76	3.24%	-32.12
	#2	-31.70			
	#3	-32.05			
	#4	-32.31			
	#5	-30.22			
	#6	-31.06			
RTFO AAK1 (PG64-22)	#1	-30.04	-30.15	2.76%	-29.29
	#2	-31.01			
	#3	-30.58			
	#4	-29.38			
	#5	-28.99			
	#6	-30.92			
PAV AAK1 (PG64-22)	#1	-24.64	-25.95	5.03%	-24.63
	#2	-26.18			
	#3	-24.84			
	#4	-28.04			
	#5	-25.23			
	#6	-26.75			

TABLE 3.19: AE Embrittlement Temperature along with BBR-based Critical Cracking Temperatures of SHRP AAM1 Asphalt Binder

Asphalt Binder ID	Rep#	AE Embrittlement Temp (°C)			BBR Cracking Temp (°C)
		T_{EMB} (°C)	Average	CoV%	
TANK AAM1 (PG64-16)	#1	-29.29	-28.01	2.67%	-24.32
	#2	-28.17			
	#3	-27.58			
	#4	-27.05			
	#5	-28.09			
	#6	-27.90			
RTFO AAM1 (PG64-16)	#1	-26.50	-26.52	3.60%	-21.13
	#2	-25.31			
	#3	-26.11			
	#4	-26.09			
	#5	-27.04			
	#6	-28.09			
PAV AAM1 (PG64-16)	#1	-21.33	-19.98	4.40%	-14.21
	#2	-20.17			
	#3	-20.32			
	#4	-19.21			
	#5	-20.02			
	#6	-18.84			

TABLE 3.20: AE-based & BBR-based Cracking Temperatures of LTC study Asphalt Binders

Asphalt Binder ID		AE Embrittlement Temp		BBR-based Cracking Temp (°C)
		T_{EMB} (°C)	CoV (%)	
MnRoad20 (PG58-28)	Tank	-35.0	0.80%	-31.9
	RTFO	-34.5	4.20%	-30.0
	PAV	-30.2	2.10%	-28.3
MnRoad20 (PG58-34)	Tank	-43.4	3.20%	-36.9
	RTFO	-40.7	2.30%	-35.5
	PAV	-38.5	1.00%	-34.2
NY (PG64-22)	Tank	-30.3	3.00%	-27.4
	RTFO	-28.6	1.80%	-27.1
	PAV	-25.5	1.40%	-22.9

TABLE 3.21: AE-based & BBR-based Cracking Temperatures of AOX-modified PG64-22

Asphalt Binder ID	AE Embrittlement Temperature		BBR-based Cracking Temp (^oC)
	T_{EMB} (^oC)	CoV (%)	
TANK-PG64-22	-29.5	6.20%	-28.6
TANK-PG64-22+AOX	-30.7	2.00%	-31.9
RTFO-PG64-22	-26.9	3.80%	-27.9
RTFO-PG64-22+AOX	-28.9	2.40%	-29.8
PAV-PG64-22	-23.3	6.30%	-24.2
PAV-PG64-22+AOX	-26.7	6.00%	-27.6

TABLE 3.22: AE-based & BBR-based Cracking Temperatures of AOX-modified PG70-22

Asphalt Binder ID	AE Embrittlement Temperature		BBR-based Cracking Temp (^oC)
	T_{EMB} (^oC)	CoV (%)	
TANK-PG70-22	-24.80	6.30%	-25.80
TANK-PG70-22+AOX	-31.50	8.10%	-30.30
RTFO-PG70-22	-23.40	5.30%	-24.60
RTFO-PG70-22+AOX	-28.60	7.20%	-29.90
PAV-PG70-22	-22.50	6.70%	-23.80
PAV-PG70-22+AOX	-27.50	3.80%	-28.00

3.4. SPECTRAL ANALYSIS OF ACOUSTIC EMISSION TEST RESULTS

A complex signal, such as AE signal, can be viewed in two different ways: time domain as well as frequency domain. Any complex time domain signal is composed of a combination of sinusoidal waves of varying frequency, amplitude, and phase [51, 52]. The 19th century French mathematician, Jean Baptiste Joseph Fourier, developed a technique to convert and express any

time domain signal as a frequency domain. In the present study, AE signals are stored digitally as time domain signals. While performing analyses in the time domain is extremely useful in many cases, some useful information can be obtained by conducting spectral analyses. The Fast Fourier Transform (FFT) method is employed to convert time signals to frequency domain and explore the frequency content of AE signals [51,52]. The FFT method is basically a computationally-efficient technique for computing the Fourier Transform on digital signals, equations below:

$$X[k] = \sum_{n=1}^{N} x[n]\omega_N^{(n-1)(k-1)} \qquad (3.13)$$

$$\omega_N = e^{(-2\pi i)/N} \qquad (3.14)$$

To perform the spectral analysis, several time domain AE signals at different stages of testing namely: beginning and middle of the transition region, stable cracking region, and beginning of fully cracked region, were picked and converted to frequency domain using FFT method. Figure 3.26 shows the approximate locations of the points on an AE events counts vs. temperature plot, where time domain AE signals were picked for spectral analysis. A typical time domain AE signal along with its frequency domain representation is illustrated in Figure 3.27.

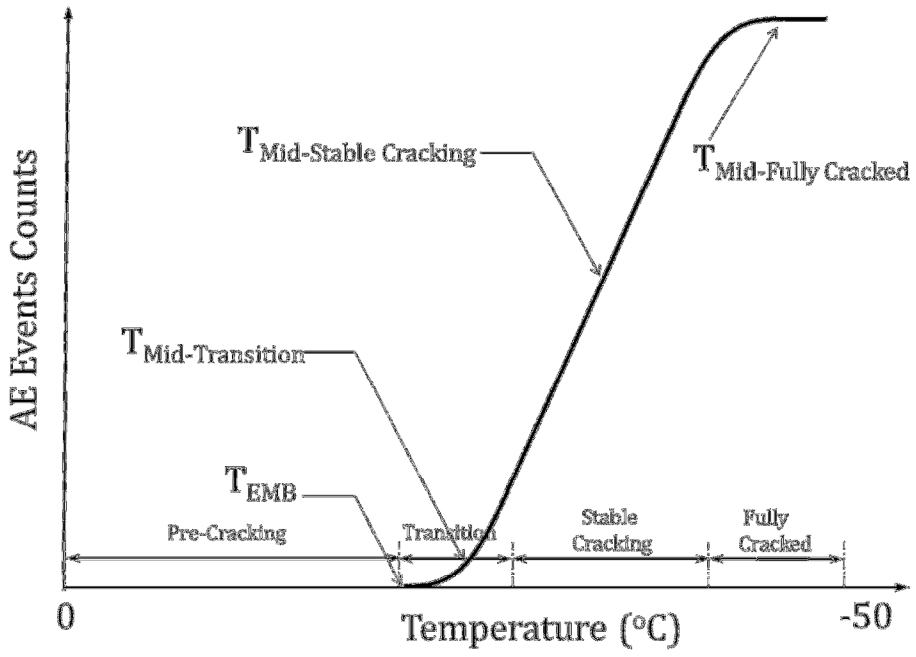

Figure 3.26: Approximate Locations of the Points Where Time Domain AE Signals were Picked for Spectral Analysis.

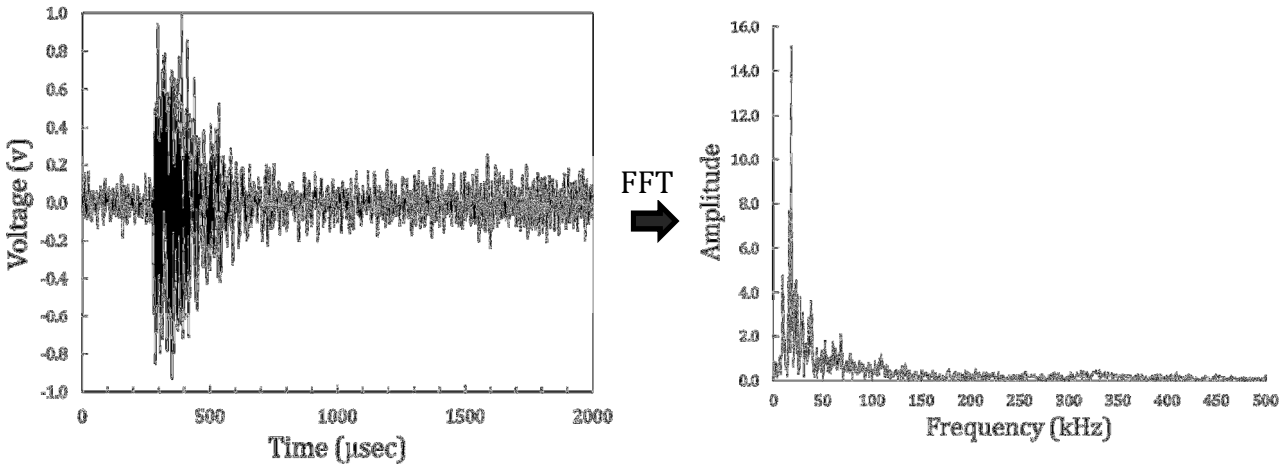

Figure 3.27: Typical Time Domain AE Signal along with its Frequency Domain Representation.

Spectral analysis results of AE signals obtained from Tank PG64-22 and Tank PG70-22 asphalt binders at different temperatures (different locations) are presented in Tables 3.23 and 3.24, respectively. It was observed that for almost all samples, the dominant frequency of AE events is higher at lower temperatures. This is mainly due to the fact that cracking of brittle materials results in AE signals with high frequency content. This has been demonstrated in different kind of materials such as concrete [53,54]. Here, as asphalt binder is cooled down, its behavior gradually changes from a quasi-brittle (locations 1 and 2) to a brittle state (locations 3 and 4). This leads to higher frequency AE signals in stable cracking and fully cracked regions as compared to the transition region. Spectral analysis results suggest that this method might be used to quantify and compare the brittleness of asphalt binders by comparing their dominant frequencies.

TABLE 3.23: Spectral Analysis Results of Tank PG64-22 Asphalt Binder

Asphalt Binder ID	Location	Rep#	Dominant Frequency (kHz)		
			f (kHz)	Average	CoV%
TANK PG 64-22	1	#1	19.00	21.36	10.47%
		#2	23.45		
		#3	21.63		
	2	#1	28.14	26.61	5.87%
		#2	26.66		
		#3	25.02		
	3	#1	43.65	44.32	5.48%
		#2	47.01		
		#3	42.29		
	4	#1	46.00	47.83	10.64%
		#2	53.58		
		#3	43.91		

TABLE 3.24: Spectral Analysis Results of Tank PG70-22 Asphalt Binder

Asphalt Binder ID	Location	Rep#	Dominant Frequency (kHz)		
			f (kHz)	Average	CoV%
TANK PG 70-22	1	#1	38.92	41.46	7.90%
		#2	40.31		
		#3	45.16		
	2	#1	49.50	46.49	5.63%
		#2	44.73		
		#3	45.24		
	3	#1	69.67	77.35	9.30%
		#2	78.43		
		#3	83.94		
	4	#1	71.04	74.69	6.91%
		#2	78.34		
		#3	-		

3.5. SHORTCOMINGS OF AE-BASED BINDER TESTING

One shortcoming of AE-based binder testing method is testing of less adhesive asphalt materials such as highly aged binders or asphalt mastics with high percentages of mineral filler. As illustrated in Figure 3.28 during conducting AE test, there are two important thermally induced stresses competing against each other: one is thermally induced tensile stresses within the sample causing transverse cracks, Figure 3.29(a), and the other one is shear stresses at the interface of asphalt binder and granite. The thermally induced shear stresses tries to debond the sample from substrate which is not desirable, Figure 3.29(b). For less adhesive binder materials, the quality of bonding between binder and granite is weak and easy to break. As a result, thermally induced shear stresses at the interface reach the shear strength of the bond causing debonding while the thermally induced tensile stresses are still below the tensile strength of the material and there is no transverse cracking in the sample. The embrittlement temperature is associated with formation of transverse cracks in the sample. Debonding of sample due to lack of proper bonding between binder and substrate prevents formation of thermal transverse cracks in the sample. As a result, it is not possible to measure the embrittlement temperature of the material when debonding occurs, unless a different test geometry is introduced.

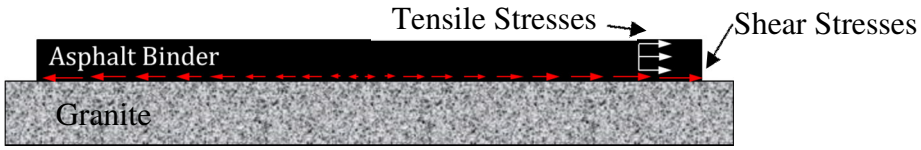

Figure 3.28: Thermally Induced Tensile and Shear Stresses in AE Binder Sample

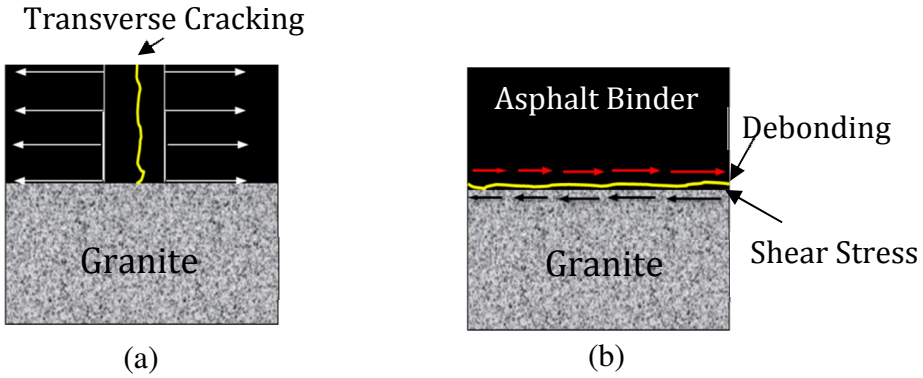

Figure 3.29: (a) Transverse Crack Cause by Thermally Induced Tensile Stresses (b) Debonding at the Interface of Asphalt and Granite due to Thermally Induced Shear Stresses

3.6. TWO-DIMENSIONAL EXPLICIT ELASTIC SOLUTION FOR AE BINDER SAMPLES

This section attempts to present a two-dimensional explicit elastic solution for a brittle film bonded to a rigid substrate. The brittle layer of asphalt binder bonded to granite which acts as a rigid substrate, subjected to cold temperatures will eventually fail by formation of several uniformly distributed cracks along the longitudinal direction of the binder sample. Figure 3.30 schematically shows a thin layer of asphalt binder (thickness h_b, elastic modulus E_b, and Poission's ratio ν_b) fully bonded to the granite (thickness h_g, elastic modulus E_g, and Poission's ratio ν_g). When the tensile strain of binder film reaches the critical level, it will be cracked in to two pieces. Considering the range of temperatures during which thermal cracking occur within the asphalt sample, behavior of asphalt binder right before thermal cracking was assumed elastic. Here we used the explicit elastic solution developed by Yin et al. [55,56] for the problems where a thin film of a ductile elastic material is fully bonded to a rigid substrate. For analysis purposes, a standard representation is employed using the superposition of a uniformly strained section with the "reduced problem" where the asphalt sample is subjected to a uniform tensile strain on its ends [55]. A 2D Cartesian coordinate system is setup with the origin at the central bottom of the section.

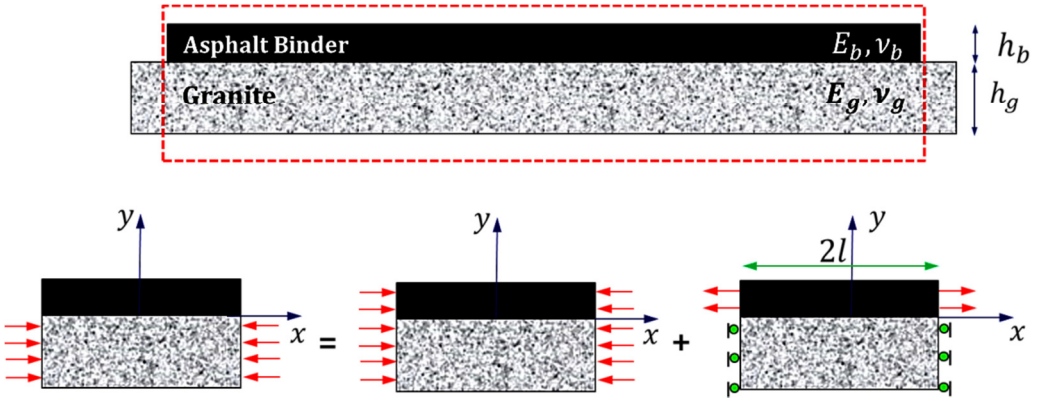

Figure 3.30: (a) Thin Film of Asphalt Binder Bonded to Granite Substrate along with a Standard Representation using the Superposition of a Uniformly Strained Section with the "Reduced Problem" where the Asphalt Sample is Subjected to a Uniform Tensile Strain on its Ends

The plane strain condition was considered for this problem. It is also assumed that the plane normal to the y direction remained perpendicular after deformation:

$$u_y(x, y) = u_y(y) \tag{3.15}$$

The equilibrium equation in the absence of body force in *x* direction is shown in equation 3.16:

$$\sigma_{x,x} + \tau_{xy,y} = 0 \tag{3.16}$$

From the 2D plain strain constitutive law we have:

$$\sigma_x = \bar{E}_b u_{x,x} \quad , \quad \tau_{xy} = \mu_b u_{x,y} \tag{3.17}$$

$\bar{E}$ and μ are the plane strain tensile and shear moduli of the sample, respectively, which are defined in equation (3.17).

$$\bar{E}_b = \frac{E_b}{1-\nu_b^2} \quad , \quad \mu_b = \frac{E_b}{2(1+\nu_b)} \tag{3.18}$$

Combining (3.16) and (3.17) yields to (3.19):

$$\bar{E}_b u_{x,xx} + \mu_b u_{x,yy} = 0 \tag{3.19}$$

The general solution can be obtained using the separation of variables technique:

$$u_x(x,y) = \left(A_1 e^{\frac{cx}{h_b}} + A_2 e^{-\frac{cx}{h_b}}\right)\left[B_1 \sin\left(\frac{dy}{h_b}\right) + B_2 \cos\left(\frac{dy}{h_b}\right)\right] \tag{3.20}$$

The $A_1, A_2, B_1,$ and B_2 coefficients in equation (3.20) are constants determined using the following boundary conditions of the problem.

$$u_x(0,y) = 0 \ ; \ u_x(l,y) = 0 \ ; \ u_{x,y}(x,h_b) = 0 \tag{3.21}$$

Applying the boundary conditions in (3.20) yield to:

$$u_x(x,y) = B \sin h\left(\frac{cx}{h_b}\right)\cos\left[d\left(1-\frac{y}{h_b}\right)\right] \tag{3.22}$$

$$\sigma_x = \bar{E}_b \varepsilon_x = \frac{1}{h_b}\int_{y=0}^{h_b} \sigma_x(l,y)dy \tag{3.23}$$

By substituting (3.22) in (3.17), and (3.17) in to (3.23) leads to:

$$B = \frac{-1}{\sqrt{\bar{E}_b \mu_1}\cosh\left(\frac{cl}{h_b}\right)\sin(d)}\frac{h_b \sigma_x}{} \tag{3.24}$$

Using the Xia and Hutchinson [57] method:

$$c = \frac{2}{\pi f(\alpha,\beta)} \quad ; d = \sqrt{\frac{\bar{E}_b}{\mu_b}}c \tag{3.25}$$

The $f(\alpha,\beta)$ function depends on Dundurs parameters namely: α and β. Dundurs [58] showed that for any problem of a composite body made of two isotropic, elastic materials with prescribed tractions, the material dependence of the problem is reduced from three dimensionless parameters to the two "Dundurs parameters". The following are Dundurs' parameters for AE binder samples:

$$\alpha = \frac{\bar{E}_b - \bar{E}_g}{\bar{E}_b + \bar{E}_g} \quad ; \quad \beta = \frac{\mu_b(1-2\nu_g) - \mu_g(1-2\nu_b)}{2\mu_b(1-\nu_g) + 2\mu_g(1-\nu_b)} \tag{3.26}$$

When both materials have the same properties, α = β = 0. For most practical material combinations, values of β typically lie between β= 0 and β=α/4 [59]. It should be noted that dependence of *f(α,β)* on β is weak except when α approaches -1. Xia and Hutchinson proposed the following equation to approximate *f(α,β)*:

$$f(\alpha,\beta) = \frac{1.258 - 0.4\alpha - 0.26\alpha^3 - 0.30\alpha^4}{1-\alpha} \tag{3.27}$$

Substituting Dundurs parameter provides closed-form elastic solution for AE binder sample:

$$u_x(x,y) = B \sin h\left(\frac{cx}{h_b}\right)\cos[d\left(1-\frac{y}{h_b}\right)] \tag{3.28}$$

$$\sigma_x = \frac{Bc\bar{E}_b}{h_b}\cos h\left(\frac{cx}{h_b}\right)\cos[d\left(1-\frac{y}{h_b}\right)] \tag{3.29}$$

$$\tau_{xy} = \frac{\mu_1 Bd}{h_b}\sinh h\left(\frac{cx}{h_b}\right)\sin[d\left(1-\frac{y}{h_b}\right)] \tag{3.30}$$

Figure 3.31 shows the thermally induced tensile stresses (σ_x) for a 100mm long AE sample along the length as well as thickness of the sample. Due to symmetry only half of the sample was analyzed. Results show that tensile stress is fairly constant in the middle of the sample. As we move towards the end of the sample tensile stresses reduce, however the rate of reduction is not the same for top and bottom of the sample. Tensile stress at the bottom of the sample (interface

of binder and granite) reduces at lower rate as compared to that of at top of the sample. The change in tensile stress distribution along the X axis as well as thickness of the sample generates shear stresses. Figure 3.32 shows the change in thermally induced shear stresses along the length of the sample. It is observed that shear stress increases from zero in the middle of sample (X=0) to its maximum at the end of the sample. The shear stress distribution through the thickness of the sample is shown in Figure 3.33. It is seen that shear stresses are maximum at the interface (Y=0) and gradually decrease until reaching zero at the surface of the sample.

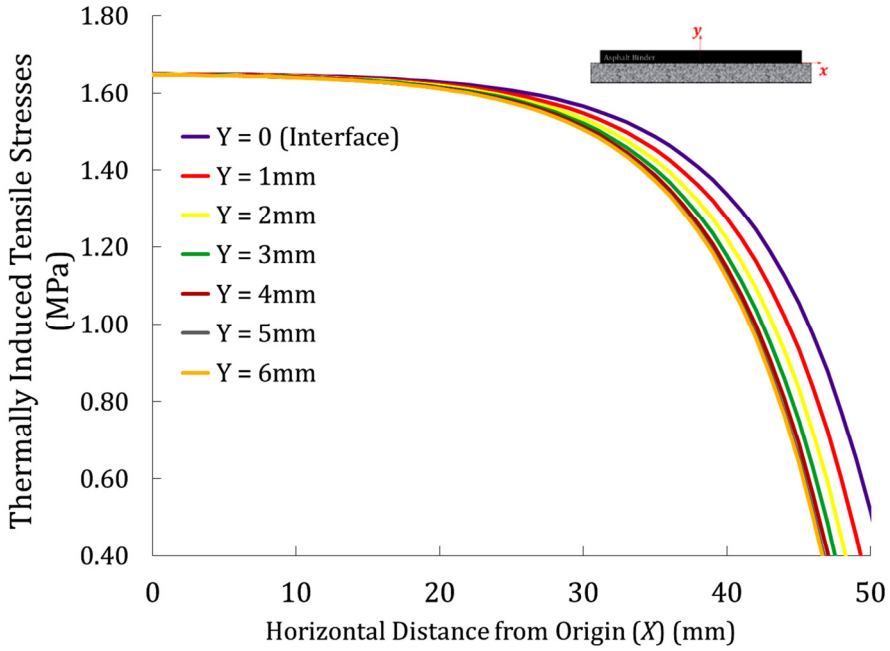

Figure 3.31: Thermally Induced Tensile Stresses (σ_x) along the Length as well as Thickness of the AE Binder Sample

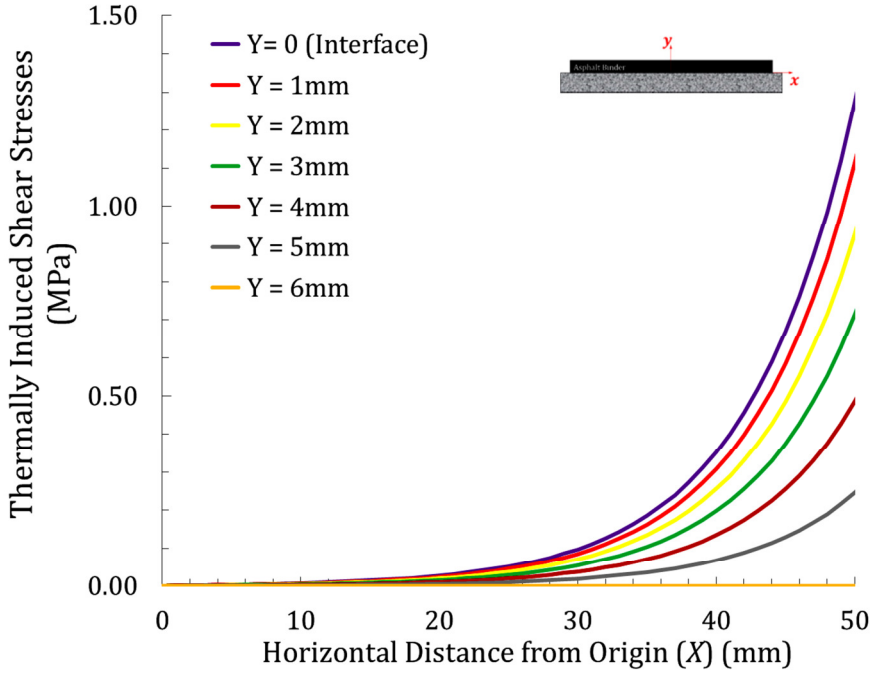

Figure 3.32: Thermally Induced Shear Stresses (τ_{xy}) along the Length as well as Thickness of the AE Binder Sample

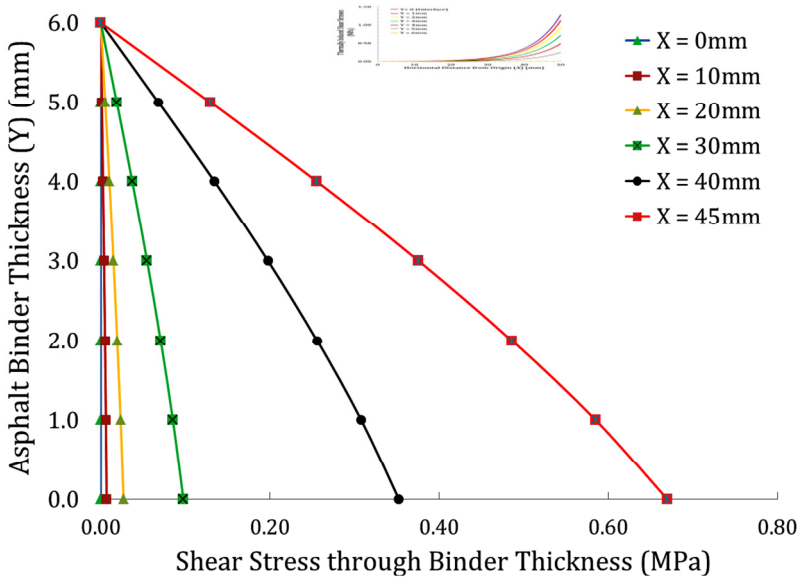

Figure 3.33: Shear Stresses (τ_{xy}) Distribution along the Thickness of the AE Binder Sample

3.7. FINITE ELEMENT ANALYSIS OF ACOUSTIC EMISSION BINDER SAMPLE

The Finite Element Method (FEM) was employed to simulate the AE binder sample. The commercially available finite element simulation software, ABAQUS [60], was used for this matter. FEM simulations performed using the two-dimensional (2D) plane stress conditions. Due to symmetry, only half of the AE sample is modeled. The boundary conditions applied to the model are shown in Figure 3.34. Various constraints are introduced to the model. The left side of the model, along the center line of the sample, is constrained in the X direction and the bottom of the sample is constrained in the Y direction. Four-noded 0.5mm long quadrilateral (Q4) elements were utilized to represent the asphalt binder and the granite substrate, Figure 3.35. In the current study, two types of FE simulations namely: elastic and viscoelastic, were performed on PG64-22 asphalt binder. Obtained results were compared against the explicit elastic solution method results.

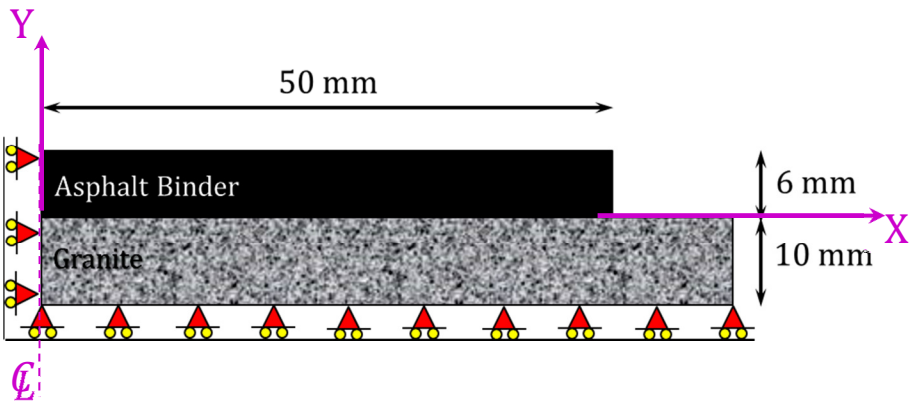

Figure 3.34: Geometry and the Boundary Conditions of the AE Model

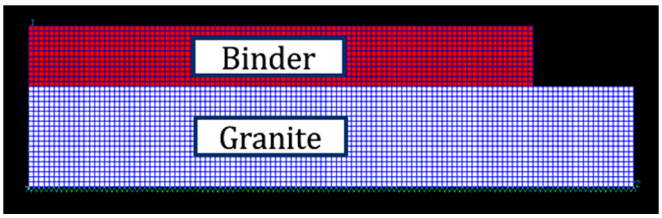

Figure 3.35: Finite Element Mesh of the AE Model using Q4 Elements

3.7.1. Material Properties

Material properties were assigned for all the Q4 elements within the model. For the elastic simulation, 1 GPa and 40GPa were assigned to the modulus of elasticity of asphalt and granite,

respectively. In reality, granite is an elastic material; however asphalt binder behaves like a viscoelastic material. The viscoelastic simulation is performed to take the linear viscoelastic behavior of asphalt material into account. To obtain viscoelastic material properties of asphalt binder, the BBR test was conducted on asphalt material at three different temperatures namely: -12, -18, and -24°C. Creep compliance master-curves were generated through time-temperature superposition (Figure 3.37). A Generalized Voigt-Kelvin (Figure 3.36) model was fitted to the master-curve using equation (3.31).

$$D(\xi) = D_0 + \sum_{i=1}^{4} D_i (1 - e^{\frac{-\xi}{\tau_i}}) + \frac{\xi}{\eta_v} \qquad (3.31)$$

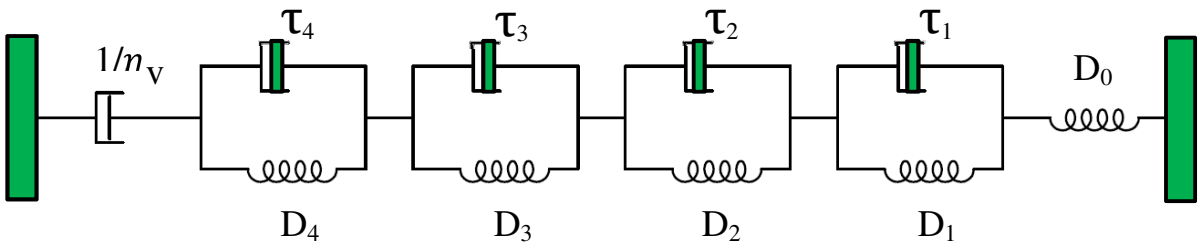

Figure 3.36: Generalized 10-Param Voigt-Kelvin (VK) Model

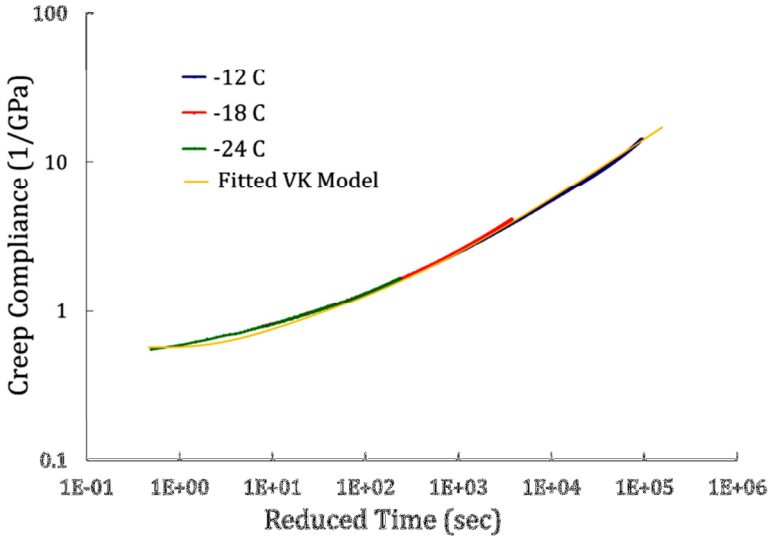

Figure 3.37: Creep Compliance Master Curve Generated from BBR Test Results Conducted at 3 Different Temperatures: -12, -18, and -24 °C.

The Prony series function of the generalized Maxwell model, equation (3.32), is used in ABAQUS to take into account the viscoelastic material properties of asphalt binder. The model parameters (Spring and Dashpot properties) were determined by means of laboratory testing. The BBR creep test provides creep compliance master curve and the generalized VK model parameters. Table 3.25 outlines the generalized VK and generalized Maxwell models parameters, where D_1, D_2, D_3, D_4 and D_5 are VK model spring compliance parameters (1/GPa); τ_1 through τ_4 and η_v are VK model dashpot coefficients (sec); E_1, E_2, E_3, E_4, and E_5, are Maxwell model spring relaxation parameters (GPa); and τ_1 through τ_5 are Maxwell model dashpot coefficients (sec). The Maxwell model parameters are calculated by interconverting the creep compliance using the convolution integral as shown in the equation (3).

$$E(t) = \sum_{i=1}^{n} E_i e^{\left(-\frac{t}{\tau_i}\right)} \qquad (3.32)$$

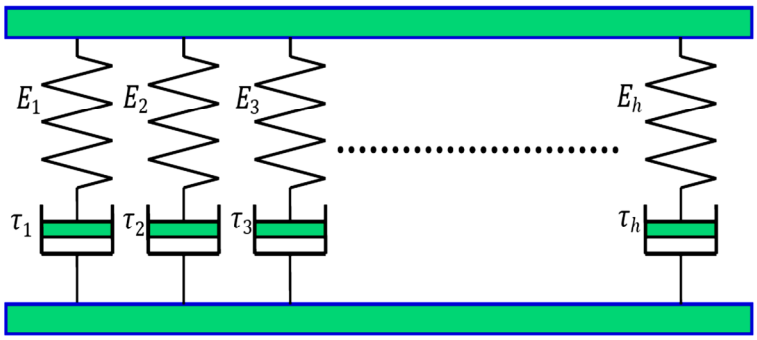

Figure 3.38: Schematic representation of the Generalized Maxwell Model [Buttlar et al, 2007]

$$\int_0^t E(t-\tau)D(\tau)d\tau = t \quad t > 0 \qquad (3.33)$$

Table 3.25: (a) VK Model Parameters (b) Maxwell Model parameters

(a)

Parameter	Value
D0	0.5581
D1	0.5939
D2	0.5891
D3	2.2457
D4	4.1210
$\tau 1$	1.518
$\tau 2$	2.668
$\tau 3$	3.45
$\tau 4$	4.6
$\log \eta_V$	10.2

(b)

Parameter	Value
E1	0.9796
E2	0.3496
E3	0.2331
E4	0.1063
E5	0.1233
$\tau 1$	15.4
$\tau 2$	286.8
$\tau 3$	1307.2
$\tau 4$	20466.6
$\tau 5$	1.285E+11

3.7.2. Finite Elements Simulations Results

Finite element elastic and viscoelastic simulations were performed on a PG64-22 AE binder sample model. Horizontal stress (Sxx) as well as shear stress (Sxy) contours are illustrated in Figures 3.39 and 3.40, respectively. Figure 3.41 shows the thermally induced tensile stresses along the interface of the binder and granite (y=0) obtained from both elastic and viscoelastic simulations and compares them against the explicit elastic solution results discussed previously. It is seen that in both elastic and viscoelastic cases, tensile stresses remain constant throughout the sample except near the end of the sample, the last 5mm, which is apparently due to stress concentration effects. Tensile stresses from the viscoelastic simulation are approximately 15% lower than those of elastic simulation. This is due to the viscoelastic behavior of asphalt material in the viscoelastic simulation which allows asphalt material to relax induced stresses. It is observed that both elastic and viscoelastic simulation results are slightly lower than the explicit elastic solution.

Thermally induced shear stresses through the thickness of the binder sample are shown in Figure 3.42. It is observed that as we go from the interface (Y=0) toward the surface (Y=6mm), thermally induced shear stresses gradually reduce from the maximum at the binder-granite

interface to zero at the surface. Due to symmetry, shear stresses are all zero in the center of the sample. They gradually increase as we go from the center toward the end of the sample where it reaches its maximum value, Figure 3.43. The rate of change of shear stresses between the interface and the surface increases as we go horizontally along the X axis from the center toward the end of the sample. A comparison between elastic and viscoelastic simulation results shows that due to stress relaxation, the viscoelastic shear stresses are approximately 12% lower than the elastic stresses. It is also seen that the explicit elastic solution underpredicts the thermally induced shear stresses in the top 4mm of the sample and overpredicts them at the bottom 2mm of the sample and at the interface.

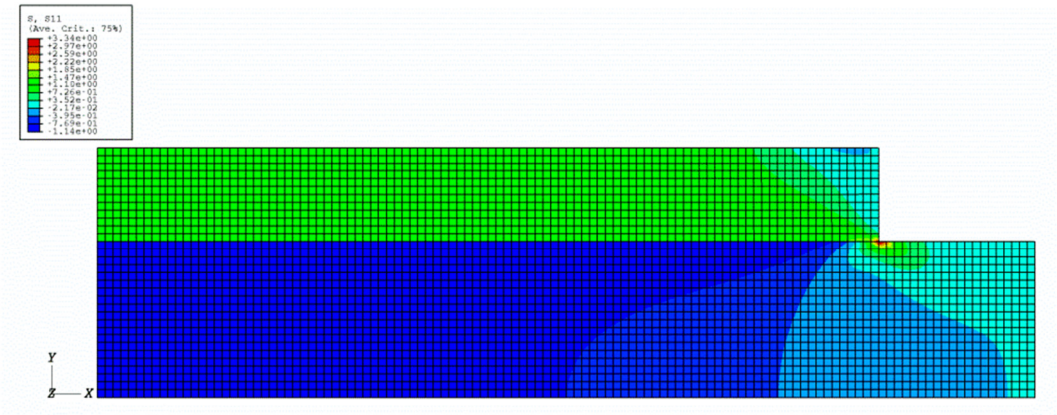

Figure 3.39: Horizontal Thermally Induced Stresses (Sxx) Contour

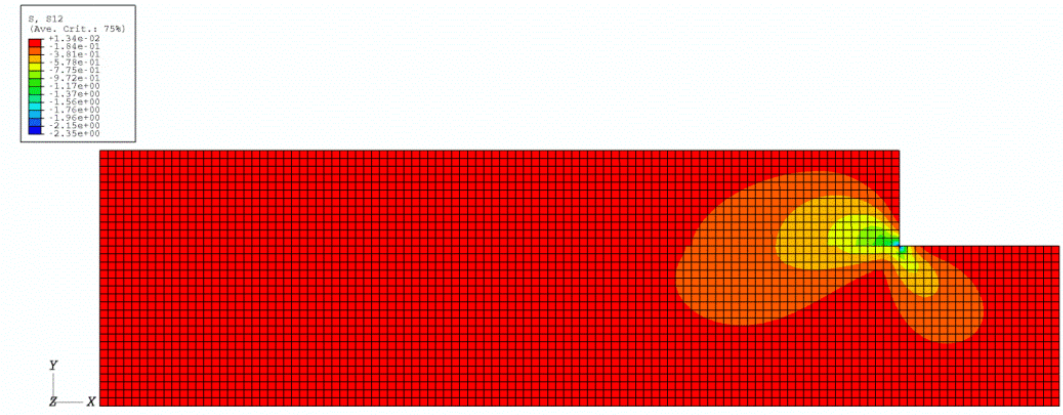

Figure 3.40: Thermally Induced Shear Stresses (Sxy) Contour

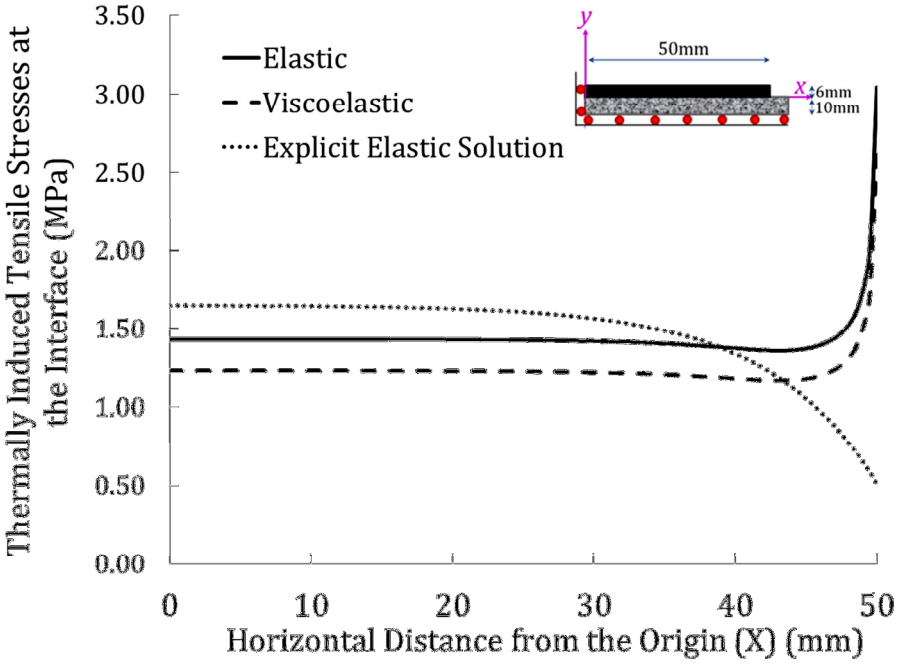

Figure 3.41: Thermally Induced Tensile Stresses along the Interface of Binder and Granite (Y=0)

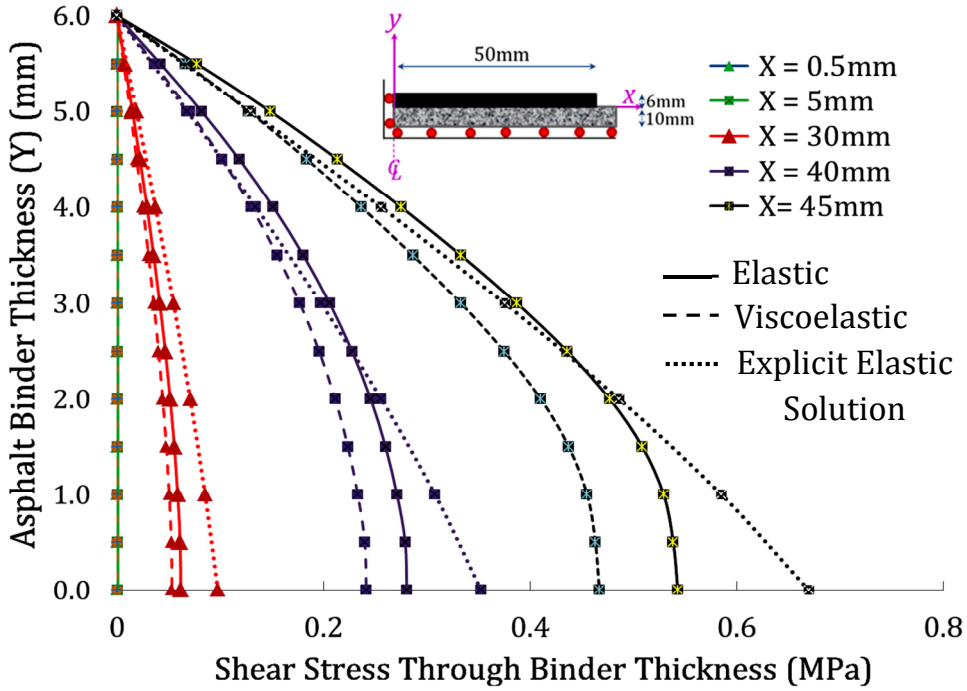

Figure 3.42: Thermally Induced Shear Stresses through the Thickness of the Binder Sample

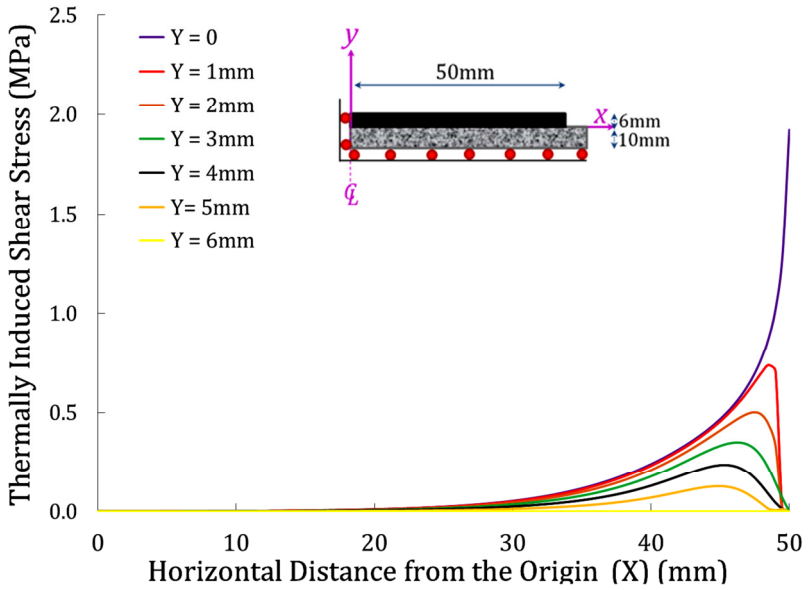

Figure 3.43: Thermally Induced Shear Stresses along the Length of the Binder Sample

3.8. SUMMARY

An acoustic emission-based test was developed to evaluate the low temperature cracking performance of asphalt binders. Several asphalt binders including: SHRP core asphalt binders (AAA-1(PG58-28), AAB-1(PG58-22) ,AAC-1 (PG 58-16), AAD-1 (PG 58-28), AAF-1 (PG 64-10), AAG-1 (PG 58-10), AAK-1 (PG 64-22), and AAM-1 (PG 64-16)), asphalt binders from an LTC study (PG64-22 (NY), PG58-28 (MN/Road-section20), and PG58-34 (MN/Road-section22)), and anti-oxidant (AOX) modified asphalt binders (PG64-22, AOX-modified PG64-22, PG70-22, and AOX-modified PG70-22), were tested. Asphalt binders were prepared at three different aging levels: Tank, RTFO, and PAV. The critical cracking temperature of asphalt binders were determined by conducting the BBR test at different temperatures. The temperature corresponding to the onset of thermal microcracks within the sample was termed as the "*Embrittlement*" temperature of the material.

Comparison of AE embrittlement temperature and BBR critical cracking temperature of asphalt binders revealed that, for most binders, the embrittlement temperature is a few degrees lower

than the BBR critical cracking temperature. It was observed that the embrittlement temperature was sensitive to aging level of asphalt material; the more aged the binder the warmer its embrittlement temperature. Results also showed that embrittlement temperature is sensitive to presence of additives in asphalt binder.

Effects of binder thickness on embrittlement temperature were investigated. It was observed that the embrittlement temperature decreases as sample thickness reduces. Results suggested that 6mm thick binder sample is a proper sample size which yield reliable results.

Cooling rate effects on embrittlement temperature of asphalt binders was examined. Different cooling rates ranging from 0.2 to 3^{o}C/min were applied. It was observed that there was not a significant difference between the embrittlement temperatures at cooling rates slower than 2^{o}C/min. As a result, the 2^{o}C/min rate was chosen as the cooling rate for binder samples.

Spectral analysis was performed on several binders at different temperatures. The dominant frequency of AE events appeared to be a good indicator of the brittleness of asphalt material; the more brittle the material the higher its dominant frequency.

Elastic and viscoelastic finite element simulations of AE binder sample were performed. Simulation results were compared against two-dimensional explicit elastic solution results. It was observed that due to stress relaxation, the viscoelastic shear stresses are approximately 12% lower than the elastic stresses. It is also seen that the explicit elastic solution underpredicts the thermally induced shear stresses in the top 4mm of the sample and overpredicts them at the bottom 2mm of the sample and at the interface.

Based on this study it can be inferred that AE-based binder test could be a viable alternative to the current AASHTO procedure for characterization of low temperature properties of asphalt material and especially advantageous when the direct tension (DTT) test is required.

CHAPTER 4
DEVELOPING ACOUSTIC EMISSION-BASED TEST FOR ASPHALT MIXTURES

4.1. INTRODUCTION

Asphalt concrete mixture is a complex heterogeneous material composed of a viscoelastic asphalt binder (mastic) matrix and aggregate particles, generally greatly varying in size, and perhaps including other modifiers and materials such as fibers. Upon rapid cooling, the asphalt mastic (the asphalt plus fine aggregate fraction) in the pavement contracts more than the aggregate particles causing thermal stresses in the pavement to develop in the material. When temperature drops below the point where asphalt mastic becomes brittle, thermal cracking can develop in the asphalt pavement. In addition to asphalt mastic cracking, debonding of asphalt mastic and aggregates at their interface is another microdamage occurs at low temperatures. This study employs acoustic emission testing technique to explore this phenomenon, through mastic and mixture testing. Two specimen configurations were proposed: loose mixtures as well as compacted asphalt mixtures [1].

In the following, first a brief review of testing techniques currently used to evaluate low temperature behavior of asphalt mixtures are presented, followed by sections focusing on AE testing of both loose and compacted mixtures.

4.1.1. Reviewing Current Thermal Cracking Evaluation Tests for Asphalt Mixtures

Over the past decades several testing methods have been developed to characterize the low temperature properties of asphalt binders. This section is divided in to two parts: first the conventional old testing techniques are presented, followed by the second part which briefly reviews current important testing techniques to evaluate and control low temperature cracking of asphalt materials.

- Indirect Tension Test (IDT),
- Disk-Shaped Compact Tension Test (DC[T]),
- Semi- Circular Bending Test (SCB),
- Thermal Stress Restrained Specimen Test (TSRST)

4.1.1.1. The Indirect Tension Test (IDT)

The indirect tension (IDT) creep test was developed in the mid 1990's to characterize the resistance of asphalt concrete mixtures to low-temperature cracking. Nowadays, the IDT creep test is widely used to predict the low-temperature performance of asphalt mixtures. It has been standardized in AASHTO T322, Standard "*Method of Test for Determining the Creep Compliance and Strength of Hot Mix Asphalt (HMA) Using the Indirect Test Device*"[61-63].

IDT creep testing is often conducted at 0, -10 and -20°C per SHRP recommendations through application of static loading for a duration of 1000 seconds. Creep compliance is determined using the horizontal and vertical deformations measured in the center of the specimen. Applied loads should be carefully selected so that the load-induced horizontal and vertical strains remain in the linear viscoelastic range during the creep test. The induced strains are measured 30 seconds after starting the creep test and compared with the allowable lower and upper limits to ensure that measurements are conducted within the linear range of material response. Figure 4.1 schematically illustrates the specimen for IDT test [61-63].

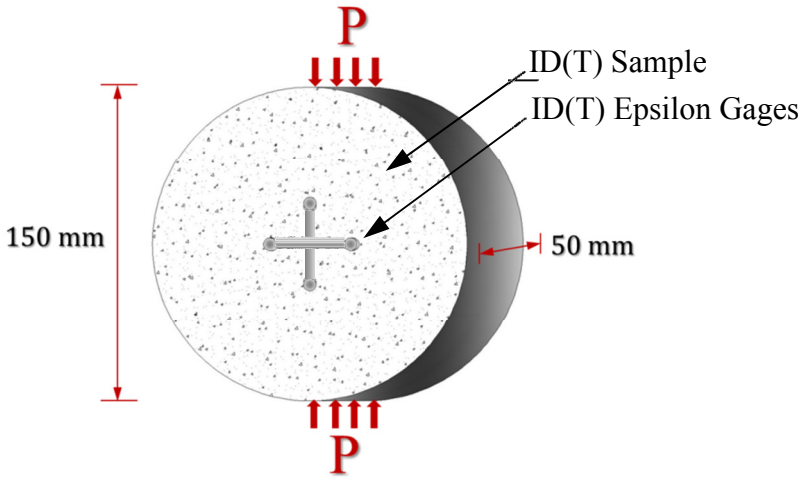

Figure 4.1: Indirect Tensile Test (IDT) Geometry and Dimensions

Creep compliance master-curves are generated through time-temperature superposition. A power-law model is fitted to the master-curves using equation (1) that shows the fitting function.

$$D(t) = D_0 + D_1 t^m \qquad (4.1)$$

The parameters D_0, D_1 and m are determined using a least-square fitting procedure. The m-value of the power law is associated with the rate of creep deformation and stress relaxation in viscoelastic materials. The higher the m-value the better the low temperature performance of asphalt mixture according to SHRP researchers [61-63].

4.1.1.2. Disk-Shaped Compact Tension Test (DC[T])

The Disk-Shaped Compact Tension Test (DC[T]) test is used to evaluate the low-temperature fracture characteristics of asphalt mixture samples. DC(T) testing is performed in accordance with ASTM D7313 at +10°C higher than the PG low temperature grade of the asphalt mixture [2]. The DC(T) sample geometry consist of a circular specimen with a single edge notch loaded in tension. Due to its simple geometry, DC(T) specimens can be obtained easily from field cores as well as laboratory compacted samples. The loading rate for the DC(T) tests was controlled through opening displacement at the crack mouth. A constant crack mouth opening displacement (CMOD) rate of 1 mm/min was utilized. The DC(T) testing setup and DC(T) specimen geometry shown in Figure 4.2. Fracture energy of the specimens was determined by calculating the normalized area under the Load-CMOD curve. Normalization is done to obtain the fracture energy required to produce a unit fracture area [64-67].

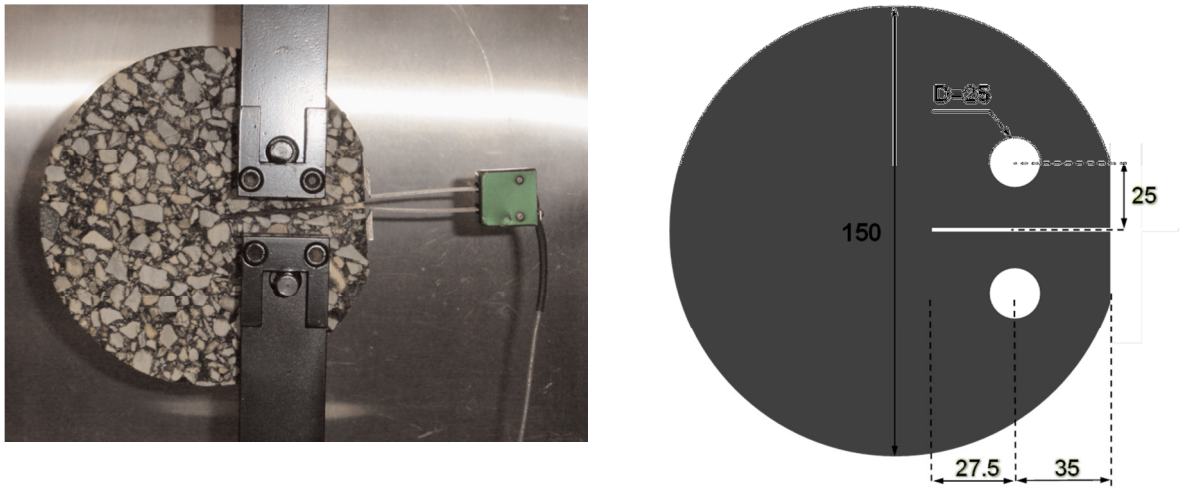

(a) (b)

Figure 4.2: (a) Disk-shaped Compact Tension (DC(T)) test setup (b) Geometry and Recommended Dimensions for the DC(T) Sample

4.1.1.3. Semi- Circular Bending Test (SCB)

The Semi-Circular Bend (SCB) test method is conducted to assess the low temperature behavior of asphalt mixtures by measuring their fracture energy and fracture toughness. The schematic representation of SC(B) test is illustrated in Figure 4.3. To conduct the SC(B) test, a vertical load which is controlled by constant rate of crack mouth opening displacement (CMOD) is applied on the top of the specimen. Fracture toughness is generally computed from the peak load, and fracture energy can be determined from the area under load vs load line displacement (LLD) plot [68,69] normalized by the fractured area.

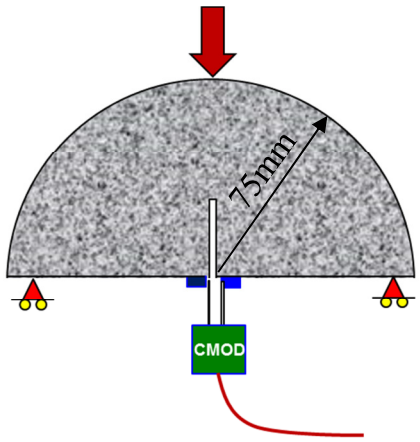

Figure 4.3: Schematic Representation of SC(B) Sample

4.1.1.4. Thermal Stress Restrained Specimen Test (TSRST)

The thermal stress restrained specimen testing (TSRST) is performed on asphalt mixtures to measure their low temperature thermal stress characteristics, tensile strength, and fracture temperature under one or more temperature cycles. It is conducted in accordance with AASHTO TP 10. TSRST specimens are 10 inches long and 2 inches square in cross-section. The TSRST testing device maintains the specimen at a constant length during a temperature cooling cycle. The TSRST device uses a displacement feedback loop to ensure that the stresses in the specimen do not relax by holding specimen length constant during the test [70]. The TSRST testing setup is shown in Figure 4.4.

Figure 4.4: Thermal Stress Restrained Specimen Testing Setup [71]

4.2. ACOUSTIC EMISSION TESTING OF ASPHALT MIXTURES

The current study employs an acoustic emission based testing method to evaluate low temperature cracking performance of asphalt mixtures. Two specimen configurations are examined:

- Loose Mixture:
    - ❖ Binder coated aggregates
    - ❖ Mastic coated aggregates
- Compacted Asphalt Mixtures (laboratory compacted mixtures as well as field cores)

The esting setup and data analysis for mixture testing are nearly identical to the asphalt binder AE test. In the following sections, AE asphalt mixture testing for both loose mixtures as well as compacted mixtures are explained in detail along with obtained test results.

4.2.1 Acoustic Emission Testing of Loose Asphalt Mixtures

Different types of asphalt binders including PG64-22, PG58-28, and PG70-22 were utilized to prepare binder coated aggregates as well as loose (uncompacted) asphalt mixtures. AE testing was conducted on asphalt binder samples, individual aggregates coated with binder, and individual mastic coated aggregates obtained from prepared loose mixtures. As illustrated in Figure 4.5, an AE sensor was mounted on the mastic/binder coated aggregate to monitor AE activity of the specimen as specimen cooling occurred. Binder-coated- and mastic-coated-aggregates are shown in Figures 4.6 (a) and 4.6(b), respectively.

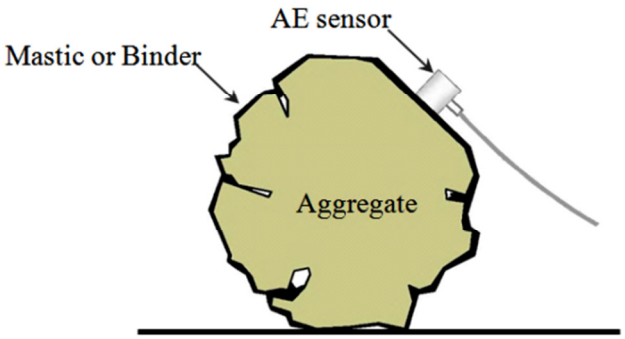

Figure 4.5: Mastic/Binder Coated Aggregate with Mounted AE Sensor [1]

(a) (b)

Figure 4.6: (a) Binder Coated Aggregate (b) Mastic Coated Aggregate [1]

Tables 4.1 through 4.3 summarize the results obtained from AE testing of binder and mastic coated aggregate particles. It was observed that the embrittlement temperature of mastic coated aggregates was slightly lower than that of binder coated aggregates. However, comparing these results with the binder testing results suggests that the embrittlement temperature of mastic/binder coated aggregates is lower than the embrittlement temperature of the binder itself. This could be linked to very thin film thickness asphalt binder covering the aggregates as compared to 6mm thick layer of binder in AE binder samples. Significant effect of asphalt film thickness on embrittlement temperature was explored and discussed previously in chapter 3 for AE binder samples with different thicknesses ranging from 6 to less than 1mm. It was also observed that the thinner the binder film thickness, the lower its embrittlement temperature. This agrees with the findings of Yin, where thin films bonded to substrates are found to be more and more fracture resistant as film thickness is reduced (Yin et al.). In addition to binder film thickness several other possibilities were hypothesized to explain the difference in embrittlement temperature measured in these three material configurations: 1) difference in temperature profiles (gradient across specimen); 2) difference in behavior at material interfaces in the three test configurations (granite-binder interface in binder testing; binder-coarse aggregate interface, and; binder-mastic-coarse aggregates interfaces), and; 3) geometry/constraint/size effects on fracture behavior. These differences suggest that the AE technique is sensitive to changes in testing configuration and material composition. Another important observation is that the embrittlement temperature of samples is sensitive to aging level of its asphalt binder. However, results shows that binder and mastic coated aggregates are less sensitive to change in aging condition of binder; the different between embrittlement temperature of tank and PAV binder/mastic coated aggregates is lower than that of binder samples.

Comparison of coefficient of variations of AE test results of all three testing configurations show an interesting trend. Results show that the COV% of binder tests are much lower than those of binder/mastic coated aggregates. Aggregates with different shapes and sizes, irregularities of aggregate surface, and different binder film thicknesses in different binder/mastic coated aggregates could be considered as possible reasons affecting the spread of AE test results on binder/mastic coated aggregates.

TABLE 4.1. PG64-22 Binder, Binder Coated Aggregate, and Mastic Coated Aggregate Test Results

Material ID	Rep#	Asphalt Binder			Binder Coated Aggregate			Mastic Coated Aggregate		
		T_{EMB} (°C)	Average	CoV%	T_{EMB} (°C)	Average	CoV%	T_{EMB} (°C)	Average	CoV%
TANK PG64-22	#1	-28.20	-27.88	4.45%	-34.12	-31.84	10.87%	-33.92	-32.86	16.20%
	#2	-27.10			-26.58			-31.32		
	#3	-29.71			-30.39			-27.11		
	#4	-26.19			-33.16			-34.84		
	#5	-28.34			-35.77			-29.91		
	#6	-26.73			-27.10			-40.95		
	#7	-27.42			-34.67			-25.96		
	#8	-29.33			-32.96			-38.88		
RTFO PG64-22	#1	-26.01	-26.34	3.84%	-25.64	-31.37	13.30%	-32.72	-32.53	13.39%
	#2	-24.93			-33.31			-35.97		
	#3	-27.19			-34.61			-31.14		
	#4	-25.34			-32.48			-38.69		
	#5	-25.72			-27.79			-29.00		
	#6	-26.84			-36.01			-27.26		
	#7	-27.92			-26.19			-37.22		
	#8	-26.78			-34.89			-28.20		
PAV PG64-22	#1	-23.91	-24.69	2.31%	-28.29	-30.81	10.69%	-32.48	-31.16	12.97%
	#2	-25.07			-34.50			-25.89		
	#3	-24.33			-28.03			-35.93		
	#4	-25.03			-30.45			-32.46		
	#5	-23.98			-34.52			-29.02		
	#6	-25.22			-27.66			-36.66		
	#7	-24.57			-28.11			-30.71		
	#8	-25.38			-34.95			-26.12		

TABLE 4.2. PG70-22 Binder, Binder Coated Aggregate, and Mastic Coated Aggregate Test

Material ID	Rep#	Asphalt Binder			Binder Coated Aggregate			Mastic Coated Aggregate		
		T_{EMB} (^{o}C)	Average	CoV%	T_{EMB} (^{o}C)	Average	CoV%	T_{EMB} (^{o}C)	Average	CoV%
TANK PG70-22	#1	-33.12	-34.84	4.22%	-37.48	-36.96	7.83%	-37.73	-37.10	4.33%
	#2	-36.18			-38.31			-35.56		
	#3	-34.70			-37.11			-38.98		
	#4	-35.45			-36.16			-38.95		
	#5	-32.71			-39.96			-36.01		
	#6	-36.64			-33.51			-38.45		
	#7	-33.91			-40.73			-36.12		
	#8	-35.99			-32.40			-35.01		
RTFO PG70-22	#1	-32.18	-33.43	2.88%	-35.16	-34.92	11.17%	-35.16	-34.54	15.22%
	#2	-34.17			-39.19			-27.22		
	#3	-33.52			-33.11			-40.31		
	#4	-31.92			-31.10			-38.16		
	#5	-33.87			-37.22			-29.11		
	#6	-34.16			-28.11			-30.17		
	#7	-33.05			-36.49			-41.19		
	#8	-34.54			-38.94			-35.02		
PAV PG70-22	#1	-27.63	-26.94	5.14%	-39.16	-35.30	16.83%	-32.14	-33.54	8.71%
	#2	-25.12			-42.11			-37.22		
	#3	-28.54			-28.01			-35.14		
	#4	-29.10			-27.16			-32.90		
	#5	-25.99			-37.87			-28.10		
	#6	-26.04			-41.73			-32.28		
	#7	-27.00			-31.00			-36.71		
	#8	-26.12			-35.32			-33.81		

TABLE 4.3. PG58-28 Binder, Binder Coated Aggregate, and Mastic Coated Aggregate Test

Material ID	Rep#	Asphalt Binder			Binder Coated Aggregate			Mastic Coated Aggregate		
		T_{EMB} (^{o}C)	Average	CoV%	T_{EMB} (^{o}C)	Average	CoV%	T_{EMB} (^{o}C)	Average	CoV%
TANK PG58-28	#1	-37.99	-36.10	4.73%	-40.12	-40.77	9.03%	-44.27	-40.92	12.19%
	#2	-36.32			-43.50			-43.28		
	#3	-35.83			-38.03			-39.37		
	#4	-37.72			-44.11			-34.92		
	#5	-33.11			-35.12			-43.29		
	#6	-34.14			-42.93			-32.17		
	#7	-37.18			-37.22			-43.88		
	#8	-36.47			-45.14			-46.21		
RTFO PG58-28	#1	-35.42	-35.47	3.08%	-42.49	-38.19	12.81%	-42.11	-40.22	5.33%
	#2	-33.49			-42.14			-40.68		
	#3	-36.59			-30.22			-43.29		
	#4	-34.11			-33.42			-39.11		
	#5	-35.97			-34.13			-41.18		
	#6	-35.91			-43.11			-40.22		
	#7	-36.01			-40.01			-36.39		
	#8	-36.24			-39.98			-38.76		
PAV PG58-28	#1	-30.11	-31.69	5.71%	-37.96	-36.55	3.62%	-38.21	-38.68	4.92%
	#2	-28.19			-35.42			-35.11		
	#3	-32.45			-34.66			-38.71		
	#4	-33.14			-37.26			-39.14		
	#5	-32.26			-35.14			-40.01		
	#6	-30.99			-38.19			-37.10		
	#7	-33.49			-36.73			-39.95		
	#8	-32.88			-37.01			-41.18		

4.2.2 Acoustic Emission Testing of Compacted Asphalt Mixtures

The acoustic emission method was implemented to evaluate the low temperature behavior of lab-compacted mixture samples from the pooled fund Low Temperature Cracking (LTC) study as well as several lab compacted PG 64-22, PG 70-22, and PG 58-28 asphalt concrete mixtures at different aging levels. Moreover, AE test conducted on several field cores and lab compacted samples provided by the Asphalt Institute. Asphalt concrete mixture samples were sliced to prepare 150 mm diameter semicircular shape with 50 mm thickness AE testing samples. In the same manner as in binder testing, AE mixture specimens were positioned inside the cooling chamber of the portable freezer. Specimen temperature was continuously recorded using a K-type thermocouple coupled to the specimen surface. Typical temperature versus time cooling

plot is shown in Figure 4.7. The average cooling rate for 50mm thick mixture specimens is around 0.8°C/min, when the global cooling unit (Shuttle) is set to its lowest temperature (-86 Celsius). Similar to the AE binder test, Wideband piezoelectric sensors (Digital Wave, Model B1025) with a nominal frequency range of 50 kHz to 1.5 MHz are utilized in order to monitor and record acoustic activities of the sample during the test. The AE testing setup specimen dimensions are schematically shown in Figure 4.8(a) and 4.8(b), respectively.

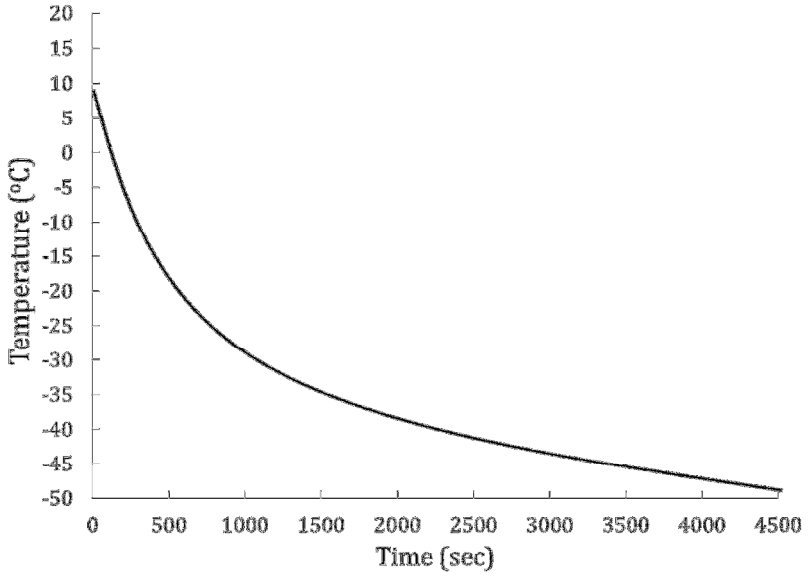

Figure 4.7: Typical Plot of Temperature vs Cooling Time of AE Asphalt Mixture Samples.

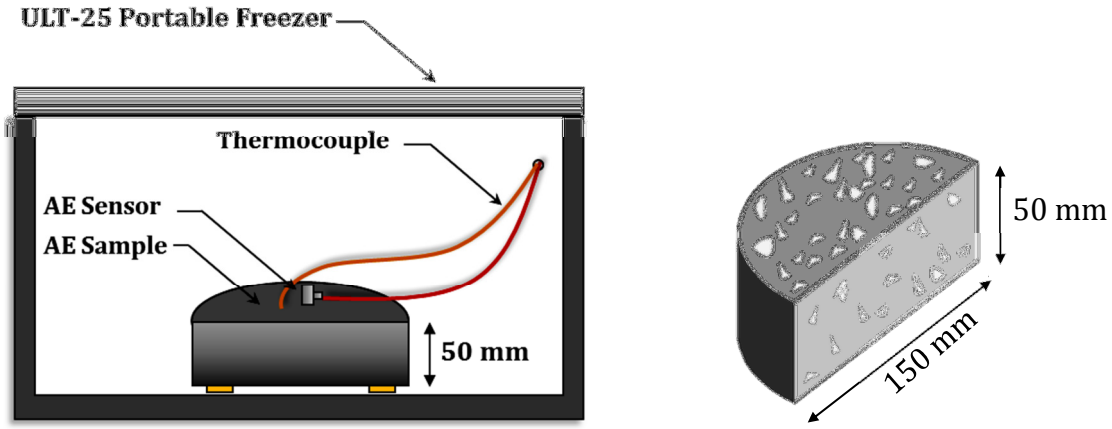

(a) (b)

Figure 4.8: (a) AE Mixture Testing Set-up (b) AE Mixture Specimen

Similar to the AE binder test, typical plots of AE events counts vs. temperature of asphalt concrete mixtures has four distinct regions namely: pre-cracking, transition, stable cracking, and fully cracked. The temperature corresponding to the first major event has termed the "e*mbrittlement*" temperature. In addition to embrittlement temperature, testing results indicated that the temperature at which a maximum acoustic energy release is observed was a very repeatable parameter for the broad range of materials tested. Like embrittlement temperature, this quantity is also expected to be an intrinsic fracture property of the material. This temperature has termed the "maximum energy event temperature ($T_{MAX)}$". The variability of T_{MAX} is higher than the variability of T_{EMB}. For asphalt mixtures, the maximum energy event temperature is always lower than its embrittlement temperature. Unlike embrittlement temperature which is mainly due to formation of local microdamages probably at the interface of asphalt mastic and aggregates, it is hypothesized that T_{MAX} might be associated with formation of a large microcrack involving several aggregate particles and surrounding asphalt mastic. In other words, embrittlement temperature is due to local micro-scale thermally induced damages, whereas T_{MAX} is due to macro-scale thermally induced cracks within the sample. Because of the indeterminate nature of asphalt concrete microstructure, formation of microcracks while releasing some strain energy locally, do not prevent those pockets of mastic from accumulating thermally induced tensile strain energy. Strain energy within mastic continues to accumulate as temperature reduces, until temperature reaches T_{MAX}. At T_{MAX} thermally induced stresses within the mastic equal mastic fracture strength leading to formation of relatively large microcrack in the mastic which is accompanied by release of accumulated strain energy in the form of a high energy AE event. The concepts of embrittlement temperature and temperature of maximum AE event energy for asphalt mixtures are shown in Figure4.9 [1,72,73].

The graphical representation of the distribution of AE events energies of asphalt concrete samples is presented as a histogram in Figure 4.10. Similar to binder samples, only a small portion of AE events contain high energy while the majority of them are low energy events. Number of recorded AE events in the testing of an asphalt concrete mixture is significantly higher than that observed in asphalt binder testing. The majority of these events are caused by microcracks resulting from asphalt mastic brittleness and the action of tensile thermal stresses

within the material. In addition, debonding of asphalt mastic and aggregates at their interface is another important source of AE events of asphalt concrete mixtures. Figure 4.11 schematically illustrates thermally induced stresses and resulting damage in the mixture sample. A typical envelope locus of AE event energies for asphalt mixtures is depicted in Figure 4.12. It schematically shows the intensity of the released energies of AE events. The envelope locus is zero throughout the pre-cracking region before a significant jump occurs at the beginning of transition region, T_{EMB}. The magnitude of energy envelope locus gradually increases until reaching its maximum value at T_{MAX}. The magnitude of AE energies envelope locus gradually tapers off at temperatures lower than T_{MAX} until reaches almost zero in the fully cracked region.

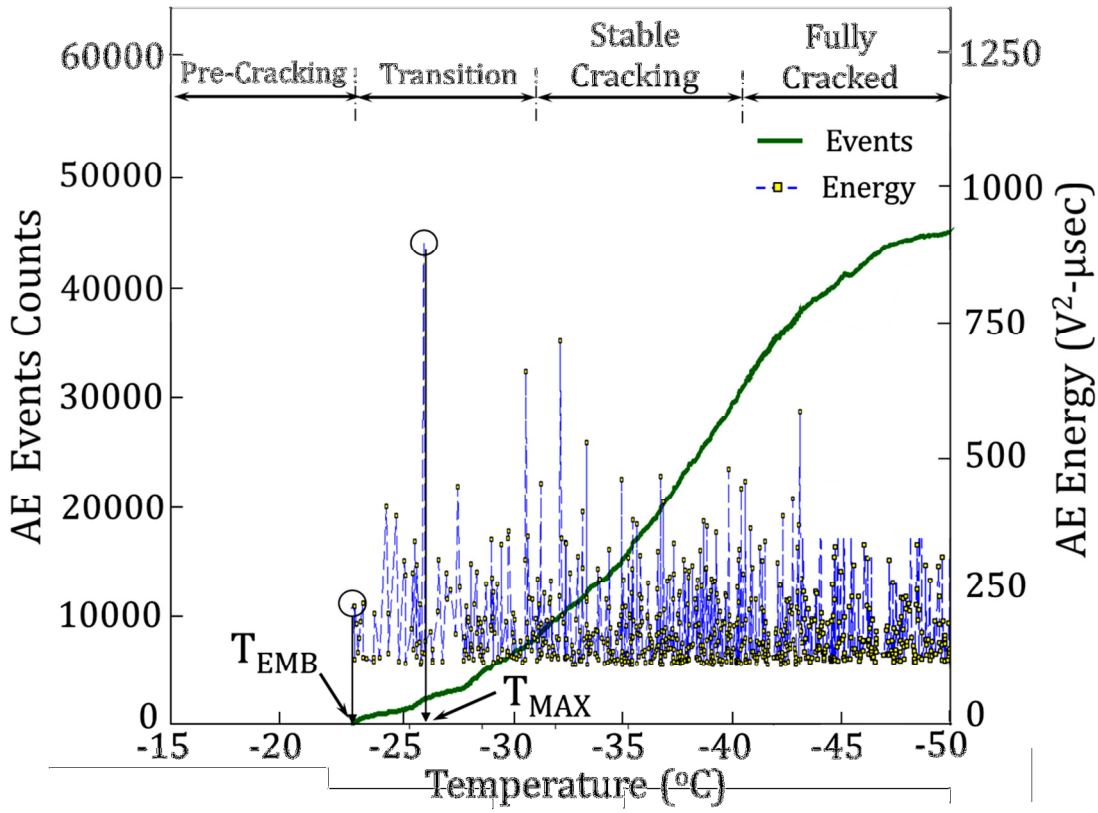

Figure 4.9: Typical Plot of AE Events Counts and AE Energy Versus Temperature

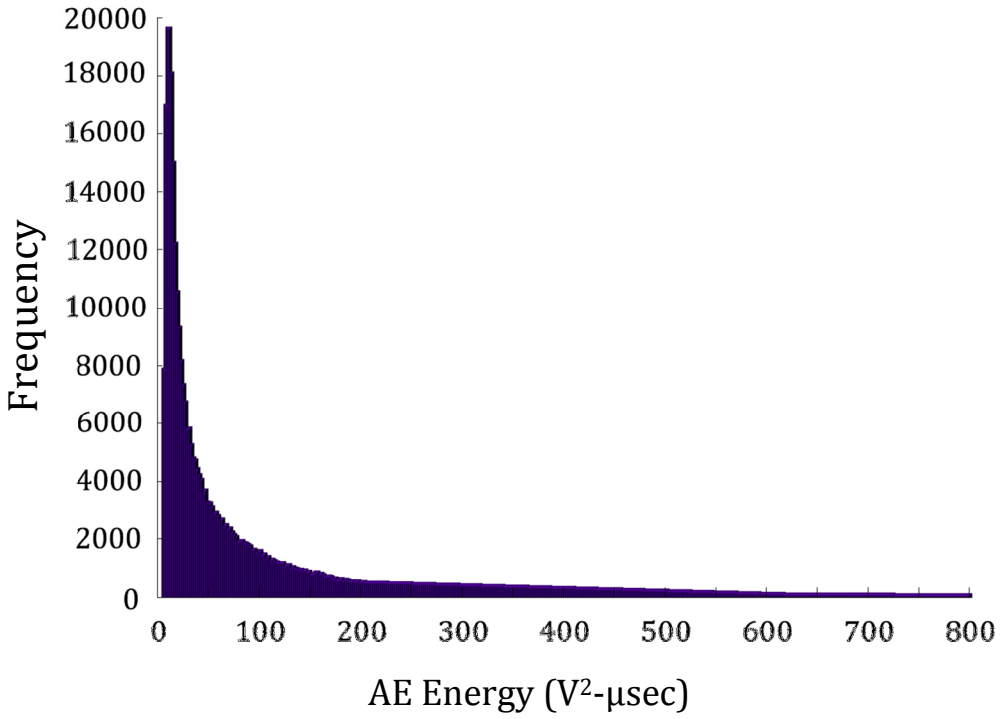

Figure 4.10: Typical Histogram of AE Events Energies of Asphalt Mixture Sample.

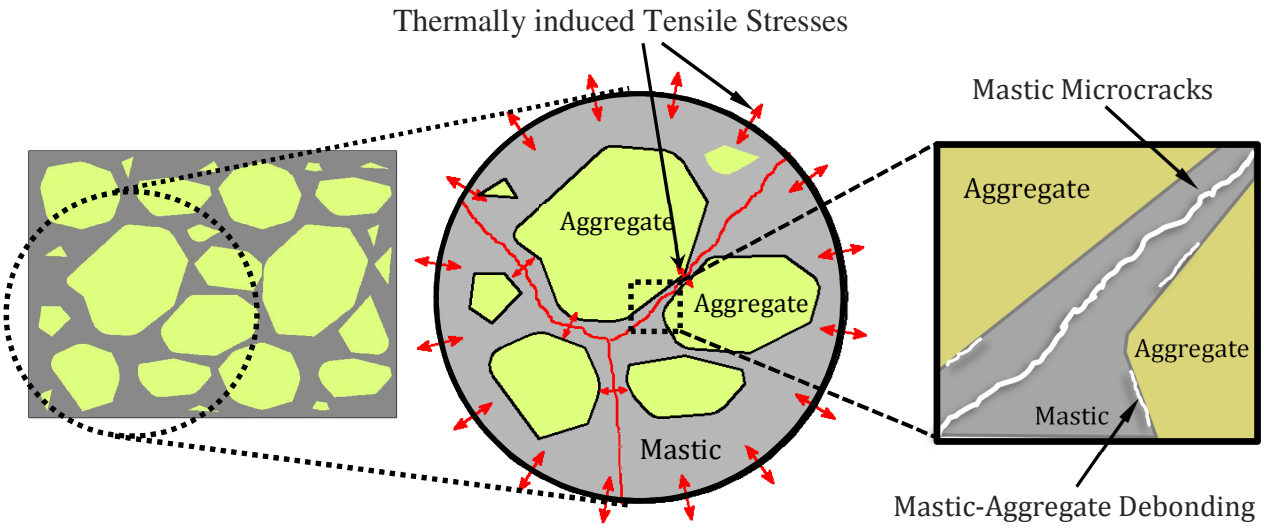

Figure 4.11: Schematic Illustration of Thermally Induced Stresses within the Asphalt Mastic along with Two Main Types of Microdamage within Mixture Sample including: Mastic Microcrack, and Mastic-Aggregate Debonding

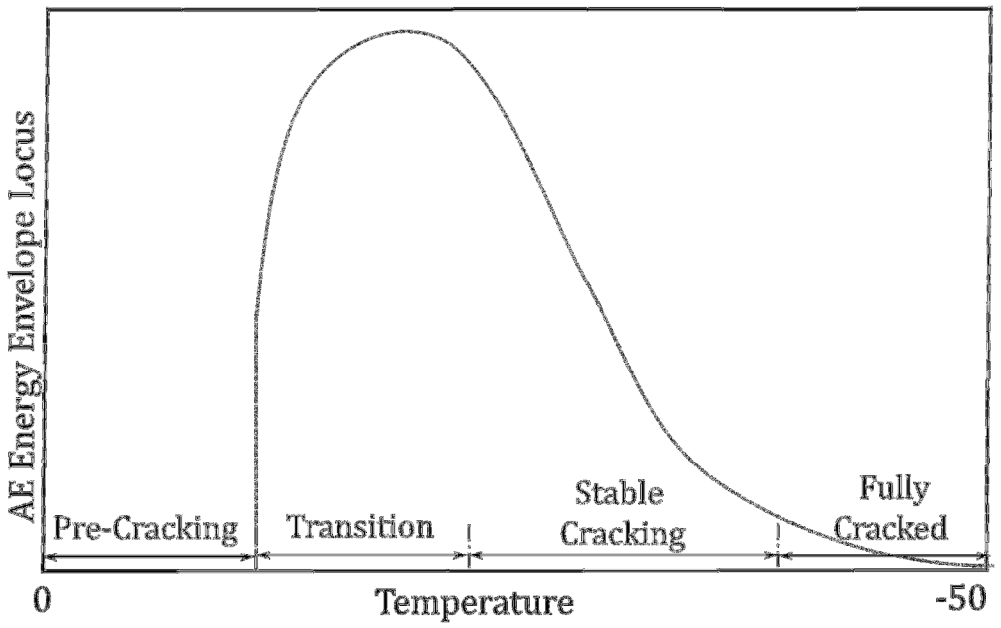

Figure 4.12: Typical Envelope Locus of AE Events Energy During Thermal Cooling

4.2.2.1 Determining the Proper Location to Measure AE Asphalt Mixture Sample Temperature

One critical aspect of AE-based testing of asphalt mixtures is to record the temperature that represents the temperature of the whole sample. Due to thickness of the sample, there might be thermal lag between the surface and inside of the sample. To determine the proper location to measure temperature, three K-type thermocouples were positioned at three different locations of the mixture sample. The first thermocouple (A) was placed on the surface of the sample, the second and the third thermocouples (B and C) were embedded 12mm and 24mm deep inside the sample, respectively. Figure 4.13 schematically depicts locations of three thermocouples A, B, and C on the sample surface, 12mm deep, and 24mm deep, respectively.

The temperature vs. time plots of mixture samples measured by thermocouples A, B, and C are shown in Figure 4.14. Results show that initially at the beginning of the test, there is a thermal lag of 9^{o}C between the surface (A) and the middle of the sample (C). The thermal lag gradually decreases as the sample cools down until it reaches around 1^{o}C at -5^{o}C. When temperature approaches -10^{o}C thermal lag reduces to 0.5^{o}C. This indicates that uniformly cooling of AE sample in the portable freezer effectively minimizes thermal lag within the sample. Thermal lag at temperatures below -10^{o}C is negligible and we can consider the temperature of sample surface

as the temperature of the whole specimen. At very low temperatures, below -40°C, temperatures of all three thermocouples of A, B, and C become almost the same. Considering the fact that the acoustic emission activity of most asphalt concrete mixtures start below -10°C, it can be concluded that sample surface could be a proper location to position a thermocouple to measure the temperature of mixture sample during AE test.

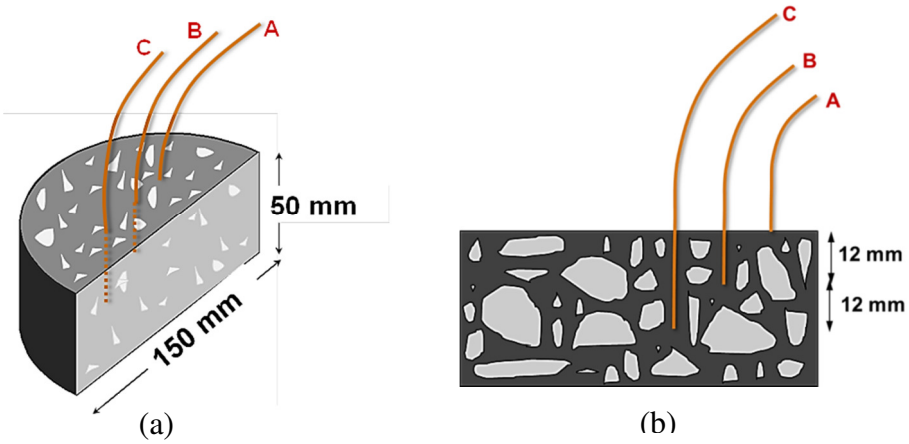

Figure 4.13: (a) AE Asphalt Mixture Sample with Three Thermocouples A, B, and C (b) Profile View of AE Mixture Samples with the Location of Thermocouples

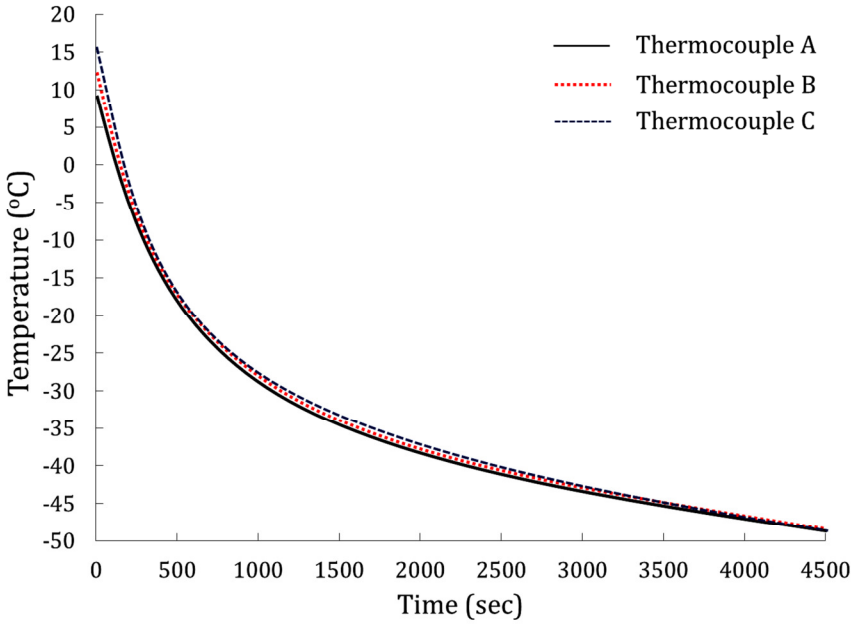

Figure 4.14: Typical Plots of Temperature vs Time of AE Mixture Sample Obtained from Thermocouples of A, B, and C.

4.2.2.2 Determining the Proper Thickness for AE Asphalt Mixture Samples

The 150mm diameter semicircular asphalt concrete samples were used for AE testing. This geometry was selected because of its easy and fast sample preparation procedure from either the gyratory compacted samples or field cores. The important issue is to determine the proper sample thickness in order to obtain accurate and reliable results. Several 150mm diameter semicircular AE mixture samples with different thicknesses ranging from 10mm to 60mm were examined. AE test was conducted on all samples with different thicknesses; Table 4.4 presents obtained results. It is seen that thinner samples exhibited warmer embrittlement temperatures. The embrittlement temperature of samples with different thicknesses is plotted in Figure 4.15. It is observed that the embrittlement temperature is sensitive to change in the thickness of the sample. It reduces from -14.76^{o}C to -29.11^{o}C when the thickness increases from 10 to 40mm. The rate of change of embrittlement temperature with respect to sample thickness is very high for 10mm thick sample (8.14^{o}C drop in T_{EMB} for 10mm increase in thickness). It gradually reduces until it reaches 0.32^{o}C/cm for 40mm thick sample. Results show that there is not much change in embrittlement temperatures of 40mm or thicker samples. Thickness of the sample significantly affects repeatability of AE test such that the COV% of 10mm samples is relatively high (22.27%), while COV% for 40mm or thicker samples is around 5%. Results suggest that AE mixture samples should be at least 40mm thick to properly represent the mixture and to yield repeatable and reliable results. In the current study 50mm thick samples were used as AE mixture sample.

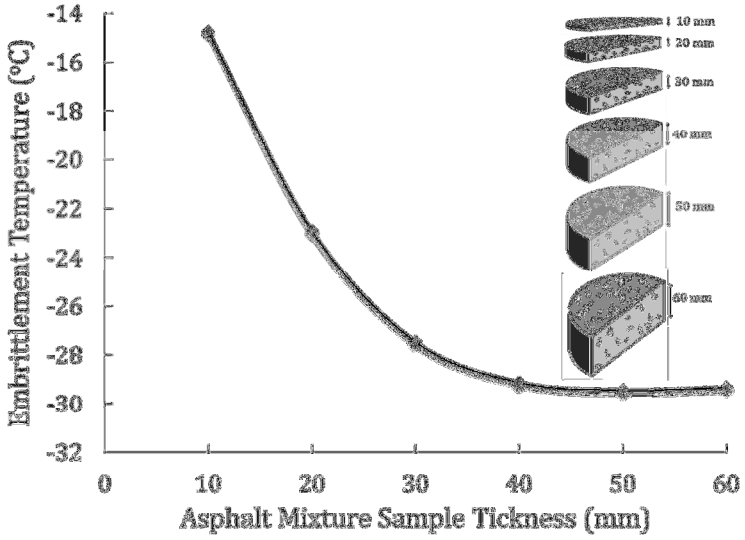

Figure 4.15: Embrittlement Temperatures vs Thickness of AE Mixture Samples

TABLE 4.4. AE Test Results for Tank PG64-22 Mixture Samples with Different Thicknesses

Mixture ID	Sample Thickness (mm)	Rep#	Embrittlement Temperature		
			T_{EMB} (^{o}C)	Average	CoV%
Mixture Tank 64-22	10 mm	#1	-11.42	-14.76	22.27%
		#2	-12.51		
		#3	-18.12		
		#4	-16.97		
	20mm	#1	-27.31	-22.89	26.83%
		#2	-18.37		
		#3	-16.89		
		#4	-28.99		
	30mm	#1	-25.67	-27.45	6.60%
		#2	-29.98		
		#3	-27.15		
		#4	-27.01		
	40mm	#1	-28.16	-29.11	4.02%
		#2	-30.11		
		#3	-30.14		
		#4	-28.04		
	50mm	#1	-31.69	-29.44	5.18%
		#2	-29.04		
		#3	-28.46		
		#4	-28.55		
	60mm	#1	-28.43	-29.32	4.14%
		#2	-29.83		
		#3	-30.79		
		#4	-28.22		

4.3. RESULTS AND DISCUSSIONS

Acoustic emission testing was conducted on several asphalt concrete mixtures including: lab compacted PG64-22, PG70-22, and PG58-28 mixtures, LTC study mixtures, and mixtures provided by Asphalt Institute. Results are presented in the following sections.

4.3.1. Lab Compacted PG64-22, PG70-22, and PG58-28 Mixtures

Asphalt mixtures with19 mm nominal maximum aggregate size and target asphalt content of 5.9% were prepared for this study. Three asphalt binders namely: PG64-22, PG70-22, and PG58-28 at different aging levels: Tank, RTFO, and PAV, were utilized as base binders. Mixing was performed at 155°C using a standard bucket mixing procedure. Acoustic emission test was conducted on all asphalt concrete mixtures. The embrittlement temperatures as well as the max energy event temperatures of mixtures are outlined in Tables 4.5 to 4.7.

Results show that both T_{EMB} and T_{MAX} are sensitive to aging level of the mixture; the higher the aging level of the mixture the warmer its T_{EMB} and T_{MAX}. However, it is observed that T_{EMB} is much more sensitive to aging level of mixture as compared to T_{MAX}. Another important observation is that for most mixtures, there is not much change in the temperature difference between T_{EMB} and T_{MAX} of a mixture at different aging levels. This indicates that oxidative aging of mixtures does not change the size of transition region of asphalt mixture; it just shifts the AE events counts plot toward warmer temperatures.

Comparison of T_{EMB} and PG low temperature (PGLT) of PAV mixtures show that the embrittlement temperature of PAV mixtures are couple of degrees lower than the PGLT of that mixture. This may suggest that the Superpave PAV aging procedure doesn't properly represent the long term aging that occurs in the field.

TABLE 4.5. Acoustic Emission Test Results of PG 64-22 Mixtures at Different Aging Levels

Mixture ID	Rep#	Embrittlement Temp (°C)			Max Energy Event Temp (°C)		
		T_{EMB} (°C)	Average	CoV%	T_{MAX} (°C)	Average	CoV%
TANK PG64-22	#1	-29.10	-30.28	8.90%	-35.14	-38.54	7.17%
	#2	-32.19			-39.17		
	#3	-27.06			-38.14		
	#4	-30.15			-40.19		
	#5	-32.71			-39.45		
	#6	-29.33			-34.09		
	#7	-33.65			-37.72		
	#8	-27.61			-35.75		
	#9	-26.33			-37.18		
	#10	-32.95			-42.32		
	#11	-33.89			-40.12		
	#12	-28.44			-43.17		
RTFO PG64-22	#1	-27.32	-29.41	5.51%	-40.16	-37.60	4.78%
	#2	-29.17			-37.11		
	#3	-29.19			-36.19		
	#4	-30.78			-35.26		
	#5	-28.27			-38.91		
	#6	-31.75			-37.99		
PAV PG64-22	#1	-25.14	-25.18	4.57%	-37.44	-35.47	7.80%
	#2	-25.64			-35.34		
	#3	-24.17			-30.91		
	#4	-26.66			-36.12		
	#5	-25.92			-34.17		
	#6	-23.55			-38.86		

TABLE 4.6. Acoustic Emission Test Results of PG 58-28 Mixtures at Different Aging Levels

Mixture ID	Rep#	Embrittlement Temp (°C)			Max Energy Event Temp (°C)		
		T_{EMB} (°C)	Average	CoV%	T_{MAX} (°C)	Average	CoV%
TANK PG58-28	#1	-35.72	-36.90	6.78%	-43.16	-42.56	5.43%
	#2	-32.13			-40.24		
	#3	-38.19			-45.01		
	#4	-34.99			-39.57		
	#5	-38.27			-40.66		
	#6	-39.81			-41.79		
	#7	-37.17			-44.70		
	#8	-38.88			-45.38		
RTFO PG58-28	#1	-36.17	-35.51	8.32%	-44.41	-42.96	4.45%
	#2	-38.18			-45.08		
	#3	-30.01			-41.17		
	#4	-37.02			-43.95		
	#5	-34.56			-40.22		
	#6	-37.14			-42.90		
PAV PG58-28	#1	-33.15	-33.51	7.75%	-42.12	-41.45	5.44%
	#2	-36.18			-38.16		
	#3	-29.06			-43.63		
	#4	-34.41			-42.81		
	#5	-32.51			-39.11		
	#6	-35.72			-42.88		

TABLE 4.7. Acoustic Emission Test Results of PG 70-22 Mixtures at Different Aging Levels

Mixture ID	Rep#	Embrittlement Temp (°C)			Max Energy Event Temp (°C)		
		T_{EMB} (°C)	Average	CoV%	T_{MAX} (°C)	Average	CoV%
TANK PG70-22	#1	-31.63	-35.01	7.47%	-46.72	-46.33	3.03%
	#2	-37.97			-44.82		
	#3	-34.52			-47.10		
	#4	-33.17			-45.24		
	#5	-37.06			-44.17		
	#6	-34.15			-47.53		
	#7	-32.81			-48.11		
	#8	-38.79			-46.91		
RTFO PG70-22	#1	-33.23	-33.14	6.06%	-44.94	-46.01	4.30%
	#2	-34.65			-47.79		
	#3	-34.17			-43.85		
	#4	-34.34			-45.78		
	#5	-29.22			-44.69		
	#6	-33.23			-48.98		
PAV PG70-22	#1	-27.11	-28.92	8.58%	-39.97	-43.13	8.63%
	#2	-29.33			-45.47		
	#3	-32.72			-46.02		
	#4	-30.67			-37.19		
	#5	-27.58			-46.22		
	#6	-26.09			-43.88		

4.3.2 LTC Study Lab Compacted Asphalt Mixtures

Acoustic emission tests were conducted on four mixtures from the LTC study, namely sections 20, 22 and 33. The embrittlement as well as the maximum energy event temperatures are listed in Table 4.8. Notice that tests were conducted for mix specimens with 4% and 7% air void levels. The embrittlement temperature data indicates that for sections 20 and 21 the onset of damage begins at temperatures well above the Superpave PG low temperature of the virgin binder. This might be linked to the presence of 30% RAP in the mix, whereby, the aged binder from RAP leads to increased brittleness and earlier onset of measured microcracking. On the other hand, the temperatures corresponding to the maximum energy events for Sections 20 and 21 seem to correspond to PGLT grade of the virgin binder. Similar observations can be made for section 22 where the first major acoustic event occurred at a temperature above the PGLT grade of the virgin binder, whereas the maximum acoustic energy was released at a temperature close to or lower than the virgin binder PGLT grade. The results for section 33 follow similar trends as the other sections, where the embrittlement temperature is higher than that of the PGLT grade of the virgin binder, whereas the temperature at maximum energy release is similar to the PGLT. The air void level did not reveal a specific trend in either the embrittlement temperature or the temperature corresponding to the maximum energy event. This is expected, as the acoustic activity is measure of fracture and fracture phase change for the mastic portion of the mixture. In addition, the 4 and 7% air void levels were targeted for a180 mm tall gyratory specimens, while AE testing was performed on 50 mm thick samples, which almost certainly had lower air void levels and possibly less difference in air void level between the two groups.

TABLE 4.8. Acoustic Emissions Test Results of LTC Mixtures

Mixture ID	Air Void %	Rep #	Embrittlement Temp			Max Energy Event Temp		
			T_{EMB} (^{o}C)	Average	CoV%	T_{MAX} (^{o}C)	Average	CoV%
Section 20 (PG58-28)-30%RAP	4%	#1	-17.45	-19.45	9.74%	-29.97	-30.06	1.40%
		#2	-21.36			-29.69		
		#3	-18.25			-29.90		
		#4	-20.75			-30.66		
	7%	#1	-24.10	-24.65	8.66%	-29.92	-30.26	6.24%
		#2	-22.87			-28.04		
		#3	-27.75			-30.44		
		#4	-23.89			-32.63		
Section 21 (PG58-28) - 30%RAP	4%	#1	-21.00	-22.24	8.55%	-29.74	-31.89	5.92%
		#2	-21.29			-32.66		
		#3	-24.43			-33.27		
	7%	#1	-19.90	-20.91	4.27%	-26.82	-28.28	5.37%
		#2	-21.59			-29.85		
		#3	-21.24			-28.16		
Section 22 (PG58-34) - 30%RAP	4%	#1	-28.05	-28.75	8.18%	-32.02	-33.70	4.27%
		#2	-29.35			-35.50		
		#3	-31.61			-33.38		
		#4	-26.00			-33.89		
	7%	#1	-29.86	-29.90	4.73%	-35.74	-36.97	2.71%
		#2	-28.33			-37.84		
		#3	-29.64			-37.73		
		#4	-31.76			-36.57		
Section 33 (PG58-34)	4%	#1	-30.40	-30.50	5.54%	-31.20	-31.16	5.24%
		#2	-28.16			-28.85		
		#3	-31.46			-32.03		
		#4	-31.97			-32.54		
	7%	#1	-29.87	-29.73	2.69%	-32.94	-33.02	4.33%
		#2	-30.74			-31.02		
		#3	-29.48			-34.12		
		#4	-28.83			-33.98		

4.3.3 Asphalt Institute Compacted Asphalt Mixtures

AE-based mixture test was conducted on several lab compacted asphalt mixtures as well as field cores provided by the Asphalt Institute, which were part of a study investigating non-load associated cracking in airfield pavements [19]. Three sets of lab compacted mixtures at three different aging levels including: 0, 4 and 24 hours were tested. All aging was performed on loose mixture before compaction to expedite and simplify the lab conditioning process. According to information provided by the Asphalt Institute, three asphalt binders namely, Gulf-Southeast (PG64-22), Western Canadian (PG64-28) and West Texas sour (PG64-16), were utilized in the study mixtures. The asphalt binders possessed different low temperature relaxation properties as defined by the BBR m-value. Table 4.9 summarizes the lab compacted AE test results. It is observed that for all samples at different aging levels, the more aged the sample, the warmer the T_{EMB} of that material. It was hypothesized that aging causes a significant loss in relaxation properties of the asphalt mastic at lower temperatures, and this change results in deteriorating fracture cracking resistance of the material. Similar to LTC mixtures, for all lab compacted samples, the T_{EMB} is warmer than the PGLT of virgin binder, whereas for most cases the maximum acoustic energy temperatures are close to virgin binder's PGLT.

In addition to lab compacted samples, several field cores provided by Asphalt Institute were tested to assess their low temperature cracking behavior using AE technique. Field cores obtained from three different projects located at different regions with different climates as well as different asphalt crude sources. Coring locations on General Aviation (GA) pavements were Montana and New Mexico. These locations and typical photos of cores are provided in Figure 4.16. The coring location selected with the goal to obtain cores from both cracked and non-cracked sections. The locations selected were matched to the binder source wherever possible. For example, it was believed that the Montana airport cores would reflect an asphalt source similar to the Western Canadian crude, whereas the New Mexico sites would more likely resemble asphalt as refined from the West Texas Sour crude.

Cores were taken from airports representing in-service pavements. In Montana, cores were taken from one airport – identified as Roundup – that had recently received an overlay of an older, cracked pavement. The estimated age of the pavement is 12 to 15 years old. A number of cracks were present in this pavement, which have been previously routed and sealed. Obtained cores

were split into layers with the upper layer representing the new pavement (Roundup Top) and the lower layer representing the older pavement (Roundup Bottom). In New Mexico, cores were taken from the Clayton airport and the Conchas Lake airport. Site reports for the Clayton airport indicate that it was paved in 2004. Some low severity longitudinal cracking and raveling was identified. The Conchas airfield was paved in 2001. Site reports from the Conchas Lake airport indicate that some moderate severity distresses were identified over most of the paved area, and that the pavement had a weathered appearance [74].

TABLE 4.9. Acoustic Emissions Test Results of Lab Compacted Mixtures

Mixture ID	Aging Level (Hours)	Embrittlement Temp (^oC)		Max Energy Event Temp (^oC)	
		T_{EMB} (^oC)	CoV%	T_{MAX} (^oC)	CoV%
Gulf South East Crude (PG64-22)	0	-18.00	1.26%	-21.71	2.18%
	4	-16.99	7.37%	-21.9	8.07%
	24	-13.96	9.17%	-20.5	7.49%
Western Canadian Crude (PG64-28)	0	-22.84	8.70%	-27.82	7.80%
	4	-20.67	1.27%	-27.78	2.80%
	24	-16.37	10.07%	-22.16	7.47%
Western Texas Sour Crude (PG 64-16)	0	-12.55	4.68%	-23.49	2.89%
	4	-10.03	4.09%	-21.71	6.42%
	24	-8.42	12.93%	-18.13	6.32%

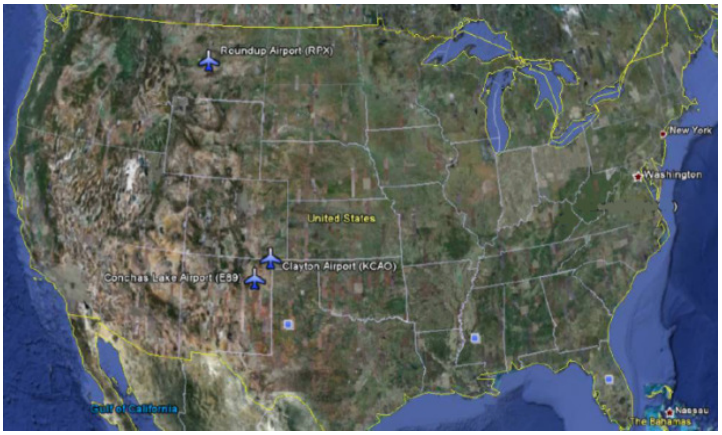

(a)

(b)

Figure 4.16: (a) Coring Sites Locations: New Mexico, Montana (b) Sample Cores from Rounup, MT and Conchas Lake, NM[74].

TABLE 4.10. Acoustic Emissions Test Results of Asphalt Institute Field Cores

Material ID	Embrittlement Temp (°C)		Max Energy Event Temp (°C)	
	T_{Emb} (°C)	CoV%	T_{Max} (°C)	CoV%
Conchas Lake Airport, NM	-12.65	4.92%	-27.64	1.77%
Clayton Airport, NM	-21.57	10.10%	-29.72	1.38%
Roundup Top Airport, MT	-13.02	17.33%	-26.06	4.91%
Roundup Bottom Airport, MT	-12.17	0.17%	-23.27	2.52%

The embrittlement temperature of field cores matches with the reported cracking condition of the airfields. Both Conchas and Clayton airfields are paved using Western Canadian Crude asphalt binder. It is seen that T_{EMB} of Conchas samples is much higher than Clayton samples. This can be attributed to the fact that Conchas pavement encountered more severe age hardening, as the pavement appears slightly oxidized already in the field compared to Clayton pavement which was reported to be in good condition. For Roundup samples, as expected, the Roundup Top samples which belong to the newly paved overlay have better T_{EMB} as compared to the Roundup Bottom samples which are from the old pavement. For both Roundup pavement layers, which experience thermal cracking during service life, poor field aged embrittlement temperatures were measured (in the -12 to -13^{o}C range). It is noted that the COV% values for the bottom of the pavement were significantly lower than the top of the pavement, indicating more consistency in the physical properties between core samples for the Roundup bottom samples.

4.4. SUMMARY

An acoustic emission-based test was developed for testing asphalt concrete mixtures. The testing setup for the AE mixture test is similar to the AE binder test. The developed AE-based mixture testing method was implemented to characterize the low temperature behavior of lab-compacted mixture samples from the pooled fund Low Temperature Cracking (LTC) study as well as several lab compacted PG 64-22, PG 70-22, and PG 58-28 asphalt concrete mixtures at different aging levels. Moreover, AE tests were conducted on several field cores and lab compacted samples provided by Asphalt Institute. The key findings are summarized as follows:

- Two important temperatures obtain as outcome of AE mixture test are:
  - ❖ Embrittlement Temperature (T_{EMB}): Temperature corresponding to the first major AE event.
  - ❖ Maximum Energy Event Temperature (T_{MAX}): Temperature corresponding to the event with maximum AE energy.

- The embrittlement temperature of asphalt mixture is an indicator of onset of thermal damage in the material. It is mainly due to formation of local microcracks most probably

at the interface of mastic and aggregates. While embrittlement temperature is due to local micro-scale thermally induced damage, T_{MAX} is due to macro-scale thermally induced cracks within the mastic.

- Investigation to determine the proper thickness of AE asphalt mixture sample showed that the minimum thickness of 40mm is required in order to obtain repeatable and reliable results.

- The proper location to measure temperature of AE mixture sample was determined using three thermocouples located at different locations in the sample. It was observed that initially there was a thermal lag between surface and inside the sample. However, at lower temperatures, below -10^{o}C, the thermal lag is negligible. As a result, the temperature measured at the surface of the sample during AE test, can be considered as the temperature of the whole specimen.

- Both T_{EMB} and T_{MAX} are sensitive to aging level of the mixture; the higher the aging level of the mixture the warmer its T_{EMB} and T_{MAX}. However, T_{EMB} is much more sensitive to aging level of mixture as compared to T_{MAX}.

- The embrittlement temperature of PAV mixtures are couple of degrees lower than the PGLT of that mixture. This may suggest that the Superpave PAV aging procedure doesn't properly represent the long term aging that occurs in the field.

- AE testing results of field cores provided by Asphalt Institute showed that the embrittlement temperatures of field cores match well with the reported cracking condition of the airfields.

CHAPTER 5

IMPLEMENTATION OF AE-BASED MIXTURE TESTING TECHNIQUE TO EVALUATE COOLING CYCLE EFFECTS ON LOW TEMPERATURE CRACKING CHARACTERISTICS OF ASPHALT CONCRETE

5.1. INTRODUCTION

The following investigates the effects of cooling cycles on low-temperature cracking characteristics of asphalt concrete by conducting non-destructive (NDT) evaluation techniques along with advanced asphalt concrete mechanical tests. The Disk-shaped Compact-Tension (DC[T]) test and Indirect Tensile test (IDT), as well as two NDT tests namely: Acoustic Emission (AE) and X-ray computed micro-tomography imaging, were employed to evaluate asphalt concrete's macro and micro-structures during various stages of cyclic cooling.

5.2. EXPERIMENTAL PROCEDURE

The asphalt mixture samples used in this study were obtained from field cores as well as laboratory compacted gyratory samples. The first set of samples consisted of field cores taken from a 50 meter long outdoor testing section located at Advanced Transportation Research Engineering Laboratory (ATREL) in Rantoul, IL. The test section was constructed about three years ago at the ATREL research center mainly to conduct NDT tests on pavements. What makes this test section unique is the absence of mechanical (traffic) loads throughout the pavement's life. This means that there is no load-related distress in the pavement and all existing damage is caused solely by the environment. Asphalt pavement of the test section has been exposed to the environment (snow, rain, hot and cold weather) reacting with the oxygen in the air even at the moderately low temperatures, causing oxidative aging.

A total of six field cores of 200 mm high and 150 mm diameter were extracted from the test section. Figure 5.1 schematically illustrates the test section from which asphalt mixture field cores were extracted. In addition to field cores, three 180 mm high, 150mm diameter lab compacted samples were prepared using loose PG64-22 asphalt mixture from the test section. Loose asphalt mixture was sampled at the time of construction of test section, properly sealed and stored to avoid aging. Lab compacted samples can be considered to have the same aging level as the test section asphalt mixture right after the pavement construction. In order to

fabricate testing samples for mechanical tests, field cores and laboratory samples were sliced into two 50 mm thick cylindrical specimens: one from the top and another one from the bottom of the sample. To avoid possible end-effects, around 10 mm of both sides was trimmed off before slicing the samples as shown in Figure 5.1. Acoustic emission, and X-ray tomography tests as well as DC(T) and IDT tests were performed on both field cores and laboratory samples.

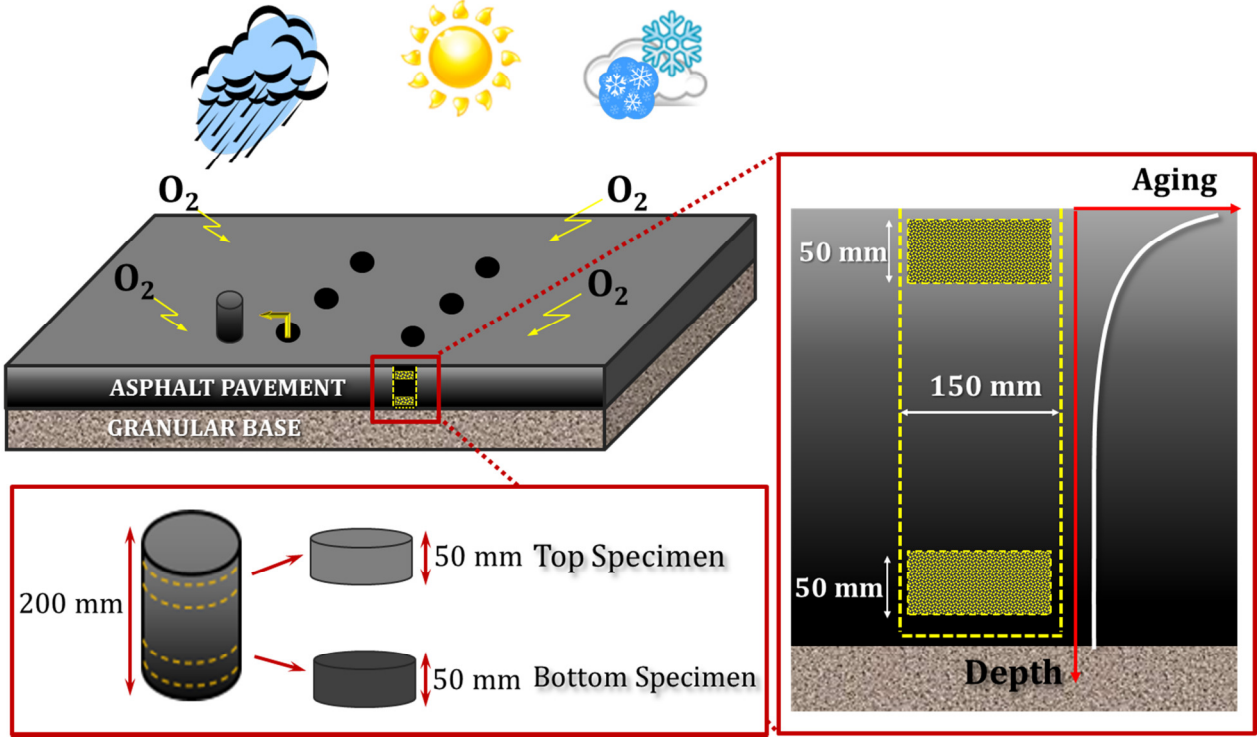

Figure 5.1: Schematic Representation of Test Section and Field Cores

5.3. RESULTS AND DISCUSSION

Brief introduction of applied NDT and mechanical performance tests along with obtained results are presented in the following sections.

5.3.1. Disk-shaped Compact Tension [DC(T)] Test

To evaluate the low-temperature fracture characteristics of asphalt mixture samples, disk-shaped compact tension [DC(T)] tests were performed for all samples in accordance with ASTM D7313 at -12°C, +10°C higher than the PG low temperature grade of the test section asphalt binder (PG64-22) [75].

To investigate effects of cooling cycles on cracking performance of asphalt concrete mixtures, half of laboratory compacted samples were subjected to intense cooling cycle by placing them inside a cooling chamber at -50^{o}C for two hours to induce thermal damage within samples. DC(T) test were performed on both intact and thermally-damaged samples. Obtained fracture energy results are presented in Figure 5.2. DC(T) fracture energy results for both thermally-damaged and intact laboratory samples are shown in Figure 5.2(a). It is observed that the average CMOD fracture energy of thermally damaged samples is about 12% less than the fracture energy of intact samples. This clearly shows the detrimental effect of a severe applied cooling cycle on fracture resistance of asphalt concrete. Reduction in fracture resistance of the asphalt concrete after one intense cooling cycle indicates the presence of thermally induced micro-damages inside the conditioned samples. Figure 5.2(b) compares the fracture energies of top and bottom specimens obtained from field cores. It is seen that the fracture energy of top specimens are lower than the fracture energy of specimens extracted from the bottom of the pavement layer. The average fracture energy of the top specimens is around 306 J/m^2, whereas for the bottom specimens the fracture energy is 362 J/m^2. The observed difference in fracture energies can be associated with the presence of environmentally induced damages in the specimens extracted from the top of the field cores, which negatively affect the fracture cracking resistance of the asphalt mixture.

Figures 5.2(c) and (d) compare CMOD fracture energies of field core samples versus laboratory compacted samples. The average CMOD fracture energy of the bottom field core samples, 362 J/m^2, is very close to that of the intact laboratory samples, 354 J/m^2. This is because field core bottom specimens were not directly exposed to the environment; i.e., they were somehow protected from oxidative aging as well as damaging intense thermal cooling gradients. That's why field cores bottom specimens and intact laboratory samples have the same performance as undamaged test section mixture, i.e., they exhibit similar cracking resistance. Surprisingly, the fracture energies of the field core top samples are close to the samples that were submitted to 1-cooling cycle, which implies that the two hours of intense cooling of the laboratory samples caused more or less the same level of thermally induced micro-damages that exist in the top field core samples.

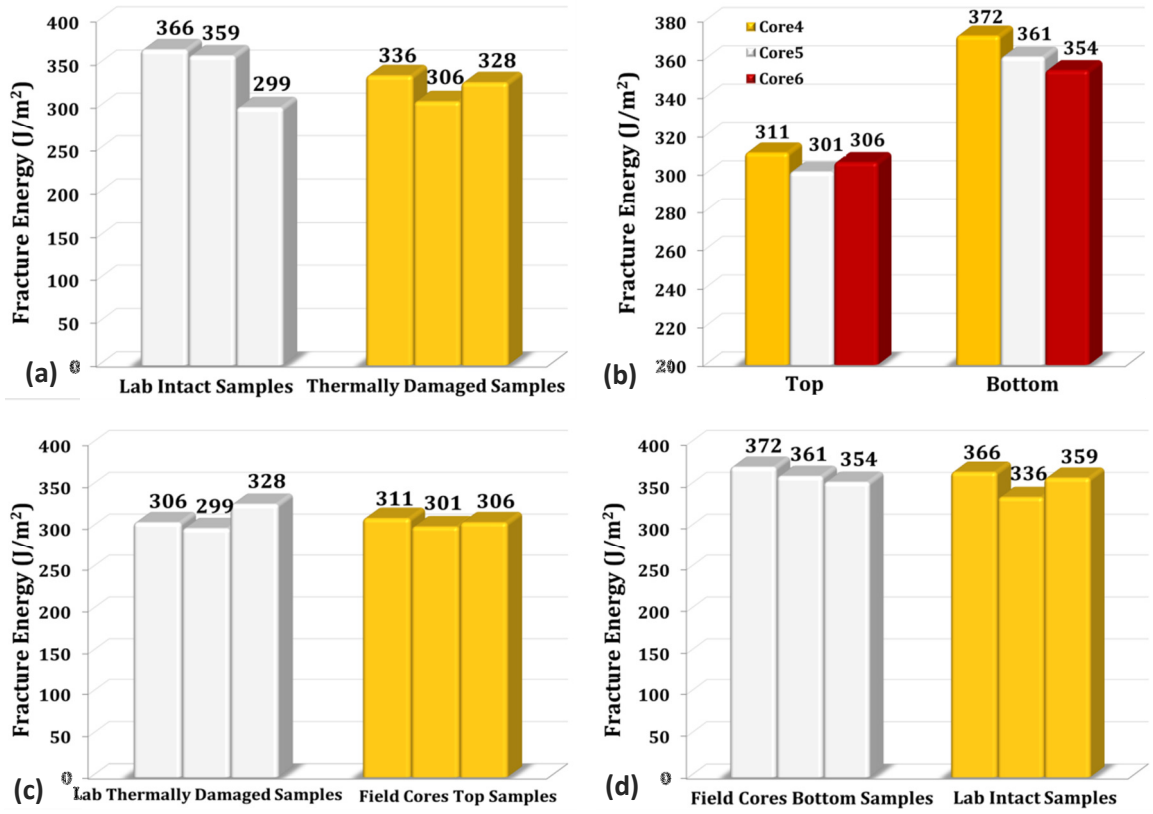

Figure 5.2: DC(T) CMOD Fracture Energy Results for Field Cores and Lab Compacted Samples: (a) Fracture Energies of Thermally Damaged and Intact Lab Specimens; (b) Fracture Energies of Top and Bottom Specimens Extracted from Field Cores; and (c) and (d) Comparison of Fracture Energies of Field Core Samples with Laboratory Compacted Samples.

5.3.2. Indirect Tensile Test (IDT)

Indirect Tensile (IDT) creep test was performed to further investigate the cooling cycle effects on low-temperature cracking performance of the asphalt mixtures. The IDT tests were performed on both laboratory compacted and field cores samples. Testing was conducted in accordance with AASHTO T322 testing procedure utilizing three test replicates [62]. Creep testing was conducted at 0, -10 and -20°C through application of static loading for the duration of 1000 seconds. Creep compliance master-curves were generated through time-temperature superposition. A power-law model was fitted to the master-curves using the fitting function.

The creep compliance results from IDT creep tests are presented in Figure 5.3, which shows the corresponding fitted power-law curves along with the exponential terms from the power-law model (m-value). The m-value represents the ability of the material to relax induced stresses during the relaxation period. The higher the m-value of asphalt concrete, the better its cracking performance. As expected, the aged-hardened field cores (i.e., top samples) had the lowest m-value and creep compliance values, which indicate they are prone to thermal cracking. On the other hand, the other field cores (i.e., from the pavement bottom) samples exhibited the best performance by exhibiting the highest m-values and creep compliance. In the case of laboratory compacted samples, test results followed the same trend; intact, i.e., virgin, samples showed higher m-values and creep compliances as compared to thermally-damaged samples. Interestingly, even though field cores bottom specimens and laboratory compacted intact samples were almost at the same aging level, field cores bottom samples performed better than lab intact samples. This can be linked to better compaction of asphalt concrete in the field which resulted in an asphalt mixture with lower potential for thermal cracking.

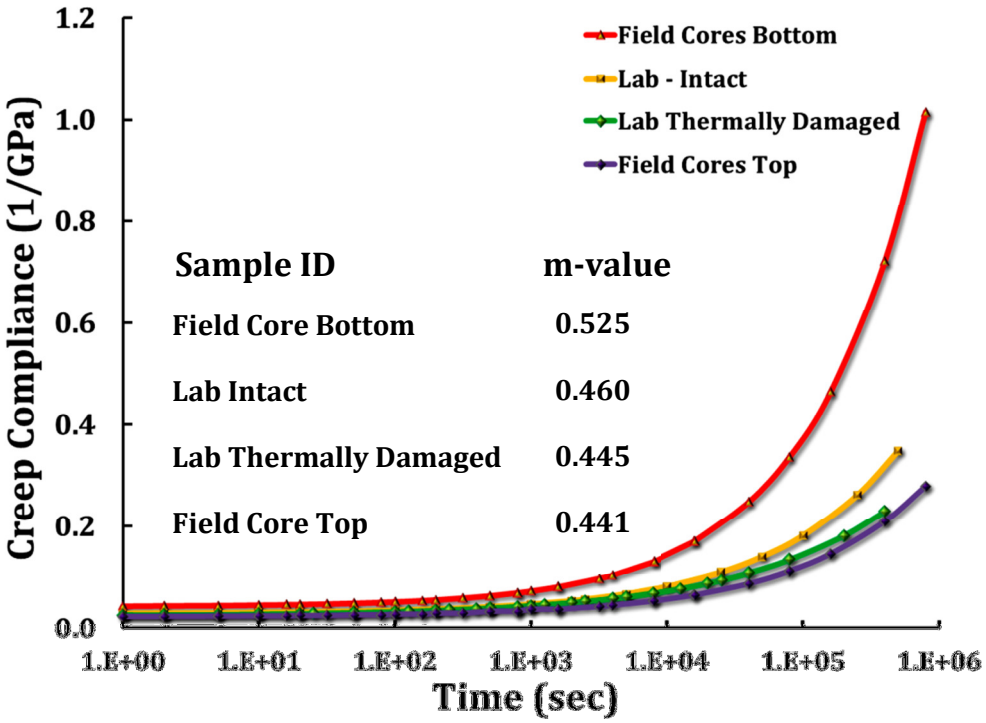

Figure 5.3: Creep Compliance Master-curves from Indirect Tensile Test Results

5.3.3. Acoustic Emission-based Mixture Test

Acoustic emission-based technique for testing asphalt mixtures was employed to detect and assess occurrence of micro-damages in asphalt mixtures due to cooling cycles. Unlike mechanical tests this technique evaluates the material from the micro-scale standpoint.

AE tests were conducted on both lab samples and field cores specimens. Analyses of thermally induced AE activities of asphalt concrete samples were performed on accumulated AE events extracted from AE tests. Temperatures corresponding to the first major high energy event, the embrittlement temperature, as well as total number of AE events counts are presented in the Table 5.1. AE results of laboratory prepared samples show that the first cooling cycle specimens consistently have much warmer embrittlement temperatures, T_A, and significantly higher number of AE events counts as compared to those of the second cooling cycle samples. The main source of AE events of the asphalt concrete samples subjected to cold temperatures is generation of thermally-induced microcracks within samples. During the first cooling cycle, shortly after starting the test, as soon as thermally induced local tensile stresses within the sample exceed the strength of the material, asphalt concrete samples encounter large number of microcracks. Formation of microcracks in the sample generates a large number of AE events, see Table 5.1.

AE asphalt concrete samples sit for 48 hours at room temperature, 20^{o}C, after manufacturing. Due to viscoelastic properties of asphalt concrete (i.e. stress relaxation), stresses induced within asphalt concrete during manufacturing (compaction and cutting) of samples are completely relieved after 48 hours. It seems reasonable to assume that AE samples were in stress-free condition before applying the first cooling cycle. Here, the room temperature is termed as the "*stress-free temperature*", T_C, and it is used as the reference temperature.

Before starting the second cooling cycle, the samples' temperature is raised to stress-free temperature (i.e., thermal unloading) by letting them sit at room temperature, 20^{o}C, for 2 hours. During this period of thermal unloading, a portion of microcracks (perhaps the smaller microcracks) are healed, while the reminder of the microcracks (i.e., the larger microcracks) may need additional time and higher temperatures to heal. During the second cooling cycle, mainly due to the presence of thermally-induced microcracks created during the first cooling cycle, the internal structure of asphalt concrete samples has become softer; yet, because of the indeterminate nature of the microstructure, it is still capable of sustaining an increase in thermal

stresses with lowering the temperature. As a result, it takes lower temperatures (higher in magnitude) to generate new microcracks within the sample. This can be clearly observed in the relative large differences between embrittlement temperatures of sample obtained during the first cooling cycle, T_A, and during the second cooling cycle, T_D. Clearly, the embrittlement temperature obtained during the second cooling cycle is lower than the one obtained during the first cooling cycle. The difference between embrittlement temperatures obtained during the first and second cooling cycles is schematically depicted in Figure 5.4, and reported in Table 5.1.

The observed phenomenon is known as the Felicity Effect. This phenomenon is witnessed during cyclic loading of materials and is defined as the absence of detectable AE activities during reloading of the material until a load level below the previous maximum applied load, in the current case a thermal load. In other words, during reloading process, the material test sample generates AE activity before the previous maximum loading level is reached. The Felicity effect is also schematically illustrated in Figure 5.4, which shows the cumulative AE events counts versus applied thermal load. The loading path from B to C (unloading) and C to D to E (reloading) clearly indicates the absence of AE activity up to a loading level (T_D), which is below the level of the previous loading cycle (T_B). It should be noted that another AE cyclic loading phenomenon known as the Kaiser effect exists. The Kaiser effects occurs when no AE activity happens until the previous maximum load level is reached, which makes the Kaiser effect a particular case of the Felicity effect (i.e., points B and D coincide). When the Kaiser effect is valid indicates that no microcrack healing occurs in the sample. Considering that the adhesive nature of asphalt concrete material depends on the chemical composition and the oxidative aging level of the asphalt mixture, some level of microcracks healing takes place within asphalt concrete during thermal unloading. This means that in thermal cyclic loading of adhesive materials such as asphalt mixtures with high potential of microcrack healing, the Felicity effect is the one that would occur rather than the Kaiser effect.

An important parameter is the Felicity Ratio (FR), which is defined as the ratio of the load at which emissions occur to the previous maximum load. In the present study, it is defined as the ratio of $(T_D - T_C)$ to $(T_B - T_C)$ as shown in equation (5.2). The average Felicity ratio for tested asphalt mixture is around 0.754. To better quantify crack healing of asphalt mixtures, a new parameter called the "*Healing Index*" is introduced and defined by equation (5.3). The Healing

Index is an indication of the amount of healing that occurred in asphalt mixture between the loading cycles over the period of thermal unloading. Depend on the sample temperature (i.e., thermal cycle), type of binder, and presence of moisture, the Healing Index of asphalt mixture ranges from 0% (no healing) to 100% (fully healed). The average Healing Index of the tested samples is around 24.56%, which indicates partial healing of the asphalt concrete mixtures during the rest period between the first and second cooling cycles.

$$FR = \frac{T_D - T_C}{T_B - T_C} \tag{5.2}$$

$$\text{Healing Index (\%)} = 100(1 - \text{FR}) \tag{5.3}$$

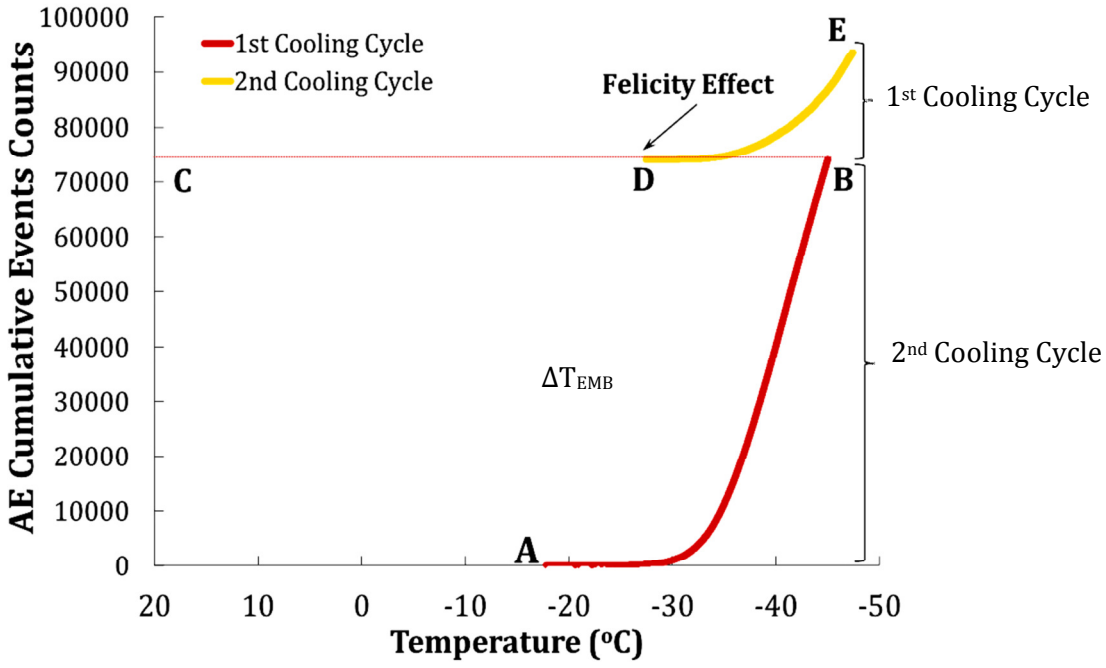

Figure 5.4: Typical AE Test Results of Thermal Cyclic Loading of Lab Samples

TABLE 5.1: AE Test Results of Lab Compacted and Field Samples

Lab Compacted									Field Cores			
Sample ID	Cooling Cycle#	AE Events Counts	T_A (^oC)	T_B (^oC)	T_D (^oC)	T_C (^oC)	FR= $(T_D-T_C)/(T_B-T_C)$	Healing Index	Sample ID		AE Events Counts	T_A(^oC)
Lab S1	1st	108000	-14.98	-46.80	-30.20	20.00	0.751	24.85%	Field S1	Top	23500	-11.13
	2nd	331								Bottom	74200	-14.69
Lab S2	1st	110500	-16.13	-46.20	-28.80	20.00	0.737	26.28%	Field S2	Top	26100	-10.04
	2nd	489								Bottom	61600	-12.83
Lab S3	1st	98100	-14.02	-45.90	-29.30	20.00	0.748	25.19%	Field S3	Top	24700	-11.36
	2nd	201								Bottom	72500	-13.54
Lab S4	1st	117400	-16.99	-46.30	-32.30	20.00	0.789	21.12%	Field S4	Top	20400	-10.32
	2nd	250								Bottom	67200	-15.97
Lab S5	1st	91700	-13.24	-45.90	-30.80	20.00	0.771	22.91%	Field S5	Top	23900	-12.27
	2nd	352								Bottom	70100	-14.99
Lab S6	1st	101300	-14.71	-45.50	-27.80	20.00	0.730	27.02%	Field S6	Top	27300	-11.48
	2nd	518								Bottom	77400	-13.72

The acoustic emission test results of the field core specimens show that the bottom field cores specimens have higher number of AE events counts as compared to the top samples. Similar to the laboratory compacted samples, this can be linked to presence of thermally induced damages in the already age-hardened top specimens due to exposure to the environment and severe thermal gradients. Another important observation regarding field cores is that the embrittlement temperatures (T_A) of the top samples are warmer than those of bottom samples. Oxidative aging of top samples lowers their thermal cracking resistance as it is also observed in DC(T) test results, see Figure 5.2. When subjected to cold temperature, the aged-hardened top samples develop microcracks at warmer temperatures than the bottom samples.

Comparison of AE events counts of the second cooling cycle of laboratory samples and the field cores top specimens is very interesting. Even though both have encountered thermally-induced damages, surprisingly the field cores top samples have higher number of AE event counts as compared to the second cooling cycle samples. The average cumulative AE event counts of field core top specimens is around 24000 while for the second cooling cycle samples the cumulative

AE events counts is only 356. This can be attributed to the healing mechanisms (adhesive healing at the asphalt-aggregate interface and cohesive healing within asphalt mastic), which occurs in the field core top samples. The second cooling cycle was conducted shortly after the first cooling cycle; as a result, laboratory samples didn't have enough time for the healing mechanism to occur to the same extent as the field core tope samples. After being severely thermally-damaged during the winter, the field core top samples had enough time for the healing mechanism to occur and to reduce the micro-damages in the pavement especially during the summer months.

5.3.4. X-ray Computed Micro-Tomography Imaging

Asphalt mixtures have a complex heterogeneous microstructure. The macro properties of asphalt mixtures strongly depend on their microstructure. X-ray Computed micro-Tomography (micro-CT) technique is a powerful tool for acquiring the internal microstructure of heterogeneous materials. It is a nondestructive evaluation technique for microscopic visualization of interior features within materials and for obtaining digital information on their 3-D geometries and properties. Tomography refers to the cross-sectional imaging of an object from either transmission or reflection data collected by illuminating the object from many different directions [76]. In X-ray micro-CT device, X-rays were sent at different angles through a rotating specimen, collected through a flat-panel detector, and a computer was used to reconstruct a 3D image of the sample's interior [77], see Figure 5.5. Using X-ray micro-CT, s numerous images of the cross-section of asphalt concrete specimens were collected. Each image has several levels of gray intensity corresponding to different densities of the materials and X-ray attenuation in the material. Attenuation is mainly a function of X-ray energy and the density and composition of the material being imaged.

In the current study, X-ray micro-CT was employed to quantitatively visualize the cooling cycle effects on asphalt mixture. Cubic samples of 1 inch on-the-side were prepared from intact, i.e., virgin, compacted lab samples utilized as testing specimens. To investigate the cooling cycle effects on asphalt mixture microstructure, X-ray micro-CT conducted on samples before and after conditioning samples at -50^{o}C for 2 hours. Figure 5.6 depicts sectional images of both undamaged and thermally-damaged mixtures. Thermally-induced damage, circled in red, are

easily detectable by comparing high resolution images before and after conditioning the sample. There are two main types of micro-damages observed: thermal microcracking inside the asphalt mastic and thermally-induced debonding between aggregate and asphalt mastic. Debonding at the interface happens due to differential thermal contraction between aggregates and asphalt mastic. Thermal microcracking of the asphalt mastic results primarily from a combination of asphalt mastic brittleness and the action of the thermally-induced tensile stresses within the material. The size of the thermal microcracks was measured using Amira ® software for all samples. Measurements show that thermally-induced microcracks have the average width and length of approximately 30µm and 350µm, respectively, see Figure 5.7. As mentioned earlier during the discussion of the DC(T) and IDT tests results, the presence of these microcracks affects macro properties of asphalt concrete mixtures such as fracture characteristics and stress relaxation ability (m-value) of the material.

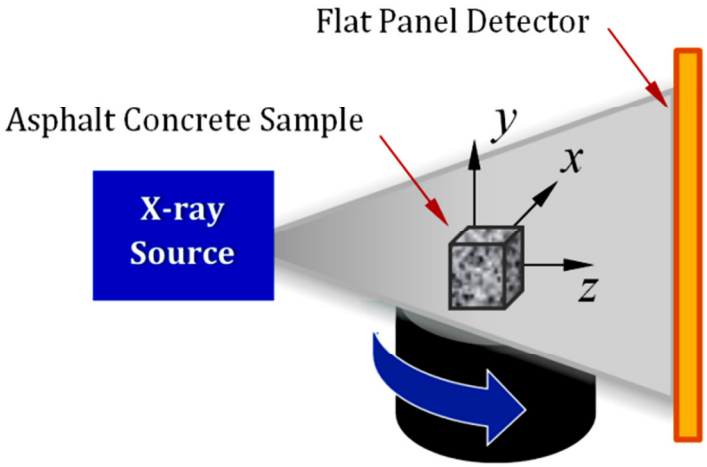

Figure 5.5: Schematic Illustration of X-ray Apparatus [16].

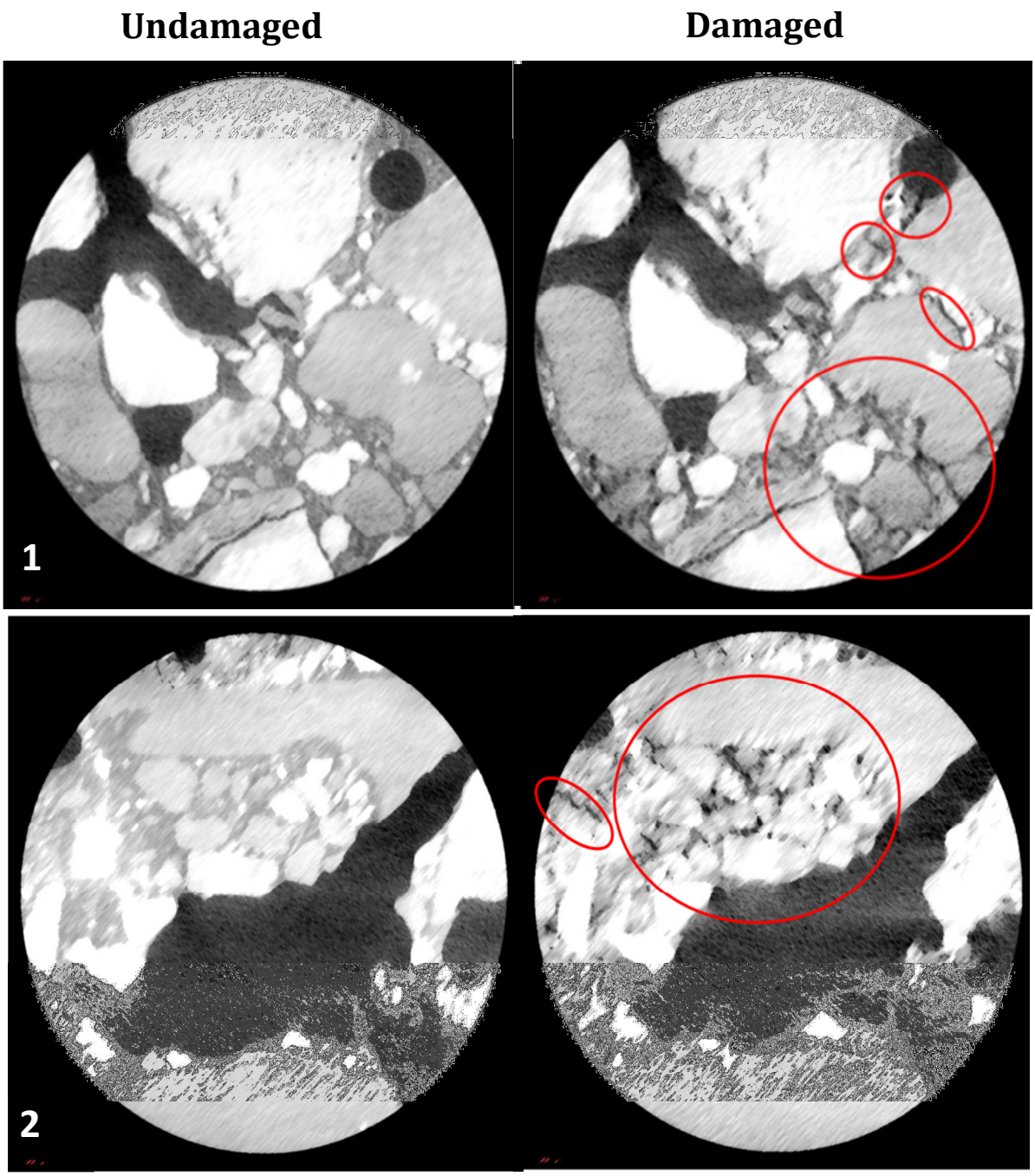

Figure 5.6: X-ray Micro-CT Images of Intact vs Thermally Damaged Samples

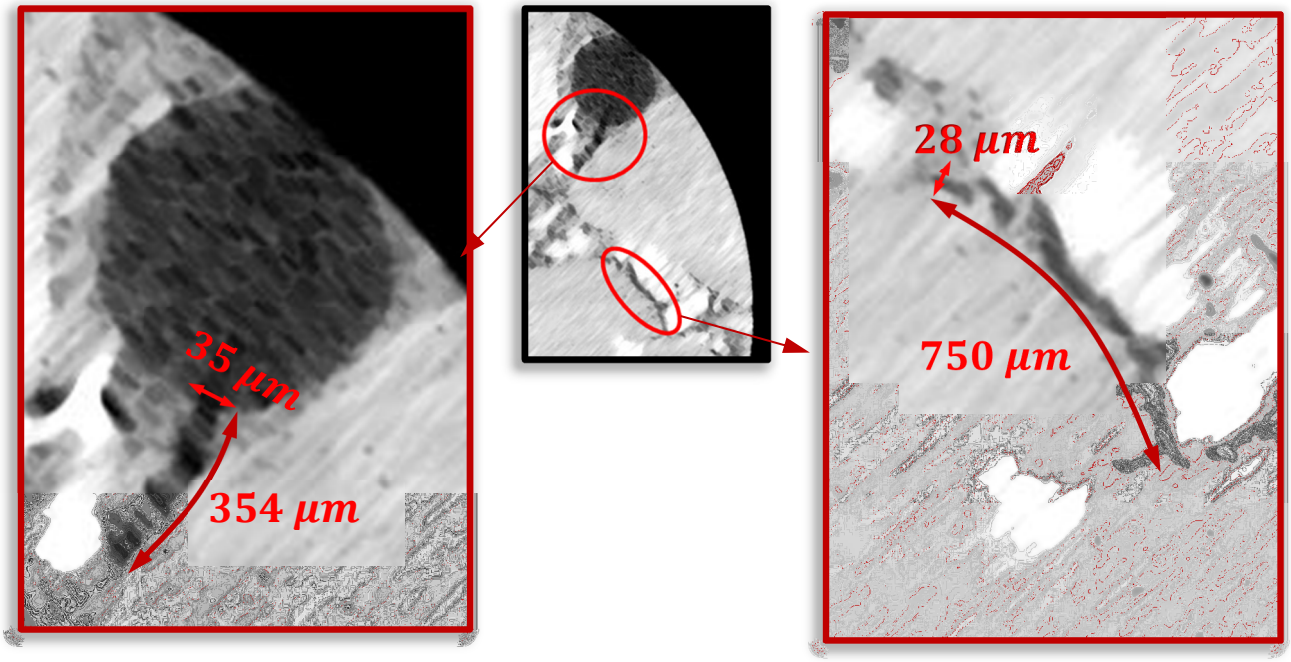

Figure 5.7: Size of Thermally Induced Damages in the Mixture

5. 4. SUMMARY

In the preceding sections, effects of cooling cycles on low temperature cracking behavior of asphalt mixtures was investigated. Two mechanical performance tests namely, DC(T) and IDT, along with two NDT tests namely, acoustic emission (AE) and X-ray micro-CT tests were conducted on field cores and laboratory compacted samples.. Based on laboratory testing results, the following conclusions can be drawn regarding the low-temperature cracking performance of asphalt concrete mixtures:

- DC(T) test results showed that surface specimens from field cores and thermally damaged laboratory samples had lower fracture energies than bottom samples obtained from field cores and intact laboratory specimens, respectively. Results shows that fracture energy measurements from DC(T) test are sensitive to the presence of thermally induced micro-damage inside the asphalt concrete and capable of capturing the effects of cooling cycles on the low-temperature cracking performance of asphalt pavements.

- The trend observed in the DC(T) test was also observed in the IDT test as thermally damaged both laboratory and field cores specimens had lower m-value as compared to intact ones. This indicates a lower rate of stress relaxation as well as higher potential for thermal cracking. In addition, field cores bottom samples exhibited the best performance in terms of thermally induced stress relaxation.

- Microscopic visualization of microstructure of the mixture was performed using X-ray micro-CT. Thermally induced micro-damage was detected and dimensions of microcracks and debonded interfaces were measured in the high resolution images obtained. These micro-cracks and aggregate-mastic debonding zones appear to be the source of the changes in the macro properties of the mixture namely: fracture energy, m-value, and the source of AE events measured in the new test device.

- One important difference between the AE technique and mechanical bulk and fracture testing is the response scale within the material. In the case of mechanical tests, the mechanical test results are a measure of the response of the whole specimen (as a structure) and thus it is difficult to extract local properties, while the AE procedure yields results that are at the local scale of the material response. Both mechanical tests and AE techniques are recommended for complete evaluation of cracking resistance of pavement mixtures.

- AE test results were consistent with DC(T) and ID(T) results. In general it was observed that thermally-induced damage from intense cooling cycles negatively affect the low temperature characteristics of asphalt concrete mixtures.

- The acoustic emission testing technique appears to be a viable approach for evaluating the cooling cycle effects on internal structure of the mixtures. It can assess the extent of thermally induced damages inside asphalt concrete mixtures.

CHAPTER 6
APPLICATION OF ACOUSTIC EMISSION TECHNIQUE IN ASSESSING AGING OF ASPHALT CONCRETE MIXTURE

6.1. INTRODUCTION

Cracks in asphalt pavements are expensive and difficult to properly treat. They drastically affect asphalt pavement life span, rideability, and lead to millions of dollars of repair and maintenance annually. If left untreated, cracks deteriorate and widen over time, allowing moisture to readily infiltrate the pavement system. Cracks enable water and oxygen to enter the pavement, which can lead to severe pavement damage over time. Oxidative aging has long been recognized as an important contributing factor to cracking of asphalt pavements. As the asphalt concrete is subjected to conditions in the field, it continuously becomes oxidized, leading to material embrittlement with time. Figure 6.1 illustrates two pictures of a pavement section: the left one was taken immediately after the construction, and the right one was taken after nineteen months [27]. Comparing the two pavement conditions clearly reveals the difference in pavement surface, texture, and color. These differences are the result of aging and climatic weathering. Aged pavements are stiffer, more brittle, and relieve stresses much slower than new pavements. In addition, crack healing in aged pavements is slower, accumulating damage more quickly [78].

Figure 6.1: Pavement Section at the University of Illinois' Advance Testing and Research Engineering Laboratory (ATREL) right after the construction and 19 months after construction [27].

The amount of aging varies significantly depending upon chemical composition (e.g. crude source, refining techniques, and additives), environmental factors, and characteristics of the mixture (e.g. asphalt content, air voids) [79-81]. The preventive maintenance of pavements is one important aspect of pavement preservation that is usually overlooked. Preservation entails repairing distresses in the pavement at very early stages as they begin to occur. One of the great challenges for the pavement engineer is determining when a pavement has become vulnerable to cracking. Currently, pavement engineers lack practical tools to determine the proper time for preventive maintenance. Maintenance can entail the application of a surface treatment or a more substantial rehabilitation, such as pavement milling and resurfacing. Accurate evaluation of aging effects of asphalt concrete could greatly benefit pavement engineers in determining the critical time for applying preventive maintenance measures to extend the pavement life.

The primary goal of this study is to assess laboratory induced oxidative aging of asphalt concrete mixtures. Acoustic emission and ultrasonic tests were conducted on asphalt concrete mixtures at different aging levels ranging from 0 to 72 hours of laboratory aging. The acoustic emission and ultrasonic test results both showed that the internal structure of asphalt mixtures improves with the increase in aging time until it reaches a peak and then continues to deteriorate with further aging. The observed trend is consistent with disk-shaped compact tension (DC[T]) fracture test results reported by Braham et al [82].

6.2. EXPERIMENTAL PROCEDURES

Nine asphalt concrete specimens with the same mix design were prepared following Superpave guidelines. A 19 mm nominal maximum aggregate size (NMAS) with a target asphalt content of 5.9% by weight of the total mixture was selected for this study. The PG 64-22 binder was utilized as the base binder. The aggregate blend consisted of aggregates from four different stockpiles: coarse (CM16), fine (FM20, FM02), and mineral filler (MF). The blend percentages are summarized in Table 6.1.

TABLE 6.1: Aggregate Blend Percentages

Aggregate Type	Blend Percentage (%)
CM16	65.3
FM20	23
FM02	10.5
Mineral Filler	1.2

Mixing of the asphalt concrete mixtures was conducted at 155°C using a standard bucket mixing procedure. The uncompacted loose asphalt concrete mixtures were laboratory aged for 0, 12, 24, 28, 32, 36, 48, 60 and 72 hours at 135°C. Laboratory aging of the asphalt mixtures was performed by placing loose mixtures in the force draft oven (at 135°C) for the appropriate amount of time (0 – 72 hours). To ensure uniform aging throughout the sample, the mixtures were hand-stirred every 12 hours. Once aged, the mixtures were compacted at 135°C using a servo-controlled gyratory compactor (IPC Servopac). The compacted gyratory specimens were then cut to obtain four AE samples as well as two 40 x 70 x 135 mm^3 rectangular specimens for ultrasonic velocity and attenuation measurements, and four half-moon 60mm thick samples, which were used to evaluate the AE response of samples during thermal cooling. Figure 6.2 shows the specimens geometry and nominal dimensions. During sample preparation, the last 5 mm of each side of the compacted samples was trimmed off to avoid the end-effects induced during compaction and to obtain a smooth surface for sensor placement.

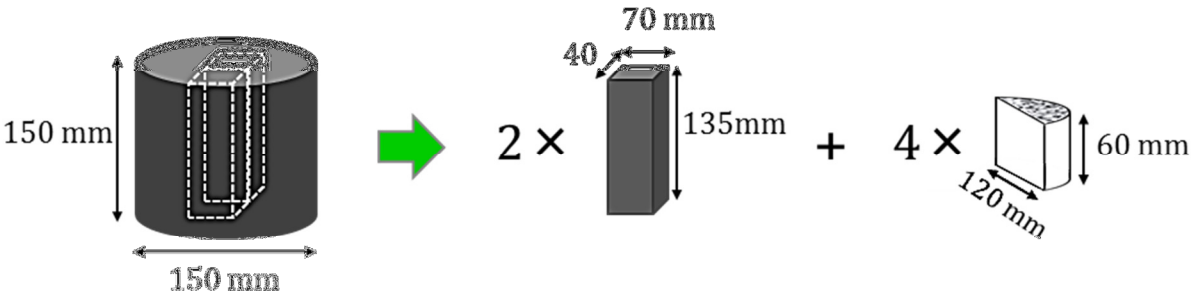

Figure 6.2: Preparation of AE and Acoustic Ultrasonic Tests Samples along with their Dimensions

6.3. RESULTS AND DISCUSSIONS

Acoustic emission-based testing was carried out for all asphalt concrete mixtures at different aging levels ranging from 0 to 72 hours. Temperatures corresponding to the first major event (embrittlement temperature) as well as the total number of AE events counts are presented in the Table 6.2. The embrittlement temperature of asphalt mixtures versus aging time is shown in Figure 6.3(a). The results reveal that embrittlement temperature increases with aging time; the higher the aging time, the warmer the onset of the thermally-induced microdamages in the asphalt concrete samples. This can be linked to the age-hardening effect of oven aging, which makes asphalt mixtures brittle and prone to cracking. The rate of change of embrittlement temperature with respect to aging time is shown in Figure 6.3(b). It is observed that initially the average rate of change of T_{EMB} versus aging time gradually increases from 0 to 24 hours of aging time, followed by significant increase in this value from 24 to 36 hours. After approximately 36 hours of aging time, average rate of change of T_{EMB} versus aging time drops drastically. This leads to a plateau in the T_{EMB} versus aging time plot at longer aging times which indicates aging beyond 36 hours does not have a significant effect on the cracking resistance of asphalt mixtures. In other words, 36 hours of oven aging appears to be a threshold up to which a majority of aging occurs. Furthermore, the significant amount of aging that occurs after 24 hours of aging time suggests that the aging level equivalent to 24 hours of oven aging can be considered as the critical point beyond which deterioration of pavement accelerates significantly.

Figure 6.4 illustrates the total number of AE events counts versus laboratory aging times. Results show that the number of AE events counts increases until 12 hours aging and then decreases for longer aging periods. Explaining the observed phenomenon requires an understanding of the aging effects on internal structure of the asphalt concrete mixtures. As a heterogeneous material, the internal structure of the asphalt concrete is influenced by the quality of asphalt mastic interparticle bonds as well as quality of bonds between aggregates and asphalt mastic. Figure 6.5 schematically depicts thermally induced stresses between mastic and aggregates along with the adhesive bonds between particles of asphalt mastic.

TABLE 6.2: Acoustic Emissions Test Results (Number of AE Events Counts and Embrittlement Temperature and Temperature)

Aging Time (hrs)	Rep #	Number of AE Events Counts			T_{Emb} (^oC)		
		N_{AE}	Average	CoV%	T_{Emb} (^oC)	Average	CoV%
0	#1	44196	43836	4.29%	-24.18	-25.18	6.99%
	#2	41593			-27.31		
	#3	43424			-25.87		
	#4	46129			-23.37		
12	#1	134550	116287	11.76%	-25.41	-24.08	4.90%
	#2	118841			-23.01		
	#3	107414			-24.72		
	#4	104342			-23.16		
24	#1	89850	98250	13.97%	-22.92	-23.36	7.33%
	#2	106400			-24.85		
	#3	113000			-21.13		
	#4	83750			-24.55		
28	#1	99820	82120	15.38%	-23.12	-22.47	6.25%
	#2	81250			-22.07		
	#3	70310			-23.98		
	#4	77100			-20.72		
32	#1	73800	61200	17.03%	-21.69	-20.28	10.33%
	#2	57100			-22.39		
	#3	49400			-19.01		
	#4	64500			-18.02		
36	#1	20002	25393	22.16%	-15.46	-15.23	9.09%
	#2	31692			-14.23		
	#3	28535			-17.09		
	#4	21344			-14.12		
48	#1	5381	5765	23.94%	-13.69	-14.19	4.06%
	#2	7402			-14.79		
	#3	6162			-13.70		
	#4	4113			-14.57		
60	#1	147	145	27.18%	-12.83	-13.89	10.48%
	#2	200			-15.19		
	#3	118			-15.09		
	#4	115			-12.44		
72	#1	138	98	34.32%	-11.12	-14.06	14.98%
	#2	91			-15.96		
	#3	107			-14.07		
	#4	57			-15.09		

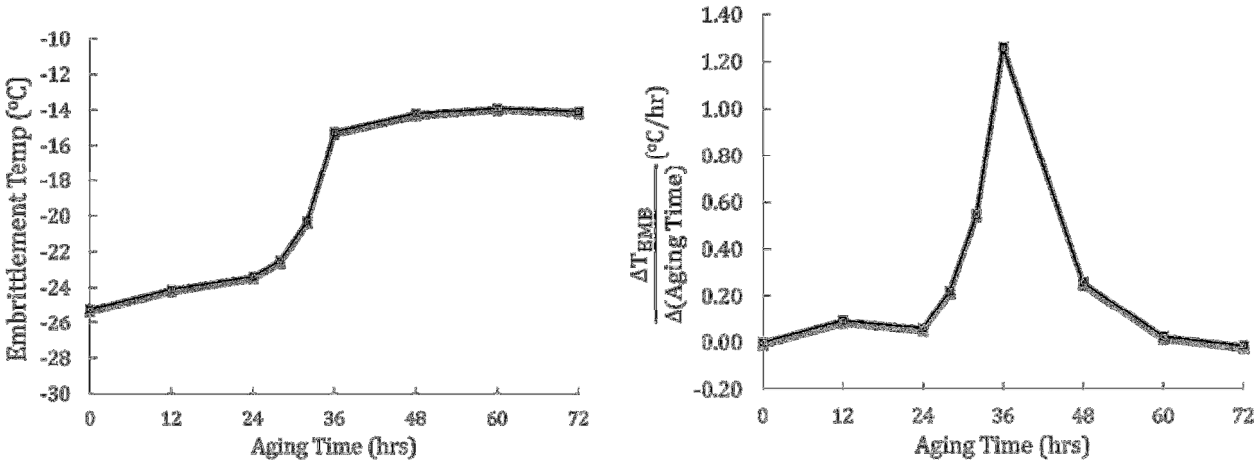

Figure 6.3:(a) The embrittlement temperature vs aging time plot (b) The average rate of change of embrittlement temperature vs aging time plot

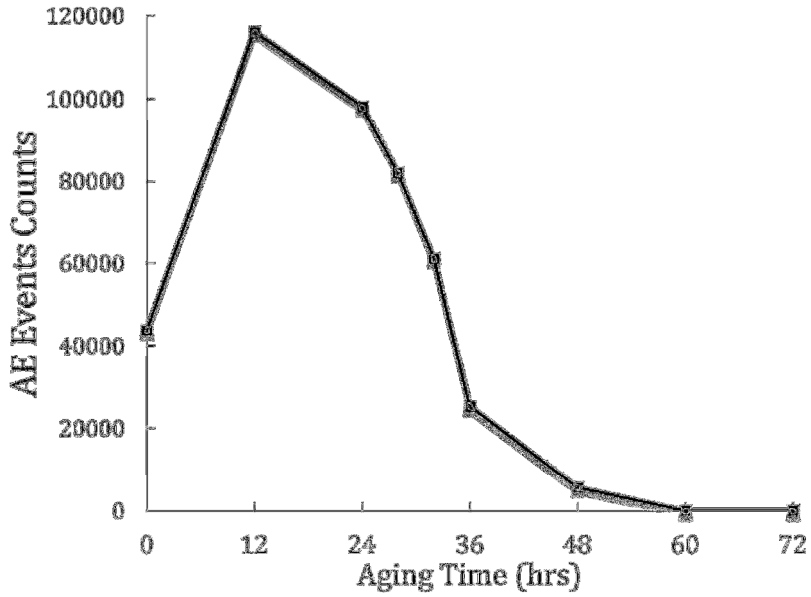

Figure 6.4: AE Events Counts vs Aging Time

The behavior of the oven-aged asphalt concrete is significantly influenced by two factors which counteract each other. These two factors are increase in stiffness and decrease in adhesion of asphalt mastic with increase in aging. Laboratory aging of loose asphalt mixtures increases the stiffness of the asphalt mastic while reducing its adhesive properties. Initially, at early stages of aging the positive effects of the increase in mastic stiffness overcome the negative effects of reduction in adhesion of asphalt mastic. As a result, short-term aged compacted samples appear to have stronger internal structure compared to virgin asphalt concrete samples. However, at

longer aging times, the deteriorating effects resulting from reduction in mastic adhesion overcome the advantageous effects of increase in mastic stiffness. This loss in mastic adhesion properties leads to weaker bonds between mastic and aggregates as well as weaker bonder between mastic particles, which leads to a weaker internal structure of the composite. This manifests itself as a significant reduction in number of detectable AE events in the aged asphalt concrete samples.

Source of AE events is generation of thermally-induced microcracks resulting primarily from breaking asphalt mastic interparticle bonds as well as bonds between asphalt mastic particles and aggregate. When compacted, less adhesive aged loose asphalt mixtures result in asphalt concrete samples with poor mastic interparticle bonds. The interparticle bonds in aged samples are not as strong as less aged mixtures. Microcracks resulted from breaking of strong bonds produce higher energy AE signals, while AE signal resulted from breaking of poor bonds are comparatively low level energy signals. In case of highly aged mixtures, for example 60 and 72 hours of aging, the quality of bonds are extremely poor. As a result, emitted AE waves are so weak, that they are not detectable by AE sensor. This explains significant drop in number of AE events counts at high aging levels.

Figure 6.4 shows that aging initially improves the internal structure in the asphalt concrete sample, as the 12 hours aging samples exhibit higher AE activities than virgin samples. When aging time exceeds 12 hours, a drastic drop in the AE event counts occurs, which indicates weakening in the internal structure of the samples. These AE test results are consistent with disk-shaped compact tension (DC[T]) fracture test results reported by Braham et al. In their study, the uncompacted samples were aged for 4, 6, 8, 12, 24, 36, and 48 hours at 135°C, compacted, and tested using the DC(T) test. The DC(T) was performed to evaluate the fracture cracking resistance of mixtures. Figure 6.6, which is reproduced after Braham et al, contains the fracture energies of the asphalt concrete samples at different aging levels. The DC(T) results are consistent with the trend observed in AE testing, i.e., the fracture energy of each asphalt mixture increases with an increase in aging until it reaches a peak and then decreases with increasing aging. This indicates that aging initially improves the internal structure of samples which leads to increase in fracture energy. At longer aging times, aging reduces the fracture resistance of the asphalt concrete, allowing cracks to propagate readily.

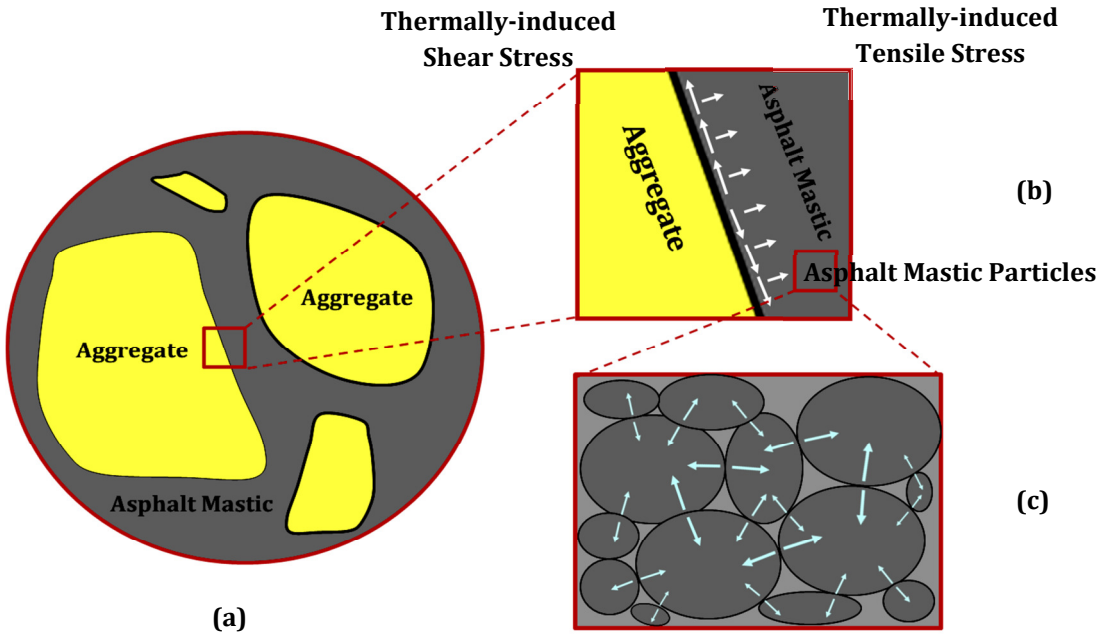

Figure 6.5:(a) Schematic representation of asphalt concrete as a heterogeneous material composed of aggregates and asphalt mastic (b) Thermally induced tensile and shear stresses inside mastic at the interface of asphalt mastic and aggregate (c) Asphalt mastic thermally-induced interparticle interactions

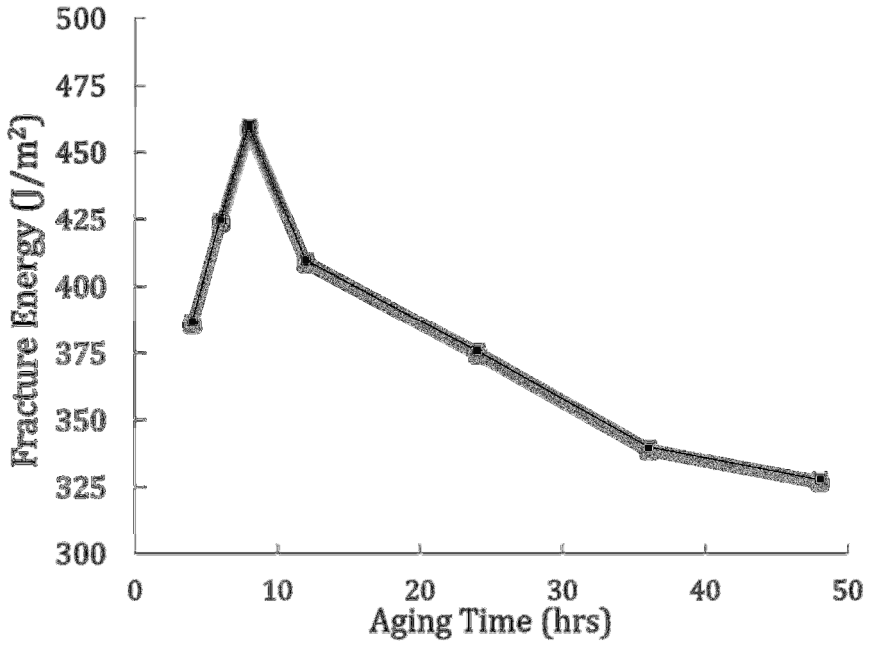

Figure 6.6: Oven Aging Effects on Fracture Energy of Asphalt Concrete [82]

6.4. SUMMARY

The main objective of this chapter was to explore the laboratory aging effects on asphalt concrete mixtures. Nine asphalt concrete specimens with the same mix design were prepared at different aging levels ranging from 0 to 72 hours. Acoustic emission-based mixture test was utilized to investigate age-related changes in asphalt concrete. Obtained results were compared against mechanical testing results reported by Braham et al. Based on the laboratory testing results of the mixtures studied herein, the following conclusions can be drawn:

- The embrittlement temperature (T_{EMB}) of asphalt concrete mixtures progressively increases with aging time. This can be attributed to age-hardening effect of oven aging, which makes asphalt mixtures brittle and prone to cracking.

- The average rate of change of embrittlement temperature with respect to aging time is not constant. There is a significant increase in T_{EMB} when the aging time exceeds 24 hours.

- Based on the limited laboratory testing results, 24 hours of laboratory aging appears to be the critical point beyond which deterioration of pavement accelerates drastically. The field aging time equivalent to 24 hours of intense laboratory oven aging seems to be a proper time to apply the preventive pavement maintenance.

- Unlike the general idea that aging always weakens the internal structure of the material, this study has shown that oxidative aging initially improves the internal structure of asphalt mixtures, beyond which it begins to deteriorate the structure. The same trend was observed in DC(T) fracture testing of aged asphalt mixtures.

CHAPTER 7
USING ACOUSTIC EMISSION TECHNIQUE TO INVESTIGATE EFFECTS OF RECYCLED ASPHALT PAVEMENT (RAP) AMOUNTS ON LOW TEMPERATURE CRACKING PERFORMANCE OF ASPHALT MIXTURES

7.1. INTRODUCTION

Reclaimed asphalt pavement (RAP) is the most frequently used by-product in hot mix asphalt (HMA), and the most recycled material in the US. The recycling of pavement materials has proven to be an economical and feasible process to rehabilitate old pavements. The economic benefits from utilizing RAP materials can provide a great boost to the highway industry by freeing funds for additional highway construction, rehabilitation, preservation or maintenance. In recent years there has also been a stronger incentive in favor of recycling based on the concern for the environment and sustainability. The general public is becoming more aware of the need to conserve natural resources through recycling. RAP usage can result in sustainable development and cost savings by reducing the amount of virgin materials required in the production of the new asphalt mixture [83].

These benefits notwithstanding, excessive amounts of RAP in the mixture can have detrimental effects on pavement performance. Xiao et al. [84] reported that inclusion of 15% RAP results in significant increase in stiffness of the mixture. In recent years, as asphalt prices have continued to escalate, a great deal of interest has been focused on the utilization of higher contents of RAP. Currently, RAP utilization varies considerably across the United States, but the average RAP content in asphalt mixtures is estimated to be around 15% [85].

The belief that pavements constructed with RAP materials are more prone to cracking than virgin mixtures is generally attributed to stiffening and embrittlement effects induced by attempting to combine weathered, age-hardened materials to virgin materials. A careful RAP mixture design will achieve proper binder stiffness by considering the aged binder stiffness, virgin binder stiffness, and the proportions of these two binder components to be present in the final blend. Extensive research has been directed towards characterization of low temperature properties of pavements containing RAP [83].

The present study employs acoustic emission method to explore the effects of RAP amounts on the low temperature fracture properties of asphalt mixtures. Study of the low temperature fracture properties of HMA with RAP is conducted in the context of five RAP levels and two virgin binder sources. RAP levels of 10, 20, 30, 40 and 50% are studied with PG 64-22 and PG 58-28 virgin binders. Disk-shaped Compact Tension [DC(T)] fracture testing was conducted to determine the fracture energy of the mixtures. In addition to DC(T) test, the Superpave Indirect Tension Test (IDT) was conducted on HMA specimens containing 20% and 40% RAP.

7.2. EXPERIMENTAL PROCEDURE

The main goal of this study was to employ the AE-based mixture testing technique to investigate the effects of RAP amounts on low temperature performance of asphalt pavements. To accomplish this goal, RAP material obtained from a portion of Interstate 72 (I-72) located in the western portion of Illinois in a previous study was selected [83]. Incomplete records were available to assess the original design and materials associated with this RAP material, and thus, forensic testing was conducted. Extraction and recovery of asphalt binder was performed on RAP samples in accordance with the AASHTO T319 test procedure to determine the RAP binder content along with evaluating the rheological properties of the extracted RAP binder. Recovered binders were tested to determine the complex modulus using the Dynamic Shear Rheometer [DSR] as per recommendations of the Superpave specified procedure (AASHTO T315-03) for testing of short term aged (RTFO aged) asphalt binder. According to DSR test results at 64°C, for the provided RAP samples, the complex modulus, phase angle and rutting parameter of RAP binder are as following: G*=94.03 kPa, δ=66.60°, G*/sin(δ)=102.49 kPa. In addition, from extraction testing results, RAP binder content was determined as 3.91%. RAP binder extraction produced a clean aggregate sample that was used to determine the RAP aggregate gradation using the AASHTO T27-88 procedure (*8*). Figure 7.1(a) and 1(b) show RAP materials before binder extraction and the clean aggregate byproduct or residue from the binder extraction, respectively. Sieve analysis was also conducted to determine RAP aggregate gradations.

(a)

(b)

Figure7.1: (a) RAP Material; (b) Extracted RAP Aggregate

Asphalt mixtures with 19 mm nominal maximum aggregate size mixtures with a target asphalt content of 5.9% and RAP amounts ranging from 0% to 50% by weight of total mixture formed the basis of the experimental design for this study. Mixing was performed at 155°C using a standard bucket mixing procedure. Details regarding the amount of RAP and virgin constituents are presented in Table 7.1. Various mixtures in this study are indicated using the naming system that shows the virgin asphalt binder grade as well as the amount of RAP. For example, "64-20%" represents asphalt mixture manufactured with PG 64-22 virgin binder and consisting of 20% RAP by total weight of the mix.

In order to evaluate the low temperature fracture characteristics of RAP mixtures, disk-shaped compact tension [DC(T)] tests were performed in accordance with ASTM D7313-07 for all mixtures at -12°C (*9*). In addition, low temperature performance of these mixtures was further investigated using indirect tensile (IDT) creep tests. IDT tests were performed on mixtures containing 20% and 40% RAP. Testing was conducted in accordance with AASHTO T322 test procedure utilizing three test replicates [62]. Creep testing was conducted at 0, -10 and -20°C through application of static load for 1000 second durations. Creep compliance master-curves were produced through time-temperature superposition. Finally AE-based testing method was conducted on all mixture samples to determine the embrittlement temperature of mixtures with different amounts of RAP.

TABLE 7.1: Mix Design for RAP Mixtures

Mix Type (64 = PG 64-22; 58 = PG 58-28)	Binder Content of RAP (%)	Mass of Constituents in the Mixture (gm) (Total batch weight = 5000 gm)			
		RAP Binder	RAP Aggregate	Virgin Binder	Virgin Aggregates
64-0% / 58-0%	3.91	0.0	0.0	295.0	4705.0
64-10% / 58-10%	3.91	19.6	480.5	275.5	4224.6
64-20% / 58-20%	3.91	39.1	960.9	255.9	3744.1
64-30% / 58-30%	3.91	58.7	1441.4	236.4	3263.7
64-40% / 58-40%	3.91	78.2	1921.8	216.8	2783.2
64-50% / 58-50%	3.91	97.8	2402.3	197.3	2302.8

7.3. RESULTS AND DISCUSSION

Fracture energies of mixtures containing RAP along with control (virgin) mixtures were determined using the DC(T) fracture test. Results obtained for mixtures containing PG 58-28 and PG 64-22 as the virgin binder are summarized in Figures 7.2(a) and 7.2(b), respectively. For mixtures using PG 58-28 as the virgin binder, adding RAP reduces the fracture energy of the material; the fracture energy is drastically reduced when the RAP amount exceeds 10%. For example, going from 10% to 20% RAP, a drop of 59% in fracture energy is observed. For RAP amounts greater than 20%, there is minor reduction in the fracture energies. Note that the amount of change of average fracture energies for RAP amounts greater than 20% is within the range of experimental error. In the case of PG 64-22 mixtures, the fracture energy initially increases with an increased amount of RAP. The increase is noticed up to 30% RAP; thereafter, it reduces with increase in RAP amount. This type of trend was observed previously by Braham

et al. (*12*) in the study of aging effects on fracture energy. In their work, the fracture energies of asphalt mixtures increased with an increase in aging levels until it reached a peak and then was noted to drop with further aging. The study by Braham et al. utilized different aging procedures; when using AASHTO R30 procedure, the results for all asphalt mixtures provided high fracture energies when compared to unaged mixtures. In the present study, if RAP is considered to represent long-term aged material, the combination of RAP and virgin material will yield improvement in fracture energies up to certain amount of RAP, after which the energy drops with an increasing amount of RAP. The fracture energy of virgin mixture manufactured with PG 64-22 is comparable to the energy for the combination of this mixture and 50% RAP, which suggests that the baseline properties of the mixture are not very different from that of the RAP. However, in the case of PG 58-28 binder, the control mixture with 0% RAP has very high fracture energy and thus there is large difference in fracture properties between the RAP and virgin mixture. This difference in the baseline fracture energy of the two control mixtures seems to underlie the drastic differences in the trends of fracture energy versus RAP amount as seen in Figure 7.2(a) and 7.2(b).

Another important observation from the fracture energy results is that using asphalt binders with lower PG grades to compensate for the presence of RAP gives favorable results from the perspective of fracture energy and therefore cracking resistance. For instance, the mixture with 50% RAP and PG 58-28 virgin binder had a fracture energy of 595 J/m^2, which is in excess of the virgin PG 64-22 mixture, which had a fracture energy of 411 J/m^2. Of course, this trend will vary from mixture to mixture and from RAP source to RAP source, which emphasizes the usefulness of the fracture energy test in the design and control of mixtures with RAP.

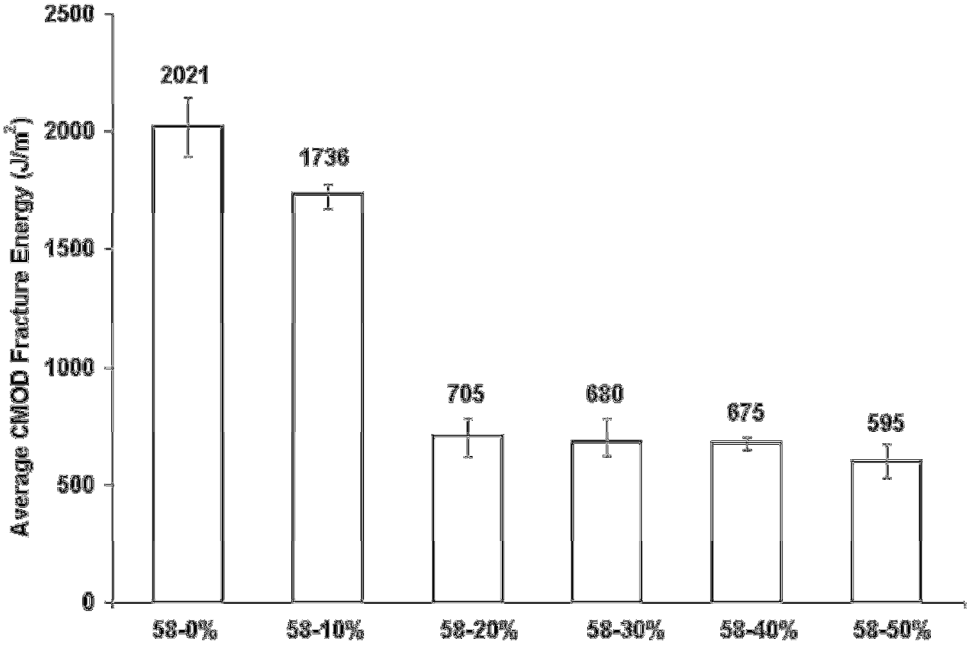

(a) PG 58-28 Mixtures

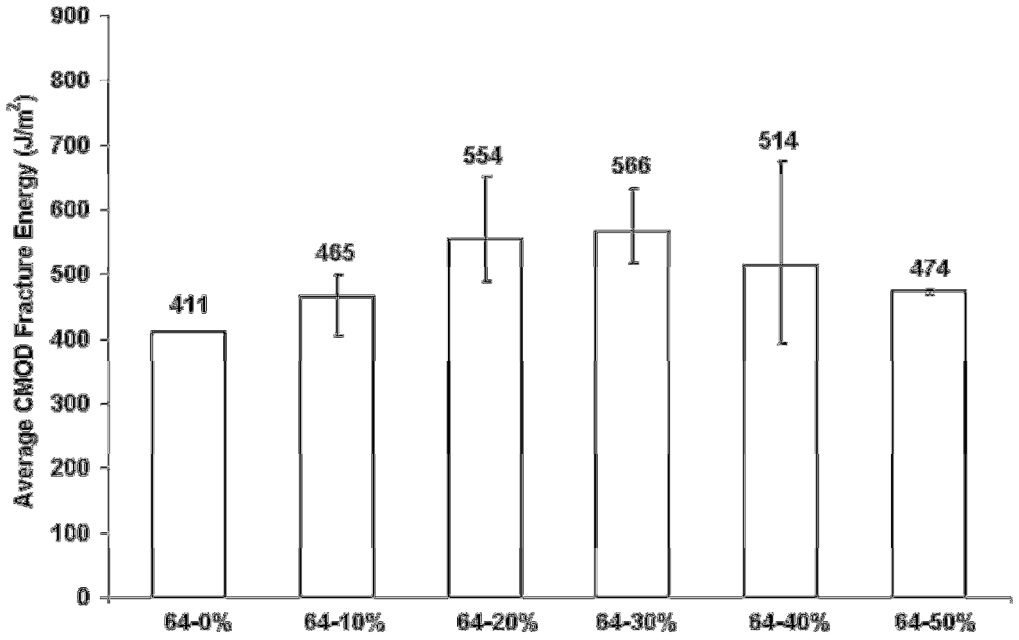

(b) PG 64-22 Mixtures

Figure7.2: Fracture Energy of RAP Mixtures Determined using the Disk-Shaped Compact Tension Test

The creep compliance evaluated from the test results for 20 and 40% RAP mixtures for both binder types are shown in Figure 7.3 along with the corresponding fitted power-law curves, and the exponential term from the power-law model (m-value). The results are as expected, which indicates that an increase in RAP amount leads to a mixture that behaves in a stiffer manner. Higher m-values were observed for PG 58-28 mixtures. The m-value drops as the RAP amount increases from 20% to 40%. The increase in m-value indicates increased viscoelastic behavior with higher rate of stress relaxation. Thus, increased m-value indicates lower potential for thermally induced cracking.

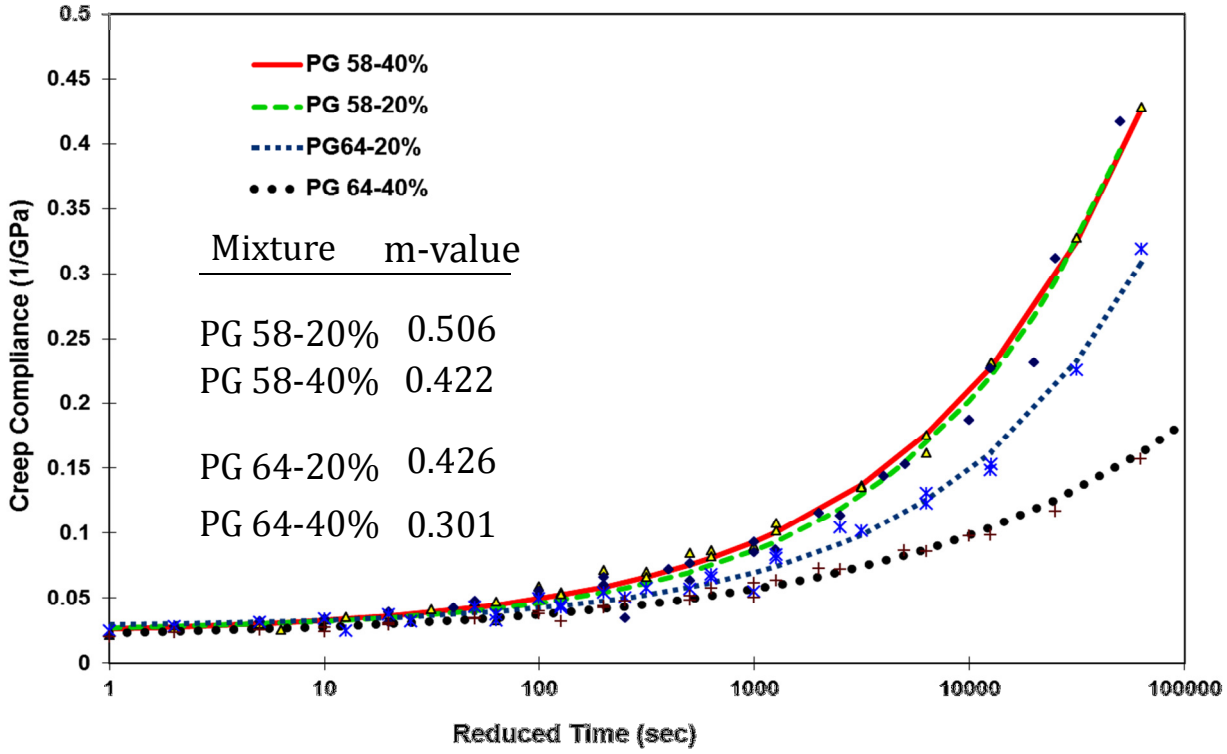

Figure7.3: Creep Compliance of RAP Mixtures Determined using the Indirect Tension Test

Embrittlement temperature results of various mixtures are presented in Figures 7.4(a) and 7.4(b). The results are shown as average of at least four test replicates for each material. For a PG 64-22 mixture with 10% RAP specimens were not available for AE testing and thus results are not presented. The embrittlement temperatures of control mixtures were found to be closer to their virgin binder low temperature PG grades. However, it was observed that the T_{EMB} of mixtures containing RAP are significantly higher than the T_{EMB} of the corresponding control mixtures.

This can be attributed to the aged hardened binder from RAP, contributing to a brittle behavior. Another observation is that the change in the embrittlement temperature is quite significant between mixtures with and without RAP; however it is not as significant for mixtures with different amounts of RAP (10 – 50% RAP). The AE testing procedure measures material properties at local scale. This can be explained through an example; if a composite material system consisting of two types of material is tested using the AE technique, the embrittlement temperature will be the temperature at which the weaker of the two materials starts to undergo damage and fracture. In the case of RAP mixtures, it is hypothesized that there is only partial blending of binder and mastic from RAP and virgin materials. During the course of AE testing, as mixtures undergo cooling, the mastic portion rich in aged material from RAP begins to accumulate damage earlier and generates earlier acoustic emission activities. This would explain the lack of significant distinction between T_{EMB} of mixtures with different RAP amounts.

The overall trends of T_{EMB} for control as well as RAP mixtures are consistent with the results observed for fracture energy and creep compliance. This provides more confidence in the use of the T_{EMB} quantity as a screening tool to quickly assess cracking resistance.

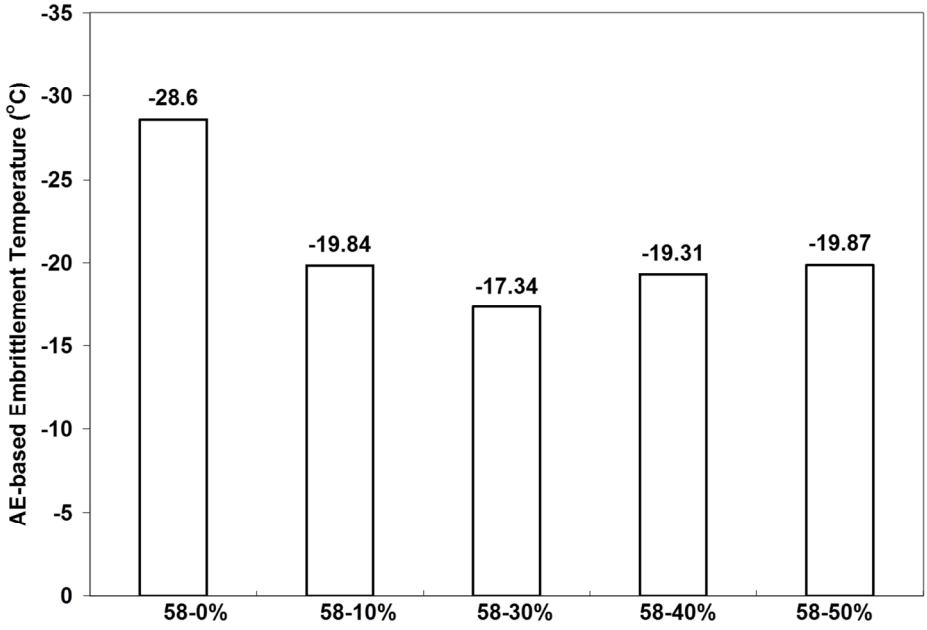

(a) PG 58-28 Mixtures

(Figure 7.4 cont. on next page)

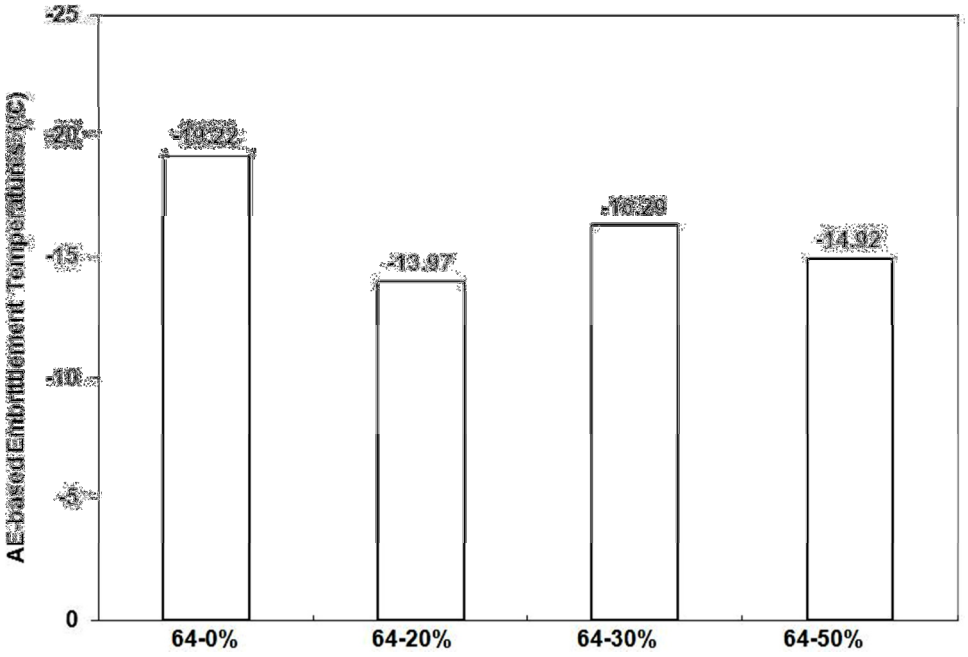

(b) PG 64-22 Mixtures

Figure7.4: Embrittlement Temperature of Asphalt Mixtures Determined using Acoustic Emission Technique

7.4. SUMMARY

This chapter describes evaluation of cracking resistance of asphalt mixtures with varying amounts of recycled asphalt pavement (RAP). A series of laboratory tests were conducted for asphalt mixtures with six RAP amounts (0 – 50%) and two virgin binder types. A newly developed acoustic emission based procedure was utilized to identify the embrittlement temperature (T_{EMB}) of the mixtures. Viscoelastic and fracture evaluation were performed using the disk-shaped compact tension test (DC[T]) and the indirect tensile test (IDT). Laboratory results indicate that it is important to thoroughly characterize the mixtures with RAP to determine their cracking resistance. In this study, mixtures produced with PG 58-28 binder showed greater sensitivity to the presence and amount of RAP as compared to mixtures with PG 64-22 binder and the same RAP source. The viscoelastic properties of RAP mixtures showed consistent trends with fracture energy results. The AE test results showed that the embrittlement

temperatures for mixtures containing RAP were much higher (warmer) than the mixtures without RAP.

One major distinction between the AE technique and mechanical bulk and fracture testing is the response scale within the material. In the case of mechanical tests, the mechanical test results are a measure of the response of the whole specimen (as a structure) and thus it is difficult to extract local properties, while the AE procedure yields results that are at the local scale of the material response. Both mechanical tests and AE techniques are recommended for complete evaluation of cracking resistance of pavement mixtures. The AE technique can provide information regarding the onset of damage and damage accumulation (i.e., cracking and crack propagation) in the material and mechanical tests (bulk and fracture) can provide information regarding overall response to loading as well as the propagation of damage and cracking once it has initialed.

CHAPTER 8
EVALUATION OF WARM MIX ASPHALT MIXTURES CONTAINING RECLAIMED ASPHALT PAVEMENT USING ACOUSTIC EMISSION TECHNIQUE

8.1. INTRODUCTION

Environmental experts define sustainability as meeting the needs of the present without depleting the resources required by future generations [86]. Civil engineering infrastructure materials can significantly contribute to the sustainability movement through the use of recycled materials and more environmentally friendly production processes. In the asphalt paving community, the most commonly employed sustainability practices involve the addition of increasingly greater amounts of reclaimed asphalt pavement (RAP) and the use of warm mix asphalt (WMA).

RAP is the primary recycled product of asphalt concrete pavements. The use of RAP leads to several advantages including reduced material costs, energy savings, and increased rutting resistance. Chiu et al. (2008) determined through cost analyses that 23% energy savings occurred with the use of RAP [87]. Furthermore, Kandhal and Mallick (1997) found a potential cost reduction of 34% available with RAP contents between 20 and 50% [88]. In terms of performance, RAP can improve rutting resistance through increased asphalt binder stiffness. Oxidative hardening significantly increases asphalt binder stiffness during pavement service life, which can provide rutting resistance when RAP is incorporated into a new asphalt paving mixture [89].

Performance issues may arise with the use of higher amounts of RAP in the area of pavement durability. Xiao et al. [84] determined that the introduction of as little as 15% RAP significantly increased mixture stiffness, which opens the door for premature development of various forms of pavement cracking. Behnia et al. (2011) reported reduced cracking resistance in PG 58-28 mixtures containing up to 50% RAP through Disk-shaped Compact Tension (DC(T)), Indirect Tensile (IDT) Creep Compliance, and Acoustic Emissions (AE) tests at low temperatures [72]. The increased stiffness associated with RAP may lead to the selection of a more costly softer asphalt binder grade and/or limit the amount of RAP that can be used in a given mixture. A current school of thought in the asphalt industry is that the reduced aging in the asphalt binder associated with lower production temperatures in WMA mixtures leaves additional ‘headroom’ for the incorporation of higher amounts of RAP in a given asphalt mixture [90]. In essence, it is

thought that the stiffer RAP binder can be 'counterbalanced' by virtue of the less aged binder resulting from the WMA production process, which reduces mixture production and laydown temperatures and hence reduces oxidative hardening, volatilization, etc.

WMA represents a growing alternative to conventional hot mix asphalt (HMA). This technology is produced at temperatures approximately 25-30^{o}C less than HMA due to chemical composition changes during the mixing process [91]. At least 20 WMA additives and processes exist on the market today, and include: foaming additives and processes, organic additives, and chemical additives. The foaming group utilizes water to foam the asphalt binder prior to or during the mixing process. The foaming processes subcategory uses water injection systems to foam the asphalt binder while the additives subcategory includes synthetic zeolites such as Advera and Aspha-min. Synthetic zeolites are metallic alumino-silicates which contain approximately 20% water by weight in their microstructure [90]. At approximately 100^{o}C, the zeolite degrades and releases the entrapped water. According to Prowell and Hurley (2005), foaming additives may have moisture sensitivity issues based on laboratory evaluations [90]. Organic additives generally include paraffin waxes, montan waxes, and fatty acid amides. This group of WMA additives stiffens the asphalt binder as shown by Prowell and Hurley (2005) who determined that the addition of 2.5% Sasobit led to a PG 58-28 asphalt binder behaving as a PG 64-22 [92]. Consequently, organic additives may reduce thermal cracking resistance for a given binder in a given climate. The chemical additive category includes liquid and solid chemical packages added to the asphalt binder prior to entering the mixing drum. Liquid chemical additives generally act as emulsifying agents and contain amine groups which lead to improved thermal cracking and moisture resistance, respectively.

Several environmental advantages occur with the use of WMA including: energy savings and emissions reductions. According to the National Asphalt Pavement Association (2007), WMA can reduce fuel consumption by as much as 10-35%, as fuel usage may decrease by as much as 3% for each 6^{o}C drop in mixing temperature [93]. European and Canadian researchers have determined that a 15-70% reduction in SO_x, NO_x, CO_2, and volatile organic compounds (VOC's) emissions are generally realized with the use of WMA [91].

Potential disadvantages of WMA include increased rutting, moisture sensitivity, and lack of long-term field performance results. In the case of the chemical and foaming groups, mixture stiffness may be reduced such that rutting resistance could be problematic according to Hurley

and Prowell (2005, 2006) [94,95]. Organic additives, on the other hand, may increase stiffness such that pavement cracking potential also increases. The lack of long-term WMA performance data in the field of practice also affects WMA use in the U.S. (the technology has only been in place for approximately 8 years). As a result, laboratory performance tests continue to fulfill a critical role in the design and deployment of existing and emerging WMA technologies.

As stated previously, WMA and RAP have the potential to perform well in combination, not to mention the two-pronged sustainability benefits that can be realized. Research to date, such as Doyle *et al.* (2011), primarily focused on the moisture and rutting resistance aspects of WMA RAP mixture performance [96]. Their study suggested that moisture and rutting resistance can be improved through the combination of WMA and RAP [96]. However, low temperature performance of WMA RAP mixtures remains in question. Therefore, this study will introduce new findings with respect to low temperature characteristics of WMA RAP mixtures, while considering rutting and moisture resistance in order to evaluate the overall durability of WMA RAP mixtures.

In this experimental investigation, four WMA additives, including one additive from each WMA group, and three different RAP levels were used to evaluate WMA-RAP mixtures in comparison to control HMA mixtures through advanced asphalt mixture tests. These tests included: DC(T), IDT Creep Compliance, and AE tests.

8.2. MATERIALS

The primary objective of this study was to evaluate the combined effects of WMA additives and RAP on asphalt mixture low temperature properties. An additional objective of the study was to compare the rutting resistance and moisture sensitivity of WMA RAP mixtures and control HMA mixtures to fully characterize WMA-RAP mixture durability properties. At least one additive from each of the WMA categories were used, namely: Sasobit, Advera, Evotherm 3G, and Rediset LQ. Sasobit is a paraffin wax product of the Fischer-Tropsch process [97]. Paraffin waxes act as stiffening agents which can potentially improve rutting resistance while increasing thermal cracking potential. Sasobit was added at a rate of 3.0% by weight of the asphalt binder. Advera is a foaming additive synthetic zeolite which was added at a rate of 0.25% by weight of the mixture. This additive may have issues with moisture sensitivity due to the moisture released during the mixing process [94]. Evotherm 3G and Rediset LQ are liquid chemical additives

added at a rate of 0.50 and 0.75% by weight of the asphalt binder, respectively. This type of additive has the potential to improve moisture and thermal cracking resistance. Sasobit, Advera, Evotherm 3G, and Rediset LQ will be referred to as F-T wax, Zeolite, Chemical-1, and Chemical-2, respectively.

PG 64-22 was used as the base asphalt binder in this study. This neat asphalt binder is commonly used across Illinois and much of the United States in applications with low to moderate traffic levels. Aggregates were sampled from a local central Illinois hot-mix asphalt producer (Open Roads Paving, LLC in Champaign, IL), including CM16 (9.5 mm nominal maximum size) coarse aggregate; FM20 (manufactured) and FM02 (natural) sand, and; a limestone-based mineral filler. The CM16 and FM20 stockpiles consisted of dolomitic limestone.. Researchers fractionated the virgin aggregate prior to mixture production to reduce variability caused by material sampling. RAP was sampled from a stockpile of material reclaimed through milling of the surface of I-72 in central Illinois, and fractionated through a 9.5mm (3/8") screening deck. The post-extraction RAP gradation can be found in Table 8.1 with the estimated RAP asphalt content, bulk specific gravity (G_{sb}), and maximum theoretical specific gravity (G_{mm}). All specific gravities, asphalt content estimations, and RAP gradations were verified with the Illinois Department of Transportation (IDOT), Bureau of Materials and Phyical Research laboratory, located in Springfield Illinois.

To determine the HMA mixing and compaction temperatures, which were found to be 160 and 150^{o}C, respectively, the Asphalt Institute Superpave mix design method for selecting mixing and compacting temperatures based upon asphalt binder viscosity was followed [98]. Separate WMA mixture designs were not utilized in this study. This approach was taken in order to compare WMA and HMA mixtures with equivalent aggregate skeletal structures. The WMA mixing and compaction temperatures were selected to comply with manufacturer recommendations. Consequently, the mixing and compacting temperatures of 135 and 125^{o}C, respectively, were selected. The number of gyrations was chosen to be 70 which meets the IDOT standard for medium-to-low volume roads receiving a 20 year traffic intensity of 3 to 10 million Equivalent Single Axle Loads (ESALs). Additionally, all mixtures met the 9.5mm nominal maximum aggregate size (NMAS) surface mixture gradation requirements designated by Superpave. RAP contents of 0, 15, and 45% were included in this study to evaluate the interaction of WMA additives and RAP. A 15% RAP content was chosen to correspond to the

maximum allowable RAP content for Illinois surface mixtures [99]. The 45% RAP mixture was selected to evaluate the characteristics of a high RAP content mixture containing WMA additives.

TABLE 8.1: RAP Gradation and Selected Volumetric Properties

Sieve (mm)	RAP Gradation	RAP Properties
25.0	100	
19.0	100	
12.5	100	RAP G_{sb}
9.5	99.3	2.641
4.75	73.8	AC Content (%)
2.36	50.5	5.50
1.18	35.5	RAP G_{mm}
0.60	25.8	2.492
0.30	18.1	
0.15	13.8	
0.075	11.2	

Figure 8.1 displays gradation plots for the virgin (0% RAP), 15% RAP, 45% RAP mixtures. The outer red lines represent the Superpave control points for 9.5mm NMAS mixtures. As shown in Figure 8.1, the gradations are approximately similar at all points, with a maximum deviation between curves of 1.5% passing. The 15 and 45% RAP mixtures contained slightly more material passing the #200 sieve than the virgin mixture, due to the relatively high content of material passing the #200 sieve for the RAP source used.

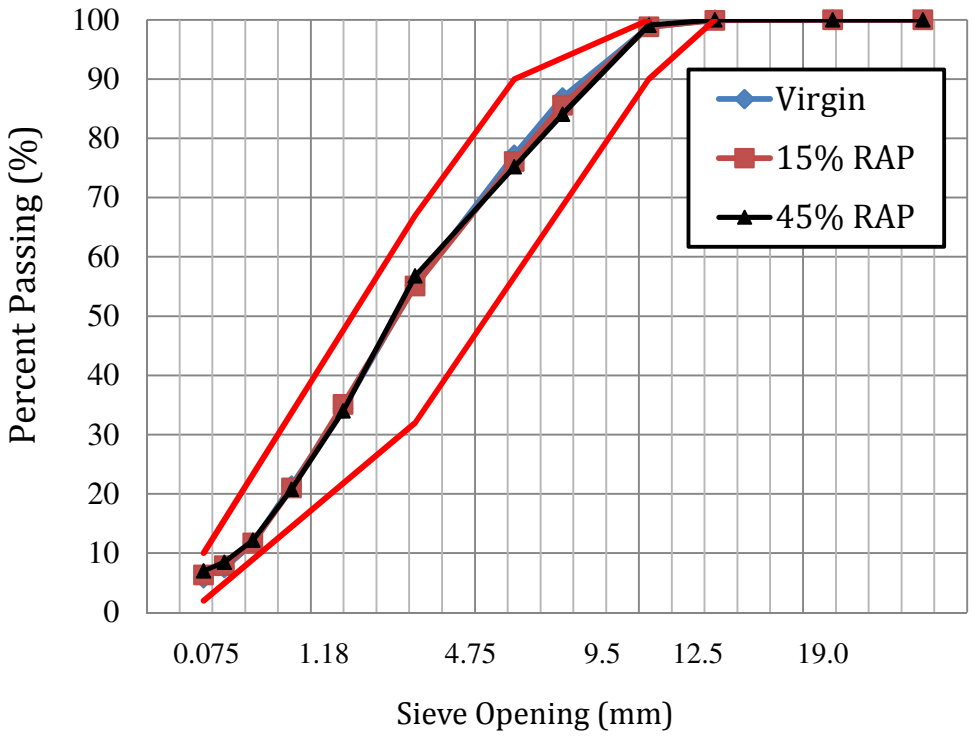

Figure 8.1: WMA-RAP Mixture Gradations

Mixture volumetric properties are summarized in Table 8.2. Similar VMA and VFA levels were achieved for the three mix types (i.e., three RAP levels). The 15 and 45% RAP mixtures contained virgin asphalt contents of 5.9 and 3.9%, respectively.

TABLE 8.2: Mixture Volumetric Properties

Mix Type	AC Content *(%)*	Air Voids *(%)*	VMA *(%)*	VFA *(%)*	DP
Virgin	6.70	4.0	15.3	73.7	1.2
15% RAP	6.70	4.0	15.5	74.4	1.3
45% RAP	6.20	4.0	15.3	73.3	1.4

8.3. EXPERIMENTAL METHODS

To characterize the low temperature cracking behavior of WMA-RAP mixtures, a suite of fracture, creep, and acoustic emission (AE) tests were performed. AE-based technique was employed to obtain a relative comparison of the expected low temperature cracking threshold of WMA mixtures containing RAP materials.

8.4. RESULTS AND DISCUSSION

Figure8.2 displays the DC(T) fracture test results. The error bars represent the high and low fracture energies produced via the DC(T) test among the three replicates tested per setIn the virgin mixtures, the chemical WMA mixtures exhibited slightly greater fracture energy, approximately 7%, as compared to the control HMA mixture. Higher fracture energy is desirable from the standpoint of resisting thermal, block, and reflective cracking. On the other hand, the F-T wax and Zeolite WMA additives had a slight adverse effect on mixture fracture energy as these mixtures exhibited fracture energies 11 and 12% lower than the control HMA, respectively. Among the five WMA and HMA virgin mixtures tested in this study, the F-T wax WMA mixture exhibited the steepest post-peak softening response in its load versus crack mouth opening displacement (CMOD) curve. Previously published simulation studies have demonstrated that steep post-peak softening behavior leads to a more brittle fracture with a higher propensity for crack propagation.

The 15% RAP mixtures showed decreased fracture energies as compared to the virgin mixtures. This result agrees with Behnia *et al.* (2011), where DC(T) fracture energy decreased with the addition of RAP for the PG 58-28 mixtures blended with several RAP sources obtained from Illinois HMA contractors [72]. The 15% RAP HMA mixture performed the best among the 15% RAP mixtures tested. Thus, perhaps unexpectedly, fracture energy (and hence thermal cracking resistance) was not aided by the fact that the WMA mixtures were produced at significantly lower production temperatures than the reference HMA mix.

The 45% RAP fracture results further demonstrated that increased RAP content led to decreased fracture resistance. This result differed from Doyle *et al.* (2011) [96]. The 45% RAP mixtures exhibited significantly higher coefficient of variation as compared to the 0 and 15% RAP mixtures. It is hypothesized that this increased variability could manifest itself in poor field performance, and also in difficulties in mixture production control, especially in meeting end-

result or performance-related specifications. However, it is acknowledged that behavior of field produced mixtures with high RAP content could vary significantly from that which is characterized in laboratory prepared specimens.

The DC(T) fracture results for RAP-WMA and HMA mixtures provided several key observations. First, the DC(T) test displayed that mixture fracture resistance can be sensitive to the WMA additive used. Thus, a case can be made for the importance of a low temperature performance test, such as the DC(T) fracture energy test. Secondly, irrespective of WMA additives used or reduced production temperatures, increasingly greater RAP contents likely lead to increased thermal cracking potential. Consequently, the addition of a softer virgin asphalt binder grade may remain the only option to combat thermal cracking in high RAP mixtures as WMA employment did not significantly improve the fracture resistance of RAP mixtures in this study. Advances in asphalt mix plant design might also aid in the production of WMA-RAP mixtures with improved low temperature properties, but again, performance tests such as the DC(T) can be used to assess such technologies.

Mixture low temperature creep compliance data can be used to assess the ability of a mixture to resist thermal stress build up upon cooling during a critical low temperature event. Higher compliance and higher slope at longer loading times (or 'm-value') are both desirable from a standpoint of minimizing stress development and maximizing stress relaxation upon cooling under restrained conditions. Creep compliance master curve results as produced from data measured in the Superpave Indirect Tension Test (IDT) are shown in Figure 8.3. Similar to the DC(T) fracture test, the Chemical-modified virgin WMA mixtures displayed the most desirable low temperature creep performance in terms of greatest creep compliance as compared to the other virgin mixtures. In addition, the virgin Chemical-1 WMA mixture produced the greatest m-value, which indicates the greatest capacity for stress relaxation. The control HMA, Zeolite, and F-T wax mixtures displayed similar creep compliance master curves. The F-T wax WMA mixture exhibited the lowest m-value and thus the lowest stress relaxation potential among the virgin mixtures tested. Among the three RAP levels investigated, the virgin mixtures displayed the greatest sensitivity to WMA additives in terms of creep compliance.

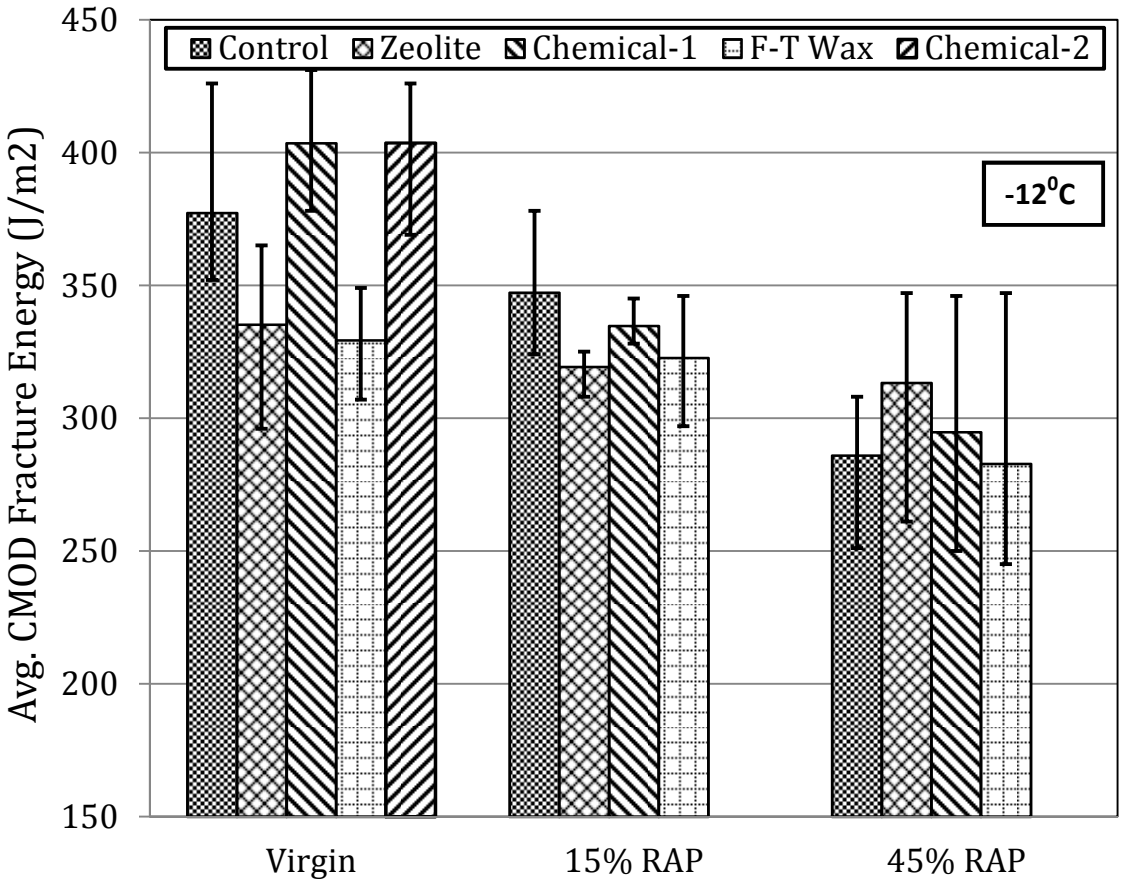

Figure 8.2**:** Average DC(T) CMOD Fracture Energy

In the 15% RAP data set, RAP addition at this level was found to reduce the m-value computed from all WMA and HMA mixture master curves. These results agreed with those found by Behnia *et al.* (2011) and showed that the presence of RAP led to reduced capacity for stress relaxation in the case of a thermal event. The m-value rankings remained the same for HMA and WMA mixtures in this data set which suggests that RAP interaction with WMA additives did not improve or reduce creep behavior. The 15% RAP WMA mixtures were slightly more compliant and therefore better able to relax stress than the control HMA mixture. This result differed from the fracture test results and likely leads to the conclusion that although the fracture energy may not be enhanced by WMA technologies, these technologies may improve the bulk material relaxation capabilities during a cooling event. Modeling and field trials will be needed to fully evaluate the relative cracking behavior of these mixes; i.e., to determine if the compliance benefit would outweigh the fracture energy reduction for a given climate and pavement structure.

The 45% RAP WMA and HMA mixtures displayed further stress relaxation losses due to the presence of RAP. In all 45% RAP mixtures, m-values decreased, which further agreed with the results found by Behnia *et al.* (2011) [72]. The presence of a high RAP content narrowed the differences in the creep compliance and m-values among the 45% RAP WMA and HMA mixtures, which naturally follows due to the high percentage of this common ingredient among the mixtures. Finally, WMA mixtures continued to display slightly better performance as compared to the control HMA mixture. In addition, the m-value rankings remained the same as the other two RAP data sets in this study.

The IDT creep compliance data results in this study provided three key findings: (1) WMA technologies affected the creep compliance characteristics of virgin asphalt mixtures. Therefore, additives and processes should be considered carefully in terms of their effect upon stress relaxation characteristics in colder climates or where rapid temperature changes exist; (2)the use of WMA slightly improved the stress relaxation characteristics of RAP mixtures, whereas fracture energy was not improved with the presence of WMA additives, and; (3) although RAP WMA mixtures performed slightly better than the control HMA RAP mixture, increased RAP contents led to significantly reduced stress relaxation capabilities in both WMA and HMA mixtures.

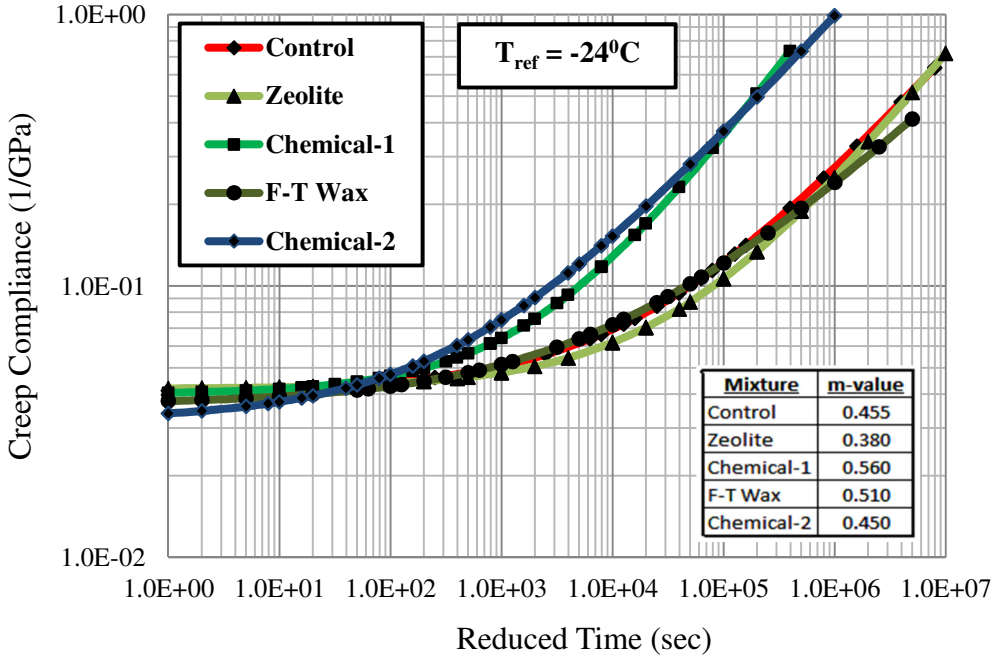

Figure 8.3**:**(a) Virgin Mixture Fitted Creep Compliance Master Curves

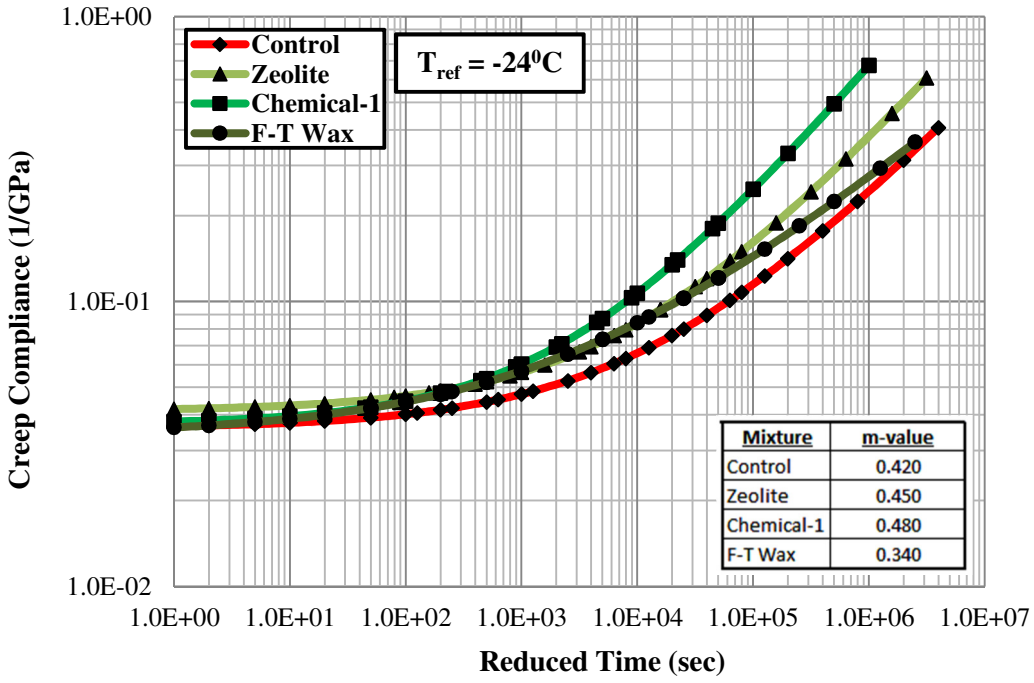

Figure 8.3:(b) 15% RAP Mixture Fitted Creep Compliance Master Curves

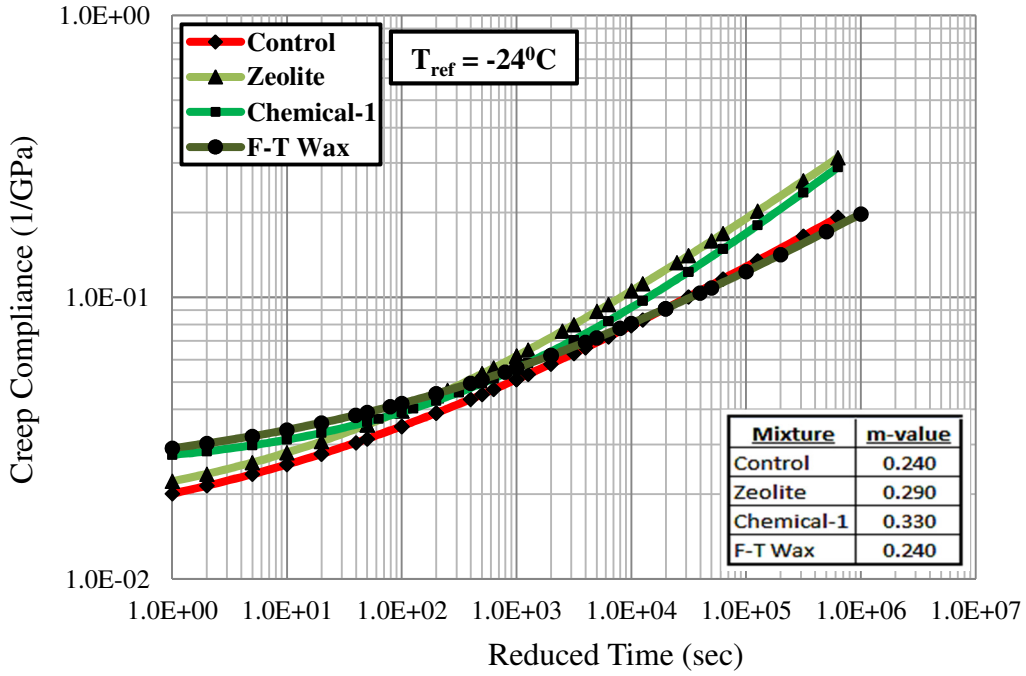

Figure 8.3:(c) 45% RAP Mixture Fitted Creep Compliance Master Curves

Acoustic Emission activity of WMA mixture samples subjected to thermal loading (rapid temperature decrease) was evaluated by analyzing recorded AE events counts, test temperature and computed AE energy.

AE test results of WMA mixtures with 0%, 15% and 45% `RAP are summarized in Figure 8.4. The provided results are an average of at least four test replicates for each material, and CoV% values in the range of 5% to 10% were fairly typical. WMA chemical-2 RAP mixtures were not available for AE testing and thus results are not presented. Comparing T_{EMB} of WMA mixtures containing different RAP amounts reveals the effect of the presence of RAP on low temperature cracking performance of mixtures. It is observed that embrittlement temperature of WMA mixtures occurs at warmer temperatures as the RAP content increases. This can be attributed to the aged-hardened binder in the RAP, which contributes to more mixture brittle behavior. A comparison of AE test results of different additives indicates that among all utilized additives, F-T Wax exhibited the most significant increase in T_{EMB} as compared to others. For WMA mixtures with 45% RAP, there was not much difference between T_{EMB} of the control HMA mixture, Zeolite and Chemical-1 mixtures. As evidenced in DC(T) and IDT tests, this can be attributed to the fact that as the RAP content increased it began to dominate the overall material behavior. This would explain the lack of significant distinction between T_{EMB} of mixtures with 45% RAP amounts. AE results of WMA mixtures showed that the T_{MAX} values for control mixtures were close to their virgin binder low temperature PG grades. This was previously reported by Behnia *et al.* (*2011*) in their study on low temperature performance of RAP mixtures *[72]*. Another observation is that unlike T_{EMB}, the T_{MAX} of mixtures was not significantly affected by RAP content or type of additive. More work is needed, including numerical simulation of the AE test, to obtain a more fundamental understanding of the damage/cracking behavior leading to AE events, especially at the thresholds of T_{MAX} and T_{EMB}.

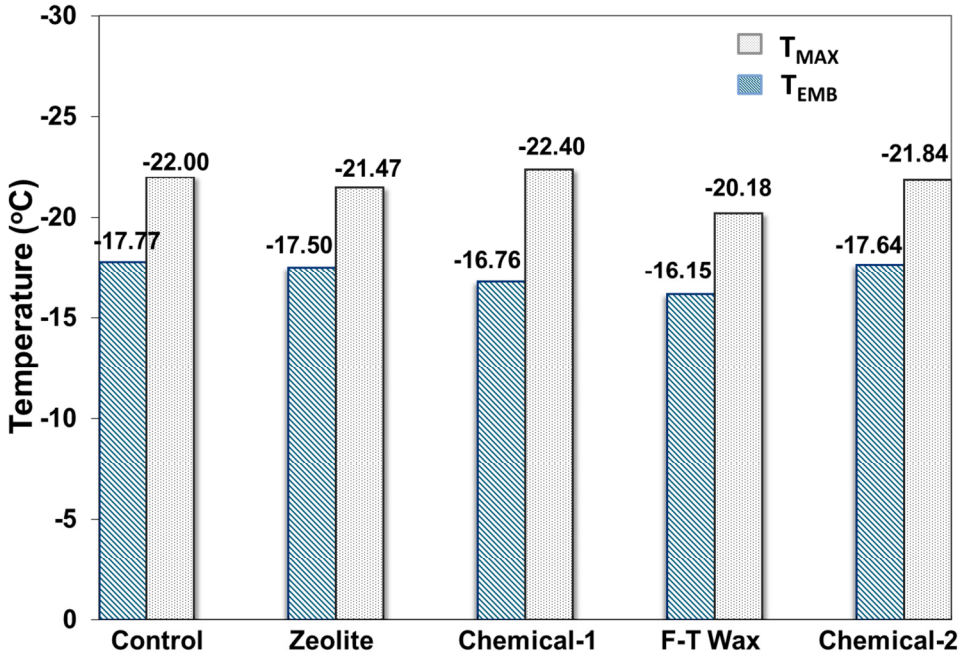

Figure 8.4(a) T_{EMB} and T_{MAX} of WMA Mixtures without RAP, Determined using Acoustic Emission Technique

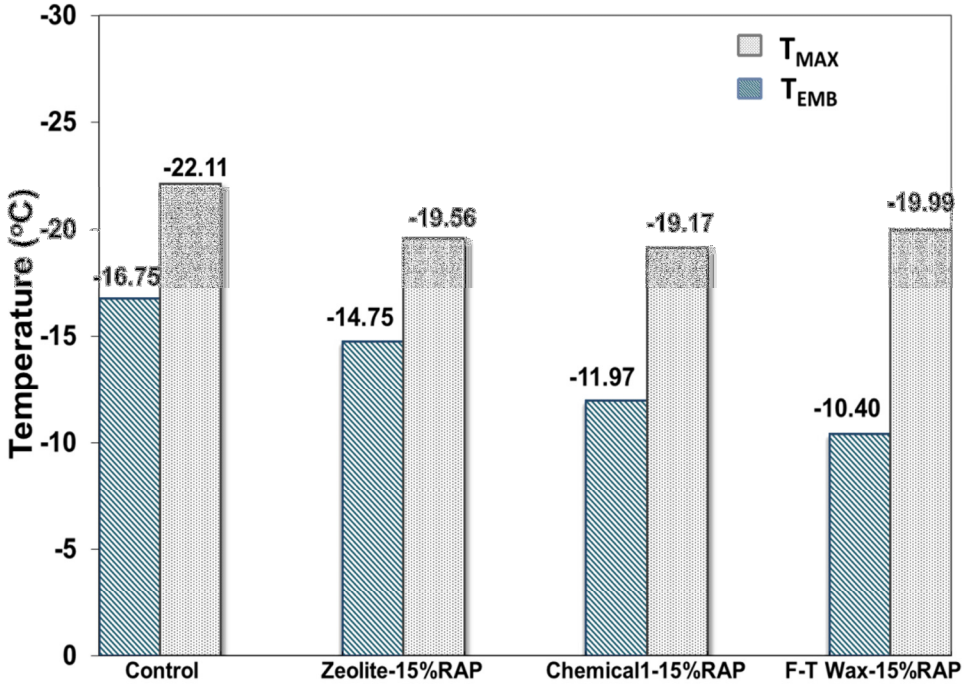

Figure 8.4(b) T_{EMB} and T_{MAX} of WMA Mixtures with 15% RAP, Determined using Acoustic Emission Technique

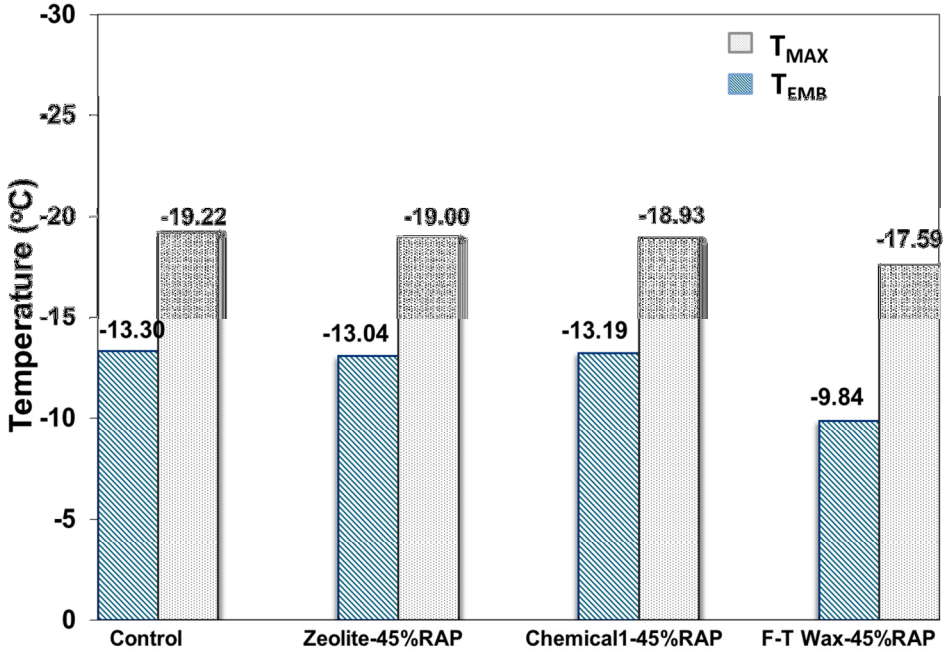

Figure 8.4(**c**) T_{EMB} and T_{MAX} of WMA Mixtures with 45% RAP, Determined using Acoustic Emission Technique

8.5. SUMMARY

This chapter investigated the low-temperature durability of WMA and HMA RAP mixtures through the use of advanced asphalt mixture performance tests. The research presented herein focused on the low temperature performance of these mixtures using the DC(T), IDT creep compliance, and AE tests. Based upon the results obtained through this experimental investigation, the following conclusions regarding the behavior of the WMA-RAP mixtures investigated were drawn:

- DC(T) fracture energy results for virgin mixtures displayed a sensitivity to WMA additives. The chemical additives improved the fracture resistance of WMA mixtures as compared to the control HMA mixture. Therefore, careful consideration of WMA additive options should be made prior to use in the field to avoid thermal cracking.
- The inclusion of RAP led to reduced DC(T) fracture energy as well as IDT creep compliance. These results show that the presence of RAP at low temperatures may lead to increased thermal cracking potential irrespective of the WMA additive employed.

- Acoustic Emission results were sensitive to RAP content as well as to the additive type used in the WMA mixtures tested. The higher the RAP content, the higher (warmer) the T_{EMB} of the mixture. In addition, T_{MAX} of control mixtures were close to their virgin binder low temperature PG grades.
- The overall trends of T_{EMB} of WMA mixtures were consistent with the results observed for fracture energy and creep compliance. This provides more confidence in the use of the T_{EMB} quantity as a screening tool to quickly assess the cracking resistance of asphalt mixtures, including those containing RAP and/or WMA.
- Advanced mechanical and AE tests such as those presented in this study may be useful in validating WMA/RAP mixture designs for important paving projects, particularly until more long-term field performance test results are available. In fact, even when long-term field performance is available, these tests may continue to serve the asphalt industry for high-profile projects, since a near infinite combination of WMA additives, RAP sources, climates, pavement structures, and production/construction variables potentially make each paving project unique.

CHAPTER 9
LOW TEMPERATURE PERFORMANCE CHARACTERIZATION OF BIO-MODIFIED ASPHALT MIXTURES CONTAINING RECLAIMED ASPHALT PAVEMENT

9.1. INTRODUCTION

Meeting sustainability requirements in asphalt concrete generally necessitates the use of recycled materials or the employment of energy saving technologies. The most common form of energy saving technology readily available to asphalt producers is warm mix asphalt (WMA). WMA research and demonstration projects up to date predominately examined the performance of WMA mixtures in terms of laboratory tests to evaluate rutting, moisture, and low temperature susceptibility [92-96,100,101]. Due to the reduced production temperatures and application of certain additives, WMA mixtures may lack stiffness at the high in-service temperature range which can result in increased permanent deformation (rutting) as compared to untreated control sections. Therefore, publications such as the WMA Best Practices guide recommend the inclusion of reclaimed asphalt pavement (RAP) to increase mixture stiffness [84]. However, studies have shown that the inclusion of RAP in the mixture can increase overall mixture stiffness at both intermediate and low temperatures [102]. While an increase in stiffness is beneficial at intermediate temperatures (reducing permanent deformation), the mixture may be more susceptible to low temperature cracking.

An additional issue remaining with the use of WMA is initial and continuous investment in asphalt plant production equipment, such as plant modifications to facilitate foaming, inclusion of WMA additives, etc. A 2009 study detailed the costs associated with WMA additives and WMA foaming devices [103]. In general, these costs may render WMA less profitable under certain conditions than initially thought. Thus, other sustainable asphalt concrete approaches such as bio-modified asphalt may provide similar performance to WMA mixtures, but with reduced production costs.

In general, bio-modified asphalt is accomplished through the replacement of neat asphalt binder (less than 10% by weight) with processed bio-oil derived from biomasses such as plant matter and residues [104-110]. However, the bio-oil used to produce bio-binder for this study is derived solely from swine waste, which has been cited as a tremendous and underutilized renewable source of energy [111]. If bio-modified binder is found feasible, it will not only provide a

reasonably abundant supply of a sustainable alternative to petroleum-based binder but also provide a viable alternative to the otherwise problematic management of excess swine waste [112]. The similarities between bitumen asphalt binder and bio binder have been well documented in previous research [113], where the chemical composition of bio-binder was compared with a petroleum-asphalt binder used in the Federal Highway Administration (FHWA) funded SHRP-1 program. The results indicated a similar carbon:hydrogen content ratio and higher contents of nitrogen and oxygen. In addition, this research determined that bio-binder had a relatively high resin content in comparison to its saturated and aromatic compounds which resulted in a net increase in the solvent phase of the asphalt thereby reducing viscosity [113].

The processing procedure, known as thermo-chemical liquefaction, subjects the manure to immense pressure and heat in the presence of anaerobic conditions. This process was chosen due to its lower energy input (200-300^{o} C) and its capability of handling materials with high moisture contents such as the swine manure. Liquefaction has become widely used and accepted amongst researchers for the conversion of biomass. The resultant of liquefaction is bio oil, which is subsequently processed through a post-processing method involving fractionalization and stabilization. Once the bio-binder is blended with the neat asphalt binder, the final product is bio-modified binder (BMB). The overall production cost of the bio-binder is estimated to be $0.54/gallon, as compared to that of asphalt binder at approximately $2/gallon.

Previous research found that increasing percentages of bio-modified binder blended with neat asphalt binder led to reduced viscosity compared to that of neat asphalt binder as shown in Figure 9.1. Consequently, bio-modified asphalt binder may reduce asphalt mixtures stiffness, which can ultimately give rise to the occurrence of permanent deformation. Such mixtures may be promising candidates to promote the usage of high RAP percentages. A 2012 study incorporated RAP in bio-modified asphalt mixtures and found significant increases in stiffness and reductions in permanent deformation, resulting in the enhancement of pavement sustainability while reducing the production cost. However, to date, no research has been conducted on the low temperature characteristics of bio-modified asphalt mixtures incorporating RAP.

The current study determines the low temperature behavior of bio-modified asphalt mixtures to examine its feasibility for use in colder regions, where distresses such as thermal cracking are prevalent. Bio-modified asphalt mixture samples were tested using the Disk-Shaped Compact

Tension (DC(T)), Superpave Indirect Tension (IDT), and Acoustic Emissions (AE) tests. The DC(T) test evaluated the fracture energy of each of the bio modified mixtures, which can be used to evaluate thermal cracking resistance. The IDT test determined the bulk mixture creep compliance master curves while the AE test evaluated the embrittlement temperature of the mixture.

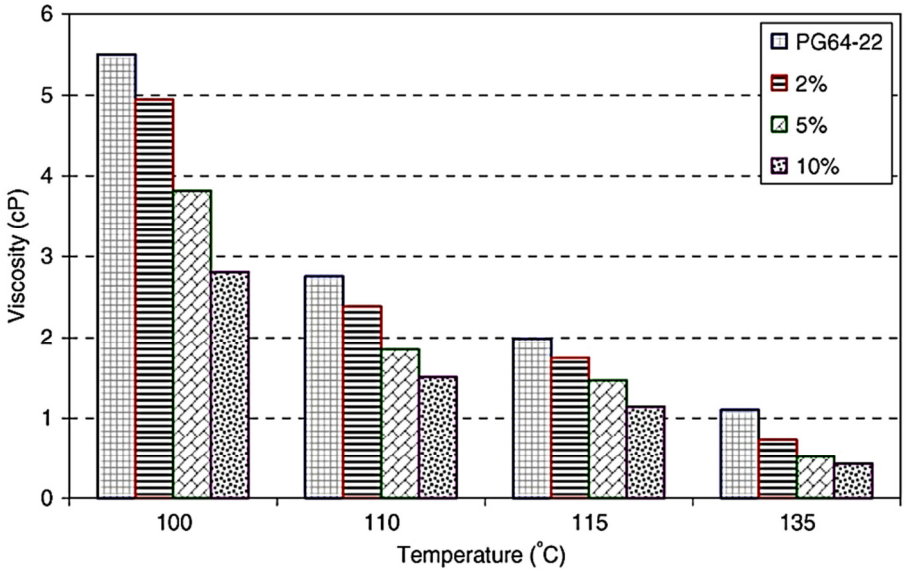

Figure 9.1: Reduction in Viscosity due to Addition of Bio-Binder to Base Binder (PG 64-22).

9.2. EXPERIMENTAL PROCEDURE

The neat asphalt binder used in this study was Superpave PG 64-22, which is the most widely used binder grade in the United States. A recently published study reported adding bio-binder to neat asphalt binder at a rate of 5.0% by mass. An identical bio binder addition rate was used in the current research study. Mixing of the neat and bio-binders occurred at a temperature of 135^{o}C for 30 minutes at a rotational speed of 1800 rpm. This temperature was chosen so that the modified asphalt binder would not stiffen excessively during the mixing period.

Aggregate sampling was conducted at a central Illinois asphalt concrete producer, Open Road Paving Co., LLC. The aggregates sampled included: CM16 (9.5 mm nominal maximum aggregate size (NMAS)), FM20 (manufactured) and FM02 (natural) sands, and limestone mineral filler. The CM16 and FM20 aggregates are characterized by the producer (Vulcan Materials, Kankakee, IL) as dolomitic limestone. Each aggregate was fractionated prior to

mixture design. RAP samples were also procured at Open Roads Paving Co., LLC. The RAP originated from surface mixtures milled from interstate I-72 in central Illinois and fractionated through a 9.5mm screening deck. All RAP data including gradation (post-extraction), estimated RAP asphalt content, bulk specific gravity (G_{sb}), and maximum theoretical specific gravity (G_{mm}) are shown in Table 9.1.

TABLE 9.1. RAP Gradation and Volumetric Properties

Sieve (mm)	RAP Gradation	RAP Properties
25.0	100.0	
19.0	100.0	
12.5	100.0	RAP G_{sb}
9.5	99.3	2.641
4.75	73.8	AC Content (%)
2.36	50.5	5.50
1.18	35.5	RAP G_{mm}
0.60	25.8	2.492
0.30	18.1	
0.15	13.8	
0.075	11.2	

Mixtures were prepared using 0, 15, and 45% RAP by weight of mixture. The 15% RAP level was chosen to coincide with the maximum RAP level recommended by IDOT without virgin asphalt grade adjustment. The 45% RAP content was chosen to evaluate the effects of high RAP levels in bio-modified asphalt mixtures. Superpave mixture design was conducted for the hot mix asphalt (HMA) mixtures at the three RAP levels (0, 15, and 45%). Bio-modified binder (BMB) mixture specific designs were not conducted, since it was desired to use the same total asphalt content and aggregate structure in the control and bio-modified mixtures. The three gradations used in this study are provided in Table 9.2.

TABLE 9.2. Asphalt Mixture Gradations

Sieve	Virgin	15% RAP	45% RAP
25.0	100.0	100.0	100.0
19.0	100.0	100.0	100.0
12.5	100.0	99.9	100.0
9.5	98.8	98.8	99.1
6.25	86.9	85.6	84.1
4.75	77.2	76.1	75.2
2.36	55.3	55.1	56.8
1.18	34.4	35.1	34.0
0.60	21.4	21.0	20.8
0.30	11.7	11.7	12.2
0.15	7.5	7.9	8.5
0.075	5.8	6.3	7.0

Each mixture gradation met the 9.5mm NMAS requirement. Additionally, the design number of gyrations was set to 70 in order to meet IDOT requirements for low to medium volume roads receiving traffic intensities between 3 and 10 million Equivalent Single Axle Loads. Compaction and mixing temperatures for HMA mixtures comply with the Asphalt Institute method for asphalt mixture design. In this case, HMA compaction and mixing temperatures were 150 and 160^{o}C, respectively. The volumetric properties of the HMA mixtures are provided in Table 9.3. Due to the reduced viscosity of bio-modified asphalt binders found in previous research and shown in Figure 9.1, BMB mixtures were mixed at reduced production temperatures similar to WMA. Consequently, a common WMA temperature reduction was chosen based on various WMA manufacturer recommendations. This study chose to reduce both mixing and compaction temperature by 25^{o}C, respectively. Obviously, a more rigorous method for determining proper mixing and compaction temperatures for bio-modified mixtures will need to be established when sufficient lab and field data is available; however, the selected temperatures used in this study appeared to be reasonable, based upon observations made during mixing and compaction.

TABLE 9.3. Mixture Volumetric Properties

Mix Type	AC Content	Design Air Voids	VMA	VFA
Virgin	6.7%	4.0	15.3	73.7
15% RAP	6.7%	4.0	15.5	74.4
45% RAP	6.3%	4.0	15.3	73.3

9.3. RESULTS AND DISCUSSION

A suite of fracture, creep, and acoustic emission (AE) tests were conducted to evaluate the low temperature properties of HMA and BMB mixtures. The average DC(T) CMOD fracture energies for the HMA and BMB mixtures are presented in Figure 9.2. The error bars represent the high and low CMOD fracture energies found for each mixture. In addition, Table 9.4 displays the DC(T) tensile peak loads (kN), CMOD fracture energies (J/m^2), and coefficients of variation. As shown in Figure 9.2, the BMB mixtures exhibited greater average fracture energy than HMA mixtures at each RAP level. This result likely can be attributed to the suppressed temperature range at which mixture embrittlement occurs due to the presence of the soft bio-modified asphalt. As shown in a previous bio-binder study, BMB mixtures consistently displayed reduced dynamic moduli in comparison to HMA. BMB mixture peak loads were approximately 0.3 kN less than HMA peak loads in the virgin and 15% RAP mixtures. The difference in peak loads was insignificant between treated and untreated mixtures at the 45% RAP level, probably due to dominant effects of the RAP in these mixtures. The source of the larger variability found in the RAP-BMB mixtures is not well understood; a larger experiment will be conducted to determine if this is a repeatable phenomenon, and if so, to determine the source of the enhanced testing variability.

Greater RAP contents adversely affected average HMA fracture energy more than average BMB fracture energy. In both mixture types, fracture energy dropped due to the presence of RAP. A previous RAP study found the stiffness of RAP generally leads to a reduction in fracture resistance. The addition of 15 and 45% RAP in the HMA mixtures led to fracture energy reductions of 8.0 and 24.2%, respectively. Conversely, in the BMB mixtures, the 15 and 45% RAP replacement reduced fracture energies by 1.5 and 13.6%, respectively. Due to the reduced

effect of RAP on BMB mixture fracture energy, the difference in fracture resistance amongst the BMB and HMA mixtures grew with larger percentages of RAP replacement in this study.

Several observations can be drawn from the DC(T) test results. First, the DC(T) test captures the effect of bio-modified binders in asphalt mixtures as fracture energy and peak load were both affected by this modification. Second, the introduction of bio-modified asphalt binders tended to improve fracture resistance in this study. Third, the introduction of RAP did not affect the ranking of BMB mixtures as compared to HMA mixtures. Consequently, in terms of fracture resistance, BMB mixtures may provide low temperature property benefits similar to those found for chemical-based additives used in WMA mixtures, particularly when used in conjunction with RAP.

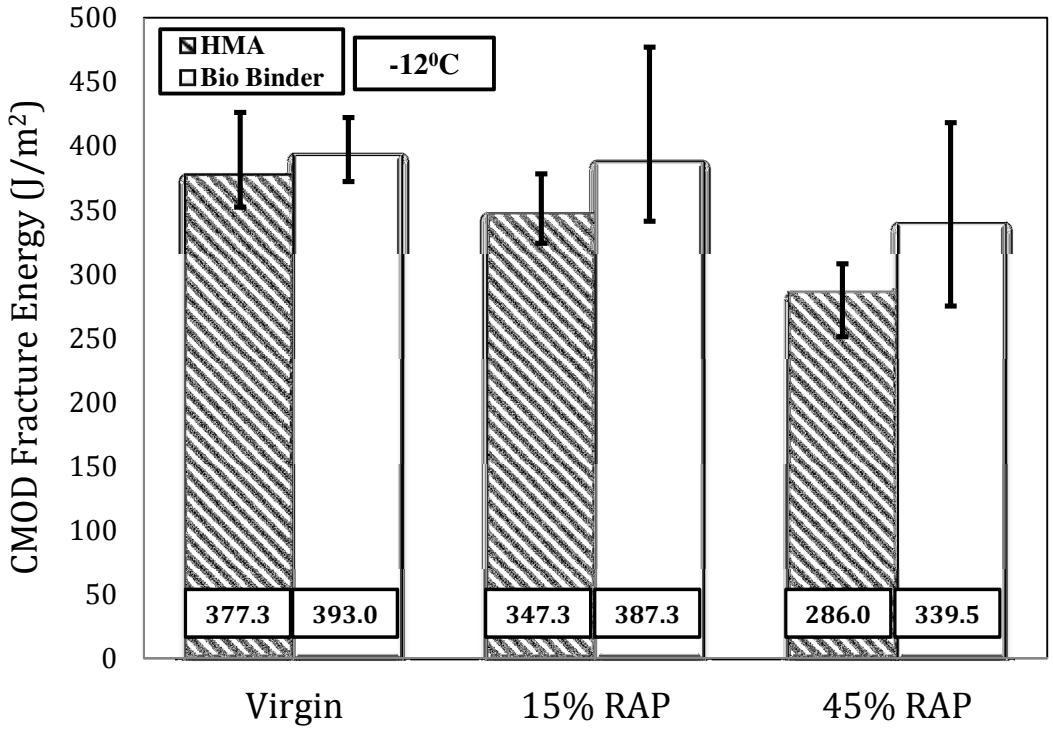

Figure 9.2: DC(T) CMOD Fracture Energy Results (-12°C).

TABLE 9.4.Virgin, 15%, and 45% RAP DC(T) Results

Specimen ID	Avg. Peak Load (kN)	Avg. CMOD G_f (J/m^2)	CMOD G_f COV (%)
HMA – 0% RAP	3.179	377.3	9.3%
Bio Binder – 0% RAP	2.897	393.0	6.6%
HMA – 15% RAP	3.374	347.3	8.0%
Bio Binder – 15% RAP	3.078	387.3	16.0%
HMA – 45% RAP	3.253	286.0	8.7%
Bio Binder – 45% RAP	3.245	339.5	19.7%

The Superpave IDT test results were used to create creep compliance master curves for virgin, 15%, and 45% RAP mixtures, as shown in Figures 9.3(a), 9.3(b), and 9.3(c), respectively. Each plot contains the m-value associated with each mixture. As stated previously, the m-value relates to the stress relaxation capabilities of the asphalt mixture during a cooling event. Similar to the DC(T) fracture energy results, the BMB mixtures produced more desirable low temperature creep compliance properties in comparison to HMA mixtures. This finding remained consistent with 15% and 45% RAP replacement as well. BMB mixtures also displayed greater m-values than HMA mixtures in virgin and RAP mixtures. Consequently, BMB mixtures in this study exhibited a greater potential for stress relaxation during critical cooling events similar to chemical additive modified WMA mixtures studied previously.

RAP adversely affected creep compliance in both BMB and HMA mixtures. As shown in Figure 9.3(a-c), m-value and creep compliance decreased with greater percentages of RAP replacement, which agreed with previous research. However, RAP affected initial creep compliance to a lesser degree in BMB mixtures compared to HMA mixtures. As shown in Fig. 4(a), HMA displayed greater creep compliance than BMB mixtures for a period of approximately 100 sec; however, as RAP contents increased, BMB mixture initial creep compliance met and exceeded HMA initial creep compliance. Therefore, the introduction of bio-modified binder in conjunction with RAP replacement in this study led to increased stress relaxation characteristics particularly in loading periods greater than 100 sec.

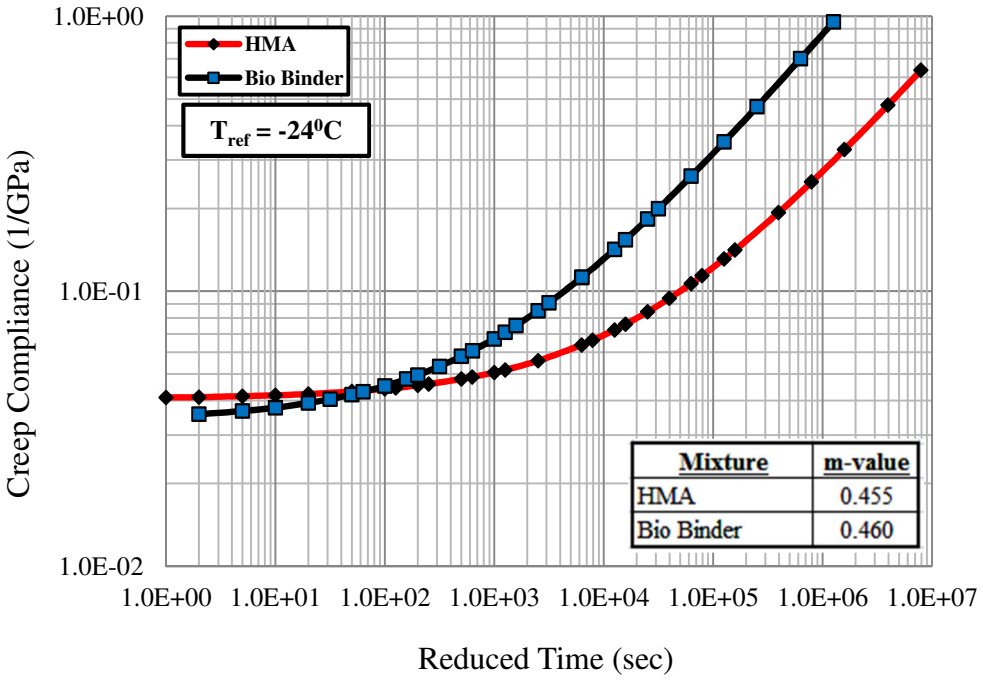

Figure 9.3(a) Virgin Mixture Fitted Creep Compliance.

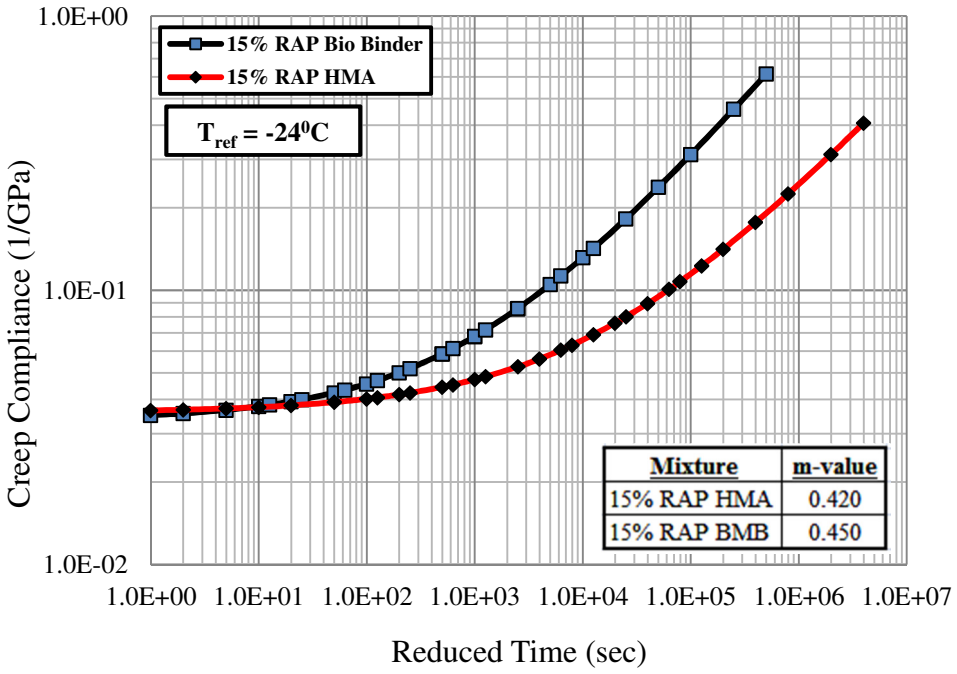

Figure 9.3(b) 15% RAP Mixture Fitted Creep Compliance.

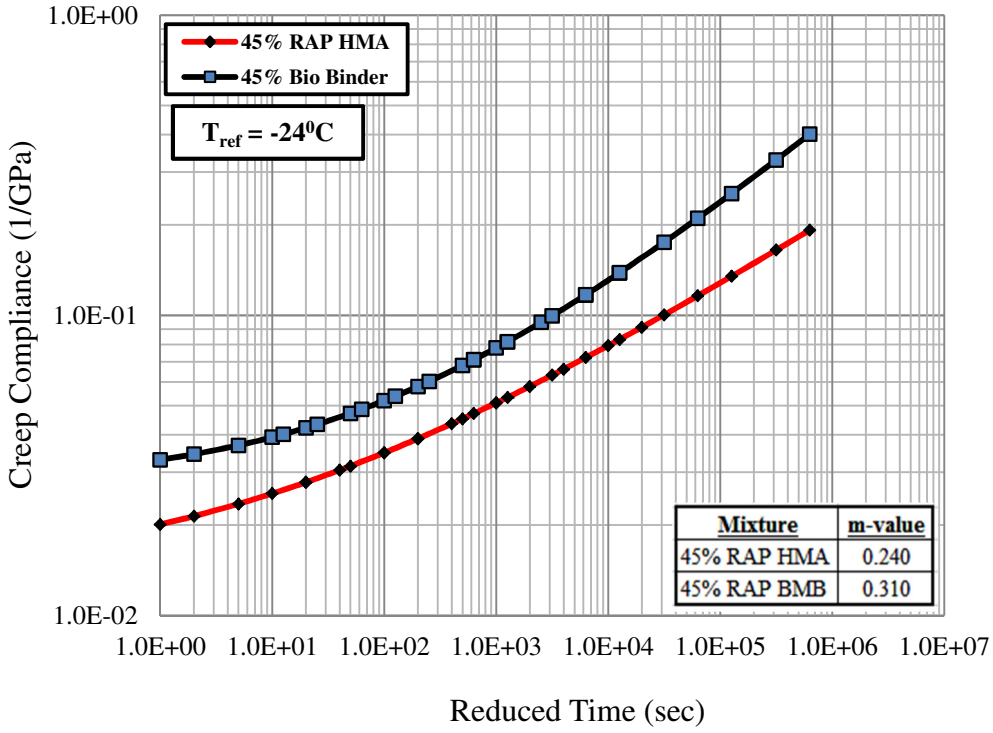

Figure 9.3(c) 45% RAP Mixture Fitted Creep Compliance.

Acoustic Emission testing results of both HMA and BMB mixtures containing 0%, 15%, and 45% RAP were determined by monitoring AE activities of mixtures specimens during thermal loading. Temperatures corresponding to the first major event (embrittlement temperature), T_{EMB}, as well as the maximum energy event, T_{MAX}, are presented in Table 9.5 and Figures 9.4(a), 9.4(b), and 9.4(c). It is observed that BMB mixtures exhibit lower T_{EMB} as compared to HMA. This indicates that for BMB mixtures the onset of damage due to thermal cooling is suppressed to lower temperatures as compared to the non-BMB mixtures. This can be linked to the presence of bio-modified binder in the mix, where the softening effects associated with bio-modified binder led to reduced brittleness in the mastic.

The effect of RAP in the mixtures was also captured by the AE test. In both HMA and BMB mixtures, T_{EMB} and T_{MAX} temperatures increased due to presence of RAP in the mixture; the higher the RAP content, the warmer the T_{EMB} and T_{MAX} temperatures. This can be attributed to the aged hardened binder from RAP, which increases the brittleness of the mixture. It was also observed that the embrittlement temperature of the mixture was drastically increased when the

RAP amount exceeded 15%. For example, going from 15% to 45% RAP, T_{EMB} temperature increased around 3^{o}C. Results show that using bio-modified binders to compensate for the presence of RAP gives favorable results from the perspective of T_{EMB} and T_{MAX}, and therefore low temperature cracking performance would be expected to be improved as a result. For instance, the BMB mixture with 45% RAP has T_{EMB} =-16.74^{o}C and T_{MAX} =-31.54^{o}C which are close to those of the virgin HMA mixture, where T_{EMB} =-17.77^{o}C and T_{MAX} =-22.00^{o}C.

Another important observation is that the change in the size of transition phase, T_{EMB}-T_{MAX}, is quite significant between HMA and BMB mixtures. As shown in Fig. 5(c) the size of transition phase of BMB mixtures is around 6 to 9^{o}C greater than that of for HMA mixtures. This might be linked to the effects of bio-modified binder in the mixture which is not only improves T_{EMB} of the material but also expands the size of transition phase. This suppresses the onset of the "stable cracking" phase, where mixtures transition to a very brittle state and encounter significant thermally induced damage in the process.

The results also suggest that thorough blending of the three binder sources, namely, virgin binder, binder from RAP material, and bio binder was achieved. In previous studies, incomplete mixing of RAP and virgin binder was detected in the AE test by observing that the RAP/virgin material mixture had similar T_{EMB} as compared to the RAP material itself. These results may suggest that the bio binder provides some benefits in terms of homogenization and rejuvenation of the RAP binder in this unique, "dually sustainable" mixture system.

TABLE 9.5. AE Test Results of 0%, 15%, and 45% RAP

Mixture ID	Rep#	Embrittlement Temperature			Max Energy Event Temp		
		T_{EMB} (^oC)	Average	CoV%	T_{Max}(^oC)	Average	CoV%
HMA-0%RAP	#1	-16.72	-17.77	6.05%	-22.68	-22.00	2.83%
	#2	-18.87			-21.86		
	#3	-17.73			-21.46		
HMA-15%RAP	#1	-17.86	-16.75	4.72%	-22.08	-22.11	8.65%
	#2	-16.65			-24.81		
	#3	-16.51			-21.01		
	#4	-15.99			-20.54		
HMA-45%RAP	#1	-14.11	-13.30	8.98%	-19.35	-19.22	3.69%
	#2	-14.08			-19.77		
	#3	-13.42			-18.19		
	#4	-11.57			-19.58		
BMB-0%RAP	#1	-20.49	-21.98	6.86%	-33.16	-33.24	4.71%
	#2	-22.69			-34.99		
	#3	-23.74			-31.20		
	#4	-20.98			-33.59		
BMB-15%RAP	#1	-23.48	-20.77	9.63%	-32.93	-32.14	3.05%
	#2	-21.06			-33.00		
	#3	-19.24			-31.59		
	#4	-19.28			-31.04		
BMB-45%RAP	#1	-18.62	-16.74	9.90%	-33.54	-31.58	5.56%
	#2	-14.63			-32.59		
	#3	-16.51			-30.07		
	#4	-17.19			-30.13		

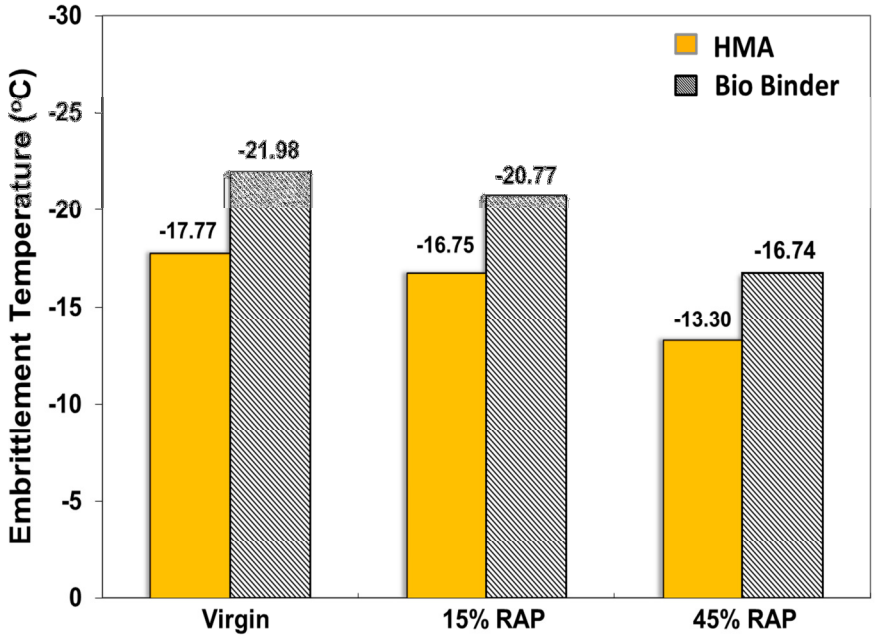

(a)

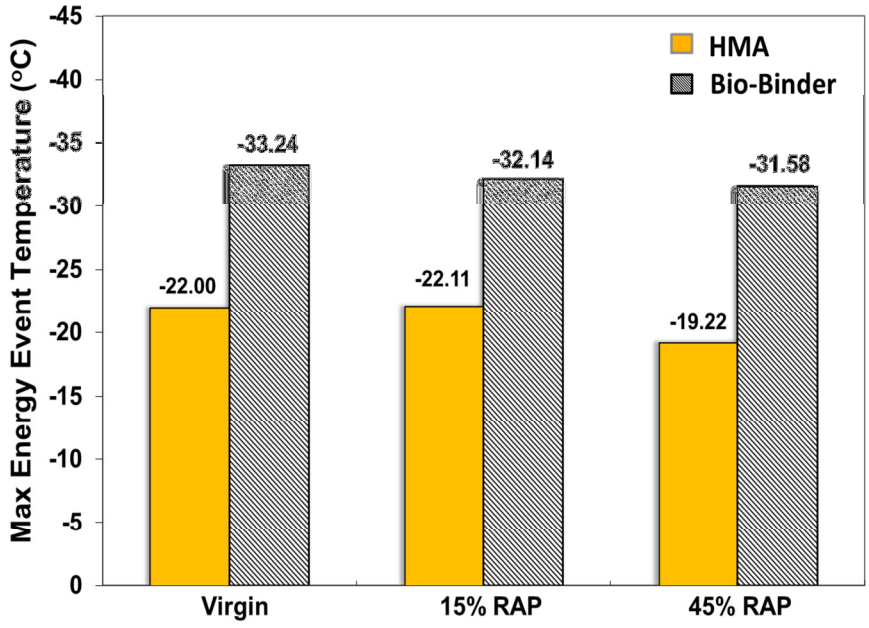

(b)

(Figure 9.4 cont. on next page)

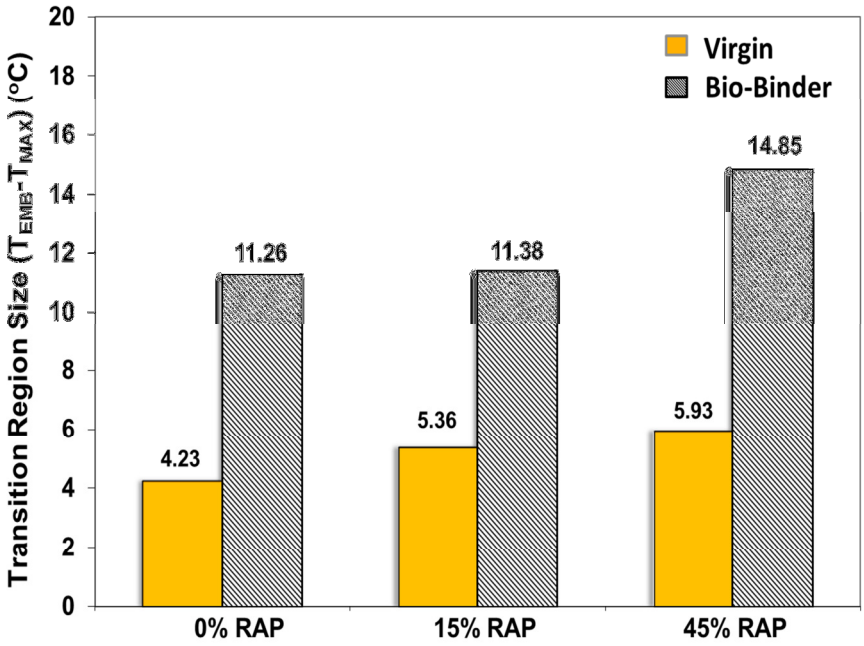

(c)

Figure 9.4**:** AE Test Results of HMA and BMB Mixtures (a) Embrittlement Temperatures Results (b) Max Energy Event Temperature Results (c) Transition Region Size of different mixtures.

9.4. SUMMARY

This study investigates the low temperature behavior of bio-modified asphalt mixtures incorporating RAP through a series of mechanical laboratory tests, including the DC(T) to obtain mixture fracture energy, the IDT test to obtain creep compliance, and a new acoustic emission test to characterize mixture phase transition to a brittle state. One of the main objectives of this study was to determine the feasibility of using bio-modified mixtures incorporating RAP in colder climates, where thermal cracking is a major cause of pavement distress. Based on the results obtained, the following conclusions were drawn:

- Fracture energy and peak load of the asphalt mixtures obtained from DC(T) test were both affected by the nature of the asphalt binder present in the mixture. Bio-modified asphalt binder was found to improve mixture fracture resistance, while RAP reduced the

fracture energy of the both BMB and HMA mixtures. However, the reduction in fracture energy caused by RAP was reduced when bio binder was present.

- The viscoelastic properties of RAP mixtures showed trends which were consistent with fracture energy results. The creep compliance as well as the m-value of the mixture was reduced as the amount of RAP increased. In contrast, BMB mixtures exhibited significantly higher creep compliance and m-values as compared to HMA mixtures.

- AE testing was able to capture and quantify the effects of RAP on the low temperature cracking performance of asphalt mixtures. Key parameters extracted from AE testing are embrittlement temperature, $T_{EMB,}$ and temperature corresponding to maximum acoustic energy event, T_{MAX}. The overall trends of T_{EMB} and T_{MAX} for virgin as well as RAP mixtures are consistent with the results observed for fracture energy and creep compliance. This provides more confidence in the use of these parameters as a screening tool to quickly assess cracking resistance of sustainable paving mixtures such as those investigated herein. In addition, the significantly larger transition zone between T_{EMB} and T_{MAX} in BMB mixtures compared to non-modified mixtures suggests good mixing of the three binder sources in these mixtures (virgin, RAP, and bio binder), and also suggests that the BMB mixtures would be more resistant to rapid crack growth in the field due to the suppression of the two mixture embrittlement thresholds (T_{EMB} and $T_{MAX)}$ measured.

- The acoustic emission (AE) test appears to be a powerful tool for characterizing the low temperature behavior of asphalt mixtures. AE test results also provide new insight into the effects of bio-modified binders on mixture low temperature fracture behavior.

CHAPTER 10
CONCLUSIONS AND FUTURE EXTENSIONS

10.1. SUMMARY AND FINDINGS

The present research aimed at developing an acoustic emissions-based testing method to accurately assess the low temperature cracking behavior of asphalt binders and asphalt concrete mixtures. During the course of this study, AE-based tests were conducted to evaluate the concept of an embrittlement temperature through the testing of a wide range of asphalt binders and mixtures, including lab and field specimens. The temperature corresponding to the first major acoustic emission event, as determined using a standardized signal analysis technique, is defined as the embrittlement temperature.

An important aspect of this investigation was the extension of the AE test method to asphalt mixture testing, which opens the door for the use of the technique for pavement condition assessment. AE tests were performed on lab compacted mixtures provided by the Asphalt Institute and a pooled fund study on low temperature cracking. Characterization was performed to identify the embrittlement temperature and the temperature corresponding to the maximum acoustic event. Both of these temperatures are thought to represent fundamental thresholds in material behavior. The key findings identified on the basis of research conducted in this study are summarized as follows:

- The AE embrittlement temperature of asphalt binder is sensitive to binder type as well as its aging level. It is also sensitive to the presence of a range of typical asphalt additives. The repeatability of the AE testing technique was improved during the course of this study and was found to be as good as or superior to other lower temperature binder tests currently in use.

- Comparison of AE embrittlement temperature and the BBR critical cracking temperature of asphalt binders showed that, for most binders, the embrittlement temperature is slightly (generally a few degrees) lower than the BBR critical cracking temperature.

- The AE based embrittlement measurement differs significantly from existing standard mechanical tests (BBR, DTT, IDT, DC(T), TSRST), and likewise differs from more recently proposed tests, such as the ABCD fracture test. None of the existing or proposed tests has all of the features of the AE embrittlement test, namely: small, portable, suitable for both binders and mixtures, suitable for in-situ measurements, and designed specifically to aid in pavement evaluation for the purpose of determining the optimum timing and method(s) for preventive maintenance and rehabilitation.

- The AE test was successfully applied to evaluate asphalt mixtures. AE test results show that the test is sensitive to aging level and binder grade of the asphalt mixtures. The embrittlement temperature was found to be a good indicator of the extent of damage which happens in the field, as the T_{EMB} results of the provided field cores matched well with the pavement condition as reported in the non-load associated cracking study for airfield pavements conducted by Asphalt Institute.

- One important difference between the AE technique and mechanical bulk and fracture testing is the response scale within the material. In the case of mechanical tests, and particularly strength or fracture tests, are strongly size dependent and thus it is difficult to extract local properties, while the AE procedure yields results that are at the local scale of the material response, and far less sample size dependent. Both mechanical tests and AE techniques are recommended to arrive at a more complete evaluation of the cracking resistance of paving mixtures.

- The developed AE-based testing technique was successfully employed to assess cooling cycle effects on low temperature characteristics of asphalt mixtures. The Felicity effect and healing was clearly shown to exist in asphalt mixtures subjected to cyclic cooling and heating cycles, and a technique was proposed to quantify the degree to which these phenomena occur under given loading conditions.

- Microscopic visualization of microstructure of the asphalt concrete mixtures using X-ray micro-CT clearly showed that microcracks within the mastic as well as debonding at the

interface of aggregate-mastic are the sources of AE activities at low temperatures.

- The AE testing technique is capable of detecting the presence of RAP material within the mixture. The embrittlement temperature is sensitive to the amount of RAP in the mixture. Stiffening effects of aged RAP binder increases the embrittlement temperature of the mixture.

- AE results of WMA mixtures containing RAP were sensitive to RAP content as well as to the additive type used in the WMA mixtures tested. Higher RAP content WMA mixtures exhibited warmer embrittlement temperatures. The inclusion of RAP in WMA mixtures results in reduction in DC(T) fracture energy as well as IDT creep compliance for the mixtures investigated herein.

- AE testing was able to capture and quantify the effects of RAP on the low temperature cracking performance of Bio-Modified Binder (BMB) mixtures. Results showed significantly larger transition zone in BMB mixtures compared to umodified mixtures. This suggests that the BMB mixtures would be more resistant to rapid crack growth in the field due to the suppression of the two mixture embrittlement thresholds (T_{EMB} and $T_{MAX)}$ measured.

- The overall trends of T_{EMB} of several different mixtures were consistent with the results observed for fracture energy and creep compliance. This provides more confidence in the use of the T_{EMB} quantity as a screening tool to quickly assess the cracking resistance of asphalt mixtures, including those containing BMB, RAP and/or WMA.

- The current study has successfully positioned the developed AE-based testing method as a market-ready, and practitioner-friendly technology based upon the following accomplishments:

1) The scientific basis for the material parameters measured in the proposed test, namely, the embrittlement temperature and max event energy temperature, have been solidly supported through lab and field sample testing and comparison to existing test methods;

2) The repeatability of the proposed method is very good, and at par or better than existing comparable low temperature asphalt binder and mixture tests;

3) The developed AE test method was shown to be versatile, with the capability to test binder, mastic, and mixture specimens, and lab and field specimens;

4) It has the ability to detect the presence of recycled asphalt pavement (RAP) in an asphalt mixture sample, which may be useful for quality assurance testing;

5) In addition to the embrittlement temperature and temperature of maximum energy event, The AE-based test method has the potential to produce other cracking information, such as: event count, event energy, and spectral (frequency) information associated with recorded acoustic emission activities, which may lead to further uses of the device in material design and forensic applications;

6) Field validation of the technique showed excellent promise for using the tool to assess current pavement condition from the standpoint of low temperature crack resistance, and;

7) The compact nature of the AE device appears to be enhanced by the availability and applicability of modern cooling devices such as thermoelectric-based systems.

10.2. CONCLUSIONS

Based on AE testing results of binders and mixtures studied herein, the following conclusions can be drawn:

- The acoustic emission testing technique appears to be a viable approach for evaluating the extent of thermally induced damage inside asphalt concrete mixtures. The presence of microcracks in test samples significantly reduced their AE activity. In other words, the

more damaged the material the lower its AE activity.

- Results suggest that the developed AE-based testing method may be a rapid, yet powerful tool for the characterization of low temperature behavior of asphalt binders and mixtures for material formulation, selection, design, and QC/QA. This method shows excellent promise as a tool to enhance pavement sustainability by allowing precise characterization of pavement surfaces, which can then be used to accurately program preventive maintenance and rehabilitation.

- The developed AE-based testing method would yield significant payoff to practice for both up-stream and down-stream suppliers and producers, i.e.:

  - ❖ Up-stream supplies of polymer, chemical, and other additives (warm-mix additives, antistrip agents) could use the proposed technology to rapidly assess the low-temperature characteristics of trial formulations, and could quickly assess the compatibility of blended additive systems.

  - ❖ Mix designers could use the technology to verify binder grade selection, optimize amount of recycled material and/or select appropriate binder grade to use in RAP mixtures, assess and design warm-mixes, verify compatibility when multiple additives are used.

  - ❖ Mix producers could use the technology to assess and adjust mix designs and controllable mix design parameters that affect aging and asphalt absorption (production rate, temperature, mixing time), and for quality control of as-produced pavement.

  - ❖ This technique could also be used to assess RAP materials to avoid the need for time-consuming and expensive extractions.

- ❖ Pavement owners could use the technology for quality assurance of binders and mixtures, and for periodic assessment of pavement condition and for the scheduling of preventive maintenance and rehabilitation, where cracking is of concern.

Based upon these findings, we conclude that the device is ready for commercial development at this time. Of course, the testing of additional material types including other available sustainable asphalt material technologies (e.g., other than the warm mix technologies tested herein) and further field validation studies are recommended to further validate the proposed testing method and to further broaden its range of applicability. Furthermore, the development of a standardized test method to be submitted to AASHTO is recommended and will be pursued soon.

10.3. FUTURE EXTENSIONS

The application of acoustic emission to evaluate low temperature behavior of asphalt materials has only begun; the future in that area appears to be promising. It is anticipated that, as more researchers in the pavement engineering area become aware of how acoustic emission technique can be applied to their specific needs, this technology will grow very fast. Based on the finding and conclusions from this study following extensions are recommended:

1) Implementation of Cohesive Zone Model (CZM) in Finite Element Simulation of AE Binder Test to Capture the Embrittlement Cracking of Asphalt Materials:

Elastic and viscoelastic finite element simulations of AE binder sample was presented in Chapter 3. However, aforementioned simulations couldn't capture thermal cracking initiation and propagation of binder sample at low temperatures. In order to model embrittlement cracking of binders, Cohesive Zone Model (CZM) should be implemented in simulations. Cohesive Zone Model (CZM) provides a powerful numerical way to simulate damage occurring in the process zone located ahead of a crack tip. It provides a phenomenological model to simulate fracture behavior such as crack nucleation, initiation, and propagation. According to the definition, the true (material) crack tip indicates a point where traction is zero and the cohesive crack tip is a point where the traction reaches a maximum. The cohesive zone is defined as the region between the material crack tip and the cohesive zone tip where complicated fracture behavior occurs. The CZM concept in the opening mode is visualized in Figure 10.1 [114-116], where:

t_n : Normal traction

δ_n : Normal opening displacement

σ_c : Material Strength

δ_c : Displacement corresponding to zero traction

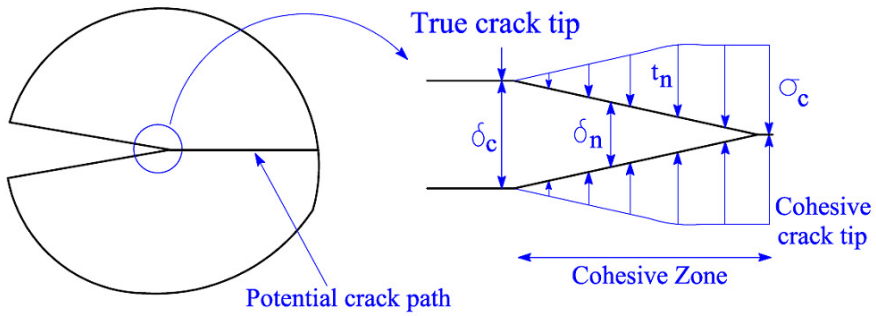

Figure 10.1: Schematic Representation of Cohesive Zone Concept [7]

Figure 10.2 schematically shows the FE model of AE binder sample along with applied boundary conditions and CZ elements located along the centerline of the sample. Fracture energy (G_f) and tensile strength of the asphalt binder are two important material properties used as inputs for the CZ model.

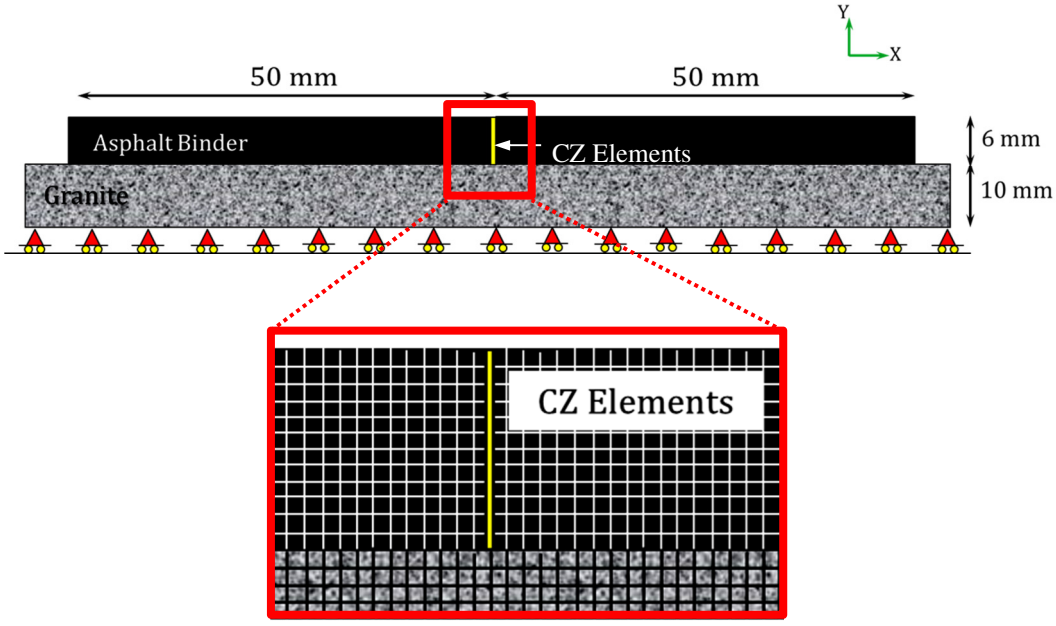

Figure 10.2: Finite Element Model of AE Binder Sample Containing Cohesive Zone Elements

Local fracture properties of asphalt binders can be estimated using the procedure presented in Figure 10.3. Global fracture properties, fracture energy and tensile strength, of asphalt material obtain from DC(T) binder test can be used as the initial local fracture properties in simulations. For simulation purposes, the fracture energy obtained from the laboratory test (or global energy) needs to be calibrated to obtain local fracture properties which are size independent. The global energy depends significantly on the mode of testing, specimen geometry, specimen size, loading rate, etc. By simulating the AE binder sample using CZM, it is possible to determine the cracking temperature of asphalt material. Obtained cracking temperature is compared against the embrittlement temperature of the material. In case $T_{EMB} \neq T_{CRACKING}$, binder fracture properties, inputted in to model initially, are adjusted accordingly in next iterations until cracking temperature and embrittlement temperature match. The binder properties used in the last iteration can be used as local fracture properties of asphalt binder.

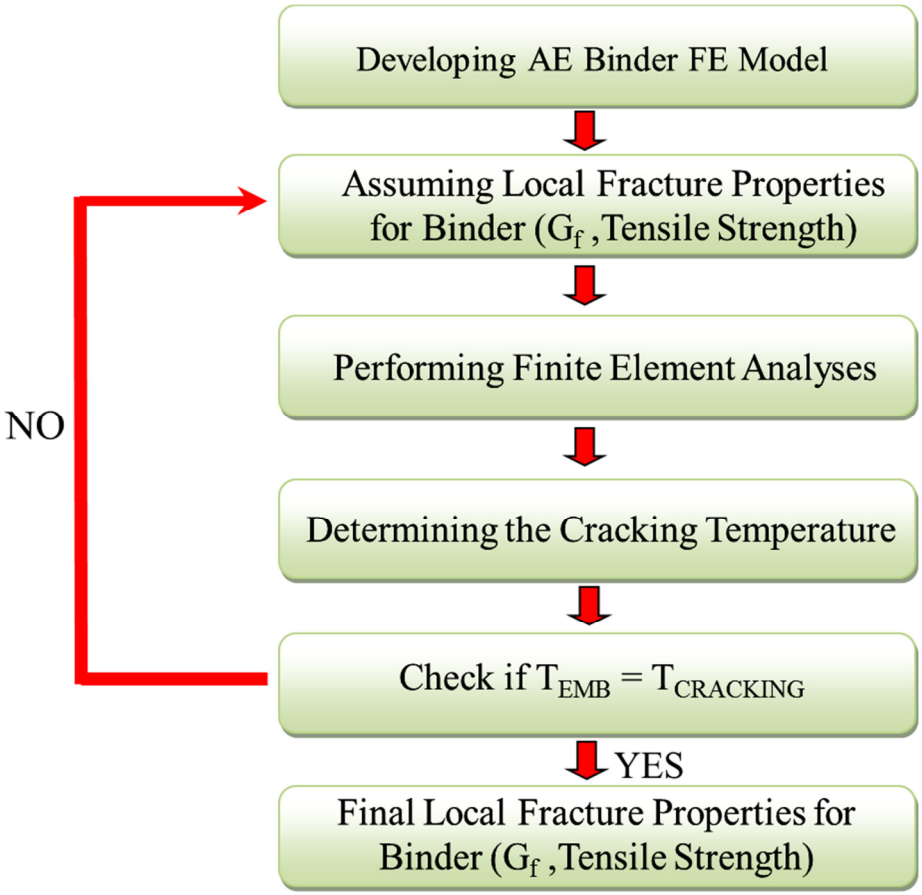

Figure 10.3: Determining Fracture Properties of Asphalt Binder Using T_{EMB}

2) Application of Developed Acoustic Emission-based Technique to Characterize Low Temperature Cracking Performance of Asphalt Concrete as a Functionally Graded Material (FGM):

Asphalt concrete pavements are inherently graded viscoelastic structures due to oxidative aging of asphalt binder and temperature cycling. As a result, asphalt concrete at the pavement surface is much more aged as compared to asphalt materials at the bottom of pavement. Developed AE-based technique can be used to determine and fully understand the aging gradient in the pavement and its effects on low temperature cracking performance of asphalt pavements. AE technique is sensitive to aging level of the asphalt materials; the more aged the pavement the warmer its embrittlement temperature. Therefore conducting AE test on asphalt concrete field cores and determining the T_{EMB} of different layers of the pavement could yield valuable information regarding aging gradient through the pavement thickness. Figure 10.4 schematically shows this procedure. Performing AE tests on asphalt concrete samples obtained from a field core and plotting cumulative AE events of all AE samples in one plot will enable us to see the aging effect on low temperature behavior of the pavement. A typical plot of cumulative AE events vs temperature is illustrated in Figure 10.5. It is seen that AE activities of sample#1 which is taken from pavement surface starts at warmer temperature as compared to other less aged samples#2&3. The less aged the material the lower their T_{EMB} ($T_{EMB1}>T_{EMB2}>T_{EMB3}$). Plotting T_{EMB} vs pavement depth reveals asphalt concrete aging gradient through the pavement thickness.

Another approach to characterize the oxidative-aging gradient of asphalt concrete involves using AE source location technique on field cores, Figure 10.6. It is expected microcracks begins where highly aged material are located, at the surface of the pavement. Conducting AE test in conjunction with AE source location technique will enable us to determine embrittlement temperatures of several points located along the pavement thickness. Plotting aforementioned T_{EMB} along with their corresponding depths in the pavement yields smooth and continuous material property gradient curve, Figure 10.7.

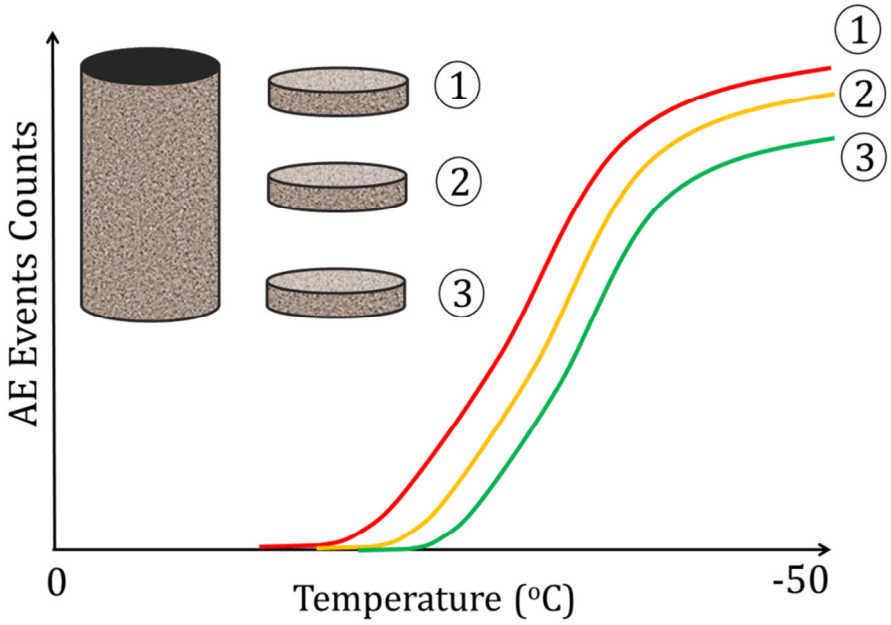

Figure 10.4: A Typical Plot of Cumulative AE Events vs Temperature for all AE Samples

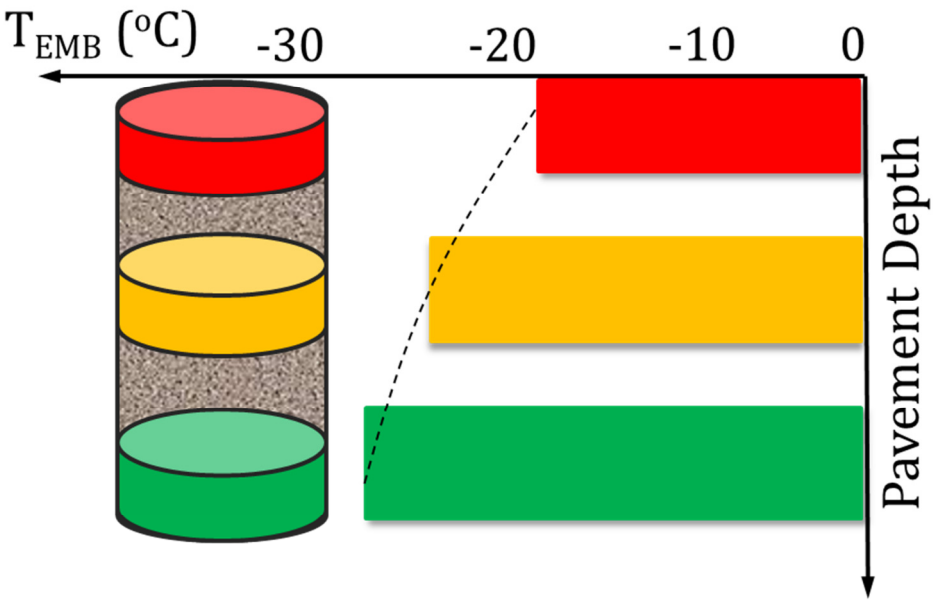

Figure 10.5: A Typical Plot of T_{EMB} of Asphalt Concrete vs Pavement Depth

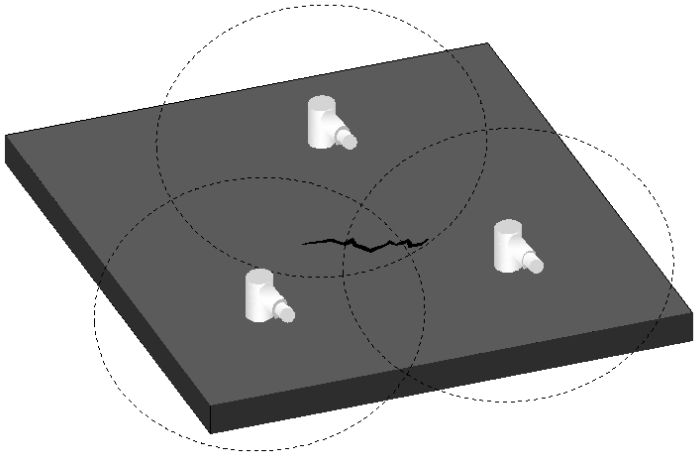

Figure 10.6: AE Source Location using Couple of Piezoelectric Sensors

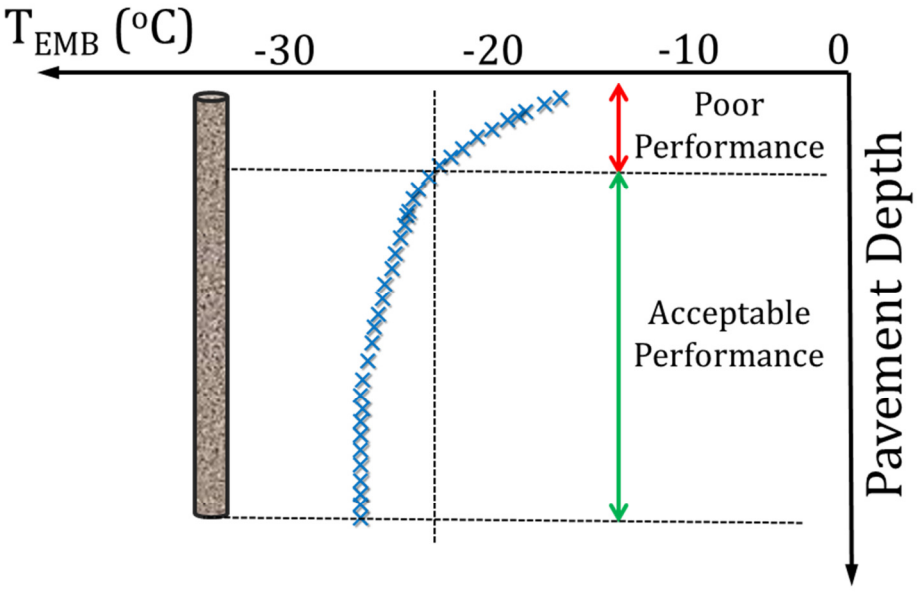

Figure 10.7: A Typical Plot of T_{EMB} Values of Asphalt Concrete vs their Corresponding Locations

REFERENCES

1. Buttlar, W. G., Behnia, B., & Reis, H. M. (2011). *An Acoustic Emission-Based Test to Determine Asphalt Binder and Mixture Embrittlement Temperature* (No. NCHRP IDEA Project 144).

2. Behnia, B., Buttlar, W.G., Apeagyei, A.K., and Reis, H. (2010). Determining the embrittlement temperature of asphalt binders using an acoustic emission approach, NDE/NDT for Highways and Bridges: Structural Materials Technology (SMT), New York

3. Kim, Y. R. (2009). Modeling of asphalt concrete. United State of America: ASCE Press.

4. Hellier, C. (2001). Handbook of nondestructive evaluation.

5. Grosse, C. U., & Ohtsu, M. (2008). *Acoustic emission testing*. Springer.

6. Scott, I. G. (1990). Basic acoustic emission (Vol. 6). Routledge.

7. Valkering, C. P., & Jongeneel, D. J. (1991). Acoustic Emission For Evaluating The Relative Performance Of Asphalt Mixes Under Thermal Loading Conditions (With Discussion). Journal of the Association of Asphalt Paving Technologists, 60.

8. Hesp, S. A., Terlouw, T., & Vonk, W. C. (2000). Low temperature performance of SBS-modified mixes. In *Association of Asphalt Paving Technologists Proc* (Vol. 69).

9. Mix, P. E. (2005). *Introduction to nondestructive testing: a training guide*. Wiley-Interscience.

10. Promboon, Y. (2000). Acoustic emission source location.

11. George, R. (1963). An investigation of AE phenomena, (Doctoral dissertation, PhD thesis, Michigan State University

12. Liptai, R. G., Harris, D. O., & Tatro, C. A. (1972). An introduction to acoustic emission. *Acoustic Emission*, *505*, 2.

13. Liptai, R. G. (1972). *Acoustic emission* (Vol. 505). ASTM International.

14. Drouillard, T. F., Liptai, R. G., & Tatro, C. A. (1975). Industrial use of acoustic emission for nondestructive testing. *Monitoring Structural Integrity by Acoustic Emission, ASTM STP*, *571*, 122-149.

15. Tatro, C. A., Drouillard, T. F., & Hamstad, M. A. (1986). *Recommendations for interagency pinch weld round robin tests* (No. UCID-20889). Lawrence Livermore National Lab., CA (USA); Rockwell International Corp., Golden, CO (USA). Rocky Flats Plant; Denver Univ., CO (USA).

16. Beattie, A. G. (1983). *Acoustic emission, principles and instrumentation* (No. SAND-82-2825). Sandia National Labs., Albuquerque, NM (USA).

17. Ziehl, P., & Fowler, T. J. (2000). *Development of a damage based design criterion for fiber reinforced polymer vessels* (Doctoral dissertation, Ph. D. dissertation, Dept. of Civil Engineering, Univ. of Texas, Austin, Tex).

18. Ziehl, P. H., Engelhardt, M. D., Fowler, T. J., Ulloa, F. V., Medlock, R. D., & Schell, E. (2009). Design and field evaluation of hybrid FRP/Reinforced concrete superstructure system. *Journal of Bridge Engineering*, *14*(5), 309-318.

19. Hamstad, M. A. (1983). Quality Control and Nondestructive Evaluation Techniques for Composites-Part VI: Acoustic Emission-A State-of-the-Art Review. *AVRADCOM Report No. TR*.

20. Hamstad, M. A. (1986). A review: acoustic emission, a tool for composite-materials studies. *Experimental Mechanics*, *26*(1), 7-13.

21. Whalley, G. S., & Cole, P. T. (1983), Development of acoustic emission techniques for quantitative use on aerospace CFRP structures. In *First International Symposium on Acoustic Emission from Reinforced Composites, The Society of the Plastics Industry Inc.*

22. Cole, P. T. (1985). Using acoustic emission (AE) to locate and identify defects in composite structures. *Composite structures*, *3*(3), 259-267.

23. Droge, M. (1983). Recommended practice for acoustic emission testing of fiberglass reinforced plastic piping systems. In *Proceedings of the 1 st international symposium on Acoutic Emission from reinforced composites* (pp. 19-21).

24. Gostautas, R. S., Ramirez, G., Peterman, R. J., & Meggers, D. (2005). Acoustic emission monitoring and analysis of glass fiber-reinforced composites bridge decks. *Journal of bridge engineering*, *10*(6), 713-721.

25. Apeagyei, A. K., Buttlar, W. G., & Reis, H. (2009). Estimation of low-temperature cracking threshold for asphalt binders using an acoustic emission approach. In *The 16th International Symposium on: Smart Structures and Materials & Nondestructive Evaluation and Health Monitoring* (pp. 72920Z-72920Z). International Society for Optics and Photonics.

26. Apeagyei, A. K., Buttlar, W. G., & Reis, H. (2009). Assessment of low-temperature embrittlement of asphalt binders using an acoustic emission approach. *Insight-Non-Destructive Testing and Condition Monitoring*, *51*(3), 129-136.

27. Dave, E. V. (2009). Asphalt Pavementagingand Temperature Dependent Properties Using Functionallygraded Viscoelastic Model, Doctoral dissertation, University of Illinois.

28. Wysong, Z. D. (2004). *Development and comparison of the asphalt binder cracking device to directly measure thermal cracking potential of asphalts*, Doctoral dissertation, Ohio University.

29. Thenoux, G., Lees, G., & Bell, C. A. (1988). Laboratory Investigation of the Fraass Brittle Point Test. In *Proc., Association of Asphalt Paving Technologists* (Vol. 57).

30. Anderson, D. A., Christensen, D. W., Dongre, R., Sharma, M. G., Runt, J., & Jordhal, P. (1990). Asphalt behavior at low service temperatures.

31. Boutin, G., & Lupien, C. (1999). Thermal cracking of asphalt pavement. In *PROCEEDINGS OF THE ANNUAL CONFERENCE-CANADIAN TECHNICAL ASPHALT ASSOCIATION* (pp. 157-174). Polyscience Publications

32. Marasteanu, M. O., Zofka, A., Turos, M., Li, X., Velasquez, R., Li, X., ... & McGraw, J. W. (2007). *Investigation of low temperature cracking in asphalt pavements: national pooled fund study 776* (No. MN/RC 2007-43).

33. H.U. Bahia, and D.A. Anderson, (1995) "Development of the bending beam rheometer; Basics and critical evaluation of the rheometer," ASTM, Proceedings of the Conference on Physical Properties of Asphalt Cement Binders, Vol. 1241 28-50.

34. Anderson, D. A., Christensen, D. W., Bahia, H. U., Dongre, R., Sharma, M. G., Antle, C. E., & Button, J. (1994). *Binder characterization and evaluation. Volume 3: Physical characterization* (Vol. 3, No. SHRP-A-369).

35. Kim, S. S., Wysong, Z. D., & Kovach, J. (2006). Low-temperature thermal cracking of asphalt binder by asphalt binder cracking device. *Transportation Research Record: Journal of the Transportation Research Board*, *1962*(1), 28-35.

36. Kim, S. S. (2007). *Development of an Asphalt Binder Cracking Device*. IDEA Program, Transportation Research Board.

37. Kim, S. S. (2010). Asphalt binder cracking device to reduce low temperature asphalt pavement cracking.

38. AASHTO, MP1a. (1998). Standard specification for performance graded asphalt binder. *American Association of State Highway and Transportation Officials*.

39. ASTM, (1999) "Standard Specification for Performance Graded Asphalt Binder," Vol. D6373-99.

40. Khosla, N. P., & Goetz, W. H. (1979). *Tensile characteristics of bituminous mixtures as affected by modified binders*. Joint Highway Research Project, Purdue University and the Indiana State Highway Commission.

41. Li, X., & Marasteanu, M. (2004). EVALUATION OF THE LOW TEMPERATURE FRACTURE RESISTANCE OF ASPHALT MIXTURES USING THE SEMI CIRCULAR BEND TEST (WITH DISCUSSION). *Journal of the Association of Asphalt Paving Technologists*, *73*.

42. Li, X., & Marasteanu, M. O. (2006). Investigation of low temperature cracking in asphalt mixtures by acoustic emission. Road materials and pavement design, 7(4), 491-512.

43. Li, X., Marasteanu, M. O., Iverson, N., & Labuz, J. F. (2006). Observation of crack propagation in asphalt mixtures with acoustic emission. *Transportation Research Record: Journal of the Transportation Research Board*, *1970*(1), 171-177.

44. Li, X., Marasteanu, M. O., & Turos, M. (2007). Study of Low Temperature Cracking in Asphalt Mixtures Using Mechanical Testing and Acoustic Emission Methods (With Discussion). *Journal of the Association of Asphalt Paving Technologists*, *76*.

45. Li, X., & Marasteanu, M. (2010). The fracture process zone in asphalt mixture at low temperature. *Engineering Fracture Mechanics*, *77*(7), 1175-1190.

46. Nesvijski, E., & Marasteanu, M. (2001). Wavelet Transform and Its Applications to Acoustic Emission Analysis of Asphalt Cold Cracking. *Journal: The e-Journal of Nondestructive Testing & Ultrasonics*, *12*(06).

47. Nesvijski, E., & Marasteanu, M. (2006). Spectral Analysis of Acoustic Emission of Cold Cracking Asphalt. *Journal: The e-Journal of Nondestructive Testing & Ultrasonics*, *11*(10).

48. ASTM D 2872 – 04, (2004), Effect of Heat and Air on a Moving Film of Asphalt (Rolling Thin-Film Oven Test)," American Society for Testing and Materials

49. ASTM D 6521 – 05, (2005) "Accelerated Aging of Asphalt Binder Using a Pressurized Aging Vessel (PAV)," American Society for Testing and Materials

50. Apeagyei, A. K. (2006). *Antioxidant treatment for asphalt binders and mixtures* (Doctoral dissertation, University of Illinois at Urbana-Champaign).

51. http://clas.mq.edu.au/acoustics/frequency/spectral.html

52. http://www.mathworks.com/help/matlab/ref/fft.html

53. Ohno, K., Ohtsu, M., 2010. Crack classification in concrete based on acoustic emission. Construction and Building Materials 24(12), 2339-2346.

54. Soulioti, D., Barkoula, N.M., Paipetis, A., Matikas, T.E., Shiotani, T., Aggelis D.G., 2009. Acoustic emission behavior of steel fibre reinforced concrete under bending. Construction and Building Materials 23,3532-3536.

55. Yin, H. M., Buttlar, W. G., & Paulino, G. H. (2007). Simplified solution for periodic thermal discontinuities in asphalt overlays bonded to rigid pavements. *Journal of transportation engineering*, *133*(1), 39-46.

56. Yin, H. M., Paulino, G. H., & Buttlar, W. G. (2008). An explicit elastic solution for a brittle film with periodic cracks. *International Journal of Fracture*, *153*(1), 39-52.

57. Xia, Z. C., & Hutchinson, J. W. (2000). Crack patterns in thin films. *Journal of the Mechanics and Physics of Solids*, *48*(6), 1107-1131.

58. Shenoy, V. B., Schwartzman, A. F., & Freund, L. B. (2001). Crack patterns in brittle thin films. *International journal of fracture*, *109*(1), 29-45.

59. Beuth Jr, J. L. (1992). Cracking of thin bonded films in residual tension. *International Journal of Solids and Structures*, *29*(13), 1657-1675.

60. Manual, ABAQUS User's (2004) "Version 6.5, Hibbitt, Karlsson & Sorensen." Inc., Pawtucket, RI

61. W.G. Buttlar, and R. Roque, (1994) "Development and evaluation of the strategic highway research program measurement and analysis system for indirect tensile testing at low temperatures," Transportation Research Record, 1454:163-171.

62. AASHTO, "Standard Test Method for Determining the Creep Compliance and Strength of Hot Mix Asphalt (HMA) Using the Indirect Tensile Test Device (T-322)," American Association of State Highway and Transportation Officials, Washington, DC, 2004.

63. D.W. Christensen, and R.F. Bonaquist, "Evaluation of Indirect Tensile Test (IDT) Procedures for Low-Temperature Performance of Hot Mix Asphalt," Federal Highway Administration, NCHRP-530, United States, 2004.

64. M.P. Wagoner, W.G. Buttlar, G.H. Paulino, and P.B. Blankenship, (2005) "Investigation of the fracture resistance of hot-mix asphalt concrete using a disk-shaped compact tension test," *Transportation Research Record,* 1929:183-192.

65. Wagnoner, M. P., Buttlar, W. G., & Paulino, G. H. (2005). Disk-shaped compact tension test for asphalt concrete fracture. *Experimental Mechanics*, *45*(3), 270-277.

66. M.P. Wagoner, W.G. Buttlar, and G.H. Paulino, (2005) "Development of a single-edge notched beam test for the study of asphalt concrete fracture," Geo-Frontiers 2005, 137-149.

67. M.P. Wagoner, W.G. Buttlar, G.H. Paulino, and P.B. Blankenship, (2006) "Laboratory testing suite for characterization of asphalt concrete mixtures obtained from field cores," *Journal of Asphalt Paving Technologists,* Proceedings of the Annual Meeting, Association of Asphalt Paving Technologists, Vol. 75 815-852.

68. Li, X., & Marasteanu, M. (2004). Evaluation Of The Low Temperature Fracture Resistance Of Asphalt Mixtures Using The Semi Circular Bend Test. *Journal of the Association of Asphalt Paving Technologists*, *73*.

69. Li, X. J., & Marasteanu, M. O. (2010). Using semi-circular bending test to evaluate low temperature fracture resistance for asphalt concrete. *Experimental mechanics*, *50*(7), 867-876.

70. Jung, D., & Vinson, T. S. (1993). Thermal stress restrained specimen test to evaluate low-temperature cracking of asphalt-aggregate mixtures. *Transportation research record*.

71. Tran, N., Taylor, A., Timm, D., Robbins, M., Powell, B., & Dongre, R. (2010), Comprehensive Laboratory Performance Evaluation, National Center for Asphalt Technology (NCAT) report 10-05.

72. Behnia, B., Dave, E. V., Ahmed, S., Buttlar, W. G., & Reis, H. (2011). Effects of Recycled Asphalt Pavement Amounts on Low-Temperature Cracking Performance of Asphalt Mixtures Using Acoustic Emissions. Transportation Research Record: Journal of the Transportation Research Board, 2208(1), 64-71.

73. Dave, E. V., Behnia, B., Ahmed, S., Buttlar, W. G., & Reis, H. (2011). Low Temperature Fracture Evaluation of Asphalt Mixtures using Mechanical Testing and Acoustic Emissions Techniques. Journal of the Association of Asphalt Paving Technologists, 80.

74. Blankenship, P. Anderson, M., King, G., Hanson, D.I., (2010), A Laboratory and Field Investigation to Develop Test Procedures for Predicting Non-Load Associated Cracking of Airfield HMA Pavements, Project 06-01 (Phase II) Final Report, August, 2010

75. ASTM 7313-07(2007) Standard Test method for determining Fracture Energy of Asphalt

Concrete-aggregate Mixtures using the Disk-Shaped Compact Tension Geometry, American Society of Testing and Materials.

76. J. Baruchel, J. Buffiere, E. Maire, P. Merle, G. Peix, "X-Ray Tomography in Material Science",Hermes science publications, Paris, 2000

77. Bordelon, A (2011), "Design of Flowable Fibrous Concrete for Thin Concrete Pavements", Ph.D. Thesis, University of Illinois at Urbana-Champaign.

78. Baek, C., Underwood, B. S., & Kim, Y. R. (2012). Effects of Oxidative Aging on Asphalt Mixture Properties. *Transportation Research Record: Journal of the Transportation Research Board*, *2296*(1), 77-85.

79. Lau, C. K., K. M. Lunsford, C. J. Glover, R. R. Davison, and J. A. Bullin, 1992, Reaction Rates and Hardening Susceptibilities as Determined from Pressure Oxygen Vessel Aging of Asphalts. *Transportation Research Record 1342*, TRB, National Research Council, 50-57.

80. Petersen, J. C., J. F. Branthaver, R. E. Robertson, P. M. Harnsberger, J. J. Duvall, and E. K.Ensley, 1993, Effects of Physicochemical Factors on Asphalt Oxidation Kinetics. *Transportation Research Record 1391*, TRB, National Research Council, 1-10.

81. Thomas, K. P., 2002, Impact of Water during the Laboratory Aging of Asphalt. *Road Materials and Pavement Design*, 3(3): 299-315.

82. Braham, A. F., Buttlar, W. G., Clyne, T. R., Marasteanu, M. O., & Turos, M. I. (2009). The effect of long-term laboratory aging on asphalt concrete fracture energy. *Journal of the Association of Asphalt Paving Technologists*, *78*.

83. Buttlar, W., Rebholz, F. E., & Nassar, W. (2004). *Detection of Recycled Asphalt Pavement (RAP) in Bituminous Mixtures* (No. ITRC FR 02-2,).

84. Xiao, F., Amirkhanian, S., & Juang, C. H. (2007). Rutting resistance of rubberized asphalt concrete pavements containing reclaimed asphalt pavement mixtures. *Journal of Materials in Civil Engineering*, *19*(6), 475-483.

85. West, R., Kvasnak, A., Tran, N., Powell, B., & Turner, P. (2009). Testing of Moderate and High Reclaimed Asphalt Pavement Content Mixes. *Transportation Research Record: Journal of the Transportation Research Board*, *2126*(1), 100-108.

86. World Commission on Environment and Development. Our Common Future. (1987), Oxford University Press.

87. Chiu, C., Hsu, T., Yang, W. (2008) Life Cycle Assessment on using Recycled Materials for Rehabilitating Asphalt Pavements. Resources Conservation and Recycling 52(3), pp. 545-556.

88. Kandhal, P.S. and Mallick, R.B. (1997), Pavement Recycling Guidelines for State and Local Government. National Center for Asphalt Technology.

89. Aurangzeb, Q., Al-Qadi, I.L., Carpenter, S., Pine, B., and Trepanier, J. (2011) , Mix Design and Laboratory Performance of Asphalt Mixtures with High RAP Content., RAP-ETG Meeting, Irvine, CA.

90. Prowell, B. and Hurley, G.C. (2007), Warm-Mix Asphalt: Best Practices. National Asphalt Pavement Association Quality Improvement Series 125. Lanham, MD, December.

91. D'Angelo, J., Harm, E., Bartoszek, J., Baumgardner, G., Corrigan, M., Cowsert, J., Harman, T., Jamshidi, M., Jones, W., Newcomb, D., Prowell, B., Sines, R., and Yeaton, B. (2008), Warm-Mix Asphalt: European Practice. FHWA Report No. FHWA-PL-08-007.

92. Prowell, B. and Hurley, G.C. (2006), Evaluation of Sasobit for Use in Warm Mix Asphalt. NCAT Report 05-06.

93. Young, T.J. (2007), Energy Conservation in Hot-Mix Asphalt Production. National Asphalt Pavement Association. Quality Improvement Series 126. Lanham, MD.

94. Prowell, B. and Hurley, G.C. (2005), Evaluation of Aspha-min Zeolite for Use in Warm Mix Asphalt. NCAT Report 05-04.

95. Prowell, B. and Hurley, G.C. (2006), Evaluation of Evotherm for Use in Warm Mix Asphalt. NCAT Report 06-02.

96. Doyle, J.D., Mejias-Santiago, M., Brown, E.R., and Howard, I.L. (2011), Performance of High RAP-WMA Surface Mixtures. Journal of the Association of Asphalt Paving Technologists, Vol. 80, pp. 403-437.

97. Sasol International. (2010)What is Sasobit®?. http://www.sasolwax.us.com/sasobit.html.

98. Roberts, F.L., Kandhal, P.S., Brown, E.R., Lee, D.Y., and Kennedy, T.W. (1996), Hot Mix Asphalt Materials, Mixture Design, and Construction. National Asphalt Pavement Association 2nd Edition. Lanham, MD.

99. Illinois Department of Transportation. (2011), Hot Mix Asphalt Level III Technician Course. Lakeland College. Chapter 2, pp. 56.

100. Hill, B. (2011), Performance Evaluation of Warm Mix Asphalt Mixtures Incorporating Reclaimed Asphalt Pavement, Master's Thesis, University of Illinois at Urbana-Champaign.

101. Hill, B., Behnia, B., Hakimzadeh, S., Buttlar, W.G., Reis, H. (2012), Evaluation of the Low Temperature Cracking Performance of WMA Mixtures, Transportation Research Record, Accepted for Publication.

102. Middleton, B. and Forfylow, R.W. 2009. Evaluation of Warm-Mix Asphalt Produced with the Double Barrel Green Process. Transportation Research Record No. 2126, pp. 19-26.

103. Appleford, J. M., Ocfernia, K. C. S., Zhang, Y., Christianson, L., Funk, T. L., and Dong, R. 2005. Analysis and Characterization of the Product Oil and Other Products of Hydrothermal Conversion of Swine Manure, *American Society of Agricultural and Biological Engineers,* Paper Number 054092.

104. Airey, G. D.,Mohammed, M. H., and Fichter, C. 2008. Rheological Characteristics of Synthetic Road Binders, *Fuel*, 87(10/11): 1763-1775.

105. Fini, E., Yang, S.H., & Shuangning, X. 2010c. Characterization and Application of Manure-Based Bio-Binder in Asphalt Industry, *Transportation Research Board Annual Meeting,* 2010: 10-2871.

106. Fini, E.H., Kalberer, E.W., & Shahbazi, A., Basti, M., You, Z., Ozer, H., & Aurangzeb, Q. 2011a. Chemical Characterization of Biobinder from Swine Manure: Sutainable Modifier for Asphalt Binder. *Journal Of Materials In Civil Engineering*, 23(11): 1506-1513.

107. Fini, E.H., Kalberer, E.W., & Shahbazi, A. 2011b. Biobinder From Swine Manure: Sustainable Alternative for Asphalt Binder, *Transportation Research Board Annual Meeting*, 2011: 11-3453.

108. Jackson, L. L., Keeney, D. R., & Gilbert, E. M. 2000. Swine Manure Management Plans in North-Central Iowa: Nutrient Loading and Policy Implications, *Journal Of Soil & Water Conservation*, 55(2): 205.

109. Keles, S. S., Kaygusuz, K. K., & Akgun, M. M. 2011. Pyrolysis of Woody Biomass for Sustainable Bio-oil, *Energy Sources Part A: Recovery, Utilization & Environmental Effects*, 33(9), 879-889.

110. Raouf, M. A., and Williams, R. C. 2010. Temperature and Shear Susceptibility of a Nonpetroleum Binder as a Pavement Material, *Transportation Research Record: Journal of the Transportation Research Board*, 2180: 9-18.

111. Roggero, C.M., Tumiatti, V.V., Scova, A.A., De Leo, C.C., Binello, A.A., & Cravotto, G. G. 2011. Characterization of Oils from Haloclean Pyrolysis of Biomasses, *Energy Sourses Part A: Recovery, Utilization & Environmental Effects,* 33(5), 467-476.

112. Xiu, S. N., Rojanala, H. K., Shahbazi, A., Fini, E. H., & Wang, L. 2011. Pyrolysis and Combustion Characteristics of Bio-Oil from Swine Manure, *Journal of Thermal Analysis and Calorimetry*, 107(2): 823-829.

113. Mogawer, W.S., Fini, E.H., Austerman, A.J., Booshehrian, A., and Zada, B. 2012. Performance Characteristics of High RAP Bio-Modified Asphalt Mixtures. *Transportation Research Record*, Accepted for Publication.

114. S.H. Song, G.H. Paulino, and W.G. Buttlar, (2006), Simulation of crack propagation in asphalt concrete using an intrinsic cohesive zone model, *Journal of Engineering Mechanics,* 132:1215-1223.

115. S.H. Song, G.H. Paulino, and W.G. Buttlar, (2006), A bilinear cohesive zone model tailored for fracture of asphalt concrete considering viscoelastic bulk material, *Engineering Fracture Mechanics,* 73:2829-2848.

116. S.H. Song, (2006), A Cohesive Zone Modeling Approach Considering Viscoelastic Effects," Doctorate Thesis, University of Illinois at Urbana-Champaign, Urbana, IL.